MODELS OF THE SPATIO-TEMPORAL DYNAMICS OF THE HIGH ALTITUDE ALPINE FAUNA IN THE CLIMATE CHANGE CONTEXT

Doctoral Dissertation of:
Andrea Mignatti

Supervisor:
Prof. Marino Gatto

Co-supervisor:
Prof. Renato Casagrandi

Tutor:
Prof. Carlo Piccardi

The Chair of the Doctoral Program:
Prof. Carlo Fiorini

Year 2013 Cycle XXVI

Acknowledgements

I would like to thank my PhD supervisors, Professors Marino Gatto and Renato Casagrandi, for supporting me during my doctorate. They have always been an example of passion and dedication to work.

I'm also grateful to prof. Stefano Focardi for having carefully revised the thesis and for his precious recommendations which helped to improve the quality of the manuscript.

I wish to acknowledge all the people that collaborated and shared ideas with me for the development of the case studies presented in this thesis. In particular, I'm grateful to Prof. Antonello Provenzale, Dr. Simona Imperio, Dr. Ramona Viterbi, Dr. Achaz von Hardenberg, Dr. Luca Pedrotti, Prof. Mauro Guglielmin and Prof. Nicoletta Cannone.

I also thank Drs. Lorenzo Mari and Giovanna Ranci Ortigosa for giving me the opportunity to taste the beauty of teaching, and to Prof. Carlo Piccardi for his tutoring.

I would like to thank Prof. Isabella Cattadori, Dr. Alexander Hernandez and all the researchers and graduate students at CIDD for their hospitality at Penn State and their precious scientific collaboration.

Thanks to Alessandro Papadopulos, Fabio della Rossa, Matteo Picozzi and all the fellows of *office 203* Daniela Anghileri, Marcello Schiavina, Marisa Rossetto and Matteo Giuliani: they are both fantastic colleagues and friends.

Many thanks also to Francesca Mattioli, Martina Cividini and Viviana Brambilla for their invaluable help in the data collection, and to the "*Prava guys*" Fabio, Francesca, Francesco and Michele which cheered up my evenings after the long days spent in the field.

A special dedication goes to Andrea, Emanuele and my room-mates Venky, Sid, Chinmay, Puneet and Sam: they made possible that the period spent at State College was truly rich.

I also thank Dr. Giorgio Corani, who had the patience to advise me for minor research projects. He taught me with passion how to carry out a productive research.

Finally, special thanks goes to my family and to Clio, which have supported me with love both in the dark and in the bright moments.

Abstract

High altitude Alpine regions are hotspots of biodiversity and are very sensitive to the occurring climate change, displaying a warming rate higher than the global average. The most evident response of Alpine species is an uphill movement towards higher elevations. Summit species are the most vulnerable because they cannot shift over the ridges or the perennial snow. This thesis's aim is to develop innovative models for the occurred and expected responses of high altitude Alpine fauna to the climate change.

We developed both species distribution models and dynamic demographic models. Species distribution models describe the relationship between environmental variables and the suitability of a territory to host a given species. Temporal dynamics is instead taken into account in demographic models, which show how the abundance of individuals changes in time. In both cases, there is a need for appropriate methods that identify, from data, which environmental and/or climatic variables have an important influence on the spatial distribution and on the demographic parameters of the target species. The identification of the best predictive models has been carried out by using standard selection criteria (e.g. the Akaike Information Criterion). When the model selection was uncertain we relied on multimodel techniques to produce predictions. Namely, we used the *Bayesian Model Averaging* (BMA) or, alternatively, the multimodel inference based on the Akaike weights. Three high altitude species, which are vulnerable to climate change, have been chosen for our study: Alpine ibex (*Capra ibex*), Alpine marmot (*Marmota marmota*) and black grouse (*Tetrao tetrix*). The choice has also been motivated by data availability.

In the Alpine marmot case study, we investigated the fine scale characteristics that determine the suitability of the habitat for the species in a high altitude Alpine valley near the Stelvio National Park (North-western Italy). Since there were no available data on marmot distribution in the valley, we performed field surveys to locate burrows. Using available data, we developed species distribution models using BMA applied to logistic regression. Results show that the position of marmot burrows is mainly dependent on the vegetation type, thus suggesting that the speed of marmot uphill shift is limited by the colonization dynamics of the vegetation.

As for the black grouse, we studied the influence of spatial position, population density and meteorological conditions on four demographic rates (growth rate and three components of fertility) that characterize the populations of 17 Alpine districts in the Piedmont region (Italy). Our results are mostly consistent with past results obtained for lowland popula-

tions. The meteorological variables that have the main influence on the demographic rates are linked with key periods of the black grouse life cycle; namely the breeding season, the hatching period and the winter season (usually characterized by a high mortality). Moreover, we found that direct density dependence is the main driver of population growth rate.

Alpine ibex populations are characterized by a strong age and sex structure, that has never been considered in a population dynamics model. On the other hand, past studies show that the main drivers of population growth rate are the population density and the accumulation of snow during winter, while survival and fertility are not constant with the age, but are typically smaller and more variable for the youngest and the oldest individuals. Using the Gran Paradiso National Park (Italy) population data, we developed models that, alongside with density and snow depth, take into account the age and sex-structure of the population at different levels of complexity. We first separate the population into four subgroups according to the sex and/or the maturation state of the individuals, and we accordingly define four demographic rates: survival of adult males, adult females and kids, and weaning success. The model identification procedure shows that population density and snow depth are still crucial for the separate population groups, and that intraspecific competition occurs mainly among the individuals of the groups that share the same environment for most of the year. Moreover, our results show that weaning success and survival of kids are maximal for intermediate levels of snow depth. We also developed models that take into account the fine age structure of the population, thus allowing the incorporation of senescence. Results show that the inclusion of senescence is particularly important for adult females survival and for the ability of adult females to breed their kids. Moreover, we found that the effect of the population density and the snow depth on survival and fertility increases with the age of the adults.

Overall, our approach permitted to detect and take into account the environmental (climatic, vegetational, etc.) and the population-specific (density, senescence, etc.) characteristics that drive the species distribution and the demography of the case-study species. Making models that take into account the specificity of each species is a key step to understand the expected impacts of climate change on the Alpine biome. However, a lot of work is still needed in this field, in particular to include the interactions between species, which is certainly of paramount importance to explain their spatial and temporal distribution.

Contents

Contents

Introduction

1.1 Climate change and the Alps

1.1.1 Alps: properties and vulnerabilities

Mountain environment is characterized by one of the highest richness in ecosystems, and a particular vulnerability to climate change and anthropogenic disturbance (Fischlin *et al.*, 2007). Geographically, mountains represent about 22% of all land, but through their ecosystem services they can influence all continental mainlands (ibidem). One of the main reasons for the high abundance in the number of different ecosystems is the temperature gradient which occurs for a variation in the altitude. The mean temperature changes in fact much more rapidly with a change in altitude than with a change in latitude; for example Wang *et al.* (2011) recently estimated, for an Himalayan plateau, an altitude gradient of -4.8°Celsius per 1000 m and a latitude gradient of -0.87°Celsius per 1000 m. Mountain regions are thus characterized by many climatic types within a short horizontal distance, and thus by an high species richness (Väre *et al.*, 2003; Moser *et al.*, 2005; Spehn, 2005).

Among the mountain regions, Alps are particularly relevant because

they host a huge quantity of endemic species (Theurillat & Guisan, 2001; Korner & Spehn, 2002). Moreover, they are regarded as one of the most important regions for the preservation of biodiversity in Europe (Theurillat *et al.*, 2003) and they are included in the set of global biodiversity conservation priority regions (Ginsberg, 1999).

The actual configuration of the alpine environment is the result of the interplay among natural conditions and centuries of anthropogenic forcing. For example, traditional pastoral practices have lowered the timberline by 100 to 400 m (Ellenberg, 1996), thus increasing the available habitat for the species that dwell on the alpine pastures, as the alpine marmot (*Marmota marmota*) and the Black grouse (*Tetrao tetrix*). However, the recent abandonment of the alpine pastures, together with the climate warming, have caused an expansion of the woods and an upward shift of the tree line, and a consequent shrinking of alpine pastures (Schweiger *et al.*, 2012). The abandonment of mountain fields, together with the intensification of the exploitation in other areas, has caused serious effects on local biodiversity (Dirnböck *et al.*, 2003; Laiolo *et al.*, 2004; Martin & Possingham, 2005). Moreover, the expansion of shrubs caused a decrease in several grassland species, together with a possible change in the host-parasite interaction (Chemini & Rizzoli, 2003).

(a) Worldwide   (b) alpine biome
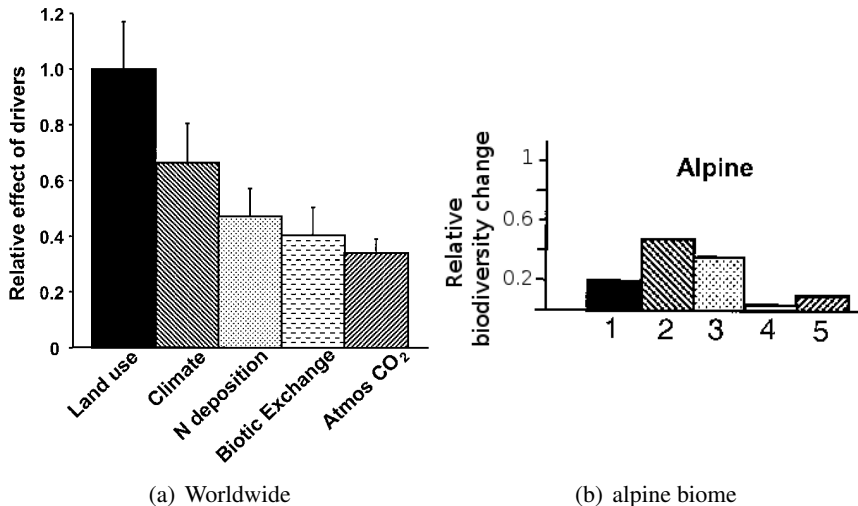
Figure 1.1: *Expected effects of different drivers in changing the biodiversity for the year 2100. Panel a) is an average of the estimates for each biome, made relative to the maximum change; Panel b) reports the effects on the alpine biome only. Adapted from (Sala* et al.*, 2000)*

More generally, Sala *et al.* (2000) shows that, worldwide, the major driver of the expected biodiversity loss for the year 2100 is the land use change (see figure 1.1.a). However, if the direct effect of the increase in the CO_2 concentrations is summed up with the climate change, the increase in the greenhouse gasses becomes the main driver of biodiversity loss (Maclean & Wilson, 2011). Moreover, Sala *et al.* (2000) predict also that, if we focus on the alpine biome, the major driver of the expected biodiversity loss is the change in climate, as reported in figure 1.1.b. In fact, climate changes are known to be most extreme in alpine regions (Beniston *et al.*, 1997). Moreover, high Altitude ecosystems are determined by low temperatures and host organisms highly specialised and that live close to the limits of their physiological tolerances. Thus, alpine communities are more like to be at risk from the predicted changes (Grabherr *et al.*, 2000; Walther *et al.*, 2005) and alpine ecosystems are expected to show the effects of climate change earlier and more clearly than other ecosystems (IPCC, 2007a; Pauli *et al.*, 2007; Pickering *et al.*, 2008).

1.1.2 Global climate change

Climate is warming at an extremely rapid rate, which is expected to increase in the near future. The climate warming has been principally caused by human activities, mainly through a variation in the greenhouse gasses balance (IPCC, 2007b). Diffenbaugh & Field (2013) recently estimated a potential increase in temperatures comparable in magnitude to the largest warming in the last 65 million years, and orders of magnitude faster. On the same line, the just published Fifth Assessment Report (AR5) of the first working group of the IPCC confirms the six main observed changes in the climatic system (IPCC, 2013):

   i an unequivocally warming of the of the ocean and the atmosphere (figure 1.2.a); the average surface warming, combining land and ocean, is 0.85 °C from 1880 to 2012;

   ii a variation in the regime of precipitations, with changes in many extreme weather and climate events (figure 1.2.d);

  iii a decrease in the ice and snow cover, with a shrinkage of the mass and the extension of the glaciers, and a reduction of the spring snow cover in the Northern Hemisphere (figure 1.2.b);

   iv a rise in the sea levels (figure 1.2.f);
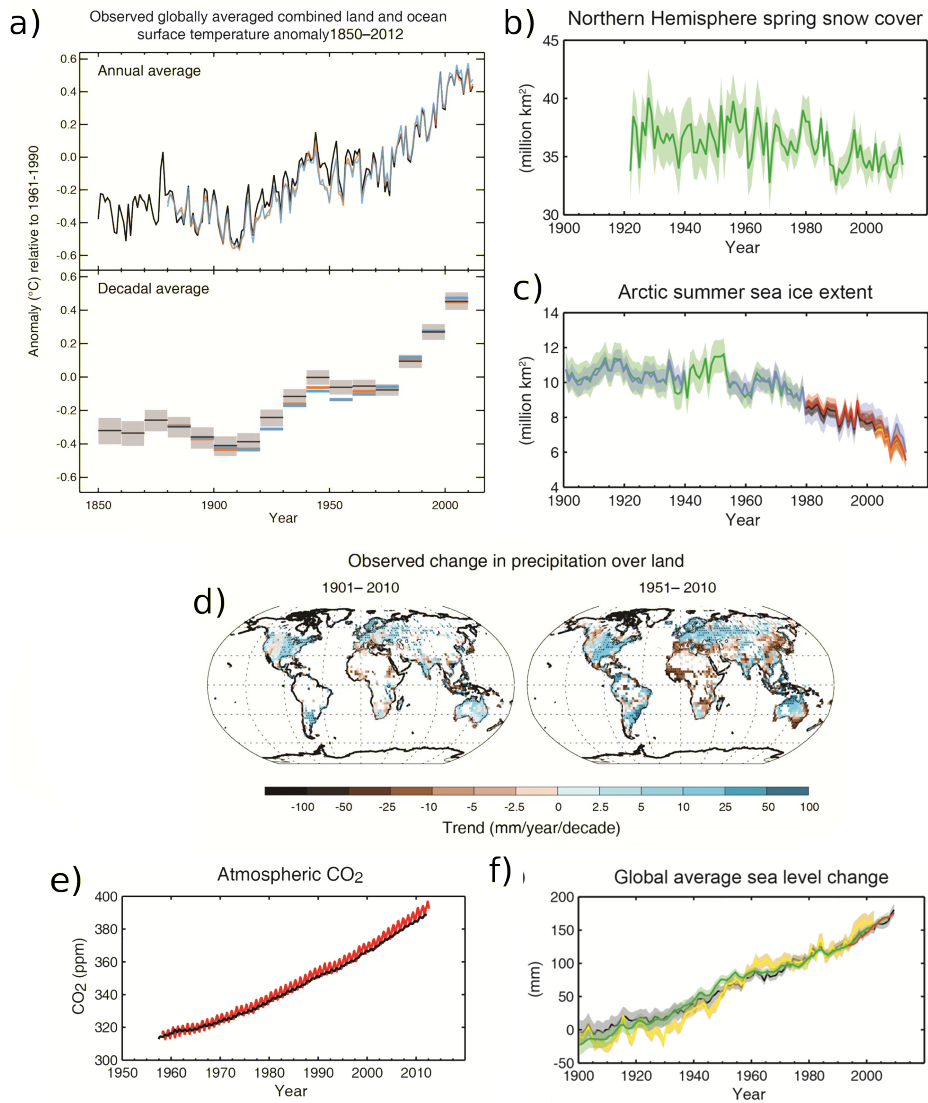
Figure 1.2: *Set of figures adapted from (IPCC, 2013) and showing the main observed changes in the climate system linked to the global climate change. We refer the reader to the original text for an accurate description of the methodologies used to develop these plots.*

  v an increase in the atmospheric concentration of the greenhouse gasses
    as carbon dioxide (CO_2), methane (CH_4) and nitrous oxide (N_2O),
    which reached the maximum concentration of the last 800000 years
    (figure 1.2.e).

  vi an acidification of the oceans, caused by the absorption of about 30%
    of the emitted anthropogenic carbon dioxide .

1.1.3 Evidences of climate change on the Alps

Effects on the abiotic components

The global climate warming is not uniform worldwide, but presents asymmetries among the different regions of the Earth, in which warming is occurring at different rates. On the Alps, the climate warming appears to be stronger than the average global signal (Beniston, 2006; Calmanti & Motta, 2007; Auer *et al.*, 2005; Rebetez & Reinhard, 2008; Keiler *et al.*, 2010) and high altitude environment can be seen as early indicator of climate change (Grabherr *et al.*, 2003). Past studies report an increase in temperature on the mountains that is at least two times higher than the global average (Diaz & Bradley, 1997; Böhm *et al.*, 2005). According to Beniston (2006), temperatures on the Alps have risen up of about 2 °C in the 20*th* century. The variation in the regime of precipitations is instead more complicated and spatially variable, and do not present a clear long term trend; however, the decrease in the amount of snowfall registered in the Northern hemisphere has been also recorded on the Alps, and has been already documented for many alpine regions (e.g. see Jacobson *et al.*, 2004; Terzago *et al.*, 2010). The warming in the Alps is projected to continue at a rate greater than the global average, with an amount of precipitations that slightly increases in winter and strongly decreases in summer. However, the increase in winter precipitations does not compensate the temperature warming, which can drastically reduce the snow cover duration. Hantel & Hirtl Wielke (2007) predict, for the Alps, that each increase of 1 degree Celsius can cause a reduction of the length of the snow cover period of 30 days at a altitude of 700 m a.s.l. and an increase of the snowline of about 150 meters.

   The cryosphere, composed by glaciers and permafrost, is sensitively responding to the change in temperatures and precipitation regimes. Glaciers have lost approximately 30-40% of the area and half of the mass (Haeberli & Beniston, 1998; EEA European Environmental Agency, 2004), and are predicted to shrink very rapidly with the temperature warming. Beniston (2006) predicts a reduction of the mass of the mountain glaciers between

50% and 90% by the end of the current century, while small glaciers will disappear (Paul, 2004). The estimated upward shift of the glacier limits is between 60 and 140 meters for each °Celsius of temperature increases (Vincent, 2002; Maisch, 2000). In agreement with the expected global trend of shrinking in the thickness and the extension of permafrost (IPCC, 2013; Haeberli, 2009), alpine observations report an increase in the temperature of permafrost (Guglielmin & Camusso, 2004). The reduction of permafrost can probably cause an increase in the frequency and the intensity of landslides and avalanches (Beniston, 2006; Bocchiola & Rosso, 2008).

The variation in the snow cover and the cryosphere will cause major changes in the water regime. The expected effect is an initial increase in the glacier runoff and in the peak flows, followed by a significantly diminished runoff total as the glaciers continue to shrink, especially in spring and summer (Hagg & Braun, 2004). The impacts of such variations will not be limited to the mountain areas, because they will affect the downstream flow reducing the amount of water available for both the mountain and lowland stakeholders needs (e.g. agriculture, drinking water, hydroelectric power). On the other hand it will also increase the hydrogeological risks such as floods and erosion (Beniston, 2006).

Effects on the biome: flora and fauna

The climatic change and its impacts on the abiotic components of the alpine habitats have strong consequences on the alpine biome, which have been already documented in many studies. The expected impacts are strong on both the fauna and the flora, because Alps host species that are adapted to extreme environments, characterized by low temperatures, and that lives on the limit of their capabilities (Eisenreich, 2005; Körner, 1999; Thuiller, 2007).

Hughes (2000) lists four main categories of direct biological consequences of global warming (see figure 1.3): (i) effects on physiology, (ii) effects on phenology, (iii) effects on distributions, and (iv) adaptation through evolution. The latter effect (iv) occurs at the evolutionary time scale and can be considered a short term strategy for adaptation to climate change only for organisms characterized by short generation times and rapid population growth. Quintero & Wiens (2013) estimate in fact that, to match the changes predicted for the current century, the climate ecological niche should evolve, for many species, more than 10000 times faster than the rates that are usually observed. As summarized in figure 1.3, the listed direct biological consequences can lead to a change in the species interaction
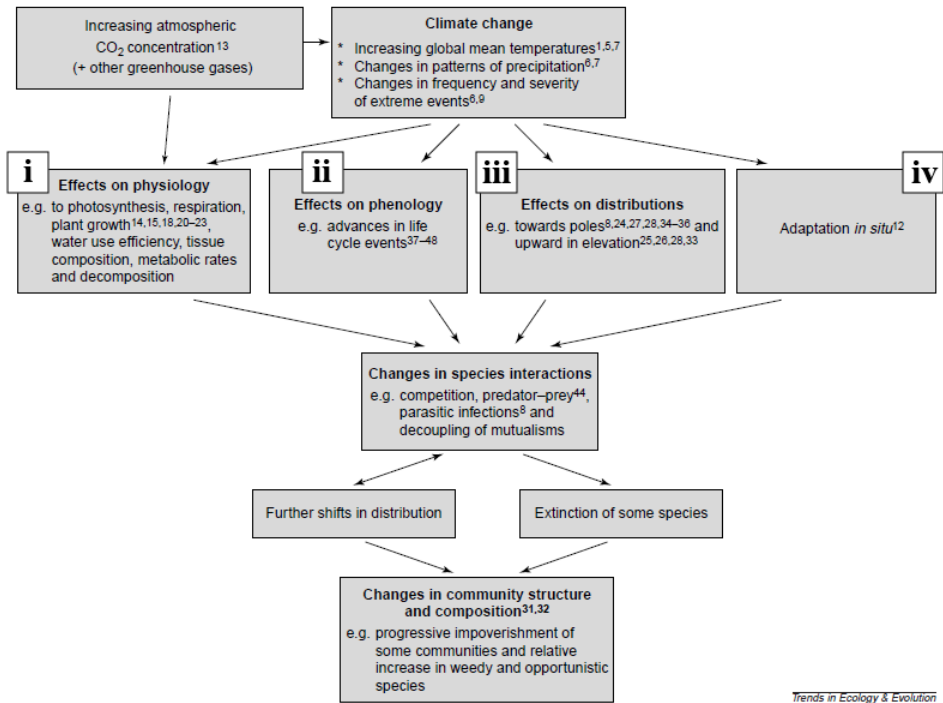
Figure 1.3: *Schematic graph, published in Hughes (2000), of the potential pathways of community change caused by the increase in the atmospheric greenhouse gasses. We report here the original caption, which summarizes the meaning of the nodes and the links of the graph:"Potential pathways of community change owing to the enhanced greenhouse effect. Increased CO2 concentration will act on species directly (via physiology) and indirectly (via climate changes) (first tier). Individual species might potentially respond in four ways (second tier), resulting in changes in species interactions (third tier). These changes might then lead either to extinctions or to further shifts in ranges (fourth tier), ultimately leading to changes in the structure and composition of communities."*

and, consequently, to the extinction of some species and a further variation in the species distribution. These variations finally cause changes in the structure and the compositions of the ecological communities.

One of the major driver that impacts the phenology (i.e. the life cycle) (iv) and physiology (ii) of alpine plants is the snow condition. An earlier snowmelt leads in fact to an anticipation of the growing phase and of the flowering in spring (Inouye, 2008; Pettorelli *et al.*, 2007; Inouye, 2008, e.g.). However, many alpine species are strongly dependent on the photoperiod and will not be able to simply anticipate their life cycle (Keller & Körner, 2003). A study conducted on the Rocky Mountains in Colorado by Inouye (2008) reports that earlier snowmelt increased the mortality of buds caused by frost, with potential effects on all the food chain. Effects on physiology are expected mainly for particularly sensitive environments, as for valley characterized by snowbed vegetation, which density and primary production are strongly affected by snow conditions (Carbognani *et al.*, 2012). Moreover, a general increase of evapotranspiration is predicted, and will probably lead to increased drought (Fischlin *et al.*, 2007).

The most evident effect of climate warming on the biome is probably the change of the distribution of the species (ii). At a global level, species are moving longitudinally away from the equator towards the poles at a very fast rate (Parmesan & Yohe, 2003; IPCC, 2007a; Thomas, 2010). Chen *et al.* (2011) recently estimate a shifting speed of 16.9 km decade^{-1}. On the mountain environments, the longitudinal shifting is substituted by a shifting toward higher elevations; the median uphill (or upslope) shifting is estimated to be 11.0 m decade^{-1} (Chen *et al.*, 2011). In figure 1.4 we summarize the possible results of an uphill shifting of the original upper boundary (dashed line in the figure) and/or lower boundary (dotted line in the figure) for a single species. Of course, if there is an uplift of the upper boundary only, the result is an enlargement of the area in which the species is distributed (mountain sketch *b* in the figure). Conversely, if the upward shift involves only the lower boundary, the area of distribution shrinks (mountain sketch *c*). On the other hand, shifting uphill often means a reduction of the geographical range of the species, because mountains have a pseudo-conical shape for which tops are smaller than bases; mountain sketch *d* in figure 1.4 shows in fact the reduction of the distribution (grey area) for the case in which the altitude uplift is equal for the lower and the upper bound of the species distribution. However, the uphill shift of the upper bound of distribution is possible only for species that live in the warmer zones of the mountains, far below the peaks, while is not possible for species that live in the proximity of the ridges (Fischlin *et al.*, 2007). An uplift of the lower

distribution boundary over the ridges determines the local extinction of the species (mountain sketch *e* in the figure). Moreover, the uphill shift of the species has the potentiality to cause non-linear effects on the population dynamics. If the areal of distribution decreases, the population abundance is in fact likely to drop, while the distance between sub-populations increases. This increase in patchiness can lead, for example, to the ignition of a type-D extinction vortex (Gilpin & Soulé, 1986). Of course, as already mentioned above in the comments of figure 1.3, a change in the distribution of a species have the potential of being a contributory cause of a variation in the ecological communities.
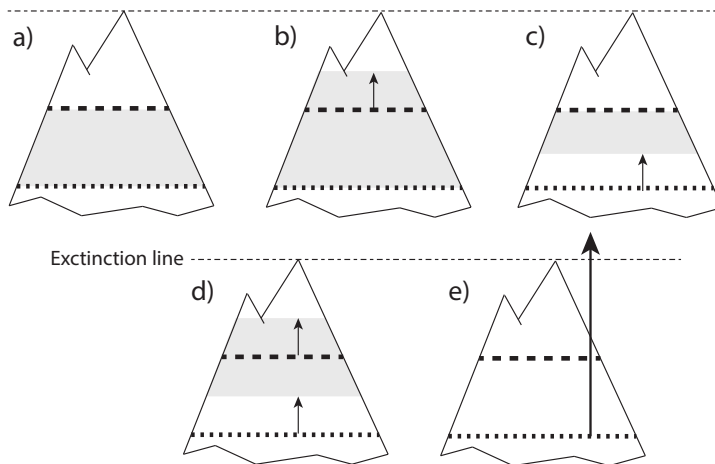
Figure 1.4: *Four remarkable possible results of uphill shifting for a single species. In the sketches of the mountains, the dashed and the dotted line represent, respectively, the upper and the lower bound of the species distribution, while the grey area is the actual distribution. a) Initial state; b) Upshift of the upper boundary only; c) upshift of the lower boundary only; d) equal upshift of the lower and the upper boundary; e) Upshift of the lower boundary over the mountain ridges, which are indicated with a dashed-dotted line (Physical Extinction line).*

On the Alps, there are clear evidences that alpine plants are shifting upwards (Walther *et al.*, 2005); the rapidity of the responses varies with the vegetation type, and is faster for ruderal plants as rockfield pioneers (Grabherr *et al.*, 1994) and snowbed vegetation (Bahn & Körner, 2003). The lower edge of nival and sub-nival plants is contracting and there is a concurrent expansion of alpine pioneer species at their leading edge (Pauli *et al.*, 2007). Parolo & Rossi (2008) showed that, in Central Alps, upper limit of vascular plants shifted between 1950s and 2000s at a speed of 23.9

m decade^{-1} (mean of 52 species), with a speed that is even faster for fast migrants, thus suggesting that the upward shift is limited by the dispersal ability. Moreover, they also registered an increase in the number of species which is maximal between 2800 and 3100 m. Cannone *et al.* (2007) report, matching the distribution of the plant communities of 1953 and 2003, an upslope shift and an expansion of the shrubs, together with a reduction of the alpine meadows and the snowbed vegetation, which results particularly sensitive to the change. The response of the treeline is slower and more complex (Leonelli *et al.*, 2010) because it involves many site-specific factors such as, for example, the abandonment of pastures. However, the most important factor in controlling the treeline position at global scale is the soil temperature (Körner, 2004), and the air temperature can be used, in the Alps, as a proxy of the treeline elevation (Ellenberg, 1996). The different rates of uphill movement leaded to a variation of the community composition at high alpine sites (Keller & Körner, 2003), with an increase of species richness (Pauli *et al.*, 2007; Parolo & Rossi, 2008). This increase in species richness is expected to be only temporary, because climate warming is likely to reduce alpine biodiversity by pushing the summit species out of their ranges (McCarthy, 2001; Theurillat & Guisan, 2001). Moreover, climate warming increases the risk of invasions by indigenous species. For example, Walther *et al.* (2002) shows that the decrease in the number of frost days favoured the invasions of evergreen broad-leaved vegetation in southern Switzerland.

Effects on the alpine fauna.   In analogy with the plants, the registered and the expected effects of climate change on the fauna are mainly related to changes in the physiology, phenology and spatial distribution. However, for the alpine fauna there are fewer study about the impacts of climate change than for flora. Theoretically, the shifting response of fauna can be faster than the response of vegetation, because mobile species do not need to wait until the following generation to change position. This characteristic increases the plasticity of the ecological niche of the animals, and makes them more efficient in responding to the extreme events. However, a mismatch in time or space of the responses in trophically interacting species can have dangerous consequences at ecological and evolutionary time scales (e.g. see Schweiger *et al.*, 2008).

The upward shift in fauna has been registered, for example, in the pine processionary moth (see figure 1.5.b), with an altitude expansion of 110-230 meters between 1972 to 2004 (Battisti *et al.*, 2005). Studies performed in the Stelvio National Park (Lombardy, Italy) have also shown one of the

firsts impacts of climate change on alpine communities; the retreat of the glaciers is in fact the main driver of the changes in spider (Gobbi *et al.*, 2006) and carabid (Gobbi *et al.*, 2007) communities. Among the mammals, the males of the Alpine ibex have shown, in the Swiss National Park, a increase in the summer altitude of about 250 meters in 19 years (Herfindal *et al.*, 2012), thus increasing the overlap between the male and the females territory. In such situation, it is likely that the interspecific competition increase, thus leading to a reduction in survival or fertility. On the same species, the Alpine ibex, many studies have been conducted to understand the role of climate in driving the population dynamics of the Gran Paradiso National Park (GPNP) population (e.g. Jacobson *et al.*, 2004; Lima & Berryman, 2006). The main reported effect is a decrease in winter survival associated to high winter snow depths. Moreover, we further improved the study of the ibex population in GPNP, and we therefore address the reader to chapters 5 and 6 for a deeper description of this case study.

(a) Change in phenology (b) Upshift
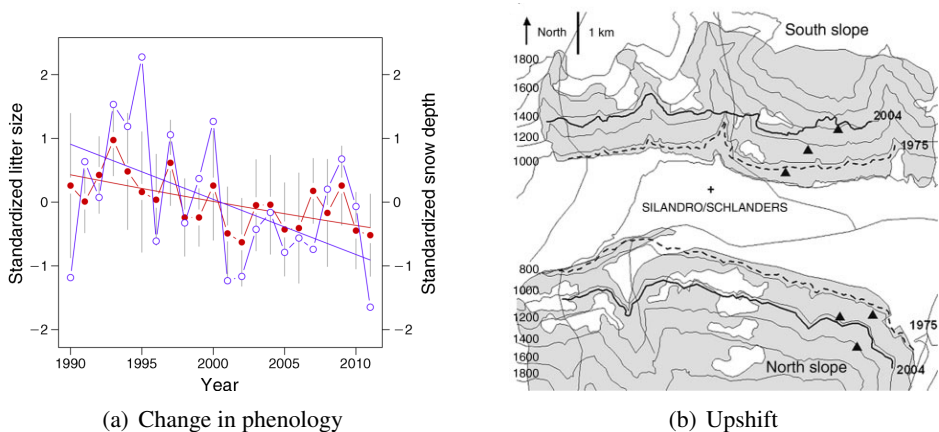
Figure 1.5: *Two examples of registered impacts of climate change on phenology and species distribution. a) plot retrieved from Tafani* et al. *(2013): the decrease in winter snow depth can explain the reduction of litter size for the Alpine marmot; b) plot retrieved from Battisti* et al. *(2005): evidences of an uphill shifting of the lower boundary of the processionary moth in northern Italy between 1975 and 2004.*

In the climate change context, the study of the habitat preferences is crucial to predict the effects, on the species, of habitat modifications. Habitat loss and fragmentation can in fact reduce the carrying capacity and increase the possibility of local extinctions. Revermann *et al.* (2006) studied the future suitability of the habitat for the rock ptarmigan (*Lagopus mutus*), an

high altitude small grouse, on the Swiss Alps. The future projections, developed according to the climatic scenarios of the 4*th* assessment report, show that the suitable habitat can decrease to less than one third until 2070. The reduction of the available habitat can also be driven by the competition with other species, as for the mountain hare (*Lepus timidus*), for which the predicted suitable habitat is shrank both by the climatic variation and the competition with the European hare (*Lepus europaeus*).

As for phenology, an example of recorded change is presented in Tafani *et al.* (2013) for an high altitude rodent: the Alpine marmot (*Marmota marmota*). The authors show that the dimension of the litter decreases over time as a consequence of the decrease in the snow cover, probably because an higher snow cover in winter increases the burrow isolation and, thus, the winter survival (see figure 1.5a). In fact, the Alpine marmot hibernates during winter and its energy consumption during hibernation is strongly dependent on the temperature in the burrow, as we will further describe in chapter 3.

1.2 Objectives and thesis structure

This thesis aims at studying the habitat preferences and the population dynamics of the high altitude alpine fauna in the climate change context. Also, we investigate the sensitivities of three species on the occurred and expected impacts of climate change in the fragile high altitude environment.

We study the habitat preferences using *Species Distribution Models* (Guisan & Thuiller, 2005; Meynard & Quinn, 2007), which describe the relationship between environmental variables (geomorphology, vegetation, climate, anthropic influence ...) and the potentiality of a territory to host a species. In particular, in chapter 3 we develop small scale species distribution models, which are more apt to identify the abiotic and the biotic variables that determine the habitat preferences. Knowing the potential response on the abiotic and biotic factors to the climate change, this type of models permits to surmise the potential indirect impacts on the species under study. However, species distribution models identify all the area that are potentially suitable for the species, thus they are static and developed under the hypothesis that the population is at its carrying capacity.

Temporal dynamics are instead taken into account in population dynamics models, which study how the number of organisms of a species, in a certain place, changes over time. This variation is mainly driven by three demographic processes (Begon *et al.*, 2009): birth, death and migration. Given the number of individuals at time t (N_t), the number of individuals

at time $t+1$ (N_{t+1}) is the result of the realization, between time t and $t+1$, of the three demographic processes listed above:

$$N_{t+1} = N_t + Births - Deaths + Immigrants - Emigrants$$

where births, deaths, immigrants and emigrants are expressed in number of individuals. The science that studies the individuals of the same species, how they make up the populations in which they exist and how these populations change over time is called *population ecology*. Our focus, in this thesis, are the birth and death processes, while we do not explicitly take into account migration processes. In chapters 4, 5 and 6, we investigate the effects of the climatic variables on the demographic parameters, such as the fertility and the survival, of the populations under study. While in chapter 4 the main target are the identification of the most important climatic variables and the detection of the density dependence, in the subsequent chapters we focus on investigating the nonlinear effects of climate and their relationship with the intrinsic characteristics of the population, namely density and age structure.

The methodological *fil rouge* that lies beneath all the chapters is the identification of the model structures and of the explanatory variables that are more likely to explain the processes under study. This analysis, often called *model selection*, is the subject of chapter 2. Model selection includes the formulation of ecological competing hypothesis, their translation into mathematical models, the model identification (or parameter calibration), and, finally, the choice of the best model (or models, if the selection of a single best model is not safe). Of course, to tackle the listed problems, there are many possible strategies and many methodologies, that is not possible, nor useful, to extensively describe in this work. Therefore, in chapter 2 we mainly concentrate on the description of the model selection methods that are used in following chapters of the thesis.

Chapters 3 - 6 present study cases and are focused on analysing the habitat preferences (chapter 3) or the population dynamics (all others) of three high altitude species, which are reported to be sensitive to climate change, and which are chosen considering the possibility of recovering data:

- Alpine marmot (*Marmota marmota*), a small mammal for which we developed species distribution models; the study on Alpine marmot is described in chapter 3.

- Black grouse (*Tetrao tetrix*), a tetraonid bird for which we studied the influences of density and meteorological variables on its demographic parameters (chapter 4);

- Alpine ibex (*Capra ibex ibex*), a large long living mammal for which we developed dynamical models considering the population structure at different levels of detail in chapters 5 and 6.

In the following, we summarize the main contents of each of the application chapters.

Chapter 3 We study the interaction between the presence of Alpine marmot and the fine scale characteristics of the environment. In the climate change context, in which there are evidences of a fast variation in the distribution of the alpine vegetation, it is important to investigate these interactions to better understand how the expected changes in the alpine flora can affect the distribution of the fauna. This species has been chosen because marmots are highly sedentary and live in burrows which are dug deep in the ground. Therefore, its habitat needs are strongly dependent on the conditions surrounding the burrows. The position of burrows is thus likely to be affected by climate change through the modification of abiotic (e.g. temperature, permafrost) and biotic (e.g. vegetation) factors. Moreover, Alpine marmot has contrasting needs that can potentially determine very different responses to climate warming. Since there are no available data, field studies were carried out in collaboration with the Stelvio National Park.

Chapter 4 We investigate the relationships between the demographic rates of the Black grouse and the interplay among population density, climate and geographical position of the population. The case study are the Black grouse populations in the alpine districts of the Piedmont region. Even if it is not considered a threatened species, Black grouse abundances have shown a declining in the last decades. However, there are still few publications that investigate, for the alpine populations of this tetraonid, the effects of climate on the population dynamics. Published studies focus mainly on populations living in "lowlands", thus in an environment which is structurally different from the Alps. For lowland populations, changes in phenology caused by climate change have already been registered (Ludwig & Alatalo, 2006). Since there are fewer informations on the interaction between climate change and alpine populations of grouse, the starting point is an high uncertainty about which climatic factors are the most important in driving the population dynamics. Unfortunately, the quality of the available data is not optimal, because data series are relatively short in time and have a coarse spatial resolution. These conditions make the model selection and model averaging methods described in chapter 2 particularly suit-

able. To investigate the potential effects of climate change on the species, the constructed models are used to make future projections of the population abundance, using exogenous variables derived from the downscaling of global climate change scenarios. The chapter is based on contributions presented at two conferences (Mignatti *et al.*, 2013a,b), and co-authored by R.Casagrandi, A.Provenzale and M.Gatto.

Chapter 5 We develop dynamical models for the Alpine ibex population of the Gran Paradiso National Park (Italy). Ibex survival has been shown to be sensitive to both the amount of snow fallen during winter and the age of the individual, but the influence of population structure on demographic parameters has never been considered in a population dynamics model. In this case, the decision about which meteorological variables are included in the model is based on previous studies, which underline the detrimental effect of winter snow depth on growth rate. We investigate the role of density and winter snow depth in affecting five demographic rates calculated using the yearly censuses: growth rate, fertility, survival of adult females, survival of adult males and survival of kids. Moreover, nonlinear effects of the climatic variable and the density are tested. The chapter is based on Mignatti *et al.* (2012), co-authored by R. Casagrandi, A. Provenzale, A. von Hardenberg and M. Gatto.

Chapter 6 Senescence, the process for which fertility and survival decrease in old individuals, is a commonly reported process for long living mammals as the Alpine ibex. Using the same case study of chapter 5, we present a method to take into account the complete age structure of the population and the senescence processes in modelling the dynamics of long-living mammals for which a relatively long data series is available. In other words, the survivals and the fertilities that in chapter 5 are defined for each population compartment (e.g. the survival of the adult females compartment), here are defined as age-specific (e.g. the survival of females of age 2, age 3, ...). However, the complete age structure is not available in the census data. The proposed methodology permits to reconstruct the age structure of the population starting from the censuses and without using Capture-marked-recapture data. Using developed models, we investigate the interplay among density dependence, age structure and climatic influence in driving the population dynamics of Alpine ibex.

Bibliography

Auer, I., Böhm, R., Jurkovi, A., Orlik, A., Potzmann, R., Schöner, W., Ungersböck, M., Brunetti, M., Nanni, T., Maugeri, M., Briffa, K., Jones, P., Efthymiadis, D., Mestre, O., Moisselin, J.M., Begert, M., Brazdil, R., Bochnicek, O., Cegnar, T., Gaji-apka, M., Zaninovi, K., Majstorovi, E., Szalai, S., Szentimrey, T. & Mercalli, L. 2005: A new instrumental precipitation dataset for the greater alpine region for the period 1800-2002. International Journal of Climatology 25(2): 139–166. doi:10.1002/joc.1135.

Bahn, M. & Körner, C. 2003: Recent increases in summit flora caused by warming in the Alps. In Alpine biodiversity in Europe, vol. 167, (pp. 437–441).

Battisti, A., Stastny, M. & Netherer, S. 2005: Expansion of geographic range in the pine processionary moth caused by increased winter temperatures. Ecological Applications 15(6): 2084–2096.

Begon, M., Townsend, C. & Harper, J. 2009: Ecology: from individuals to ecosystems. John Wiley & Sons, 5th edn. ISBN 978-1-4051-1117-1, 752 pp.

Beniston, M. 2006: Mountain Weather and Climate: A General Overview and a Focus on Climatic Change in the Alps. Hydrobiologia 562(1): 3–16. doi:10.1007/s10750-005-1802-0.

Beniston, M., Diaz, H.F. & Bradley, R.S. 1997: Climatic change at high elevation sites: an overview. Climatic change 36: 233–251.

Bocchiola, D. & Rosso, R. 2008: Application of a regional approach for hazard mapping at an avalanche site in northern Italy. Advances in Geosciences 14(2006): 201–209.

Böhm, R., Auer, I. & Schöner, W. 2005: Exploring past climate variability in the greater alpine region. Hrvatski meteorološki časopis 40: 106–110.

Calmanti, S. & Motta, L. 2007: Impact of climate variability on Alpine glaciers in northwestern Italy. International journal of climatology 2053(March): 2041–2053. doi:10.1002/joc.

Cannone, N., Sgorbati, S. & Guglielmin, M. 2007: Unexpected impacts of climate change on alpine vegetation. Frontiers in Ecology and the Environment 5(7): 360–364. doi:10.1890/060141.

Carbognani, M., Petraglia, A. & Tomaselli, M. 2012: Influence of snowmelt time on species richness, density and production in a late snow-bed community. Acta Oecologica 43: 113–120. doi:10.1016/j.actao. 2012.06.003.

Chemini, C. & Rizzoli, A. 2003: Land use change and biodiversity conservation in the Alps. Journal of Mountain Ecology 7 (Suppl): 1–7.

Chen, I.C., Hill, J.K., Ohlemuller, R., Roy, D.B. & Thomas, C.D. 2011: Rapid Range Shifts of Species Associated with High Levels of Climate Warming. Science 333(6045): 1024–1026. doi:10.1126/science. 1206432.

Diaz, H. & Bradley, R. 1997: Temperature variations during the last century at high elevation sites. Climatic Change at High Elevation Sites 36: 253–279.

Diffenbaugh, N.S. & Field, C.B. 2013: Changes in ecologically critical terrestrial climate conditions. Science (New York, N.Y.) 341(6145): 486–92. doi:10.1126/science.1237123.

Dirnböck, T., Dullinger, S. & Grabherr, G. 2003: A regional impact assessment of climate and land use change on alpine vegetation. Journal of Biogeography 30: 401–417.

EEA European Environmental Agency 2004: Impacts of Europe's changing climate - An indicator based assessment. Tech. rep.

Eisenreich, S. 2005: Climate change and the European water dimension. EU Report .

Ellenberg, H. 1996: VEGETATION MITTELEUROPAS DEN ALPEN IN OKOLOGISCHER, MIT DYNAMISCHER UND HISTORISCHER SICHT.Funfte, stark veranderte und verbesserte Auflage. EugenUlme, Stuttgart, 5th edn., 1095 pp.

Fischlin, A., Midgley, G.F., Price, J., Leemans, R., Gopal, B., Turley, C., Rounsevell, M., Dube, P., Tarazona, J. & Velichko, A. 2007: Ecosystems, their properties, goods and services. In: Climate Change 2007: Impacts, Adaptation and Vulnerability. Contribution of Working Group II to the Fourth Assessment Report of the Intergovernmental Panel on Climate Change / Parry, M.L., Canziani, O. In Notes, Cambridge University Press, Cambridge, UK, chap. 4, (pp. 211–272).

Gilpin, M. & Soulé, M. 1986: Minimum viable populations: processes of species extinction. In Conservation Biology: The Science of Scarcity and Diversity., (pp. 19–34).

Ginsberg, J. 1999: Global conservation priorities. Conservation Biology 13(1): 5.

Gobbi, M., Fontaneto, D. & De Bernardi, F. 2006: Influence of climate changes on animal communities in space and time: the case of spider assemblages along an alpine glacier foreland. Global Change Biology 12(10): 1985–1992. doi:10.1111/j.1365-2486.2006.01236.x.

Gobbi, M., Rossaro, B., Vater, A., De Bernardi, F., Pelfini, M. & Brandmayr, P. 2007: Environmental features influencing Carabid beetle (Coleoptera) assemblages along a recently deglaciated area in the Alpine region. Ecological Entomology 32(6): 682–689. doi:10.1111/j.1365-2311.2007.00912.x.

Grabherr, G., Gottfried, M. & Pauli, H. 1994: Climate effects on mountain plants. Nature 369: 448.

Grabherr, G., Gottfried, M. & Pauli, H. 2000: GLORIA: A Global Observation Research Initiative in Alpine Environments. Mountain Research and Development 20(2): 190–191. doi:10.1659/0276-4741(2000)020[0190:GAGORI]2.0.CO;2.

Grabherr, G., Gottfried, M. & Pauli, H. 2003: High Mountain Environment as Indicator of Global Change. In G. Visconti, M. Beniston, E.D. Iannorelli & D. Barba, eds., Advances in Global Change Research, Springer Netherlands, vol. 9 of *Advances in Global Change Research*, (pp. 331–345). ISBN 0-7923-6918-1. doi:10.1007/0-306-48051-4_32.

Guglielmin, M. & Camusso, M. 2004: An old relict glacier body preserved in permafrost environment: The Foscagno rock glacier ice core (Upper Valtellina, Italian Central Alps). Arctic, Antarctic, and Alpine Research 36(1): 108–116.

Guisan, A. & Thuiller, W. 2005: Predicting species distribution: offering more than simple habitat models. Ecology Letters 8(9): 993–1009. doi:10.1111/j.1461-0248.2005.00792.x.

Haeberli, W. 2009: Climate change and high-mountain regions - adaptation strategies for the Alps. Tech. rep., University of Zurich, Zurich Open Repository and Archive Climate.

Haeberli, W. & Beniston, M. 1998: change and its impacts on glaciers and permafrost in the Alps. Ambio 27: 258–268.

Hagg, W. & Braun, L. 2004: The Influence of Glacier Retreat on Water Yield from High Mountain Areas: Comparison of Alps and Central Asia. In Climate and hydrology in mountain areas C De Jong D Collins and R Ranzi Eds John Wiley and Sons London, (pp. 263–275).

Hantel, M. & Hirtl Wielke, L. 2007: Sensitivity of Alpine snow cover to European temperature. International journal of climatology 1275(March): 1265–1275. doi:10.1002/joc.

Herfindal, I., Filli, F. & Campell Andri, S. 2012: Dynamics of sex-specific utilisation of altitudes in Swiss Ibex. In Dynamics of sex-specific utilisation of altitudes in Swiss Ibex. (p. 35).

Hughes, L. 2000: Biological consequences of global warming: is the signal already apparent? Trends in Ecology & Evolution 15(2): 56–61.

Inouye, D. 2008: Effects of climate change on phenology, frost damage, and floral abundance of montane wildflowers. Ecology 89(2): 353–362.

IPCC(Intergovernmental Panel on Climate Change) 2007a: Climate Change 2007: Impacts, Adaptation and Vulnerability, vol. 114. ISBN 0521705975, 976 pp.

IPCC(Intergovernmental Panel on Climate Change) 2007b: Climate Change 2007: The Physical Science Basis, vol. 18. ISBN 0521705967, 433–440 pp. doi:10.1260/095830507781076194.

IPCC(Intergovernmental Panel on Climate Change) 2013: Climate Change 2013: The Physical Science Basis. September 2013. 1–36 pp.

Jacobson, A., Provenzale, A., Von Hardenberg, A., Bassano, B. & Festa-Bianchet, M. 2004: Climate forcing and density dependence in a mountain ungulate population. Ecology 85(6): 1598–1610.

Keiler, M., Knight, J. & Harrison, S. 2010: Climate change and geomorphological hazards in the eastern European Alps. Philosophical transactions. Series A, Mathematical, physical, and engineering sciences 368(1919): 2461–79. doi:10.1098/rsta.2010.0047.

Keller, F. & Körner, C. 2003: The role of photoperiodism in alpine plant development. Arctic, Antarctic, and Alpine Research 35(3): 361–368.

Körner, C. 1999: Alpine Plant Life: Functional Plant Ecology of High Mountain Ecosystems; with 47 Tables. Springer. ISBN 3540003479, 344 pp.

Körner, C. 2004: Mountain biodiversity, its causes and function. Ambio (13): 11–17.

Korner, C. & Spehn, E. 2002: Mountain biodiversity: a global assessment 24(3): 269–270.

Laiolo, P., Dondero, F., Ciliento, E. & Rolando, A. 2004: Consequence of Pastoral Abandonment for the structure and diversity of the alpine avifauna. Journal of Applied Ecology 41(2): 294–304.

Leonelli, G., Pelfini, M., Morra di Cella, U. & Garavaglia, V. 2010: Climate Warming and the Recent Treeline Shift in the European Alps: The Role of Geomorphological Factors in High-Altitude Sites. Ambio 40(3): 264–273. doi:10.1007/s13280-010-0096-2.

Lima, M. & Berryman, A. 2006: Predicting nonlinear and non-additive effects of climate: the Alpine ibex revisited. Climate Research 32(2): 129.

Ludwig, G. & Alatalo, R. 2006: Short-and long-term population dynamical consequences of asymmetric climate change in black grouse. Proceedings of the Royal Society B 273: 2009–2016. doi:10.1098/rspb.2006.3538.

Maclean, I.M.D. & Wilson, R.J. 2011: Recent ecological responses to climate change support predictions of high extinction risk. Proceedings of the National Academy of Sciences of the United States of America 108(30): 12 337–42. doi:10.1073/pnas.1017352108.

Maisch, M. 2000: The long-term signal of climate change in the Swiss Alps: Glacier retreat since the end of the Little Ice Age and future ice decay scenarios. Geogr. Fis. Dinam. Quat. 23: 139–151.

Martin, T. & Possingham, H. 2005: Predicting the impact of livestock grazing on birds using foraging height data. Journal of Applied Ecology 42(2): 400–408.

McCarthy, J. 2001: Review : Ecological Consequences of Recent Climate Change. Conservation Biology 15(2): 320–331.

Meynard, C.N. & Quinn, J.F. 2007: Predicting species distributions: a critical comparison of the most common statistical models using artificial species. Journal of Biogeography 34(8): 1455–1469. doi: 10.1111/j.1365-2699.2007.01720.x.

Mignatti, A., Casagrandi, R., Provenzale, A. & Gatto, M. 2013a: Effects of climate and population density on the fertility components of the Black grouse (Tetrao tetrix) in the Piedmont region (Italy). In XXIII Congresso della Società Italiana di Ecologia (SItE): Ecology for a Sustainable Blue and Green Growth. 16-18 September. Università Politecnica delle Marche, Ancona, Italy.

Mignatti, A., Casagrandi, R., Provenzale, A. & Gatto, M. 2013b: Influence of population density and climate on the dynamics of the black grouse (Tetrao tetrix) popula ons in the Piedmont region (Italy). In First Annual Conference of the Italian Society for Climate Sciences. From the Integration of Scientific disciplines, Research and Innovation to Face the Climate Change. 23-24 September, Castle of Charles V, Lecce, Italy.

Mignatti, A., Casagrandi, R., Provenzale, A., von Hardenberg, A. & Gatto, M. 2012: Sex- and age-structured models for Alpine ibex Capra ibex ibex population dynamics. Wildlife Biology 18(3): 318–332. doi:10. 2981/11-084.

Moser, D., Dullinger, S., Englisch, T., Niklfeld, H., Plutzar, C., Sauberer, N., Zechmeister, H.G. & Grabherr, G. 2005: Environmental determinants of vascular plant species richness in the Austrian Alps. Journal of Biogeography 32(7): 1117–1127. doi:10.1111/j.1365-2699.2005.01265.x.

Parmesan, C. & Yohe, G. 2003: A globally coherent fingerprint of climate change impacts across natural systems. Nature 421(6918): 37–42. doi: 10.1038/nature01286.

Parolo, G. & Rossi, G. 2008: Upward migration of vascular plants following a climate warming trend in the Alps. Basic and Applied Ecology 9(2): 100–107. doi:10.1016/j.baae.2007.01.005.

Paul, F. 2004: Rapid disintegration of Alpine glaciers observed with satellite data. Geophysical Research Letters 31(21): L21 402. doi: 10.1029/2004GL020816.

Pauli, H., Gottfried, M., Reiter, K., Klettner, C. & Grabherr, G. 2007: Signals of range expansions and contractions of vascular plants in the high

Alps: observations (1994-2004) at the GLORIA master site Schrankogel, Tyrol, Austria. Global Change Biology 13(1): 147–156. doi: 10.1111/j.1365-2486.2006.01282.x.

Pettorelli, N., Pelletier, F., von Hardenberg, A., Festa-Bianchet, M. & Côoté, S.D. 2007: Early onset of vegetation growth vs. rapid green-up: impacts on juvenile mountain ungulates. Ecology 88(2): 381–390.

Pickering, C., Hill, W. & Green, K. 2008: Vascular plant diversity and climate change in the alpine zone of the Snowy Mountains, Australia. Biodiversity and Conservation 17(7): 1627–1644. doi:10.1007/s10531-008-9371-y.

Quintero, I. & Wiens, J.J. 2013: Rates of projected climate change dramatically exceed past rates of climatic niche evolution among vertebrate species. Ecology letters 16(8): 1095–103. doi:10.1111/ele.12144.

Rebetez, M. & Reinhard, M. 2008: Monthly air temperature trends in Switzerland 1901–2000 and 1975–2004. Theoretical and Applied Climatology 91: 27–34.

Revermann, R., Zbinden, N., Schmid, H., Spaar, R. & Schröder, B. 2006: Suitable habitat for ptarmigan (Lagopus muta helvetica Thienemann 1829) in the SwissAlps and its response torapid climate change inthe 21st century: a multi-scale approach. Ph.D. thesis, Potsdam University.

Sala, O., Chapin, F. & Armesto, J. 2000: Global biodiversity scenarios for the year 2100. science 287(5459): 1770. doi:10.1126/science.287.5459.1770.

Schweiger, A., Nopp-Mayr, U. & Zohmann, M. 2012: Small-scale habitat use of black grouse (*Tetrao tetrix L.*) and rock ptarmigan (*Lagopus muta helvetica* Thienemann) in the Austrian Alps. European Journal of Wildlife Research 58: 35–45.

Schweiger, O., Settele, J., Kudrna, O., Klotz, S. & Kühn, I. 2008: Climate change can cause spatial mismatch of trophically interacting species. Ecology 89(12): 3472–9.

Spehn, E.M. 2005: High diversity in Europe 's mountains. Diversity and Distributions 11(6): 592–593. doi:10.1111/j.1366-9516.2005.00221.x.

Tafani, M., Cohas, A., Bonenfant, C., Gaillard, J.M. & Allainé, D. 2013: Decreasing litter size of marmots over time: a life history response to climate change? Ecology 94(3): 580–6.

Terzago, S., Cassardo, C., Cremonini, R. & Fratianni, S. 2010: Snow Precipitation and Snow Cover Climatic Variability for the Period 1971–2009 in the Southwestern Italian Alps: The 2008–2009 Snow Season Case Study. Water 2(4): 773–787.

Theurillat, J. & Guisan, A. 2001: Potential impact of climate change on vegetation in the European Alps: a review. Climatic change 50: 77–109.

Theurillat, J.P., Schlüssel, A., Geissler, P., Guisan, A., Velluti, C. & Wiget, L. 2003: Vascular Plant and Bryophyte Diversity Along Elevation Gradients in the Alps. In Alpine biodiversity in Europe, vol. 167, (pp. 185–193).

Thomas, C.D. 2010: Climate, climate change and range boundaries. Diversity and Distributions 16(3): 488–495. doi:10.1111/j.1472-4642.2010.00642.x.

Thuiller, W. 2007: Biodiversity: climate change and the ecologist. Nature 448(August): 550–552.

Väre, H., Lampinen, R., Humphries, C. & Williams, P. 2003: Taxonomic diversity of vascular plants in the European alpine areas.

Vincent, C. 2002: Influence of climate change over the 20th Century on four French glacier mass balances. Journal of Geophysical Research 107(D19): 4375. doi:10.1029/2001JD000832.

Walther, G., Beiß ner, S. & Burga, C. 2005: Trends in the upward shift of alpine plants. Journal of Vegetation Science (1998): 541–548.

Walther, G.G.R., Post, E., Convey, P., Menzel, A., Parmesan, C., Beebee, T.J.C., Fromentin, J.M., Hoegh-Guldberg, O. & Bairlein, F. 2002: Ecological responses to recent climate change. Nature 416(6879): 389–395. doi:10.1038/416389a.

Wang, K., Sun, J., Cheng, G. & Jiang, H. 2011: Effect of altitude and latitude on surface air temperature across the Qinghai-Tibet Plateau. Journal of Mountain Science 8(6): 808–816. doi:10.1007/s11629-011-1090-2.

Model Selection and Multimodelling

Aim of this chapter is to describe the model selection techniques that will be used in the thesis to choose the best models for representing the systems under study. Modelling has here two main objectives, and the term "best" used in the previous sentence embraces both. The first objective is to select models that have a good *predictive ability*, while the second objective is to select models that can *help in the ecological interpretation of the system*. It is therefore important to focus the attention both on the formulation of the ecological hypothesis and on the mathematical and statistical methods to be adopted. The formulation of ecological hypothesis is necessarily and strongly problem-dependent, therefore it is only marginally discussed in this chapter, while it is specifically treated for each application in each of the following chapters.

Of course, the chapter is not intended to be an exhaustive dissertation on the model selection *per se*, which would be impossible since a massive quantity of books and papers have been (fully or partially) devoted to this argument. We rather concentrate on the most important concepts that are needed to understand the methodologies used in the applications presented in this thesis.

The traditional way of estimating model parameters assumes that the

model structure (or meta-model) is *a-priori* known, and that it is the true model that generated the data (Box *et al.*, 1994). If the system under study is too complex or involves mechanisms that are not deeply understood, the *a-priori* knowledge is often too weak or too complicated to define a unique model structure. Effects of climate change on the species distribution and population dynamics is a prototypical example of such a complex phenomenon. In fact, even if one restricts the focus on the effects of a variation in temperatures, only some specific effects of this variation on some particular biological parameter of the species might have been studied (e.g. see the studies on the hibernation of marmots in Arnold (1988); Arnold *et al.* (1991); Ruf & Arnold (2000)). Unfortunately, though, the overall effects of this process on population dynamics and habitat preferences are usually less (or not) known. A variation in the climatic conditions have in fact both direct effects on the species (e.g. thermoregulation, water needs), and indirect effects, since it can influence either the biotic and the abiotic components of the ecosystems.

However, as brilliantly summarized by Box & Draper (1987):

"essentially, all models are wrong, but some are useful.",

thus, scientists can formulate competing hypotheses on the subject of the study and translate them into mathematical models that can be rigorously compared. Once the set of competing models ($\mathcal{M} = \{m_1, \ldots, m_z\}$) is defined, the objective of model selection is to find the most useful model among all the *wrong* (sensu Box & Draper, 1987) candidates, taking into account that its maximum complexity must be limited by the number of available observations (principle of parsimony). The model selection permits to simultaneously contrast several hypotheses against data, and it is a sound alternative to the classical null hypotheses testing, in which only two alternative hypothesis can be confronted at a time.

Johnson & Omland (2004) provides an interesting review of the model selection approach in the context of ecology and evolution, which we used as a starting hint to define the following model selection steps:

step 1. *Formulate ecological competing hypotheses.*

> This step is based on the prior knowledge that the scientist might have of the system, taking into account his/her personal experience and/or the previous works published on the matter. It involves the description of the most important physical mechanisms that can influence the system under study.

This step is important to avoid the testing of "all" the possible models, thus limiting the backward hypothesis formulation, on which Burnham & Anderson (2002) put a particular warning:

> *"Even in a very exploratory analysis it seems poor practice to consider all possible models; surely, some science can be brought to bear on such an unthinking approach (otherwise, the scientist is superfluous and the work could be done by a technician)."*

step 2. *Translate the competing hypotheses into competing models*

Roughly speaking, at this step we need to:

- identify the dependent variable (or variables), i.e. the effects;
- identify the possible explanatory (independent) variables, i.e. the causes or the covariates;
- identify the possible functional forms that link the independent and the dependent variables.

The difference between the dependent and the independent variables is not always as sharp as it would be desired. For example, in an autoregressive model the value of a dependent variable at time t depend on itself at the previous time steps. The different functional forms and the inclusion of different sets of explanatory variables leads to the definition of the competing model structures.

In the cases where the number of candidate model structures based on our a-priori knowledge is too large, it is a good practice to reduce the model space at this step through a pre-analysis of data. This typically happens when there are weak prior informations about the system. For example, in chapter 3, before model selection, if two explanatory variables are too correlated with each other, we remove one of the two. Another example is reported in chapter 4: in this case we reduced the number of explanatory variables by removing those that are not significantly correlated with the dependent variable. Moreover, we reduced the possible functional forms properly aggregating data (see the specific chapter for the methodological details).

step 3. *Calibrate the model parameters*

Once the set of candidate model structures is designed, each model must be fit to the observed data to calibrate its parameters. The model

fitting is usually performed through the optimization (minimization or maximisation) of a suitable figure of merit. Two paradigmatic examples of figure of merit are the *Likelihood* and the *sum of squared errors*. A notable counterexample is the Bayesian fitting, which does not involve any optimization, as will be clear at the end of the next section.

step 4. *Choose the best model(s)*

The objective is to find which model is the more supported by the data. Several methods have been proposed to solve this problem. The simplest way is to directly match the figures of merit used for the model fitting, or other indicators of fitting performances (e.g. the R^2 statistic). This approach does not consider the Occam's razor principle of parsimony, which states to *"shave away all the unnecessary"*. Indeed, a too complex model has structurally a good model fitting on the data used for calibration but it has also a poor predictive power. In the case of nested models (models that can be obtained by restricting a parameter in a more complex model to be zero) a model selection strategy is to perform a series of null hypothesis testing, matching a couple of models at each iteration (stepwise regression). For example, the likelihood ratio test uses the χ^2 statistic. These methods have several problems, e.g. the order of comparison can influence which is the best model selected. For this and other reasons (see Whittingham *et al.*, 2006) model selection criteria are to be preferred over the stepwise regression or analogous methods. Two notable examples of model selection criteria are the *Akaike Information Criterion* (described in section 2.2) and the *Schwartz Information Criterion* (described in section 2.2).

When model selection does not clearly select a single model, multimodel approaches permit to make inferences based on a set of competing models.

step 5. *Use the model*

Remembering the famous quote of Box & Draper reported above, the developed model must be useful in some way. Once the model has been selected, it can be used to make inferences on new data, either to test the predictive power of the model or to know the outcome in points that are actually unknown. Moreover, the choice of a particular model against its competitors permits to confirm or deny the initial ecological hypothesis, or to provide the basis of some back-

ward interpretation. As stated while describing step 2, the backward interpretation is not always recommended. However, it is sometimes useful to "let the data speak" if a clear interpretation of the results can be produced.

Steps 1 and 2 are clearly problem-dependent and are specifically defined for each problem, thus they are described in the following chapters for each specific case study. Conversely, steps 3 and 4 are less problem specific, and are described in sections 2.1 and 2.2, respectively.

2.1 The estimation problem

Broadly speaking, given the structure of a mathematical model and a set of observations, the estimation problem consists in assigning a value to the parameters of the model, so that the model fits the data in the best way it can. This generic definition can be applied both to statistical and dynamical models. According to this definition, the estimation problem typically takes the form of an optimization problem (but we describe below a remarkable exception), in which the objective function to be minimized is a measure of the distance between the observations and the model (or the predictions of the observations, made by using the model). Here, we summarize three paradigmatic approaches to perform the estimation of the parameters. The first two approaches, *least squares* and *maximum likelihood* are basically optimization problems, while the latter, the *Bayesian estimation*, can not be confined in this definition. Section (2.2) is useful to understand the model selection criteria and the estimation choices made in chapters 5 and 6, while the other section of the chapter present and discuss the *Multimodel inference* and the *Bayesian Model Averaging* that will be used, respectively, in chapters 6 and chapters 3 and 4.

2.1.1 Least squares

The *sum of squared errors* (*SSE*) is probably the most used figure of merit in many scientific fields. Given a set of n observations, $\boldsymbol{y} = [y_1, ..., y_n]$ and the corresponding estimates produced by a model ($\hat{\boldsymbol{y}} = [\hat{y}_1, ..., \hat{y}_n]$), the sum of squared errors is calculated as:

$$SSE = \sum_{i=1}^{n} (y_i - \hat{y}_i)^2 \tag{2.1}$$

With the terminology *least square* methods (*LS*) the literature refers to set of standard approaches that aim at minimizing the *SSE*. The key for the

success of *LS* methods is that they are particularly simple to computed for linear regression models of the type:

$$\boldsymbol{y} = \beta_0 + X\boldsymbol{\beta} + \boldsymbol{\varepsilon} \tag{2.2}$$

where X is the $(n \times k)$ *design matrix*, i.e. the matrix having as columns the values of the k explanatory variables. β_0 is the unknown intercept, $\boldsymbol{\beta}$ is the $(k \times 1)$ vector of unknown coefficients and $\boldsymbol{\varepsilon}$ is the $(n \times 1)$ vector of the error terms, which are often modelled as independent identically normally distributed random variables with mean 0 and variance σ^2: $\varepsilon_i \sim N(0, \sigma^2)$. The vector of the unknown parameter is $\boldsymbol{\theta} = \{\beta_0, \boldsymbol{\beta}, \sigma\}$, which is characterized by the length $K = k + 2$. The parameter estimates $\hat{\boldsymbol{\theta}}$ are those that minimize the squared error $\sum_{i=1}^{n} \varepsilon_i^2$, and define a regression line that is the "best fit" (Burnham & Anderson, 2002). In this case, the SSE can be computed as:

$$SSE = \sum_{i=1}^{n}(y_i - \hat{\beta}_0 - \boldsymbol{x_i}\hat{\boldsymbol{\beta}})^2 = \sum_{i=1}^{n}(\varepsilon_i)^2 \tag{2.3}$$

where $\hat{\beta}_0$ and $\hat{\boldsymbol{\beta}}$ are, respectively, the LS intercept LS vector of estimated coefficients, while $\boldsymbol{x_i}$ is the vector of values of the explanatory variables for the i*th* observation.

2.1.2 Maximum Likelihood estimation

Maximum Likelihood (*ML*) was explicitly developed as a technique by R.A. Fisher between 1912 and 1922 (Aldrich, 1997) and it is almost as widely used as the *LS*. As suggested by its name, this technique aims at finding the values of the parameters for which the model likelihood reaches its maximum value. For a single observation, the likekihood is the probability that the model generates exactly the measured observation: $Pr(y_i|model, \boldsymbol{\theta})$. In words, this is the probability of observing y_i given the model structure and the parameter vector. For example, assuming that the $y_i \sim N(\mu, \sigma^2)$ and the unknown parameters are $\boldsymbol{\theta} = (\mu, \sigma)$, then:

$$Pr(y_i|model, \boldsymbol{\theta}) = \frac{1}{\sqrt{2\pi\sigma^2}}\exp\left(-\frac{(y_i - \mu)^2}{2\sigma^2}\right) \tag{2.4}$$

For a set of data, the *Likelihood* is the probability of all the measured data, given the model structure and its parameters. If all the individual

outcomes are independent then the *Likelihood* is:

$$\mathcal{L}(\boldsymbol{\theta}|\boldsymbol{y}, model) = Pr(\boldsymbol{y}|model, \boldsymbol{\theta}) = \prod_{i=1}^{n} Pr(y_i|model, \boldsymbol{\theta}) \qquad (2.5)$$

Notice that equation 2.5 is a product of probabilities. Thus, being each of the terms of the product a product of values smaller than 1, the exact value of the likelihood can be numerically difficult (or impossible) to calculate. It is therefore often and more safely calculated the *Loglikelihood*

$$\log \mathcal{L}(\boldsymbol{\theta}|\boldsymbol{y}, model) = \sum_{i=1}^{n} \log[Pr(y_i|model, \boldsymbol{\theta})] \qquad (2.6)$$

The value of $\boldsymbol{\theta}$ that maximizes the *Likelihood* is usually called *Maximum Likelihood Estimation* (MLE), and is indicated as $\hat{\boldsymbol{\theta}}$. $\hat{\boldsymbol{\theta}}$ is an asymptotically unbiased estimator of $\boldsymbol{\theta}$, and it is also asymptotically normally distributed (Wasserman, 2000)

To clarify the concepts, focus again on the example of the linear regression model reported in equation 4.5, for which the SSE has been shown. In that case the vector $\boldsymbol{\theta}$ has $K = k + 2$ parameters, namely the intercept β_0, the k parameters of the vector $\boldsymbol{\beta}$ and the unknown error variance σ^2. Since the errors are supposed to be normally distributed, given the parameter vector $\boldsymbol{\theta}$, the probability of the i*th* observation is

$$Pr(y_i|\boldsymbol{\theta}) = \frac{1}{\sqrt{2\pi\sigma^2}} \exp\left(-\frac{\varepsilon_i^2}{2\sigma^2}\right) \qquad (2.7)$$

Consequently, the *Likelihood* measured on the entire dataset is the product of these over the n observations:

$$\mathcal{L}(\boldsymbol{\theta}|\boldsymbol{y}) = Pr(\boldsymbol{y}|\boldsymbol{\theta}) = \prod_{i=1}^{n} \frac{1}{\sqrt{2\pi\sigma^2}} \exp\left[-\frac{1}{2}\left(\frac{\varepsilon_i}{\sigma}\right)^2\right] =$$
$$\left(\frac{1}{\sqrt{2\pi\sigma^2}}\right)^n \exp\left[-\frac{1}{2}\sum_{i=1}^{n}\left(\frac{\varepsilon_i}{\sigma}\right)^2\right] \qquad (2.8)$$

Since the *ML* estimator of the error variance is $\hat{\sigma}^2_{ML} = SSE/n$ (see for example Gnanadesikan & Wilk, 1970), the maximised *Likelihood* is:

$$\mathcal{L}(\hat{\boldsymbol{\theta}}|\boldsymbol{y}) = \left(\frac{1}{\sqrt{2\pi\hat{\sigma}^2_{ML}}}\right)^n \exp\left[-\frac{1}{2}n\right] \qquad (2.9)$$

or, equivalently, as *Log-likelihood*

$$\log \mathcal{L}(\hat{\boldsymbol{\theta}}|\boldsymbol{y}) = -\frac{1}{2}n\log(\hat{\sigma}^2) - \frac{1}{2}n\log(2\pi) - \frac{n}{2} \qquad (2.10)$$

In the *Loglikelihood* calculations the two constant terms are often omitted, leading to the approximation $\log \mathcal{L}(\hat{\boldsymbol{\theta}}|\boldsymbol{y}) \approx -\frac{1}{2}n log(\hat{\sigma}^2)$.

By contrasting equations 2.3 and 2.10, it is easy to see that the maximum of both functions is obtained for the same parameter setting. More generally, assuming that the errors are independently and normally distributed, then the MLE and the LS methods produce the same values for the estimates of the structural parameters (but not for σ^2) for linear and nonlinear models (Burnham & Anderson, 2002). In the linear case, the *LS* estimator of σ^2 is in fact $\hat{\sigma}^2_{LS} = SSE/(n - (k + 2))$, while the corresponding ML estimator is $\hat{\sigma}^2_{ML} = SSE/n$.

2.1.3 Bayesian approach

The Bayesian method has been invented by Reverend Thomas Bayes (Bayes, 1736). The central idea of the method is that, before using of the observations, we do have beliefs on the system that are determined by our *a priori* knowledge, which depends on our past experiences and past observations. The existing beliefs are called *prior*, and are usually defined as probabilistic distributions. For example the prior over the parameters is $Pr(\boldsymbol{\theta})$ and represents how likely are the different values of $\boldsymbol{\theta}$ (King *et al.*, 2010). The "new" observations that come in can modify our prior, which has to be taken into account. The distribution of a quantity of interest calculated using both the prior and the observations is called *posterior*, because it is defined after having incorporated the new informations. The posterior distribution of the parameters, given the observations, is $Pr(\boldsymbol{\theta}|\boldsymbol{y})$. Of course, the posterior distribution (and in some cases the prior distribution) of the parameters depends also on the design matrix (X), but here we simplify the notation omitting this dependency. However, we will explicit the use of X in the next section, while describing the *g* prior (see below).

Given the observations ($\boldsymbol{y}$) and the prior($Pr(\boldsymbol{\theta})$), Bayesian parameter estimation calculates the joint distribution of all the posterior values of the parameters using the Bayes' theorem:

$$Pr(\boldsymbol{\theta}|\boldsymbol{y}) = \frac{Pr(\boldsymbol{y}|\boldsymbol{\theta})Pr(\boldsymbol{\theta})}{\int Pr(\boldsymbol{y}|\boldsymbol{\theta})Pr(\boldsymbol{\theta})d\boldsymbol{\theta}} = \frac{\mathcal{L}(\boldsymbol{\theta}|\boldsymbol{y})Pr(\boldsymbol{\theta})}{\int \mathcal{L}(\boldsymbol{\theta}|\boldsymbol{y})Pr(\boldsymbol{\theta})d\boldsymbol{\theta}} \propto \mathcal{L}(\boldsymbol{\theta}|\boldsymbol{y})Pr(\boldsymbol{\theta})$$

$$(2.11)$$

As stated by the equation, the Bayesian estimation of the parameters: i) returns the posterior distribution of the parameters and not a point as the *MLE* and the *LS* methods (which, by contrast, return the confidence intervals); ii) does not need to solve any optimization problem. However, other computational problems arise from this method, since an analytical computation of the posterior is seldom available and in most of the cases Bayesian estimation problems have to be solved numerically. King *et al.* (2010) states in fact:

> *"The optimisation of classical analysis has been replaced by integration for the Bayesian approach"*

For example the expected values of the model parameters is calculated as:

$$\overline{\boldsymbol{\theta}} = \int_{\boldsymbol{\theta}} \boldsymbol{\theta} Pr(\boldsymbol{\theta}|\boldsymbol{y})d\boldsymbol{\theta} \tag{2.12}$$

while the predictive distribution of y_i is computed as:

$$\hat{Pr}(y_i|\boldsymbol{y}) = \int_{\boldsymbol{\theta}} \boldsymbol{\theta} Pr(y_i|\boldsymbol{\theta})Pr(\boldsymbol{\theta}|\boldsymbol{y})d\boldsymbol{\theta} \tag{2.13}$$

To solve these problems of computing the posterior and the desired integrals, the main idea is to employ simulation procedures which result in samples from the posterior distribution, from which the posterior distribution can be approximated. A noteworthy method that follows this idea is the so called *Markov Chain Monte Carlo* (MCMC). For a description of MCMC the reader can refer, for example, to chapter 5 of the book by King *et al.* (2010) and the references therein. Another interesting approach is the *Integrated Nested Laplace Approximation* (INLA, Rue *et al.*, 2009), which is much faster than MCMC and applies to latent Gaussian models, which are additive Bayesian models with Gaussian priors (*ibidem*).

Parameter prior

Integrating priors in the analysis is a peculiar characteristic of Bayesian statistic, and constitutes the main difference with the Frequentist approach. The prior is subjective by definition, since it represents prior beliefs on the system. However, the importance of the prior in influencing the posterior decreases with the evidence provided by the data. Thus, if the data are compelling, the posterior will be dominated by the likelihood. Conversely, if data bring little evidence, the posterior is likely to be near the prior (Wintle *et al.*, 2003).

Unfortunately, prior beliefs are often lacking because the system under study is little known and/or an expert opinion is not available. In these cases, a typical choice is to assign an "uninformative" prior to the parameters, such as the *Jeffrey's prior* (Kass & Raftery, 1995, see). Actually, it is impossible to define a completely uninformative prior. For example, the *locally uniform prior*, namely a uniform prior defined over $\mathbb{R}$ ($Pr(\theta) \propto 1$ for range $[-\inf, +\inf]$) brings the information that each point in $\mathbb{R}$ is equally likely to be the parameter value.

A convenient choice is to adopt a conjugate prior, which is characterised by the interesting property of leading to posterior distributions of the same family of the prior. The main advantage is that the marginal distributions can be expressed in closed form, thus they can be often calculated analytically or, in the other cases, rapidly computed using a numerical method.

A convenient (informative) conjugate prior for the linear regression model (equation 4.5) is the *Zellner g-prior* (Zellner, 1983). Papers by Fernandez *et al.* (2001) and George & Clyde (2004) provide the details for using the g-prior. The prior on the $\boldsymbol{\beta}$ parameters is defined as a normal distribution depending on the design matrix X, the variance of the residuals σ^2 and a hyperparameter (i.e. a parameter of the prior distribution) g; the prior on σ and β_0 are instead defined with improper distributions:

$$
\begin{aligned}
Pr(\boldsymbol{\beta}|\sigma, X) &\sim \mathcal{N}(\boldsymbol{\beta}_p, g\sigma^2(X^TX)^{-1}) \\
Pr(\sigma) &\propto \sigma^{-1} \\
Pr(\beta_0) &\propto 1
\end{aligned}
\tag{2.14}
$$

where $\boldsymbol{\beta}_p$ is the prior expected values of the parameters. Notice that g is the only hyperparameter that must be defined a priori. In linear regression models, the *g* prior leads to the conditional posterior:

$$
Pr(\boldsymbol{\beta}|\boldsymbol{y}, \sigma, X) \sim \mathcal{N}\left(\frac{1}{g+1}(\boldsymbol{\beta}_p + g\hat{\boldsymbol{\beta}}), \frac{g\sigma^2}{g+1}(X^TX)^{-1}\right)
\tag{2.15}
$$

where $\hat{\boldsymbol{\beta}}$ is the maximum likelihood estimate of the parameters.

The expected values of the parameters is then a weighted sum of the prior and of the maximum likelihood estimate of the parameters, where the weights depend on the value assigned to g:

$$
Pr(\boldsymbol{\beta}|\boldsymbol{y}, X) \sim \mathcal{N}\left(\frac{1}{g+1}\boldsymbol{\beta}_p + \frac{g}{g+1}\hat{\boldsymbol{\beta}}\right)
\tag{2.16}
$$

Ley & Steel (2009) reports a useful discussion of the possible values of g. If the value of g is set proportional to the number of observations the weights

of the prior and the likelihood depends on the available information. In the *Unit Information Prior* (UIP), for example, g is equal to the sample size. Using UIP, the log Bayes factors behave asymptotically like the Schwarz criterion (BIC) (Fernandez *et al.*, 2001). In chapter 4 we use a Zellner g prior with $g = n$, while in chapter 3 we avoid the definition of a prior through the use of the BIC approximation of the Bayes factor and the MLE approximation for the *Likelihood*.

2.2   Model selection

Once the models belonging to the model set $\mathcal{M}$ have been identified, we pass to step 4 at page 28. The objective becomes that of selecting the "best" model, i.e. the one that better represents the system under study. The best model should have a good fitting on the data used for calibration and, potentially, good predictive performance on new data. This means that the goodness of fit can not be the only measure used to select the best model, but also the model simplicity must be taken into account. In fact, while the model fitting generally increases with the model complexity, the predictive power of a model has a maximum for an intermediate model complexity. Therefore, the best model is a model that has a good fit and also respects the Occam's razor principle of parsimony.

Model selection criteria are rules that permits to simultaneously compare a set of models by taking into account both the goodness of fit and the principle of parsimony. In the model selection criteria, the model complexity is generally taken into account through the number of parameters included in the model. In the following subsections, we present four model selection criteria that we use in the applications' chapters: the *Akaike's Information criterion* (*AIC*) and it's second order approximation version (AIC_c), the *Bayesian Information criterion* (BIC, also called *Schwartz Information crition*) and the *Structural Risk Minimization* (*SRM*). Moreover, we present the Bayesian method for model selection. The presented criteria are apt at analysing small data series, as is typical for several ecological problems like those that are tackled in the following chapters. Of course, there are other interesting selection criteria which have been proposed in literature, such as the Akaike's *Final Prediction Error* (FPE Akaike, 1970) and the *Deviance Information Criterion* (DIC Spiegelhalter *et al.*, 2002). The former is one of the first Akaike's attempts to develop a selection criterion while the latter is a recent criterion specifically proposed for Bayesian models. For a detailed description of these criteria we refer the reader to the provided references.

Akaike's Information criterion

The Akaike's Information criterion (AIC, Akaike, 1973, 1974) is a model selection criterion developed in the context of the information theory. This criteria is based on the Kullback-Leibler distance (Kullback, 1959), which is a measure of the distance between two models. The AIC is an estimate of the K-L distance between the candidate model and the "true" model that generated the data, and it is defined as:

$$AIC = -2\log\mathcal{L}(\hat{\boldsymbol{\theta}}|\boldsymbol{y}) + 2K \tag{2.17}$$

where K is the length of the parameter vector $\boldsymbol{\theta}$, and $\hat{\boldsymbol{\theta}}$ is the MLE estimate of he parameter vector. The AIC takes into account the model complexity through the number of parameters K, and how well the model fits the data through the *Loglikelihood*.

The numerical value of the AIC has not a value *per se* but only if the goal is to compare at least two different models. The selected model is then the one that, among the candidates, is characterised by the minimum value of AIC (AIC_{best}). These competing models can have a different model structure and a different parameter setting, but they must have some common features:

1. the same response variable y;

2. the same error structure;

3. the same dataset used for calibration.

As stated in the previous section, if the model errors are independently normally distributed with a constant error variance, $\log\mathcal{L}(\hat{\boldsymbol{\theta}}|y)$ can be approximated, up to a constant, by $-\frac{1}{2}nlog(\hat{\sigma}^2)$. In this case, AIC can be calculated as:

$$AIC = n\log\left(\hat{\sigma}^2\right) + 2K \tag{2.18}$$

As mentioned above, ecological problems are often characterised by relatively small datasets. For small sample sizes, Sugiura (1978) developed a second order bias correction for the AIC:

$$AIC_c = AIC + \frac{2K(K+1)}{n-K-1} \tag{2.19}$$

The second order bias correction tends to zero for n going to infinity. Burnham & Anderson (2002) suggest to use the AIC_c instead of the AIC when $n/K < 40$.

Even if the best model is defined as the one that minimizes the AIC (or the AIC_c), when the distance between the best model and other models is sufficiently small, there is no a clear evidence in favour of a single model, or, said in another way, some of the models can be indistinguishably good. To overcome this problem, and following the principle of parsimony, Richards (2005) propose the following alternative procedure to select the best model. We define AIC_{best} as the minimum AIC value among the AIC values of all the models in the model set. Given a model $m_j \in \mathcal{M}$, $\Delta AIC_j = AIC_j - AIC_{best}$ is a measure of the distance between the best model and m_j. The strategy is than to select the model with the minimum number of parameters among those models that are characterized by $\Delta AIC_j < 4$.

Bayesian Information Criterion

The Bayesian Information Criterion (BIC), also called *Shwartz's Information Criterion* has been developed by Schwarz (1978) as an alternative to the AIC. The difference between the two information criteria is that the BIC imposes a smaller penalty on the number of parameters than the AIC, thus generally leading to select less complex models. BIC is defined as:

$$BIC = -2 \log \mathcal{L}(\hat{\boldsymbol{\theta}}|\boldsymbol{y}) + K \log(n) \tag{2.20}$$

where, as above, K is the length of the parameter vector $\boldsymbol{\theta}$, and $\hat{\boldsymbol{\theta}}$ is the MLE estimate of the parameter vector. The BIC can be applied under the same conditions listed for the AIC.

As for the AIC, the best model according to BIC is the one that minimizes the criterion. Raftery (1995) proposes a rule to deal with the cases in which there are models that have a BIC value near the minimum BIC (BIC_{best}). The distance from the model m_j to the model with the minimum BIC is $\Delta BIC_j = BIC_j - BIC_{best}$ The rule is then to choose the model with the minimum number of parameters among the models for which $\Delta BIC_j < 2$.

As we discuss in section 2.2, the BIC has some interesting properties and, under certain hypothesis, it is an estimator of the posterior probability of the models.

Structural Risk Minimization

The *Structural Risk Minimization*, developed by Cherkassky *et al.* (1999) in the Statistical Learning Theory framework (see Vapnik *et al.*, 1994, for an

overview), is probably the less used (and known) selection criterion among those described here. Despite its weak popularity it has interesting performances in model selection when the available dataset is small. The criterion has been introduced in ecological modelling and tested against BIC and AIC by Corani & Gatto (2007), which also provide a clear and concise description of the criterion.

The key idea is that the elements of x are independently drawn from a fixed but unknown distribution $Pr(x)$ and $\boldsymbol{y}$ is drawn independently form an unknown distribution conditional on x. $Pr(x, y)$ is the joint probability of x and y. The best model is the function $f(x, \boldsymbol{\theta})$ which minimizes the risk functional:

$$R(\theta) = \int_X \int_y (y - f(x, \theta))^2 Pr(x, y) dx dy \qquad (2.21)$$

The quantity can not be computed because $Pr(x, y)$ is not known. However, for regression problems, Cherkassky *et al.* (1999) define a distribution-independent upper bound for the risk functional:

$$\max\left(0, \frac{R(\theta)_{emp}}{1 - \sqrt{\frac{d}{n} - \frac{d}{n}log(\frac{d}{n}) + ln(n)/2n}}\right) \qquad (2.22)$$

Where d is the Vapnik-Chervonenkis dimension (VC-dimension) and $R(\theta)_{emp}$ is the empirical risk, which corresponds to the fitting error of the model ($R(\theta)_{emp} = SSE/n$). The VC-dimension is a measure of the model complexity, which corresponds, in the linear case, to the number of parameters of the model (k). The upper bound in equation 2.22 holds with a probability of $1 - 1/\sqrt{n}$. According to the SRM criterion, the best model is the one that minimizes equation 2.22. SRM_{best} is the value of SRM associated to the best model.

As for BIC and AIC, it is possible that models other than the best one have a value of the criterion near SRM_{best}. Mignatti *et al.* (2012a) propose to consider all the model which differ less than 6% from the best one, namely the models m_j for which $SRM_j/SRM_{best} < 1.06$.

Bayesian model selection

The idea in the Bayesian model selection is to choose, as best model, the one with the highest posterior probability. As for the posterior probability of the parameters (equation 2.11), the posterior probability of the j*th* model

is calculated using the Bayes' formula:

$$Pr(m_j|\boldsymbol{y}, X) = \frac{Pr(\boldsymbol{y}|m_j, X)Pr(m_j)}{\sum_{m_j \in \mathcal{M}} Pr(\boldsymbol{y}|m_j, X)Pr(m_j)} \qquad (2.23)$$

where $Pr(m_j)$ and and $Pr((y)|m_j, X)$ are, respectively, the prior probability and the *marginal likelihood* of model m_j.

The marginal likelihood of model m_j is then:

$$Pr(\boldsymbol{y}|m_j, X) = \int Pr(\boldsymbol{y}|\boldsymbol{\beta_j}, m_j, X)Pr(\boldsymbol{\beta_j}|m_j, X)d\boldsymbol{\beta_j} \qquad (2.24)$$

Where $Pr(\boldsymbol{y}|\boldsymbol{\theta}_j, m_j, X)$ is the likelihood for m_j under parameters $\boldsymbol{\theta}_j$. Often, the integral in equation 2.24 can not computed analytically, thus requiring numerical methods. We refer the reader to Raftery *et al.* (1997) for the details about the computation of the marginal likelihood in case of linear regression.

Here, we use the solution of equation 2.24 calculated for two specific cases:

i- the linear regression with Zellner g-prior for the parameters;

ii- the logistic regression.

The former is the base of the models developed to study the dynamics of the black grouse and presented in chapter 4 while the latter is the structural shape of the models used to classify the suitability of the territory for the Alpine marmot in chapter 3

Linear regression models have the structure presented in equation 4.5, and the prior probability of their parameter is fixed here as in equations 2.14. Moreover, to take into account the principle of parsimony the expected value of the parameter prior $\boldsymbol{\beta}_p$ is set to 0. Under this hypothesis, the marginal Likelihood is:

$$Pr(D|m_j, g, X) \propto (y - \overline{y})'(y - \overline{y})^{-\frac{n-1}{2}}(1+g)^{-k_j}\left(1 - \frac{g}{1+g}\right)^{-\frac{n-1}{2}} \qquad (2.25)$$

which takes into account the model complexity through the model size k_j. (George & Clyde, 2004) show that for known σ^2 model selection with this prior exactly corresponds to the use of BIC.

The logistic regression is a model structure that permits to model the probabilities on a transformed scale (see Dalgaard, 2008). Logistic regression is a generalised linear model in which the response distribution

is the binomial distribution and the link function is the *logit*. If $Pr(c_1)$ is the probability of the event (or class) c_1 that to be modelled, the *logit* is $logit(c_1) = log\left(Pr(c_1)/(1 - Pr(c_1))\right)$. The *logit* link permits to describe the relation between $Pr(c_1)$ and the independent variables as a linear function:

$$logit(Pr(c_1)) = \beta_0 + X\boldsymbol{\beta} \qquad (2.26)$$

where the symbols have the same meaning as for the linear regression. A deeper description of the logistic regression model for the specific problem of modelling the distribution of a species is given in chapter 3. A convenient approximation for computing the models' marginal likelihood in the generalised linear models is based on the BIC, described here in section 2.2. The marginal likelihood of model m_j can be approximated as:

$$Pr(D|m_j) \approx \frac{\exp(-BIC_i/2)}{\sum_{m_j \in \mathcal{M}} \exp(-BIC_i/2)}. \qquad (2.27)$$

This approximation is convenient from a computational viewpoint and generally accurate, thus, it is often adopted (e.g see Wintle *et al.*, 2003; Link & Barker, 2006; St-Louis *et al.*, 2012). Using this approximation there is no need to define a specific model prior (Kass & Raftery, 1995). The estimation of the parameters for each single model is approximated using the maximum likelihood estimation.

One of the most debated points of the Bayesian Model selection is how to choose the model prior. This debate is enhanced by the fact that often, as for the model parameters, the prior information on which is the prior probability of a model is not available. Therefore, there are many attempts to define model priors that can be considered "uninformative", as we further discuss at the very end of the chapter.

2.3 Multimodel

The selection of a single best model can be uncertain because many models can perform rather similarly for the chosen criterion. This problem is referred to with the wording *Model Uncertainty*. Models with similar performances could (i) include only few common covariates, and (ii) lead to drastically different predictions. Effect (i) is critical if the aim is to discuss the ecological relevance of the covariates, while effect (ii) is a serious drawback when models are used as forecast tools. In these cases, several authors have suggested to incorporate model uncertainty into statistical inference (Buckland *et al.*, 1997; Link & Barker, 2006, e.g. see), applying

a multimodel approach. In the multimodel approach, final inferences are calculated as the weighted sum of the inferences produced by each single model in the set. The multimodel methods have been developed several years ago and are popular in statistic. However, they are still seldom used and known in ecological applications. We present here the two most used multimodel methodologies: i) the *Multimodel Inference* based on the Akaike weights and ii) the *Bayesian Model Averaging*.

Although the multimodel is theoretically a generic approach, several computational problems arise in the analysis of complicated models, especially using *Bayesian Model Averaging*. Therefore, multimodel approaches have been mainly used on sets of linear regressors or on generalised linear models. In this section we therefore discuss the multimodel approach mainly focusing on these two families of models, in which the different model structures arise from the selection of different sets of explanatory variables. Consider, for example a simple linear regression model structure with no interaction terms, of the type:

$$y = \beta_{0,j} + X_j \boldsymbol{\beta}_j + \varepsilon_j \tag{2.28}$$

which is a version of equation 4.5 slightly modified to account for the fact that we refer to the particular model m_j. Thus, for example, X_j is the $(k_j \times n)$ design matrix containing only the k_j explanatory variables included in the model m_j. Given k covariates, the model space $\mathcal{M}$ is then composed by 2^k candidate model structures, which are composed combining the k available covariates in all the possible ways.

2.3.1 Multimodel Inference

A way to avoid excessive reliance on the single best model is the *multimodel inference*, thoroughly analysed in the influential book by Burnham & Anderson (2002). Briefly speaking, multi-model inference is realized by assigning to each competing model in the model set $\mathcal{M}$ a weight which depends on its AIC or BIC score: models with better AIC (or BIC) scores get higher weights when the multi-model inference is computed.

For example, the Akaike weight is defined, for the model m_j, as:

$$w_j = \frac{exp(-\frac{1}{2}\Delta AIC_j)}{\sum_{m_j \in \mathcal{M}} exp(-\frac{1}{2}\Delta AIC_j)} \tag{2.29}$$

The prediction of the observation y_i made using a single model (m_j) is $\hat{y}_{i,j}$. Using the Akaike weights, the multimodel prediction made using the

entire model set $\mathcal{M}$ is then:

$$\hat{y}_{i,\mathcal{M}} = \sum_{m_j \in \mathcal{M}} \hat{y}_{i,j} w_j \qquad (2.30)$$

The equations 2.29 and 2.30 can be computed using all the competing models or, as suggested by Burnham & Anderson (2002), using only the models that are more likely to be good models, thus the model for which ΔAIC_j is relatively small (e.g. $\Delta AIC_j < 4$).

2.3.2   Bayesian Model Averaging

Bayesian Model Averaging (BMA) (Hoeting *et al.*, 1999) is a theoretically sound solution to model uncertainty. BMA overcomes model uncertainty by combining different competing models. The weights of the combination are the posterior probabilities of the competing models. BMA has been introduced in ecology by Wintle *et al.* (2003) to analyse presence-absence data, which is still the most common ecological application. For this specific application, BMA has shown in many works better performances than the single model approach (Wintle *et al.*, 2003; Thomson *et al.*, 2007; Hamilton *et al.*, 2009; St-Louis *et al.*, 2012).

The link between multi-model inference and BMA has been discussed by Link & Barker (2006) showing that multi-model inference can be seen as a special case of BMA, in which the prior probabilities of the models are turned into posteriors on the basis of their AIC (or BIC) scores. Therefore multi-model inference can be fully interpreted within the BMA framework.

BMA addresses model uncertainty by combining the inferences of multiple models, and weighting them by the models' posterior probability. The BMA prediction is obtained by marginalizing the model variable (Hoeting *et al.*, 1999):

$$Pr(y_i|D) = \sum_{m_j \in \mathcal{M}} Pr(y_i|D, m_j) Pr(m_j|D) \qquad (2.31)$$

where $\mathcal{M}$ denotes the model space and D the available dataset: $D = \{\boldsymbol{y}, X\}$. In the logistic regression case, the prediction to compute is the probability of observing one of the two classes, namely, following equation 2.26, $Pr(c_1)$.

Equation 2.31 requires an extensive summation over 2^k models. To keep the computation feasible, *Markov Chain Monte Carlo* methods (MCMC) are generally adopted to sample the model space, without thus implementing all the 2^k models. For small k_j it is possible to exhaustively treat the model space.

Having used more than one model, instead of using a single model, it can be difficult to make the proper ecological considerations on which of the initial hypothesis is the more supported by the data. However, BMA provides also a measure that permits to rank the contribution of each covariate to the final prediction. The posterior probability of inclusion of the qth covariate (x_q) is in fact a direct measure of its importance. It is computed by summing the posterior probabilities of the model structures which do include x_q:

$$Pr(\beta_q \neq 0) = \sum_{m_j \in \mathcal{M}_q} Pr(m_j|D) \qquad (2.32)$$

where $\mathcal{M}_q$ denotes the set of model structures which do include $\boldsymbol{x}_q$.

The posterior mean of the coefficient β_q referring to covariate $\boldsymbol{x}_q$ is estimated as (Hoeting *et al.*, 1999):

$$E[\beta_q|D] = \sum_{m_j \in \mathcal{M}_q} \hat{\beta}_{qj} Pr(m_j|D) \qquad (2.33)$$

where $\hat{\beta}_{qj}$ is the estimate of the coefficient of covariate $\boldsymbol{x}_q$ within model m_j.

Priors over the models

If a strong knowledge about the system is available, it is possible to directly assign a prior probability to each model. However, this information is seldom alternative.

An attractive solution for linear and generalised linear models is to determine the prior probability of each model through the probability of inclusion of the explanatory variables included in set of the k available covariates. A simple approach is to set the prior probability of the models using the independent Bernoulli prior. Under this prior, each covariate is independently included in the model with identical probability δ. Denoting by k_j the number of covariates included by model m_j and by k the total number of covariates, the prior probability of model m_j is (Clyde & George, 2004):

$$Pr(m_j) = \delta^{k_j}(1-\delta)^{k-k_j} \qquad (2.34)$$

which depends on the single parameter δ. This prior is also called *binomial prior*, because the model size, measured as the number of covariates included in the model, turns out to be binomially distributed with an expected value of $k\delta$.

By setting $\delta = 1/2$ one obtains a *uniform* prior *over the models*. This choice was initially considered as a non-informative choice, but it is informative when analysed from the viewpoint of the *model size*. The distribution is in fact quite concentrated around the value of $k/2$ value (Ley & Steel, 2009), as can be seen in the example of figure 2.1. The same figure reports also the distribution of the model priors obtained using the remarkable priors described hereinafter.

If the objective is to be uninformative with respect to the model size, it has been recommended the adoption of a hierarchical prior (Ley & Steel, 2009; Clyde & George, 2004). In this case, parameter δ is treated as a random variable, with its own prior distribution. The hierarchical prior results in posterior inferences which are less sensitive on the value chosen for δ. A possible choice for the distribution of δ is a *Beta*, which generates a *Beta-binomial* distribution of the prior model size, with 2 hyperparameters. If both hyperparameters are fixed to 1, the expected model size is $k/2$ (as for the uniform prior defined above), but the distribution of the prior model size is flat (see Ley & Steel, 2009) The prior probability of model m_j which includes k_j covariates is:

$$Pr(m_j) = \frac{1/(k+1)}{\binom{k}{k_j}} \tag{2.35}$$

where $1/(k+1)$ is the probability of the model size to be equal to k_j and $\binom{k}{k_j}$ is the number of possible model structures which contain k_j covariates.

Alternative prior over the models have been also proposed. For instance the K-L prior (Burnham & Anderson, 2002) yields posterior model probabilities which correspond to the AIC weights adopted in multi-model inference (Link & Barker, 2006). The K-L prior tends to favour complex models over simple ones, especially on large data sets:

$$Pr(m_j) = \frac{\exp[k_j \log(n)/2 - k_j]}{\sum_{m_j \in \mathcal{M}} \exp[k_j \log(n)/2 - k_j]} \tag{2.36}$$

The Occam prior favours instead simple models:

$$Pr(m_j) = \frac{\exp[-k_j]}{\sum_{m_j \in \mathcal{M}} \exp[-k_j]} \tag{2.37}$$

,while the complex prior favours more complicated models:

$$Pr(m_j) = \frac{\exp[k_j]}{\sum_{m_j \in \mathcal{M}} \exp[k_j]} \tag{2.38}$$
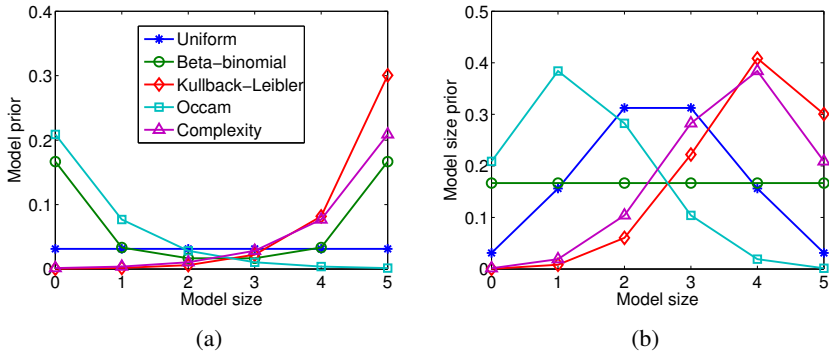
Figure 2.1: *Prior probabilities of the models as a function of the model size, obtained setting $k = 5$ and $n = 100$. Five remarkable model priors (described in the main text) are presented using different colours and markers according to the legend. The model priors are: uniform over the models, uniform over the model size (i.e. beta-binomial with hyperparameters fixed to 1), Kullback-Leibler, Occam, Complexity. Panel a) prior probability of a single model having a specific model size. Panel b) prior probability of the model size, i.e. sum of the priors of all the models having a specific model size.*

The predictive performances of these different priors depends on the specific case study and sometimes the results are presented under different sets of priors. In fact, the discussion about which is the best prior to adopt is still open. For example, we proposed a methodology that, extending the binomial prior, permits to automatize the sensitivity on the model prior in the linear regression (Mignatti *et al.*, 2012b) and in the logistic regression (Corani & Mignatti, 2013b,a).

Among this variety of priors, we chose to use, for the problems in chapters 3 and 4, the uniform prior, in which each model has the same prior probability.

Bibliography

Akaike, H. 1970: Statistical predictor identification. Annals of the Institute of Statistical Mathematics 22: 203–217.

Akaike, H. 1973: Information theory and an extension of the maximum likelihood principle. In B. Petrov & F. Csaki, eds., Second International Symposium on Information Theory. Akademiai Kiado, Budapest, (pp. 267–281).

Akaike, H. 1974: A new look at the statistical model identification. IEEE Transactions on Automatic Control 19(6): 716–723. doi:10.1109/TAC.1974.1100705.

Aldrich, J. 1997: R.A. Fisher and the making of maximum likelihood 1912-1922. Statistical Science 12(3): 162–176. doi:10.1214/ss/1030037906.

Arnold, W. 1988: Social thermoregulation during hibernation in alpine marmots (Marmota marmota). Journal of Comparative Physiology B: Biochemical, Systemic, and Environmental Physiology 158(2): 151–156.

Arnold, W., Heldmaier, G., Ortmann, S., Pohl, H., Ruf, T. & Steinlechner, S. 1991: Ambient temperatures in hibernacula and their energetic consequences for alpine marmots Marmota marmota. Journal of Thermal Biology 16(4): 223–226.

Bayes, T. 1736: An Introduction to the Doctrine of Fluxions: And, Defense of the Mathematicians Aganist the Objections of the Author of the Analyst, So Far as They are Designed to Affect Their General Methods of Reasoning. John Noon, London.

Box, G. & Draper, N. 1987: Empirical model-building and response surfaces. Wiley, first edn., 688 pp. doi:0471810339.

Box, G., Jenkins, G. & Reinsel, G. 1994: Time series analysis: forecasting and control. Prentice-Hall, Upper Saddle River, NJ, 3rd edn.

Buckland, S.T., Burnham, K.P.K. & Augustin, N.H.N.H. 1997: Model selection: an integral part of inference. Biometrics 53(2): 603–618. doi:10.2307/2533961.

Burnham, K. & Anderson, D. 2002: Model selection and multimodel inference: a practical information-theoretic approach. - Springer Verlag, 496 pp. doi:10.1198/tech.2003.s146.

Cherkassky, V., Shao, X., Mulier, F. & Vapnik, V. 1999: Model complexity control for regression using VC generalization bounds. Neural Networks, IEEE Transactions on 10(5): 1075–1089. doi:10.1109/72.788648.

Clyde, M. & George, E.I. 2004: Model uncertainty. Statistical science (pp. 81–94).

Corani, G. & Gatto, M. 2007: Structural risk minimization: a robust method for density-dependence detection and model selection. Ecography 30(3): 400–416. doi:10.1111/j.2007.0906-7590.04863.x.

Corani, G. & Mignatti, A. 2013a: Credal Model Averaging for modeling presence-absence. Ecography in review.

Corani, G. & Mignatti, A. 2013b: Credal model averaging of logistic regression for modeling the distribution of marmot burrows. In Eighth International Symposium on Imprecise Probability: Theories and Applications. Compiègne, France, (p. In press.).

Dalgaard, P. 2008: Logistic regression. In Introductory Statistics with R, Springer New York, New York, NY, Statistics and Computing, (p. 364). ISBN 978-0-387-79053-4. doi:10.1007/978-0-387-79054-1.

Fernandez, C., Ley, E. & Steel, M. 2001: Benchmark priors for Bayesian model averaging. Journal of Econometrics 100: 381–427.

George, E.I. & Clyde, M. 2004: Model Uncertainty. Statistical Science 19(1): 81–94. doi:10.1214/088342304000000035.

Gnanadesikan, R. & Wilk, M. 1970: Use of maximum likelihood for estimating error variance from a collection of analysis of variance mean squares. The Annals of Mathematical Statistics 41(1): 292–304.

Hamilton, G., McVinish, R. & Mengersen, K. 2009: Bayesian model averaging for harmful algal bloom prediction. Ecological Applications 19: 1805–1814.

Hoeting, J.A., Madigan, D., Raftery, A.E. & Volinsky, C.T. 1999: Bayesian model averaging: A tutorial. Statistical science (pp. 382–401).

Johnson, J.B. & Omland, K.S. 2004: Model selection in ecology and evolution. Trends in ecology & evolution 19(2): 101–8. doi:10.1016/j.tree.2003.10.013.

Kass, R. & Raftery, A. 1995: Bayes factor. Journal of the American Statistical Association 90(430): 773–795.

King, R., Morgan, B., Gimenez, O. & Brooks, S. 2010: Bayesian analysis for population ecology. Chapman & Hall/CRC Interdisciplinary Statistics. ISBN 9781439811870, 434 pp.

Kullback, S. 1959: Information Theory and Statistics. Wiley, New York, NY, 1 edn., 395 pp.

Ley, E. & Steel, M. 2009: On the effect of prior assumptions in Bayesian model averaging with applications to growth regression. Journal of Applied Econometrics 24: 651–674. doi:10.1002/jae.

Link, W. & Barker, R. 2006: Model weights and the foundations of multimodel inference. Ecology 87(10): 2626–2635.

Mignatti, A., Casagrandi, R., Provenzale, A., von Hardenberg, A. & Gatto, M. 2012a: Sex- and age-structured models for Alpine ibex Capra ibex ibex population dynamics. Wildlife Biology 18(3): 318–332. doi:10.2981/11-084.

Mignatti, A., Corani, G. & Rizzoli, A. 2012b: Credal Model Averaging: dealing robustly with model uncertainty on small datasets. In R. Seppelt, A.A. Voinov, S. Lange & D.Bankamp, eds., International Environmental Modelling and Software Society (iEMSs) 2012 International Congress on Environmental Modelling and Software. Managing Resources of a Limited Planet: Pathways and Visions under Uncertainty, Sixth Biennial Meeting. Helmholtz Centre for Environmental Research (UFZ), Leipzig (Germany). ISBN "978-88-9035-742-8".

Raftery, A. 1995: Bayesian model selection in social research. Sociological methodology 25(1): 111–163.

Raftery, A.E., Madigan, D. & Hoeting, J.A. 1997: Bayesian Model Averaging for Linear Regression Models. Journal of the American Statistical Association 92: 179–191. doi:10.2307/2291462.

Richards, S. 2005: Testing ecological theory using the information-theoretic approach: Examples and cautionary results. Ecology 86(10): 2805–2814.

Rue, H.v., Martino, S. & Chopin, N. 2009: Approximate Bayesian inference for latent Gaussian models by using integrated nested Laplace approximations. Journal of the Royal Statistical Society 71, Part 2: 319–392.

Ruf, T. & Arnold, W. 2000: Mechanisms of Social Thermoregulation in Hibernating Alpine Marmots. In Life in the Cold: Eleventh International Hibernation Symposium. (p. 546).

Schwarz, G. 1978: Estimating the dimension of a model. The annals of statistics 6(2): 461–464.

Spiegelhalter, D., Best, N., Carlin, B.P. & van del Linde, A. 2002: Bayesian measures of model complexity and fit. Journal of the Royal Statistical Society 64(4): 583–639.

St-Louis, V., Clayton, M.K., Pidgeon, A.M. & Radeloff, V.C. 2012: An evaluation of prior influence on the predictive ability of Bayesian model averaging. Oecologia 168(3): 719–726.

Sugiura, N. 1978: Further analysis of the data by Akaike's information criterion and the finite correction. Comm. Statist. A-Theory. Meth. 7(1): 13–26.

Thomson, J.R., Mac Nally, R., Fleishman, E. & Horrocks, G. 2007: Predicting bird species distributions in reconstructed landscapes. Conservation Biology 21(3): 752–766.

Vapnik, V., Levin, E., Cun, Y.L. & Cun, L. 1994: Measuring the VC-Dimension of a Learning Machine. Neural Computation 6(5): 851–876. doi:10.1162/neco.1994.6.5.851.

Wasserman, L. 2000: Bayesian Model Selection and Model Averaging. Journal of mathematical psychology 44(1): 92–107. doi:10.1006/jmps.1999.1278.

Whittingham, M.J., Stephens, P.A., Bradbury, R.B. & Freckleton, R.P. 2006: Why do we still use stepwise modelling in ecology and behaviour? Journal of animal ecology 75(5): 1182–1189.

Wintle, B., McCarthy, M., Volinsky, C. & Kavanagh, R. 2003: The use of Bayesian model averaging to better represent uncertainty in ecological models. Conservation Biology 17(6): 1579–1590.

Zellner, A. 1983: Bayesian analysis of a simple multinomial logit model. Economics Letters 11(1-2): 133–136.

Fine scale site selection of Alpine Marmot

3.1 Abstract

As described in the introduction (chapter 1) in the mountain environment there are clear evidences of a recent upslope of many plant taxa, that is faster for summit species. The different speed at which this upslope occurs according to the plant type leads to potentially complicated rearrangements of the habitats. To figure out the possible impacts of these variations on the alpine fauna, it is important to better understand the habitat preferences of the alpine animal species. We investigated the fine scale site selection of the Alpine marmot in an high altitude Alpine valley, at the upper edge of its distribution. To retrieve presence-absence data of marmot burrows in the valley we performed fieldworks in two consecutive years (2010 and 2011). The models were developed using the Bayesian model averaging applied to logistic regression, and matching two alternative classification thresholds. As potential explanatory variables, we included both variables linked with the geomorphology of the valley and the vegetation types. To study the influence of vegetation on the probability of presence of marmot burrows, we used a fine scale vegetation map specifically developed for the study area. The developed models have a very good predictive ability, which is more

balanced if the *prevalence* threshold is adopted. Environmental variables that are more important in modelling the distribution of burrows are the vegetation cover, the curvature and the aspect, while the altitude has a less important role. The Alpine marmot shows in fact a preference for southerly exposed slopes of the valley characterized by a moderate concavity. The importance of the variables obtained from the vegetation map confirms the strong relationship between the presence of marmot and the availability of the appropriate vegetation. In particular, the areas covered with pioneer vegetation are strongly avoided and the areas with no vegetation cover are moderately avoided, while the other vegetation covers present in the valley (shrubs, meadows and snowbed vegetation) favour the presence of burrows. The obtained results, and in particular the different role of the pioneer and the snowbed vegetation, which are both fast upshifting summit species, underline the importance of understanding the pattern of vegetation change to estimate the potential upshift of the upper bound of Alpine marmot distribution.

3.2 Introduction

The study of interactions between the habitat type and the presence of the species is a central issue in ecology (Guisan & Zimmermann, 2000). As described in the introductory chapter of this thesis one of the main effect of the climate change already registered on the Alps is the upward shifting of many plant species, thus resulting in an increase of the altitude of the tree line (Körner *et al.*, 2007), an even faster uplift of snowbed vegetation (Bahn & Körner, 2003) and rockfield pioneers (Grabherr *et al.*, 1994), and an increase of the species richness on many high altitude summits (Bahn & Körner, 2003). To understand the possible effects of climate change on the high altitude fauna, it is therefore important to disentangle the specific roles of topographic characteristics (especially of the altitude, which can be seen as a proxy of the temperature) and of the vegetation types in driving the choice of the habitat. To this aim we choose to study the distribution of marmot burrows in an high altitude Alpine valley, which is not affected by human disturbance and for which a fine scale vegetation map is available. The study area is located nearby the Stelvio National Park (Northwestern Alps, Italy), in which a rapid expansion of the area covered by shrubs has been already registered in the last 50 years (Cannone *et al.*, 2007). Moreover, in the last two decades the valley has been the subject of several geological studies (see the description of the study area at section 3.3.1).

The Alpine marmot (*Marmota marmota*) is a rodent endemic to Europe and mainly distributed in the Alps (Herrero *et al.*, 2008), that inhabits burrow systems at high altitude and hibernate during winter. During the hibernation period, which occurs between October and March, the alpine marmot relies on the body fat stored during the short summer (Arnold, 1992). Moreover, the dependency on the body fat continues also after the termination of hibernation in spring (Arnold & Walter, 1990) and an insufficient reserve of fat in spring can prevent the reproduction in either sexes. If the temperatures are low in spring and reproduction takes place too late offspring survival is reduced because newborns do not have the necessary time to accumulate body fat (Armitage *et al.*, 1976). In winter, the consumption of fat resources increases as the temperatures decrease in the hibernacula, and individuals can interrupt the hibernation and return to euthermy if temperatures are too low (Arnold *et al.*, 1991). The social hibernation of Alpine marmot is thus explained as a mechanism to increase the probability of winter survival. The winter survival of the individuals and their reproductive success depend therefore on climate via winter temperatures, availability of food resources and length of the growing season (Allainé *et al.*, 1994). All these conditions are likely to improve with a moderate increase in temperatures. On the other hand, Alpine marmots are well adapted to cold environments and they have poor thermoregulatory abilities in dumping the excess heat (see Hayes, 1976, for another species of marmot). As a consequence, the animals reduce the time spend in above ground activity and foraging in hot summer days (Melcher *et al.*, 1990). Türk & Arnold (1988) reports an increase in the activities until 25 degree Celsius, than a decrease. This behaviour is important in limiting the lower bound of the vertical distribution of the species, because at low altitudes the time available to store sufficient fat for hibernation can be too limited (Türk & Arnold, 1988). Moreover, the decrease in winter snow cover can lead to a decrease in the litter size (Tafani *et al.*, 2013). These particular and contrasting needs act in determining the habitat preferences of the Alpine marmot.

Past quantitative studies on the habitat preferences revealed that Alpine marmot is a generalist species that can live in a wide range of environmental conditions (Allainé *et al.*, 1994; López *et al.*, 2010), and usually inhabits meadows covered with grass or shrubs (Borgo, 2003; Cantini *et al.*, 1997; López *et al.*, 2010). The altitude range is really variable on the Alps, from 1000 to 3000 m a.s.l. (Lenti Boero, 2003), with the highest suitability for intermediate altitudes (1700-1900 m a.s.l., Cantini *et al.*, 1997). Past studies conducted on the Alps found also a preference for southerly exposed slopes with high solar radiation and an intermediate slope (Cantini *et al.*,

1997; Allainé *et al.*, 1994; Borgo, 2003). Allainé *et al.* (1994) conducted also a study on the quantity (and not quality) of the plant cover and anthropogenic disturbance, and found a maximal suitability for medium level of plant cover and low levels of human disturbance. The presence of big boulders or tall grass favours the presence of winter hibernacula (Borgo, 2003; López *et al.*, 2010).

Species distribution models (Guisan & Thuiller, 2005; Meynard & Quinn, 2007) quantify the relationship between the characteristics of the habitat and the presence of a species. They can be developed at different spatial scale according to the aim of the study (Schweiger *et al.*, 2012); for example, for habitat connectivity the models developed at the landscape scale are usually preferred, while fine scale models are more appropriate to study the habitat preferences (Graf *et al.*, 2005).

The objective of this chapter is to identify the fine scale environmental variables that have the main influence on the presence of marmot burrows in a high altitude Alpine valley, at the upper limit of marmot distribution. To this aim, we performed a census of the marmot burrows and developed a logistic regression model which takes into account, as explanatory variables, a fine classification of the vegetation and the topographic characteristics of the area.

In Corani & Mignatti (2013b,a) we used the same presence/absence dataset to test a novel Bayesian classification methodology. However, for that work the fine vegetation map was not available and we used only a map reporting a coarse classification of the vegetation. The results presented in this chapter confirm the preferences reported in literature and provide new insights on the importance of both the vegetation cover and the topography.

3.3 Materials

3.3.1 Study area

The study area is "La Vallaccia", an Alpine valley in Northwestern Italy, near the Stelvio National Park (see Figure 3.1). The valley has an altitude comprised between 2100 and 3100 m above sea level, and has been chosen because many informations are available on its geological and vegetation characteristics. In particular, the status of the permafrost is constantly monitored and a model that predicts the presence of permafrost is available for the area (Guglielmin, 2003; Guglielmin & Camusso, 2004). Moreover, a detailed map of the vegetation, reporting the main vegetation associations in the valley, has been developed by N. Cannone (personal communication)

and is reported in figure 3.2. Another important factor that determined the choice of the "La Vallaccia" is the limited human disturbance, since no marked trails are present, and only a winter mountaineering route is reported in the tourist maps.

3.3.2 Field surveys

The field surveys where performed in two consecutive summers in July and August by myself together with professor Casagrandi, professor Gatto and three bachelor students. Surveys aimed at the identification of the position of the Alpine marmot burrows and at the classification of the characteristics of their surrounding territory. The areas of the valley in which we performed the censuses were chosen in order to explore the different habitat present in the valley, taking into account the objective of collecting data in areas characterized by different altitude, slope, aspect, vegetation associations and geological formations.

Each census area was exhaustively explored by the operators, to assure with an high expectation that all the excavations were detected. Each found burrow was geo-referenced using a GPS receiver (MobileMapper® Thales), and positional data were post-processed to obtain sub-metric precision. Census areas and position of the burrows are reported in Figure 3.1. The burrows were also assigned to two alternative categories (called types), *main burrows* or *refugees* according to their depth measured using a walking stick or by hand. The former category was assigned if the bottom of the burrow was not reached, while the latter was assigned if the bottom was reached. Winter burrows were not distinguished from main burrows since the censused were performed in summer. Moreover, the activity status of the burrows (*used* or *abandoned*) was assigned according to evident traces of recent use. Other informations were recorded to characterize the burrows and their surroundings, as we summarize in table 3.1. The recorded values refer to a square of 5m x 5m designed around the burrow, fixing the position of the square so that the burrow is at the intersection of its diagonals, and two of its sides are parallel to the maximum slope direction. However, a full description of the data collected during censuses is out of the scope of this chapter, since we used only the positioning of the burrows to develop the species distribution models.

The total area censused in the two years was around 94 hectares and data about 446 burrows were collected, among which 412 are reported to be active. To develop the species distribution model, we divided the area into cells of 10 x 10m, thus obtaining a dataset of 9429 observations. The
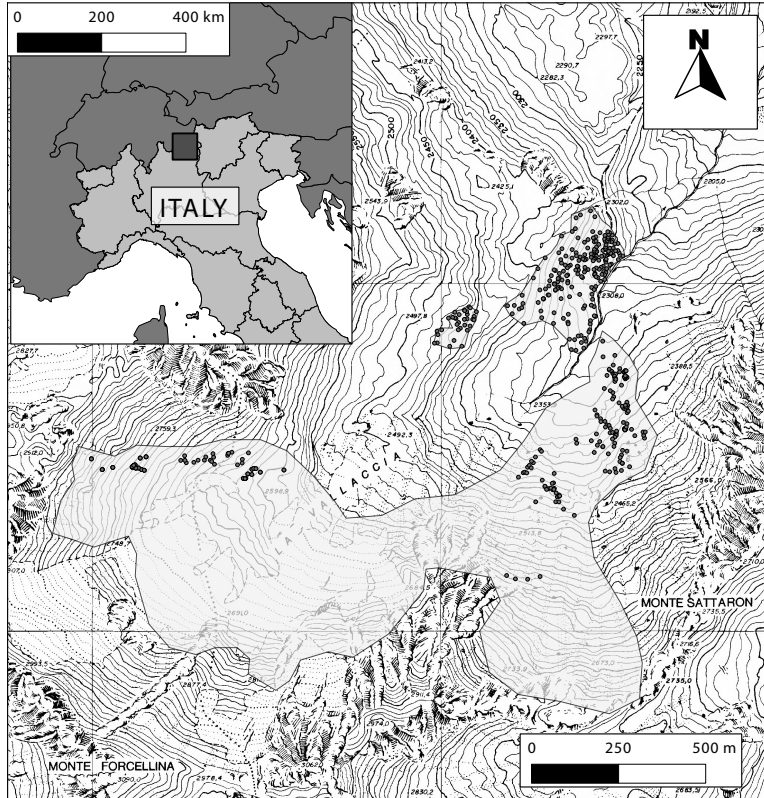
Figure 3.1: *Map of the marmot censuses. The census areas are shown with a transparent mask, while the burrows are shown as small circles.*

Table 3.1: *Data collected to characterize the burrows and their surroundings, sub-divided in three categories. The entrance data refer to the burrows only, while the data belonging to the other categories refer to the 5mx5m square designed around the burrow. The values that can take the the entrance data type and the activity are described in the main text. The predominant grain size has 4 categories: sand (<2mm), gravel (2-60mm), shingle (60-250mm) and blocks (>250mm). The vegetation context has 6 categories: woodland, continuous Alpine meadows, discontinuous Alpine meadows, shrubs, dwarf shrubs and pioneer vegetation. The geomorphological localization has 4 categories: slopes, scree slopes, valley floor and morainic ridge.*

Entrance data	Geomorphological data	Vegetation data
Date	Aspect	Vegetation context
GPS coordinates	Slope	% of tree cover
Type	Predominant grain size	% of shrub cover
Activity	Geomorphological localization	% of grass cover
		List of predominant species

fraction of presence (*prevalence*) is 0.046.

3.3.3 Environmental data

The environmental data used in the study were calculated using the information from five meteorological stations and from two digital maps: the digital terrain model (DTM), available with a resolution of 10 x 10m and a fine scale vegetation map (Nicoletta Cannone, Università dell'Insubria, personal communication).

The original categories of the vegetation, reporting a fine description of the vegetation biocenoses, were redefined into six categories, which are more general and likely to be more representative to model the habitat choices of the Alpine marmot:

- Alpine shrubs (including also dwarf shrubs);

- Alpine meadows;

- Mosaic of Alpine meadows and Alpine shrubs;

- Snowbed vegetation;

- Pioneer vegetation;

- No vegetation cover.
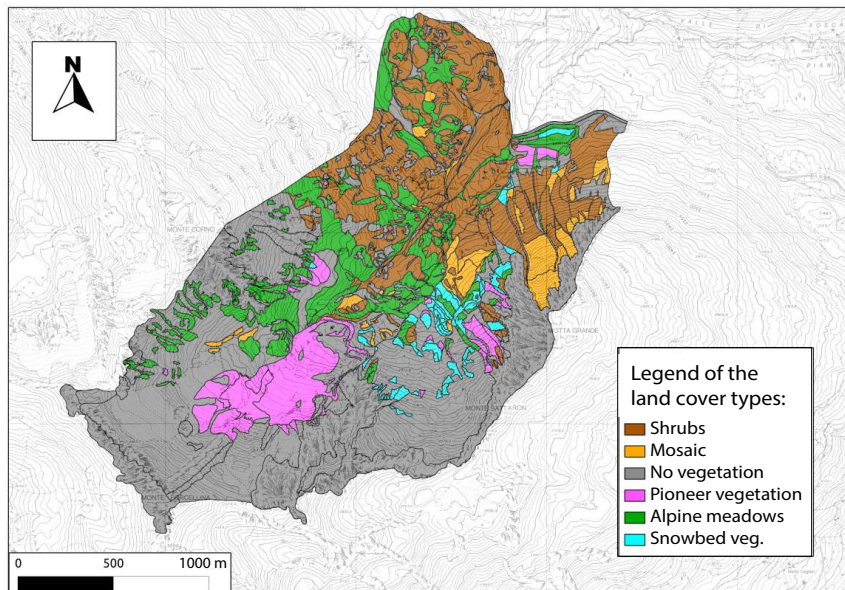
Figure 3.2: *Map of the vegetation cover, where the categories are defined according to the description given in the main text.*

The air temperature and the snow depth variables were used to calibrate the permafrost (soil temperature) model and were taken from five different meteorological stations located near the "Vallaccia" Valley, as summarized in table 3.2. Meteorological data were provided by the regional environmental agency ARPA Lombardia upon request.

Table 3.2: *List of the meteorological stations used to calibrate the permafrost model.*

Station name	Snow depth	Air temperature	Elevation (m a.s.l.)
Livigno, La Vallaccia	available	available	2650
Livigno, San Rocco	not available from June to October		1865
San Colombano, Oga	available	available	2290
Valdidentro, Cancano	not available from June to October		1940
Valfurva-S.Caterina	available	not available	2135

3.4 Methods

The covariates obtained by the DTM and the meteorological data are altitude, slope, aspect (the direction in which the slope faces) topographic ruggedness index (TRI, Riley *et al.*, 1999), hillshade, curvature and soil temperature. The aspect, usually reported as the the angle from North, was divided into two sub-variables, called *northitude* and *eastitude*. The *northitude* is calculated as the cosine of the angle from North, while the *eastitude* as the sine of the same quantity. The *northitude* is therefore an indirect measure of the attitude of a slope to receive the sunlight in the hottest hours of the day, and it assumes the value +1 if the slope is northerly exposed while a value of -1 if it is southerly exposed. The *eastitude* measures the distribution of the sunlight during the day, assuming a value close to +1 if a slope is sunny mostly during the sunrise, and close to -1 if it is sunny during sunset. The TRI is measured in meters and measures the topographic heterogeneity of the terrain. Hillshade and curvature were calculated using the default functions of ArcGIS10®. The hillshade is an estimate of the light received per unit area in each cell. A positive curvature indicates the surface is upwardly convex, while a negative curvature indicates the surface is upwardly concave. The soil temperature is a yearly mean value and was calculated starting from the DEM and the data of air temperature and snow depth, using the model developed by Guglielmin (2003). As a preprocessing step we removed too highly cross-correlated covariates, namely those that have a Pearson correlation coefficient (ρ in this chapter) larger than 0.8 or smaller than -0.8 ($|\rho| > .8$).

The Alpine marmot is a mobile species, which uses a wide territory for its activities. Therefore we hypothesize that the decision of digging a burrow in a given cell depends also on the conditions of the surrounding cells. The value of each environmental variable is therefore averaged over a circular area designed around each cell, which we refer to as the *buffer area*. The dimension of the buffer area has been set to according to the typical extension of the Alpine marmot home range, which is comprised between one and three hectares (Perrin & Berre, 1993; Lenti Boero, 2003). We therefore tested three different options for the buffer area size: one, two and three hectares. The values of the covariates, previously defined on the cell basis, were therefore recalculated as their mean value in the buffer area. We used a different aggregation strategy for the categorical vegetation variables. Using the buffer area they were in fact redefined as the % of cells with a given vegetation cover in the buffer area. Moreover, the % of vegetation cover covariates were log-transformed, and one of them was

alternatively removed from the dataset, in order to reduce their correlation and avoid singularities.

Following the concept of ecological niche, it is often unlikely that the best environment for a species occur at the maximum or a minimum of the values of an environmental variable, while it is more probable to have a range of intermediate values that are suitable for the species. The covariates obtained from the DTM were therefore potentially included in the models both linearly and quadratically. However, we did not consider the quadratic terms of the aspect variables, because the preference on intermediate values is already potentially included having defined the two quantities *Northitude* and *Eastitude*.

The goal is to predict the outcome of the binary class variable C, whose classes c_0 and c_1 denote, respectively, the absence or presence of a species. To achieve this goal we used the BMA (see section 2.3.2 for a description) applied to the *logistic regression* . The main aspects of the *logistic regression* are described in section 2.2. To calculate the marginal likelihood of each model we used the BIC approximation (see equation 2.27 at page 40), which is implemented in the R package *"BMA"*. Usually, the logistic regression returns, as prediction, the most probable class, i.e. the class c_1 (presence) is returned if $Pr(c_1) > 0.5$. However other choices are possible for setting the probability threshold τ above which the class c_1 is returned, as we explain below.

Since both the predictions and the observations of the classes are boolean (i.e. 1=presence or 0=absence), there are four possible configurations for each validation point: (i) right predicted presence (true positive), (ii) wrong predicted presence (false negative), (iii) right predicted absence (true negative) and wrong predicted absence (false negative). From now on we will use TP to indicate the number of true positives in a validation set, FP for the number of false positives, TN for the number of true negatives and FN for the number of false negatives, as summarized in Table 3.3.

Predicted	Actual	
	0	**1**
0	True Negative (TN)	False Negative (FN)
1	False Positive (FP)	True Positive (TP)

Table 3.3: *Contingency table.*

Starting from the contingency table, two measures that separately consider the two types of errors are:

   i the true positive rate, or sensitivity, calculated as $TP/(TP + FN)$;

   ii the false negative rate, or sensitivity, calculated as $TN/(TN + FP)$.

The accuracy (ACC) is instead a measure that combines both the error types, and it is defined as the fraction of correct predictions: $ACC = \frac{TP+TN}{TP+TN+FP+FN}$.

Accuracy, sensitivity and specificity are functions of the chosen threshold τ and generally, if τ is changed in order to increase sensitivity, specificity decreases. As said above, the usual value of τ is 0.5, because it corresponds to choice the most probable class. Nevertheless, there are other possible choices of τ, considering that the two types of error could imply a different cost. The costs matrix is the matrix reporting the costs (or utilities) of predicting a certain class for an instance, given the actual class of the same instance:

		Actual	
		0	**1**
Predicted	**0**	c_{00}	c_{01}
	1	c_{10}	c_{11}

Table 3.4: *Costs matrix.*

The value of the threshold τ can in fact be easily calculated once the costs (or benefits) matrix has been fully defined (Elkan, 2001):

$$\tau = \frac{c_{10} - c_{00}}{c_{10} - c_{00} + c_{01} - c_{11}} \tag{3.1}$$

where c_{ij} are the elements of the cost matrix, thus the cost of predicting j when the actual value is i.

A common alternative for the cost matrix is to use $c_{11} = c_{00} = 0$, $c_{10} = \pi$ and $c_{01} = 1 - \pi$, where π represents the prevalence (frequency of occurrence) of the positive values in the dataset. This definition of costs is used in the Kolmogorov-Smirnov statistic, as explained in terms of sensitivity and specificity by Hand (2010). In this case, following Eq. 3.1, the threshold value becomes $\tau = \pi$. We here compare the performances of the classifications obtained using, alternatively, the thresholds $\tau = 0.5$ and $\tau = \pi$. The prevalence is in fact an important characteristic of the dataset, which has been shown to systematically affect the predictive accuracy of the logistic regression models on ecological datasets (Manel *et al.*, 2001). For example, in the present case study, in which the prevalence is below

5%, a model that returns always absence would have a very high value for the accuracy, of more than 0.95. It is therefore useful to use also other measures of performance.

To overcome the problem of defining a classification threshold, some alternative threshold-independent measures have been proposed, among which the **AUC** (**A**rea **U**nder the *"Receiver Operating Characteristic"* **C**urve) is the most used. **AUC** value lies between 0 (completely wrong classifier) and 1 (perfect classifier), and is > 0.5 if the classifier works better than a random guesser. The **R**eceiver **O**perating **C**haracteristic (**ROC**) is a plot of the sensitivity, given a specific value for the 1-specificity, thus, it is a curve plotted using all the possible threshold values τ. Figure 3.3 report an example of **ROC** curves retrieved from Hand (2010) and concerning the performances of two competing medical treatments. In the **ROC** plot, the chosen classifier works better than random, for a given 1-specificity, only if the curve is above the 45 degrees line, which correspond to a perfectly random classifier.
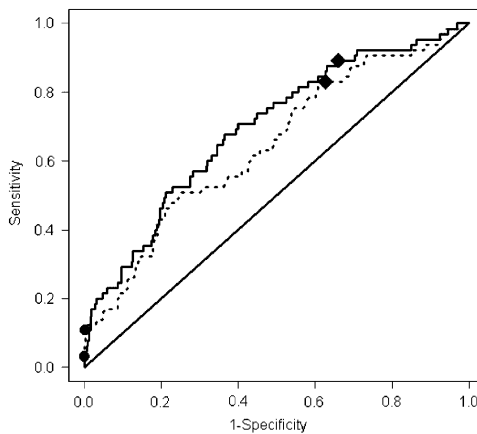
Figure 3.3: *Examples of two ROC curves, retrieved from Hand (2010).*

Even if the **AUC** is a sound alternative to measure the performances of a binary classifier, it has the lack of being equivalently defined regardless the threshold value actually used to perform the classification. The **AUC** is in fact an aggregate measure that equivalently weights all the possible values of τ, so that it could misrepresent the performance of a classifier, that must be defined giving a specific τ value (Hand, 2010).

Experimental settings

The % of vegetation type variables sum up to one for every instance and, thus, each of them can be calculated as a linear combination of the others. As already stated, to reduce the correlation among the % of vegetation type we log-transformed them. Moreover, to avoid singularities that would prevent to solve the system, we excluded one of the % of vegetation variables from the pool of explanatory variables. For each buffering area, we therefore repeated the calibration of the models six times alternatively excluding one of the % of vegetation type variables. The repeated calibrations were also used to calculate an estimate of the variance of the parameters. After having calibrated the BMA models, we used them to predict the probability of presence of burrows in all the valley.

To evaluate the performances of the models and to compare the two threshold choices, we performed a cross validation based on bootstrap samplings of the dataseries. Naming n the number of observations in the dataset, for each bootstrap sampling we executed the following procedure:

1. take a bootstrap sample of the data, i.e. a sample of size n with replacement. we also stratified the sample with respect to the presence/absence data, thus the bootstrap sample has the same prevalence of the original dataset;

2. calibrate the BMA model using the bootstrap sample;

3. evaluate the statistics (sensitivity, specificity, accuracy, **AUC**) on the training set, thus on the instances belonging to the bootstrap sample.

4. evaluate the statistics on the validation set, thus on the instance which are exclude fro the bootstrap sample.

We repeated the procedure using 600 different bootstrap samplings.

3.5 Results

From the pool of environmental data described above, we removed three of them because they are highly correlated with other variables. When two covariates have an high Pearson's correlation coefficient, we removed the one that has a less straightforward ecological interpretation. The removed variables were: TRI, correlated with the slope ($|\rho| = 0.98$); hillshade, correlated with the *northitude* ($|\rho| = 0.94$) and the soil temperature, highly correlated with the altitude ($|\rho| = 0.99$).

3.5.1 Prediction performances

The performances of the models obtained when the most probable class is returned in classification (i.e. $\tau = 0.5$) are summarized in figure 3.4. The plots show the performances on both the training and the validation bootstrapped sets. The values of the accuracy (fraction of correctly classified instances) and the specificity (fraction of correctly classified absences) are extremely high (above 0.9), while the sensitivity (fraction of correctly classified presences) is very low. However, the **AUC**, which its an integral over all the possible threshold values, is remarkably high, with a value near 0.9. The prediction performances of the models are therefore good regardless the chosen threshold. Moreover, the model is much robust for predictive aims, because the values obtained on the training and the validation sets are really similar. Furthermore the performances do not change sensitively with the size of the buffer area.
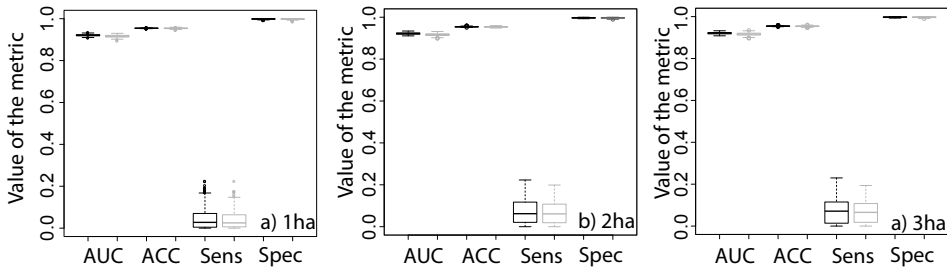
Figure 3.4: *Performances of the models obtained when the most probable class is returned ($\tau = 0.5$). The measures of performance are: **AUC**, accuracy (**ACC**), sensitivity (**Sens**) and specificity (**Spec**). For each indicator, we report the value obtained on the training set (same set of points used in calibration) in black and on the validation set (set of points not used in calibration) in grey. Training and validation sets are defined using bootstrap as explained in the main text.*

Results obtained using the prevalence threshold ($\tau = \pi$) are reported in figure 3.5 and show that in this case there is a dramatic increase on the sensitivity with respect to the results obtained using $\tau = 0.5$. The median value of the sensitivity is in fact in this case above 0.9, thus it is almost 9 times the value obtained than using $\tau = 0.5$. The cost of this strong increase in sensitivity is a decrease in the specificity and in the accuracy. However, the decrease in specificity from a value near one to a value around 0.8 is far less pronounced than the increase in the sensitivity. Since the most of data are absence, this result in specificity leads to a similar decrease in the accuracy. However, the decrease in the accuracy is an expected result, because accu-

racy is a measure based on the hypothesis of equal costs for false negative (predict an absence in an actual presence cell) and false positive (predict a presence in an actual absence cell) errors, which is not the case since we used a τ different from 0.5. Overall, even if the number of misclassified cells is larger using the prevalence threshold, the errors are better balanced among false positives and false negatives. Moreover, if the aim is to find the existing burrows, it is reasonable that the cost paid for a false negative should be set to be higher than the cost paid for false positives, thus leading to a τ smaller than 0.5 (see equation 3.1).
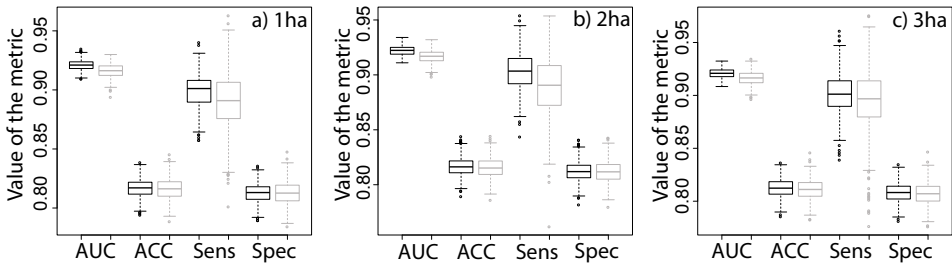
Figure 3.5: *Performances of the models obtained when the prevalence is used as the classification threshold ($\tau = \pi$). Metrics, box colours and box types are as in figure 3.4.*

As stated by equation 2.32 (page 42) while describing BMA, the importance of single covariates can be measured as the sum of the posterior probabilities of the models in which the given covariate is included. Table 3.5 reports the percentage of inclusion and the values of the covariates obtained using the three different buffer areas. The variables that have a very high probability of inclusion (>0.7) using all the buffer area sizes are *northitude*, *squared curvatures* and the *% of pioneer vegetation*, all included with a negative effect. However, for the other covariates the probability of inclusion can change drastically from a buffer area size to the other and there are no covariates that always have a very small probability of inclusion. Even if the probability of inclusion quantitatively varies for the different buffer area sizes, the effects of the single covariates are qualitatively coherent since the signs of the parameters are consistent.

To study the effects of the covariates on the probability of presence, figures 3.6 and 3.7 report the *habitat suitability curve* of each environmental variable. The *habitat suitability curves* show how the probability of presence changes with the value of a specific covariates, while the other variables are fixed to a given value (the mean value in this case), thus, the curves indicate how the environmental variables drive the habitat prefer-

Table 3.5: *Tables of the posterior probability of inclusion and the parameter values obtained with BMA (defined in section 2.3.2 at page 41) and for the models considering the three different buffer areas. The left part of the table report the results obtained using all available data, while the right part lists the results obtained with the bootstrap samples of the dataset. The % inc. is calculated as 100 times the posterior probability of inclusion.*

	all the data				bootstrap					
	% inc.	parameter value			% inc.			parameter value		
one hectare										
Intercept		$4.76 \cdot 10^1$	$\pm$	$2.05 \cdot 10^1$				$5.67 \cdot 10^1$	$\pm$	$6.11 \cdot 10^1$
Altitude	51	$-3.80 \cdot 10^{-2}$	$\pm$	$1.55 \cdot 10^{-2}$	54	$\pm$	40	$-4.49 \cdot 10^{-2}$	$\pm$	$4.49 \cdot 10^{-2}$
Altitude^2	50	$6.95 \cdot 10^{-6}$	$\pm$	$2.90 \cdot 10^{-6}$	51	$\pm$	40	$8.22 \cdot 10^{-6}$	$\pm$	$8.36 \cdot 10^{-6}$
Slope	59	$2.52 \cdot 10^{-2}$	$\pm$	$1.22 \cdot 10^{-2}$	49	$\pm$	33	$3.60 \cdot 10^{-2}$	$\pm$	$4.59 \cdot 10^{-2}$
Slope^2	19	$-6.80 \cdot 10^{-5}$	$\pm$	$2.08 \cdot 10^{-4}$	22	$\pm$	19	$-1.90 \cdot 10^{-4}$	$\pm$	$8.25 \cdot 10^{-4}$
Curvature	68	$6.08 \cdot 10^{-1}$	$\pm$	$1.55 \cdot 10^{-1}$	72	$\pm$	35	$6.87 \cdot 10^{-1}$	$\pm$	$4.46 \cdot 10^{-1}$
Curvature^2	72	$-6.83 \cdot 10^{-1}$	$\pm$	$1.78 \cdot 10^{-1}$	69	$\pm$	35	$-7.61 \cdot 10^{-1}$	$\pm$	$4.88 \cdot 10^{-1}$
Northitude	100	-1.42	$\pm$	$9.30 \cdot 10^{-2}$	100	$\pm$	1	-1.49	$\pm$	$3.31 \cdot 10^{-1}$
Eastitude	95	-1.00	$\pm$	$1.17 \cdot 10^{-1}$	84	$\pm$	29	$-9.71 \cdot 10^{-1}$	$\pm$	$4.43 \cdot 10^{-1}$
Shrubs	67	5.00	$\pm$	$7.38 \cdot 10^{-1}$	72	$\pm$	37	4.96	$\pm$	4.84
Mosaic	41	3.21	$\pm$	$2.93 \cdot 10^{-1}$	41	$\pm$	44	3.18	$\pm$	4.81
No veg.	97	$-4.97 \cdot 10^{-1}$	$\pm$	$4.61 \cdot 10^{-1}$	81	$\pm$	31	$-1.89 \cdot 10^{-1}$	$\pm$	4.45
Pioneer veg.	99	$-1.17 \cdot 10^1$	$\pm$	1.37	98	$\pm$	10	$-1.21 \cdot 10^1$	$\pm$	3.53
Alpine meadows	43	3.12	$\pm$	$2.25 \cdot 10^{-1}$	45	$\pm$	44	2.98	$\pm$	4.37
Snowbed veg.	49	$3.73 \cdot 10^{-1}$	$\pm$	$3.93 \cdot 10^{-1}$	56	$\pm$	42	3.97	$\pm$	4.93
two hectares										
Intercept		$6.17 \cdot 10^1$	$\pm$	$2.21 \cdot 10^1$				$5.40 \cdot 10^1$	$\pm$	$6.60 \cdot 10^1$
Altitude	51	$-4.81 \cdot 10^{-2}$	$\pm$	$1.67 \cdot 10^{-2}$	51	$\pm$	39	$-4.32 \cdot 10^{-2}$	$\pm$	$4.84 \cdot 10^{-2}$
Altitude^2	50	$8.73 \cdot 10^{-6}$	$\pm$	$3.12 \cdot 10^{-6}$	47	$\pm$	38	$7.75 \cdot 10^{-6}$	$\pm$	$8.96 \cdot 10^{-6}$
Slope	55	$7.90 \cdot 10^{-2}$	$\pm$	$3.60 \cdot 10^{-2}$	63	$\pm$	36	$8.51 \cdot 10^{-2}$	$\pm$	$8.88 \cdot 10^{-2}$
Slope^2	33	$-9.85 \cdot 10^{-4}$	$\pm$	$6.91 \cdot 10^{-4}$	30	$\pm$	28	$-8.71 \cdot 10^{-4}$	$\pm$	$1.61 \cdot 10^{-3}$
Curve	59	$7.21 \cdot 10^{-1}$	$\pm$	$2.21 \cdot 10^{-1}$	55	$\pm$	39	$7.01 \cdot 10^{-1}$	$\pm$	$6.16 \cdot 10^{-1}$
Curve^2	99	-2.25	$\pm$	$2.39 \cdot 10^{-1}$	92	$\pm$	19	-2.17	$\pm$	$7.75 \cdot 10^{-1}$
Northitude	100	-1.84	$\pm$	$1.09 \cdot 10^{-1}$	100	$\pm$	0	-1.79	$\pm$	$3.75 \cdot 10^{-1}$
Eastitude	66	$-9.27 \cdot 10^{-1}$	$\pm$	$1.97 \cdot 10^{-1}$	63	$\pm$	40	$-8.62 \cdot 10^{-1}$	$\pm$	$6.52 \cdot 10^{-1}$
Shrubs	81	4.45	$\pm$	$7.95 \cdot 10^{-1}$	74	$\pm$	37	6.00	$\pm$	5.56
Mosaic	50	2.33	$\pm$	$6.55 \cdot 10^{-1}$	56	$\pm$	42	4.30	$\pm$	5.46
No veg.	38	$-9.20 \cdot 10^{-1}$	$\pm$	$6.04 \cdot 10^{-1}$	57	$\pm$	40	$8.66 \cdot 10^{-1}$	$\pm$	4.93
Pioneer veg.	91	-9.39	$\pm$	1.26	93	$\pm$	19	$-1.01 \cdot 10^1$	$\pm$	3.67
Alpine meadows	38	1.19	$\pm$	$3.46 \cdot 10^{-1}$	44	$\pm$	44	3.12	$\pm$	4.82
Snowbed veg.	96	4.74	$\pm$	$7.25 \cdot 10^{-1}$	85	$\pm$	28	6.55	$\pm$	5.57
three hectares										
Intercept		$5.42 \cdot 10^1$	$\pm$	$1.92 \cdot 10^1$				$5.31 \cdot 10^1$	$\pm$	$6.48 \cdot 10^1$
Altitude	62	$-4.16 \cdot 10^{-2}$	$\pm$	$1.48 \cdot 10^{-2}$	60	$\pm$	35	$-4.18 \cdot 10^{-2}$	$\pm$	$4.70 \cdot 10^{-2}$
Altitude^2	53	$7.16 \cdot 10^{-6}$	$\pm$	$2.80 \cdot 10^{-6}$	52	$\pm$	34	$7.14 \cdot 10^{-6}$	$\pm$	$8.73 \cdot 10^{-6}$
Slope	67	$1.34 \cdot 10^{-1}$	$\pm$	$4.22 \cdot 10^{-1}$	73	$\pm$	32	$1.42 \cdot 10^{-1}$	$\pm$	$1.24 \cdot 10^{-1}$
Slope^2	45	$-1.61 \cdot 10^{-3}$	$\pm$	$8.19 \cdot 10^{-4}$	40	$\pm$	32	$-1.53 \cdot 10^{-3}$	$\pm$	$2.33 \cdot 10^{-3}$
Curvature	29	$3.50 \cdot 10^{-1}$	$\pm$	$1.85 \cdot 10^{-1}$	26	$\pm$	34	$3.46 \cdot 10^{-1}$	$\pm$	$5.32 \cdot 10^{-1}$
Curvature^2	100	-3.31	$\pm$	$3.47 \cdot 10^{-1}$	93	$\pm$	18	-3.16	$\pm$	1.09
Northitude	100	-2.24	$\pm$	$1.22 \cdot 10^{-1}$	100	$\pm$	0	-2.18	$\pm$	$4.74 \cdot 10^{-1}$
Eastitude	61	-1.02	$\pm$	$2.20 \cdot 10^{-1}$	57	$\pm$	42	$-9.41 \cdot 10^{-1}$	$\pm$	$7.91 \cdot 10^{-1}$
Shrubs	74	4.31	$\pm$	$8.17 \cdot 10^{-1}$	67	$\pm$	40	6.04	$\pm$	6.10
Mosaic	53	2.90	$\pm$	$7.46 \cdot 10^{-1}$	61	$\pm$	41	5.07	$\pm$	5.93
No veg.	17	$-3.87 \cdot 10^1$	$\pm$	$4.48 \cdot 10^{-1}$	40	$\pm$	41	1.81	$\pm$	5.19
Pioneer veg.	89	-9.22	$\pm$	1.24	92	$\pm$	20	$-1.00 \cdot 10^1$	$\pm$	3.54
Alpine meadows	32	1.01	$\pm$	$2.98 \cdot 10^{-1}$	40	$\pm$	43	3.23	$\pm$	5.18
Snowbed veg.	96	5.97	$\pm$	$8.35 \cdot 10^{-1}$	88	$\pm$	24	7.98	$\pm$	6.18

ence. Although we here present the results obtained using a buffer area of two hectares, we found that the curves are similar for all the buffer areas.

The linear and the quadratic terms of the altitude are included in the model with a posterior probability around 0.5 using all the buffer areas. The coefficients for the altitude are negative in the linear term and positive in the quadratic term. However, the habitat suitability curve reported in figure 3.6.a suggests that the suitability decreases with the altitude and reaches a minimum at the highest elevations in the valley. According to literature, the most suitable altitudes for the species ranges approximately between 1650 m a.s.l. and 1950 m a.s.l. (Cantini *et al.*, 1997; Borgo, 2003) with a maximum of about 3000 m a.s.l.. Since the valley ranges between 2200 and 3100 m a.s.l., at the higher limit of the marmot altitude range, the decrease of the suitability with the altitude is in line with findings of past studies.

The slope is included with a positive linear term and a negative quadratic term; the suitability is therefore maximal for intermediate values of slope. However, the quadratic term of slope is included with a low probability (always below 0.5), and the habitat suitability curves reported in figure 3.6.b show that the suitability is practically an increasing function of the slope for the interval of slopes present in the study area is considered. In this case, we have conflicting results reported in literature, with an optimal slope that varies from 0 to 60° (López *et al.*, 2009).

For the curvature, the linear term is included with a positive effect and the quadratic term with a negative effect, thus the maximum of the suitability is reached for intermediate values of the curvature; the peak is in fact evident in all the habitat suitability curves of figure 3.6.c. The peak of the habitat suitability curves occur at positive values of the curvatures, i.e. convex terrains, which favour the presence of burrows. The two terms have a probability of inclusion that, with the size of the buffer area, decreases for the linear term and increases for the quadratic term. Strongly convex and concave terrains are therefore strongly avoided.

The *northitude* negatively influences the presence of burrows, thus suggesting that marmot prefers southerly exposed slopes, as previously reported in several studies (e.g. Borgo, 2003). Differently from what is reported in literature, in our case the Alpine marmot shows a preference for the westerly exposed slopes, since the parameter of *eastitude* is negative. This result can be partially due to the valley shape, because easterly exposed areas mainly located at a high elevation in the valley and are characterized by absence of vegetation and low suitability.

The vegetation covers that reduce the probability of presence are the pioneer vegetation and the no vegetation cover. The former has a clear neg-

(a) Altitude

(b) Slope

(c) Curvature

(d) Northitude

(e) Eastitude
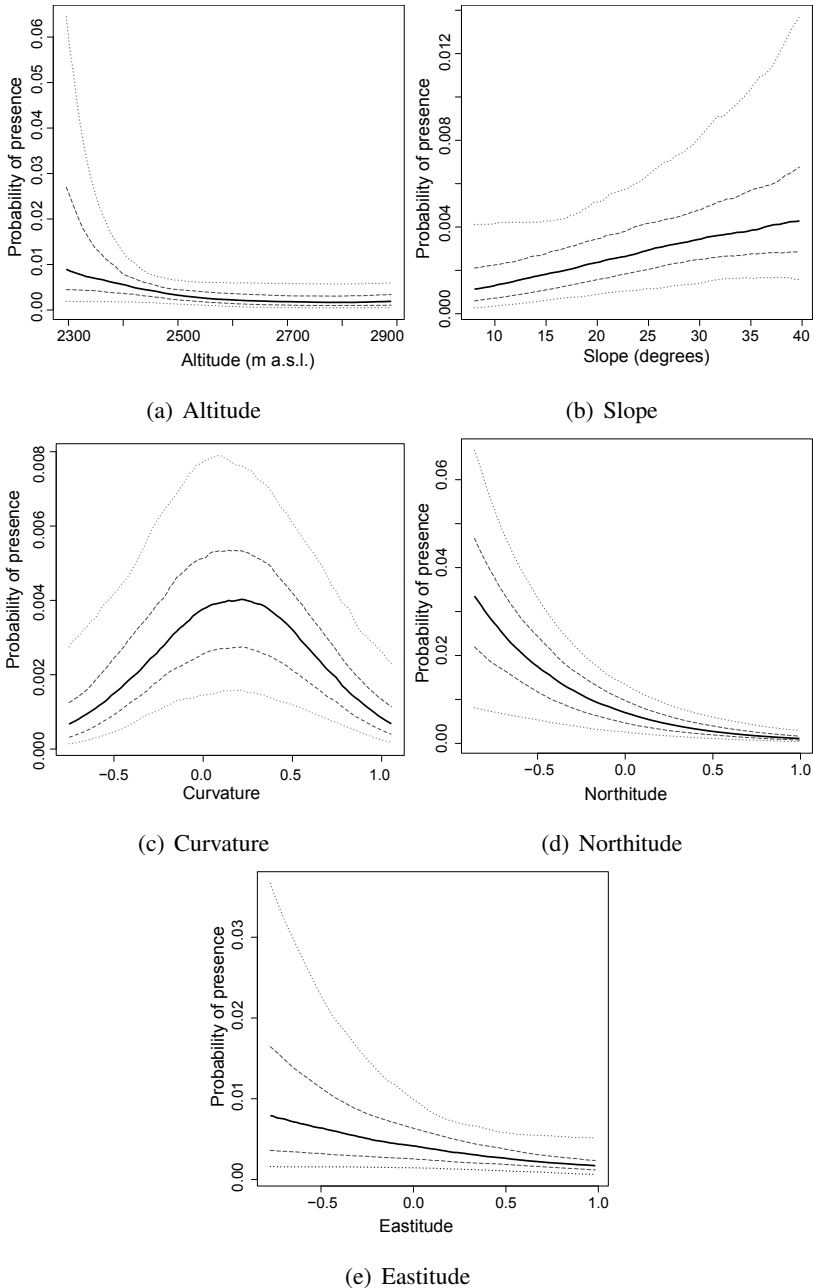
Figure 3.6: *Habitat suitability curves: probabilities of presence of burrows as functions of each non-vegetation covariate, obtained fixing the remaining covariates at their average value. The different curves represent bootstrap percentiles: black thick solid line is the 50th percentile, black dashed lines the quartiles and grey dotted lines the 5th-95th percentile. Results refer to a buffer area of 2 hectares.*

68

(a) Shrubs

(b) Mosaic: shrubs & meadows

(c) No vegetation

(d) Pioneer vegetation

(e) Alpine meadows

(f) Snowbed vegetation
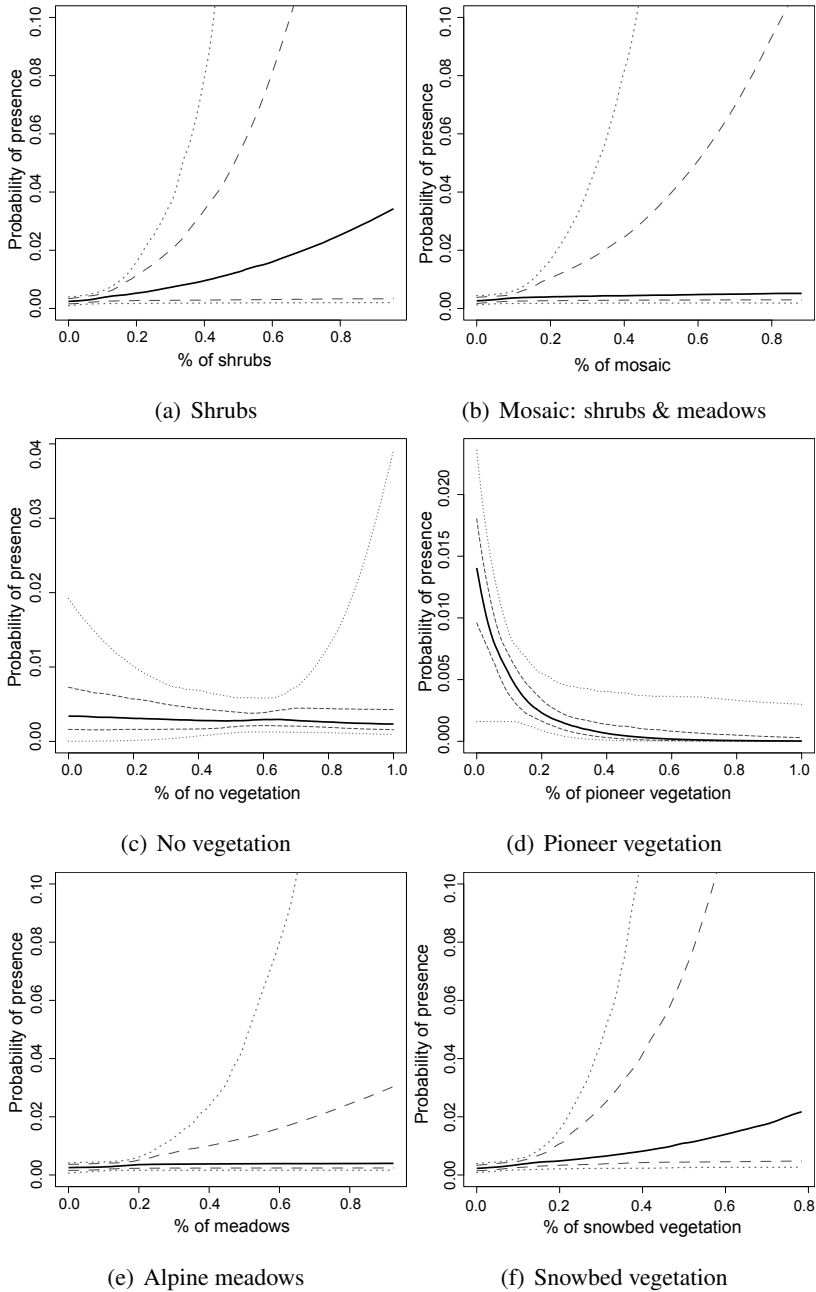
Figure 3.7: *Habitat suitability curves: probability of presence of burrows as a function of each vegetation covariate, obtained fixing the remaining covariates at their mean value. Curves have the same meaning as in figure 3.6.*

ative effect using all the buffer area sizes, and the probability of presence decreases rapidly even if a small portion of pioneer vegetation cover is included in the buffer area (see figure 3.7.d). The effect of the no vegetation cover is less strong. A cell is in fact clearly avoided if there is an high proportion of bare ground in close proximity, since the probability of inclusion of this variable in the model is 0.97 for a buffer area of one hectare (see table 3.5). This covariate is instead less important if a larger buffer area is considered. The habitat suitability curves of figure 3.7.c show that, from the 5th to the 75th percentile, the probability of presence slightly decreases with the % of no vegetation. However, for a small fraction of the bootstrap extractions, an high percentage of no vegetation cover favours the presence of the species (see the 95th percentile of figure 3.7). This result suggests that a consistent subset of the presence data has a relevant % of no vegetation cover in the surrounding. A possible interpretation of this result is that marmots can take advantage of the loose soil for digging in scree slopes.

The other vegetation covers, namely Alpine meadows, shrubs, snowbed vegetation and mosaic of shrubs and meadows favour the presence of marmot burrows. This result is in line with the preferences reported in the literature for which Alpine meadows and shrubs are the preferred type of vegetation cover (Borgo, 2003). The result on the snowbed vegetation is instead completely innovative since in literature there are no species distribution studies that report a fine classification of the vegetation as the one used here. Moreover, the posterior probability of inclusion of the snowbed vegetation covariate is near one for the buffer areas of two and three hectares, while it is below 0.5 for a buffer area of one hectare. This result suggests that the presence of alpine valley vegetation favours the presence of the species even it is not in the immediate surrounding of the burrows. The suitability curves of the vegetation covers that favour the presence of the species have all a similar shape. In all the cases there are some bootstrap extractions for which the given % of cover can strongly drive the probability of presence. The 95th percentile of the bootstrapped suitability curve is in fact widely variable from near zero to one. However, the majority of the bootstrap extractions have a less strong effect, as can be seen in the other percentiles reported in figure 3.7.a,b,e and f.

The results of the predictions on the entire area are reported in figure 3.8 for the model that consider a buffer area of two hectares, while they are reported in the appendices for the other buffer area sizes. The mapped predictions are the mean of the predictions of the six models calibrated alternatively excluding one of the vegetation variable, as explained in the methodological section. The results show that the predictions are similar
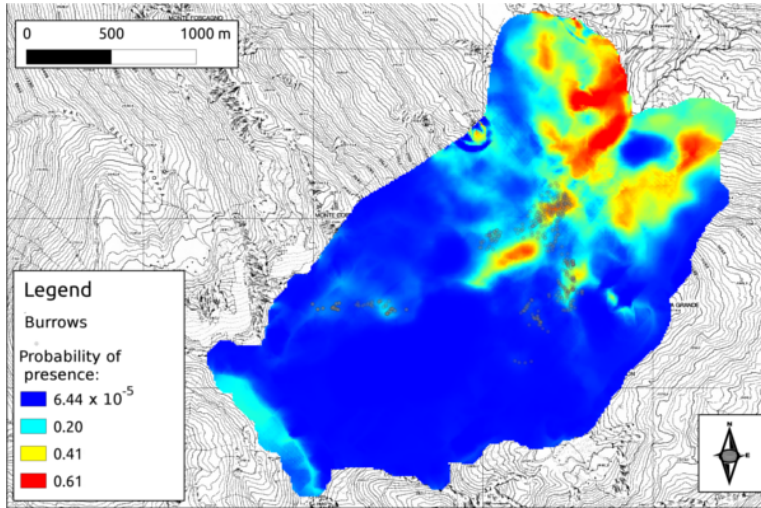
Figure 3.8: *Map of the predicted probability of presence of the burrows in all the valley, made using the results of the model that consider a buffer area of two hectares. The positions of censused burrows are reported as grey circles.*

for all the buffer areas, even if the predictions obtained with larger buffer area sizes are, as expected, spatially more smoothed. As suggested by the good results obtained with the performances criteria, in all the prediction maps, the probability of presence is consistently higher were the presence of burrows were actually observed.

3.6 Discussion and conclusions

In this chapter, we used fine scale habitat characteristics and presence-absence data we personally collected in two campaigns of 2011 and 2012 to develop marmot burrows distribution models in a high altitude Alpine valley. In particular, the availability of an accurate vegetation map of the valley permits to study the precise role of the different soil covers.

The developed models have good performances using both the **AUC** (**A**rea **U**nder the "*Receiver Operating Characteristic*" **C**urve) and the accuracy (fraction of correctly classified instances), and show a good predictive ability. However, if the classical threshold of 0.5 is used for classification, the sensitivity (fraction of correctly classified presence) of the models in prediction is very low. The alternative prevalence threshold permits to have more balanced performances among sensitivity and specificity, with a small reduction of the overall accuracy. Thus, to effectively predict the presence

of marmot burrows in unexplored areas, the results strongly suggest the use of prevalence threshold rather than the 0.5 threshold

The most important variables are the aspect, the curvature and the vegetation cover. The Alpine marmot prefers in fact southerly exposed slopes and ground that are moderately convex. The former result is coherent with the preferences reported in literature, for which the Alpine marmot generally prefers southerly exposed slopes that are warmer in the hibernation period. A possible explanation of the curvature effects is that burrows excavated on concave terrains are more likely to be affected by flooding. On the other hand, burrows on strongly convex grounds can be greatly exposed to predation or other risks.

Surprisingly enough, the altitude is an important covariate but not a major factor in the developed species distribution models for our case study, in contrast with what is reported in the majority of previous studies. A possible explanation is that the altitude is usually included also as a proxy for the vegetation cover, which is instead explicitly included here as an independent set of covariates. This hypothesis is supported by the fact that, if a coarse vegetation map is used in place of the fine scale map, altitude becomes one of the most important variables to be included in the model (Corani & Mignatti, 2013b,a). Moreover, a similar variable result is reported also in a study conducted on the Pyreneese by López *et al.* (2010), for which the altitude is in the pool of potential covariates but is not selected in the final model.

The results on the vegetation show that the pioneer vegetation and the no vegetation cover are strongly avoided while alpine meadows, shrubs and snowbed vegetation favour the presence of burrows. The crucial role of the vegetation against the altitude in affecting the probability of presence of the species is clear. This suggests that the potentialities for upward shift of the areal of distribution of marmots could be mainly regulated by the changes in the vegetation, rather than by the direct effect of the changes in temperature. In this sense, the uplift of the tree line, which occurs both for the increases in temperature and the abandonment of pastures (Gehrig-Fasel *et al.*, 2007), directly reduces the territory suitable for the Alpine marmot invading Alpine meadows and shrublands. On the other hand, the invasion of the Alpine meadows in new areas at high altitude follows precise successional stages (Caccianiga & Andreis, 2004), in which pioneer or snowbed species are usually the first invaders. This two vegetation covers are both responding very fast to the climatic change (Grabherr *et al.*, 1994; Bahn & Körner, 2003), but we showed that they have a clear different impact on the distribution of Alpine marmot. Moreover, the snowbed vegetation is

extremely sensitive to the variations of the snow cover period, and are therefore regarded to be particularly vulnerable to predicted decrease in snowfall (Carbognani *et al.*, 2012). It is therefore very important to understand the patterns of changes in the vegetation to understand the potential impact on the distribution of the Alpine marmot.

The work presented in this chapter highlights how, for a high altitude species, the potential distribution of the fauna is strongly dependent the vegetation. In the climate change context, the potential intensity and timing of variation in the distribution of fauna due to changes in the meteorological conditions is therefore likely to be mediated by the response of the vegetation. It is also clear that the availability of suitable territories might strongly influence also the population dynamics of the species. However, considering all these aspect for modelling the dynamics is often hard because of deficiencies in data or in the existing literature. Being aware of these limitations, in the next chapters we study the dynamics of two high altitude alpine species using the meteorological variables as a proxy for all the potential variations in the status of the environment.

Bibliography

Allainé, D., Rodrigue, I., Le Berre, M. & Ramousse, R. 1994: Habitat preferences of alpine marmots, Marmota marmota. Canadian Journal of Zoology 72(12): 2193–2198.

Armitage, K.B., Downhower, J.F. & Svendsen, G.E. 1976: Seasonal Changes in Weights of Marmots of Marmots in Weights Seasonal Changes. American Midland Naturalist 96(1): 36–51.

Arnold, W. 1992: Adaptation to the cold—the physiology of marmot hibernation. In Proceedings of the 1st international symposium on alpine marmots. (pp. 31–39).

Arnold, W., Heldmaier, G., Ortmann, S., Pohl, H., Ruf, T. & Steinlechner, S. 1991: Ambient temperatures in hibernacula and their energetic consequences for alpine marmots Marmota marmota. Journal of Thermal Biology 16(4): 223–226.

Arnold, W. & Walter, A. 1990: The evolution of marmot sociality: II. Costs and benefits of joint hibernation. Behavioral Ecology and Sociobiology 27(4): 239–246.

Bahn, M. & Körner, C. 2003: Recent increases in summit flora caused by warming in the Alps. In Alpine biodiversity in Europe, vol. 167, (pp. 437–441).

Borgo, A. 2003: Habitat requirements of the Alpine marmot Marmota marmota in re-introduction areas of the Eastern Italian Alps. Formulation and validation of habitat suitability models. Acta Theriologica 48(4): 557–569.

Caccianiga, M. & Andreis, C. 2004: Pioneer herbaceous vegetation on glacier forelands in the Italian Alps. Phytocoenologia 34(1): 55–89. doi: 10.1127/0340-269X/2004/0034-0055.

Cannone, N., Sgorbati, S. & Guglielmin, M. 2007: Unexpected impacts of climate change on alpine vegetation. Frontiers in Ecology and the Environment 5(7): 360–364. doi:10.1890/060141.

Cantini, M., Bianchi, C., Bovone, N. & Preatoni, D. 1997: Suitability study for the alpine marmot (Marmota marmota marmota) reintroduction on the Grigne massif. Hystrix, the Italian Journal of Mammalogy 9(1-2).

Carbognani, M., Petraglia, A. & Tomaselli, M. 2012: Influence of snowmelt time on species richness, density and production in a late snow-bed community. Acta Oecologica 43: 113–120. doi:10.1016/j.actao.2012.06.003.

Corani, G. & Mignatti, A. 2013a: Credal Model Averaging for modeling presence-absence. Ecography in review.

Corani, G. & Mignatti, A. 2013b: Credal model averaging of logistic regression for modeling the distribution of marmot burrows. In Eighth International Symposium on Imprecise Probability: Theories and Applications. Compiègne, France, (p. In press.).

Elkan, C. 2001: The foundations of cost-sensitive learning. Proc. Int. Joint Conference on Artificial Intelligence (IJCAI - 01) (pp. 973–978).

Gehrig-Fasel, J., Guisan, A. & Zimmermann, N.E. 2007: Tree line shifts in the Swiss Alps: Climate change or land abandonment? Journal of Vegetation Science 18(4): 571–582.

Grabherr, G., Gottfried, M. & Pauli, H. 1994: Climate effects on mountain plants. Nature 369: 448.

Graf, R.F., Bollmann, K., Suter, W. & Bugmann, H. 2005: The Importance of Spatial Scale in Habitat Models: Capercaillie in the Swiss Alps. Landscape Ecology 20(6): 703–717. doi:10.1007/s10980-005-0063-7.

Guglielmin, M. 2003: Permaclim: a model for the distribution of mountain permafrost, based on climatic observations. Geomorphology 51(4): 245–257. doi:10.1016/S0169-555X(02)00221-0.

Guglielmin, M. & Camusso, M. 2004: An old relict glacier body preserved in permafrost environment: The Foscagno rock glacier ice core (Upper Valtellina, Italian Central Alps). Arctic, Antarctic, and Alpine Research 36(1): 108–116.

Guisan, A. & Thuiller, W. 2005: Predicting species distribution: offering more than simple habitat models. Ecology Letters 8(9): 993–1009. doi:10.1111/j.1461-0248.2005.00792.x.

Guisan, A. & Zimmermann, N. 2000: Predictive habitat distribution models in ecology. Ecological modelling 135(2-3): 147–186. doi:10.1016/S0304-3800(00)00354-9.

Hand, D. 2010: Evaluating diagnostic tests: The area under the ROC curve and the balance of errors. Statistics in medicine 29(14): 1502–10. doi: 10.1002/sim.3859.

Hayes, S.R. 1976: Daily Activity and Body Temperature of the Southern Woodchuck , Marmota monax monax , in Northwestern Arkansas. Journal of Mammalogy 57(2): 291–299.

Herrero, J., Zima, J. & Coroiu, I. 2008: Marmota marmota. In: IUCN Red List of Threatened Species. Version 2013.1. `www.iuncredlist.org`. Downloaded on 19 July 2013.

Körner, C., All, A.M. & Terms, J. 2007: Climatic treelines: conventions, global patterns, causes. Erdkunde 61: 316–324. doi:10.3112/erdkunde.2007.04.02.

Lenti Boero, D. 2003: Long-term dynamics of space and summer resource use in the alpine marmot (Marmota marmota L.). Ethology Ecology & Evolution 15(4): 309–327.

López, B., Figueroa, I., Pino, J., López, A. & Potrony, D. 2009: Potential distribution of the alpine marmot in Southern Pyrenees. Ethology Ecology & Evolution 21(3-4): 225–235.

López, B., Pino, J. & López, A. 2010: Explaining the successful introduction of the alpine marmot in the Pyrenees. Biological Invasions 12: 3205–3217. doi:10.1007/s10530-010-9712-0.

Manel, S., Williams, H.C. & Ormerod, S.J. 2001: Evaluating presence–absence models in ecology: the need to account for prevalence. Journal of applied Ecology 38(5): 921–931.

Melcher, J.C., Armitage, K.B. & Porter, W.P. 1990: Thermal on the Activity and Energetics of Influences Marmots (Marmota flaviventris). Physiological Zoology 63(4): 803–820.

Meynard, C.N. & Quinn, J.F. 2007: Predicting species distributions: a critical comparison of the most common statistical models using artificial species. Journal of Biogeography 34(8): 1455–1469. doi: 10.1111/j.1365-2699.2007.01720.x.

Perrin, C. & Berre, D. 1993: Socio-spatial Organization and Activity Distribution of the Alpine Marmot Marmota marmota: Preliminary Results. Ethology 93: 21–30.

Riley, S.J., DeGloria, S. & Elliot, R. 1999: A terrain ruggedness index that quantifies topographic heterogeneity. Intermountain Journal of sciences 5(1-4): 23–27.

Schweiger, A., Nopp-Mayr, U. & Zohmann, M. 2012: Small-scale habitat use of black grouse (*Tetrao tetrix L.*) and rock ptarmigan (*Lagopus muta helvetica* Thienemann) in the Austrian Alps. European Journal of Wildlife Research 58: 35–45.

Tafani, M., Cohas, A., Bonenfant, C., Gaillard, J.M. & Allainé, D. 2013: Decreasing litter size of marmots over time: a life history response to climate change? Ecology 94(3): 580–6.

Türk, A. & Arnold, W. 1988: Thermoregulation as a limit to habitat use in alpine marmots (Marmota marmota). Oecologia 76(4): 544–548.

3.A   Appendix I
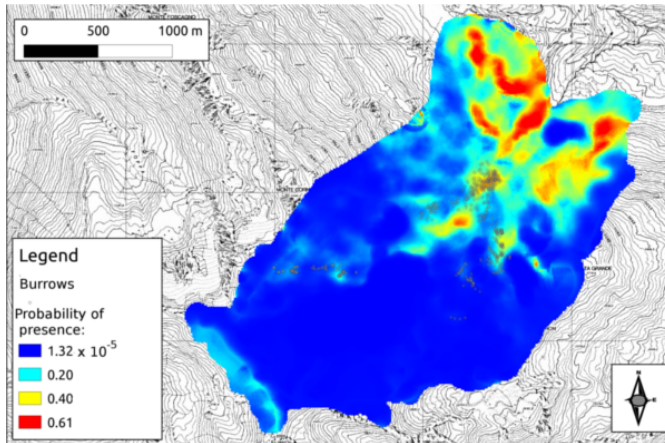
(a) One hectare
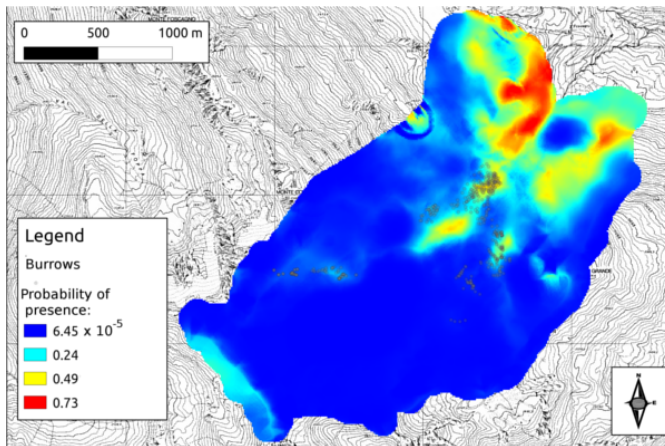
(b) Three hectares

Figure 3.9: *Map of the predicted probability of presence of the burrows in all the valley, made using the results of the models that consider a buffer area of one or three hectares. The positions of censused burrows are reported as grey circles.*

Interplay between population density and climate on the dynamics of the black grouse in the Piedmont region

4.1 Abstract

Because of its particular environmental needs and sensitivity to the human disturbance, *Tetrao tetrix* may be a key species in studying the effects of climate change on the Alpine fauna. Previous studies outlined the importance of (a) winter snow, that must be sufficiently abundant to let individuals dig their dens, (b) not so cold winters and (c) good meteorological conditions in the post-hatching period. However, the majority of the studies on how the climate affects black grouse dynamics are conducted on the "lowland" populations at the northern latitudes, while less is known about Alpine populations, at the Southern edge of the species distribution. The population abundance of black grouse in the Italian Alps constantly declined in the last decades.

Here we study the influence of geographical localization, population density and meteorological conditions on four demographic parameters of the black grouse populations in 17 Alpine districts of the Piedmont region

(Italy), using census data from 1999 to 2009. The demographic parameters under study are the annual growth rate and three components of fertility: the percentage of nesting females, the brood size and the breeding success.

First, we cluster the districts where demographic parameters are similar and we properly reduce the number of meteorological variables that can affect the population dynamics. Then we develop predictive models using Bayesian Model Averaging techniques (BMA) and project the population abundance and the demographic parameters in future decades, using a realization of a regional climatic model based the IPCC climate scenario A1B (Protheus model).

Overall, the results show that density dependence is, in all districts, the major driver of population growth rate. Quite surprisingly, we found that male population density significantly and positively affects the breeding success and the brood size, but not the percentage of nesting females.

As for climate, the growth rate decreases with the increasing of the mean temperature measured in the second half of April, just before the critical period of the formation of leks. The results provide quantitative support for the importance of meteorological conditions in the post hatching period for the percentage of nesting females (positively affected by high temperatures), the breeding success and the brood size (negatively affected by high precipitations). Moreover, the breeding success is positively affected by high precipitations in late November of the previous year, while the brood size is negatively affected by high precipitations in late January, which probably decreases food availability.

Using climatic simulations based on the IPCC scenario A1B as forcing of the best multivariate model, we found that climate change should not cause, *per se*, a major risk of extinction for the population, even though it might be responsible for relevant changes of the dynamics.

4.2   Introduction

The black grouse (*Tetrao tetrix*) is a large tetraonid mainly distributed in the northern part of Eurasia, but also present on the Alps, which represent the southern edge of its areal distribution. The species has a direct economical relevance because it is a game bird. Many populations are reported to have decreased in the last years in the western-central part of Europe (Storch, 2007), in Scotland (Geary *et al.*, 2012) and on the Italian Alps (Brichetti & Fracasso, 2004). However BirdLife International (2012) classify the species in the *least concern* category.

The Alpine populations of black grouse show a preference for patchy

habitat in which dwarf shrub and rock covers are available. As a consequence, the species has, in the past, expanded its areal distribution on the Alps with the lowering of the timberline caused by pasturing (Schweiger *et al.*, 2012). Nowadays, the abandonment of the pastures and the increase in temperatures have caused an upward shift of the vegetation, thus to a shrinking of the habitat suitable for the species. The altitude range is approximately 2000-2400 m a.s.l. (Cattadori & Hudson, 1999). In winter, to reduce the energetic consumption, black grouse stays in holes dug in the snow. These peculiar needs make the species particularly sensitive to human disturbance, such as the land use change, road network in the forests and tourism (Ortigosa *et al.*, 2003), and winter outdoor activities (Arlettaz & Patthey, 2007; Patthey *et al.*, 2008).

The life cycle, sketched in figure 4.1 is differentiated by sex. The mating season occurs between April and May, when the females reach the leks where the males sing. The females that successfully mate, move to areas suitable for nesting to lay their eggs, which hatch after 3-4 weeks. The hens and their chicks live together until autumn, when the young males leave their mother. In autumn, some of the females visit the "autumnal leks", probably to evaluate the breeding potentiality for the following spring. The female juveniles disperse in two different periods, in October and in the subsequent spring (Marjakangas & Kiviniemi, 2005; Caizergues & Ellison, 2002). Males have the same dispersion period. However they tend to remain near their birthplace. They in fact disperse less frequently and at a shorter distance then females. During winter, males and females live together is sexually mixed groups. The first days after hatching, in June, are the period characterized by the highest mortality rate for both hens and chicks. Hens are in fact more susceptible to predation (Hannon & Martin, 2006), while the chicks are sensitive to cold and humidity because of their lack in thermoregulation (Boggs *et al.*, 1977). Moreover, since the Black grouse is a ground nesting bird, high rainfalls can wash away the eggs from the nests.

Only few studies have been published on the influence of climate on the population dynamics of black grouse, and mainly on lowland populations. Moreover, the different studies have sometimes contrasting results, reporting negative or positive effects on the same (or analogous) variable. Loneux *et al.* (2003) published a study in which they attempt to model the dynamics of a lowland population in Belgium using linear autoregressive models which include exogenous meteorological variables. They identify a positive effect of high precipitations in January and high temperatures in June. The former effect is probably linked with the availability of a snow
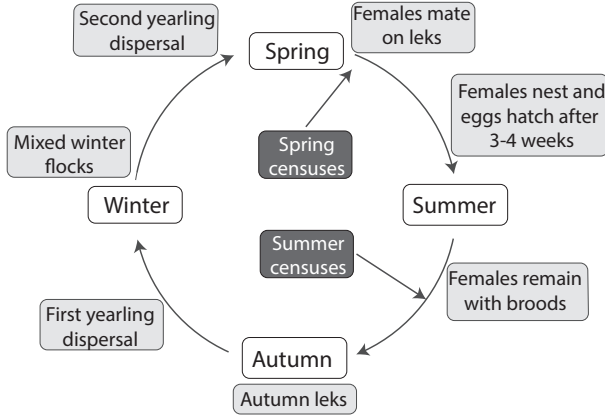
Figure 4.1: *Sketch of the main events in the yearly life cycle of Black grouse, adapted from `http://blackgrouseresearch.jyu.fi/index.html`. Moreover, we report the timing of the two yearly censuses performed in the Piedmont Alpine districts.*

surface tick enough to dig the winter shelters. Conversely, high winter temperatures (from November to March) and high precipitations in September seems detrimental for the population. Precipitations in June are also taken into account with a negative sign. However, the model proposed by the author is probably overfitted, because only 36 years of data are available, while 13 parameters have to be estimated.

A negative effect of high precipitations in June on the breeding success of the females (number of chicks per female) is reported for a Scottish population (Summers & Green, 2004). Selås *et al.* (2010) found a delayed negative effect of warm summer temperatures on the breeding success. An interesting effect of climate change on the population dynamics is described in Ludwig & Alatalo (2006) for a declining population of black grouse in Sweden. The spring warming caused an anticipation of the egg-laying and hatching. Since the early summer warming was less strong, the chicks have to face colder post-hatching conditions, thus leading to an overall decrease of the breeding success and to a consequest decrease in the population abundance. The importance of snow depth and snow melting has been studied for other species of grouse (Novoa *et al.*, 2008; Clarke & Johnson, 1992; Wang & Hobbs, 2002).

According to the Ph.D. thesis of Viterbi (2012), both density and climate affect the black grouse population in the Orsiera-Rocciavrè Park (Piedmont, Italy). In particular, they found that local populations suffer the high pre-

cipitation in the first half of June (critical post-hatching period) and benefit from high daily temperature range in December.

We here study the dynamics of the Piedmont populations of black grouse using censuses performed in 17 Alpine districts. In particular we concentrate on growth rate obtained by spring counts of males, and on three fertility components calculated using summer censuses. Before analysing the joint effects of population density and climatic conditions on the growth rate, we study their independent role. Projections of the future climatic conditions given by a regional model are used to assess the future status of the population.

4.3 Materials

4.3.1 Population data

The study area is located in the Alpine territory of the Piedmont Region, North-Western Italy (see figure 4.2). This territory is administratively divided into 17 Alpine districts in six provinces: one in Biella (BI1), one in Vercelli (VC1), three in Verbano-Cusio-Ossola (VCO1, ..., VCO3), five in Turin (TO1, ..., TO5) and seven in Cuneo (CN1, ..., CN7). Hunting is permitted in the districts in autumn.
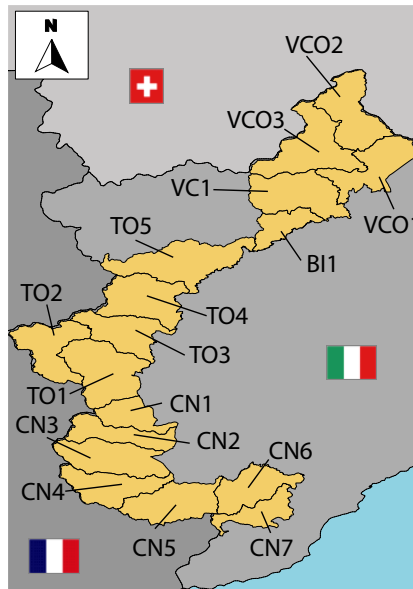
Figure 4.2: *Map of the 17 Alpine districts of the Piedmont region.*

The counts of the black grouse populations are performed two times a year in each district, in spring and in late summer. Spring censuses estimate male population density in each district ($M_{t,c}$), where t is the year and c is the district. Counts are carried out during lek formation, in suitable areas characterized by the presence of important leks. Operators are distributed in fixed points inside the census areas. The late summer censuses are carried out using hunting dogs to estimate the number of females ($F_{t,c}$), nesting females ($B_{t,c}$) and juveniles ($J_{t,c}$). Summer data are less reliable than spring data, and counts of females and juveniles suffer from the risk of underestimation. Moreover, the original dataset does not report some important details, such as the paths travelled by the dogs, that would be useful to estimate the detectability and correct the counts (e.g. see the distance sampling techniques described in Dahlgren *et al.*, 2012). However, for each detected nest, there is an high confidence that the number of juveniles is correctly reported; therefore, the mean number of juveniles per nest is not expected to be affected by underestimates in the counts. Furthermore, it is interesting to analyse also the other summer data to detect if there are strong signals in the data series. Male density data are available from 1998 to 2010 in the district TO1, and from 1999 to 2010 in all the other districts. Late summer censuses are available from 1996 to 2010 for $F_{t,c}$ and $J_{t,c}$, with only few data before 1999 (only TO1 in 1996 and 1997, and 11 districts in 1998) and only few missing data since 1999 (TO4 and TO5 in 1999, TO2 in 2000). B_t data are available only from 2001, with two missing data: BI1 in 2001 and TO5 in 2002.

Male density data for all the districts are reported in figure 4.3, in which no clear trends can be detected. Moreover, the inter-cluster (intra-annual) variability appears to be wider than the inter-annual variability. Late summer censuses are instead not directly reported here, because they are given only as absolute values, while the census area change both among districts and among different years for the same district. It has therefore no sense to directly compare the values of the abundances ($J_{t,c}$, $F_{t,c}$ and $B_{t,c}$), which we instead used to calculate comparable rates.

Despite the fact that spring censuses are performed in the proximity of important leks, and thus an overestimation in densities is expected, the densities are comparable with those reported for an Alpine French population (Caizergues & Ellison, 2002) (12-37 $birds/km^2$).

To study the dynamics we calculated, using the available data, four components of the fitness; the instantaneous growth rate and three fertility components:
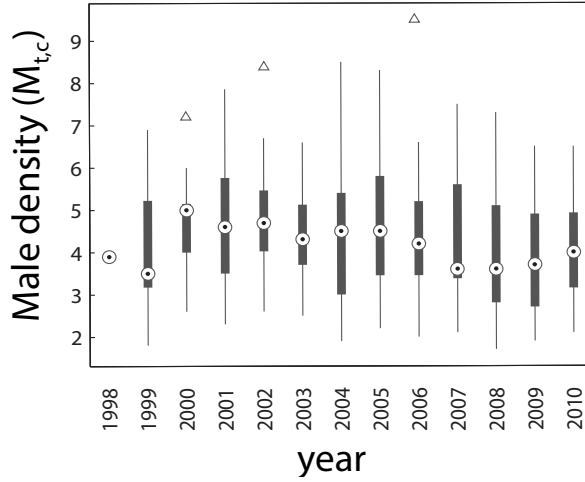
Figure 4.3: *Boxplots of the temporal dynamics of male densities ($M_{t,c}$) measured in the 17 Alpine districts. The median values are plotted as circles with an inner dot, the interquartile ranges with thick lines, the entire range of data with thin lines, excluding outliers (empty triangles). Outliers are defined as points larger than the 75th percentile plus 1.5 times the interquartile range, or smaller than the 25th percentile minus 1.5 times the interquartile range.*

- The instantaneous growth rate:

$$\log(\lambda_{t,c}) = log\left(\frac{M_{t+1,c}}{M_{t,c}}\right) \tag{4.1}$$

- the percentage of nesting females:

$$\psi_{t,c} = 100\frac{B_{t,c}}{F_{t,c}}$$

- the breeding success:

$$\rho_{t,c} = \frac{J_{t,c}}{F_{t,c}}$$

- the brood size:

$$\phi_{t,c} = \frac{J_{t,c}}{B_{t,c}}$$

Fitness components for the 17 districts are reported in figure 4.4, while their mean values and standard deviations for all the 17 districts are listed in table 4.6. The global temporal mean of the growth rate ($\log(\bar{\lambda})$) is close

to 0 in each district, with a minimum of $log(\overline{\lambda}_{TO4}) = -0.045$ years^{-1} and a maximum of $log(\overline{\lambda}_{CN3}) = 0.069$ years^{-1}. The overall mean breeding success ($\overline{\rho} =\sim 2.4$ Juveniles/Female) is higher than the value reported in literature for other populations in the Alpine region, which is between 1 and 2 juveniles per female (see Caizergues & Ellison, 2000; Barnagaud *et al.*, 2011, for a French population and Ortigosa *et al.* (2003) for a population of Trentino, Italy). Also the overall average brood size ($\overline{\phi} =\sim 3.9$ Juveniles/Breeding hen) is higher than the value reported in literature (~ 3 in Barnagaud *et al.* (2011) and 3.42 in Ortigosa *et al.* (2003)). The mean percentage of nesting females ($\overline{\psi} \sim 58\%$) is instead similar to the values reported for the French and the Italian populations.
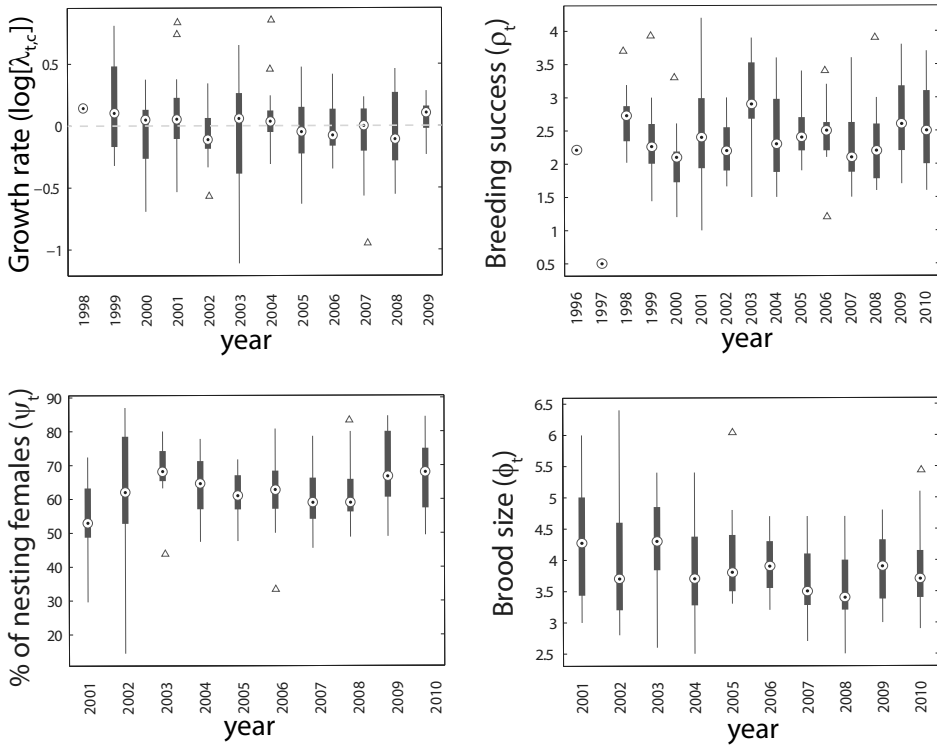
Figure 4.4: *Boxplots of the temporal dynamics of the demographic parameters measured in the 17 Alpine districts. The median values are plotted as circles with an inner dot, the interquartile ranges with thick lines, the entire range of data with thin lines, excluding outliers (empty triangles). Panels: a) istantaneous growth rate; b) breeding success; c) percentage of nesting females; d) brood size.*

4.3.2 Meteorological data

The historical meteorological data used for model calibration were provided by the Regional Environmental Agency (ARPA) of the Piedmont region as spatially distributed values referring to cells with a side of 0.125 degrees (about 14 km). For the future projections, we used the climatic predictions given by a realization of the regional climatic model PROTHEUS (Artale *et al.*, 2010; Dell'Aquila & Calmanti, 2012), based on the IPCC scenario A1B and provided by A. Provenzale. This model has a spatial resolution of 30 km (about 0.27 degrees) and its predictions are available until 2049.

The meteorological variables available in both datasets are the daily amount of precipitation ($P_t(\tau)$), the maximum ($T_{Max,t}(\tau)$) and the minimum ($T_{min,t}(\tau)$) temperature, where τ is the day of the year and t the year. The mean daily temperature and the daily temperature range were calculated, respectively, as $T_{m,t}(\tau) = (T_{Max,t}(\tau) + T_{min,t}(\tau))/2$ and $\Delta T_t(\tau) = T_{Max,t}(\tau) - T_{min,t}(\tau)$. The meteorological data were then standardized using the reference period 1991-2009.

The values assigned to a district for each meteorological variable were calculated by elaborating its values in cells of the meteorological model that overlap with the suitable territory of the district. We define as "suitable" area (A_c) the portion of territory of district c in which the probability of presence of the species is greater than 0.5, according to a suitability map provided by R. Viterbi from the Institute of Atmospheric Sciences and Climate, CNR, Turin. Let us call $A_{l,c}$ the fraction of suitable area of the district c that also belongs to the cell l. The value of the generic climatic variable $X_{c,t}(\tau)$, for the day τ of the year t and for the district c, was calculated as:

$$X_{c,t}(\tau) = \sum_{\chi_c} \frac{A_{l,c}}{A_c} X_{t,l}(\tau) \tag{4.2}$$

where χ_c is the set of climatic cells overlapped with the suitable area of the district c.

To develop the models, we used the semi-month averaged meteorological variables, thus we averaged the meteorological values in the first half (1st-15th day, labelled as 1) and in the second half (16th-last day, labelled as 2) of each month, except for February (in which the first and the second half are, respectively, 1st-14th and 15th-last day). Therefore, as an example, with the notation $P_{Apr1,t+1}$ we name the standardized precipitation averaged in the first half of April of year $t + 1$. This averaging permits

to balance the necessity to have narrow temporal window reflecting the necessity of the species, and to filter out the high frequencies.

We limited the potential semi-months that can influence the growth rate at time t using a specific temporal window: from the first half of January of year t to the second half of April of year $t + 1$. The temporal window closes just before the counts of M_{t+1}, thus avoiding the inclusion of anti casual effects of climate. Similarly, we defined a temporal window that limits the potential influence of climate on the fertility components. This window starts in the first half of September of year $t - 1$ and ends in the second half of August of year t, thus including the entire 1 year period between two consecutive late summer censuses.

4.4   Methods

The strategy described in the previous section leads to the definition of many meteorological variables that can potentially influence the demographic parameters. Since there is uncertainty about which of these variables have to be included in the model, the model space obtained considering all the possible combinations of the variables is huge. Moreover, for each Alpine district and each fitness component, only few years of observations are available.

Since there are only few observations, the alternative of separately modelling each district would probably lead to the choice of really simple models (see chapter 2), thus to the risk of excluding weak (but important) effects. On the other hand, if data from all districts are aggregated, there is a considerable quantity of data for calibration, but the information on the spatial position of data is completely discarded (i.e. all the districts are considered as equivalent).

A theoretically sound solution to overcome this problem would be to use the so-called *mixed models* (Bolker *et al.*, 2009), in which the Alpine district (thus, spatial position) is included as a random categorical variable. However, a well established selection criteria that permits to discern among models with different fixed and random structures is still not available (Vaida & Blanchard, 2005). Moreover, the possible inclusion of random effects on the intercept or on the covariates further increases the model space dimension. Therefore, we decided to use an alternative approach, in which we reduce both the number of possible meteorological variables and the possible model structures. We used a clustering algorithm to decide which parameters can be regarded as common among groups of districts that have a similar behaviour, thus increasing the data to parameters ratio.

Overall, the methodology used to develop the predictive models for each component of fertility consisted therefore of two main steps:

1. a screening, in which the most important meteorological variables are selected, and data from different Alpine districts are potentially merged (cluster analysis);

2. calibration of the model parameters using Bayesian Model Averaging technique (BMA).

To select the most important meteorological variables, we studied the separate effect of each meteorological variable using the Pearson's coefficient for the linear correlation. The adopted criterion is to include, in the multivariate analysis, only the meteorological variables that are significantly linearly correlated with the given fitness component. The significance threshold is set to 0.2 to include also variables that have a weak effect *per se* but can be important when included in a multivariate model.

The clustering procedure aims at simplifying the model complexity with respect to a model that treats all the districts separately. More precisely, the basic model to perform the clustering is a linear regression in which the only explanatory variable is the male density (M_t):

$$y_{t,c} = \beta_{0,c} + \beta_{M,c}M_{t,c} \tag{4.3}$$

where $y_{t,c}$ is one of the defined demographic parameters in year t and in district c, while $\beta_{0,c}$ and $\beta_{M,c}$ are district specific intercept and slope. The complete clustering procedure is summarized in the flowchart of figure 4.5, and can be briefly described as follows. To better clarify the entire process, the details of the steps applied along this procedure to the four demographic parameters are provided in section 4.5 for the growth rate and in appendix 4.A for the fertility components.

Conceptually, the clustering is performed on two different levels: i) a clustering on the values of the slope ($\beta_{M,c}$), thus grouping districts that have similar density-dependence and ii) a clustering on the intercepts ($\beta_{0,c}$), grouping districts with a similar intrinsic value of the given fitting component:

i) *Clustering for the same density dependence (slope)*

If, using data from all the districts, I) the overall correlation between male density ($M_{t,c}$) and the demographic parameters is significant (Pearson's p value < 0.05) and II) there is evidence to suppose that the slope is not the same for all the districts (through an F-test), then
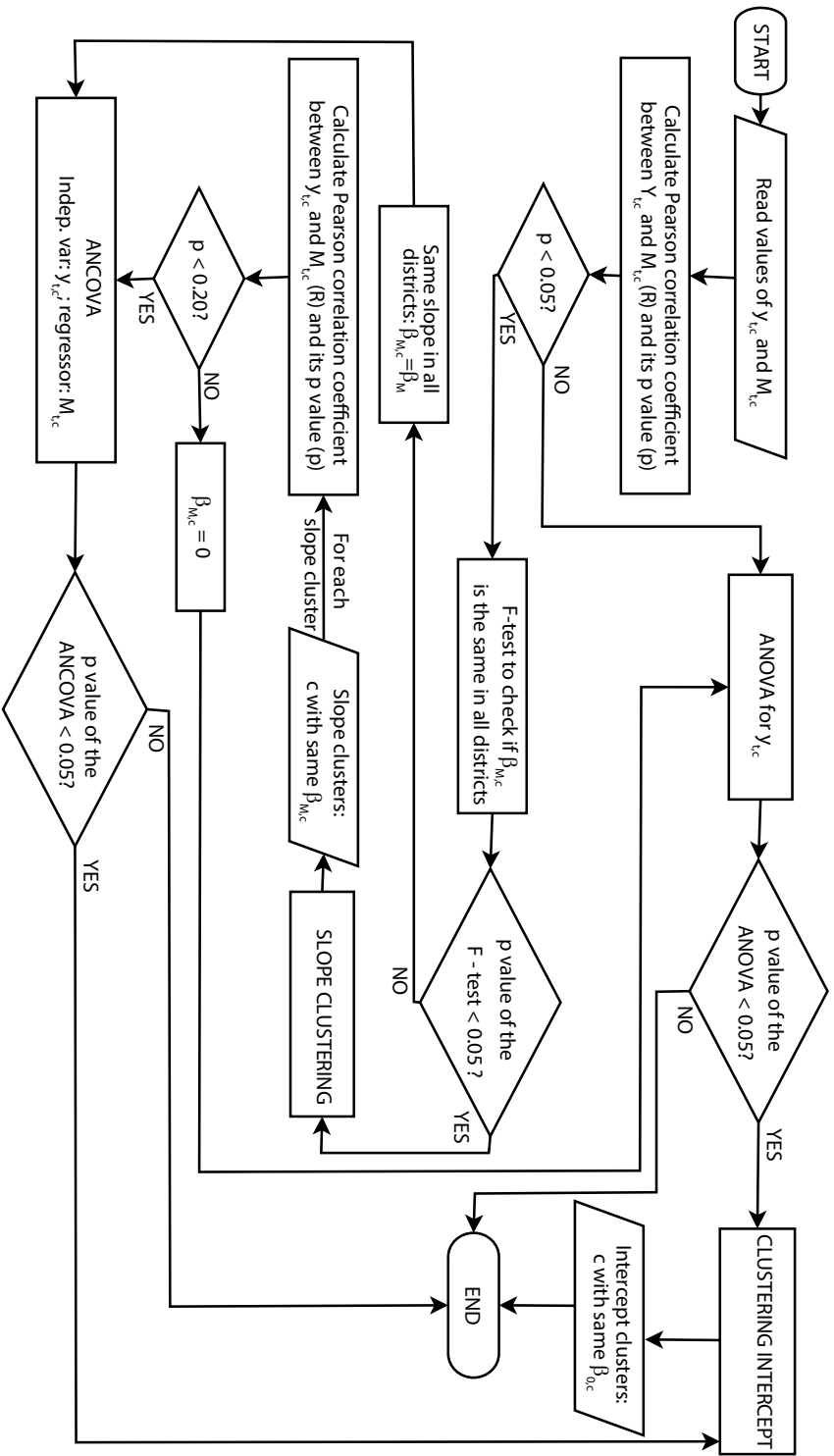
Figure 4.5: *Flowchart of the main aspects of the algorithm used to cluster the data from different Alpine districts. The meaning of the variables included in the blocks is explained in the text*

the slope $\beta_{M,c}$ is not regarded to be the same for all the districts. Districts are therefore grouped according to their value of $\hat{\beta}_{M,c}$ (box ‘‘SLOPE CLUSTERING’’ in figure 4.5), where $\hat{\beta}_{M,c}$ is the maximum likelihood estimation (MLE) of the slope, separately calibrated for each district.

The possible results of this first step are:

- a unique cluster that groups all the districts and has $\hat{\beta}_{M,c} = 0$;

- a unique cluster that groups all the districts and has $\hat{\beta}_{M,c} \neq 0$;

- a set of clusters (*cluster* **a**, *cluster* **b**,. . .), each of which can have $\hat{\beta}_M^{\mathbf{sl}} = 0$ or $\hat{\beta}_M^{\mathbf{sl}} \neq 0$. *sl* is the index of slope clusters. $\hat{\beta}_M^{\mathbf{sl}}$ is set to zero if, considering only the districts belonging to cluster *sl*, the correlation between $M_{t,c}$ and $y_{t,c}$ is not significant. The significant threshold is set to 0.20 to take into account that only a subset of observations is used.

The cluster index (**sl**) is omitted in the first two cases.

ii) *Clustering on the intrinsic value of the fitness component (intercept)*

For each slope cluster, an *Analysis of Variance* (ANOVA) or an *Analysis of Covariance* (ANCOVA) is performed to assess if all the districts have the same intercept. The ANOVA is performed if $\hat{\beta}_M^{\mathbf{sl}} = 0$, while the ANCOVA if $\hat{\beta}_M^{\mathbf{sl}} \neq 0$. If the test is passed ($p < 0.05$), districts are clustered on the basis of the value of the intercept (*cluster* **sl1**, *cluster* **sl2**,. . .). Intercept clusters are therefore sub-clusters of slope clusters (box ‘‘INTERCEPT CLUSTERING’’ in figure 4.5). At the end of the procedure, the districts belonging to the same cluster (*cluster* $\{\mathbf{sl}, \mathbf{in}\}$, where **in** is the index of intercept clusters) have the same intercept and the same slope:

$$\forall c \in cluster\ \{\mathbf{sl}, \mathbf{in}\} \quad \hat{y}_{t,c} = \hat{\beta}_0^{\mathbf{sl},\mathbf{in}} + \hat{\beta}_M^{\mathbf{sl}} M_{t,c} \qquad (4.4)$$

In the blocks ‘‘INTERCEPT CLUSTERING’’ and ‘‘SLOPE CLUSTERING’’, we used the agglomerative *hierarchical clustering* (Jain & Dubes, 1988). The adjective agglomerative means that, at the first step, each object (district) is in its own cluster and the algorithm gradually merges the atomic clusters into larger and larger clusters until a unique cluster is formed. The decision of which clusters are merged first is based on the pairwise distances between clusters. For simplicity, we

summarize here the main concepts referring to the procedure used for the "SLOPE CLUSTERING". The procedure for clustering intercept is in fact completely analogous.

When the hierarchical cluster starts, the distance $d_{i,j}$ between each pair of atomic clusters is calculated as the distance between the MLE estimates of the slopes $\hat{\beta}_{M,i}$ and $\hat{\beta}_{M,j}$. Moreover, if the distance between two clusters is significant (*p* value of the *t-test*<0.05), its value is set equal to $\max\limits_{i,j}(d_{i,j})$.

The matrix containing all the pairwise distances is the *proximity matrix* ($\mathcal{D} = d_{i,j}$). The couple of nearest clusters (say a and b) are then merged together to form a new (non-atomic) cluster, and the new *proximity matrix* is calculated substituting the clusters a and b with a unique cluster. We calculated the distance between two non-atomic clusters (or a non-atomic cluster and an atomic cluster) using the *furthest neighbour strategy*. Using this strategy, the distance is calculated as the maximum distance among all the pairwise distances between the elements of the two clusters. The algorithm is repeated until all the atomic clusters are merged, and a single cluster is obtained.

The entire procedure can be summarized in a *cluster tree* (see figure 4.7 for an example) in which the leaves of the tree are the atomic clusters. At each merging step, a branch of the tree is drawn to connect the merged clusters; the length of the branch represents the distance between the two merged clusters. For each branch of the resulting tree, we calculated an *inconsistency coefficient* (Jain & Dubes, 1988, see) using a depth of three links. To define the final clusters, we cut the tree branches where the *inconsistency coefficient* is bigger than 0.95 times the highest *inconsistency coefficient* of the entire tree.

After having completely defined the clusters, and having selected the meteorological variables, we performed a BMA analysis (see section 2.3.2) in which the basic model has a simple linear regression model structure with no interaction terms:

$$y_{t,c} = \beta_0 + \sum_{\mathcal{X}_i} \beta_j x_{j,t,c} + \varepsilon_{t,c} \tag{4.5}$$

where $y_{t,c}$ and $x_{j,t,c}$ are, respectively, the fitness component and the value of the $j-th$ covariate at time t in district c, $\mathcal{X}_i$ is the set of the covariates included in the $i-th$ model (m_i) and $\varepsilon_{t,c}$ a white noise.

To account for the intercept clustering, for each cluster $cluster$ $\{\mathbf{sl}, \mathbf{in}\}$

(but the first one, already included in β_0), a new covariate is defined as:

$$\Delta Intercept_{c,t,sl,in} = \begin{cases} 1, & \text{if } c \in cluster \; \{\mathbf{sl}, \mathbf{in}\} \\ 0, & \text{if } c \notin cluster \; \{\mathbf{sl}, \mathbf{in}\} \end{cases} \tag{4.6}$$

To take into account of this covariate, it is added to the set of potential covariates $\mathcal{X}_i$.

Similarly, a covariate is added to $\mathcal{X}_i$ for each slope cluster (*cluster* **sl**). The slope covariates are defined as:

$$slope_{sl,t,c} = \begin{cases} M_{t,c}, & \text{if } c \in cluster \; \mathbf{sl} \\ 0, & \text{if } c \notin cluster \; \mathbf{sl} \end{cases} \tag{4.7}$$

If only one slope cluster is defined, $slope_a = M_{t,c}$. The other covariates potentially included in the model are the meteorological variables that significantly (with $\alpha = 0.2$) correlate with the given fitness component.

Using the BMA models and the meteorological variables given by the realization of the Protheus model, we calculated the future projections of the male densities and the demographic parameters. The equations used for the simulations are:

$$\log(\hat{\boldsymbol{\Lambda}}_t) = \hat{\beta}_{0,\lambda} + \hat{X}_{t,\lambda}\hat{\beta}_\lambda + \hat{Z}_{t,\lambda}$$
$$\hat{\mathbf{M}}_{t+1} = \hat{\boldsymbol{\Lambda}}_t\hat{\mathbf{M}}_t$$
$$\log(\hat{\boldsymbol{\Phi}}_t) = \hat{\beta}_{0,\phi} + \hat{X}_{t,\phi}\hat{\beta}_\phi + \hat{Z}_{t,\phi} \tag{4.8}$$
$$\log(\hat{\boldsymbol{\Psi}}_t) = \hat{\beta}_{0,\psi} + \hat{X}_{t,\psi}\hat{\beta}_\psi + \hat{Z}_{t,\psi}$$
$$\log(\hat{\mathbf{P}}_t) = \hat{\beta}_{0,\rho} + \hat{X}_{t,\rho}\hat{\beta}_\rho + \hat{Z}_{t,\rho}$$

where $\log(\hat{\boldsymbol{\Lambda}}_t)$, $\log(\hat{\boldsymbol{\Phi}}_t)$, $\log(\hat{\boldsymbol{\Psi}}_t)$ and $\log(\hat{\mathbf{P}}_t)$ are, respectively, the vector of the predicted values for the growth rate, the brood size, the percentage of nesting females and the breeding success in the different Alpine districts at time t. $\hat{X}_{t,y}$ is the matrix of covariates included in the model of the quantity y (each row contains the value, at time t, for a district), $\hat{\beta}_y$ is the vector of the β parameters calculated using BMA and $\hat{Z}_{ty} \sim (0, \Sigma_y)$ are multivariate normal noises where Σ_y is the variance-covariance matrix of residuals of the BMA model for y. Therefore, the simulations include a realistic spatial effect *via* the variance-covariance matrix Σ. The matrix $\hat{X}_{t,y}$ is expressed using the *hat* because it contains the simulations of the male density. We initialized the simulation setting $\hat{\mathbf{M}}_{2010} = \mathbf{M}_{2010}$. To reconstruct the future projections, simulations are repeated 1000 times extracting the noise from the distributions of $\hat{Z}_{ty}$.

4.5 Results

4.5.1 Growth rate

Correlation with climatic variables

Figure 4.6 summarizes with colours different from white which of the many meteorological variables have a significant (even if potentially weak, $p < 0.20$) correlation with the growth rate. More precisely, red and blue indicate respectively positive or negative correlation while the colour intensity is proportional to the value of the Pearson's coefficient. So, the darker the colour, the stronger the correlation. These plots permit to visual inspect if some specific period of the year have a clear influence on population fitness and if there is any seasonal pattern. In spite of the huge number of tested meteorological variables, only few of them are significantly correlated with the growth rate. The more significant correlations are with the precipitations in the second half of October of year t ($P_{Oct2,t}$, $R = 0.19$, $p = 0.012$) and in the first half of January of year t ($P_{Jan1,t}$, $R = 0.19$, $p = 0.012$), and the mean temperature in the second half of April of year t ($Tm_{Apr2,t}$, $R = -0.18$, $p = 0.016$). However, the significant correlations appear to be connected only with those specific semi-months, since there are no sets of consecutive semi-months that influence the species in the same way. As we will see later, the situation is different with other fertility components, for which a seasonal effect is more clearly visible.

The most important meteorological variables highlighted by the univariate analysis are linked with important periods of the species' life cycle. The second half of April is in fact just before the lek formation, while October overlaps with one of the two dispersion periods and January is critical for the survival, since black grouse need good snow conditions to dig winter shelters and the food availability is scarce.

Density dependence and clustering

Studying the influence of population density on growth rate is complex, because of the intrinsic correlations between the two quantities (see eq.4.1). Therefore, besides the calculation of the correlation between growth rate and population density made pooling data from all districts (see the clustering procedure), we also calculated the correlation between growth rate and population density in each Alpine district.

The growth rate and total male density are significantly and negatively correlated ($R = -0.43$, $p < 0.001$). Moreover, the correlation is significant
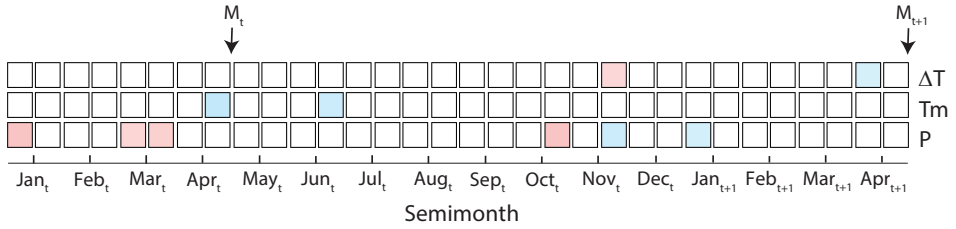
Figure 4.6: *Correlations between the growth rate* $\log(\lambda_{t,c})$ *and the semi-monthly meteorological variables: the average of the standardized precipitation P; the average of the standardized daily temperature range* ΔT; *the average of the standardized mean temperature* Tm. *Every cell in the plot refers to a single correlation between the growth rate and a meteorological variable. For each month label on the x-axis, the left column of cells refers to the first half of the month while the right column of cells to the second half of the month. Red [blue] cells indicate a positive [negative] and significant (p < 0.20) correlation, and the intensity of the colours is proportional to the Pearson correlation coefficient. On the top of the figure, we reported the timing of the spring censuses used to calculate* $\log(\lambda_{t,c}) = \log(M_{t+1,c}/M_{t,c})$.

(with $\alpha = 0.05$) also for 11 out of 17 single districts. We note that p-values of the other 6 districts (BI1, CN6, T01, T03, VC1 and VCO2) are also small ($p = 0.12$, $p = 0.12$, 0.19, 0.13, $p = 0.10$ and $p = 0.11$, respectively).

The slopes of the regression lines between the male density and the growth rate does not significantly differ among the districts ($F = 1.23$, $p = 0.25$). Interestingly, the analysis of covariance performed under the hypothesis of "same slopes" for all districts shows that intercepts are not identical ($F = 2.92$, $p = 0.0003$). Thus, we clustered the districts on the basis of the value of their intercepts, performing the "intercept clustering" described in the methodological section and reported in figure 4.5.

The described algorithm leaded us to define two clusters for the intercepts, as summarized in figure 4.7. One of the two clusters includes districts CN3, CN4, TO2 and TO5, while the other cluster includes all the other districts. For simplicity of notation, we will refer to *cluster 1* for the former cluster (red cluster in figures 4.7 and 4.8) and *cluster 2* for the latter (green cluster in the figures). Even if the districts CN3 and CN4 are adjacent and the districts TO2 and TO5 belong to the same province (Turin), it is not possible to find a clear geographical structure in the two clusters. Since both clusters are characterized by lines with different intercepts but same
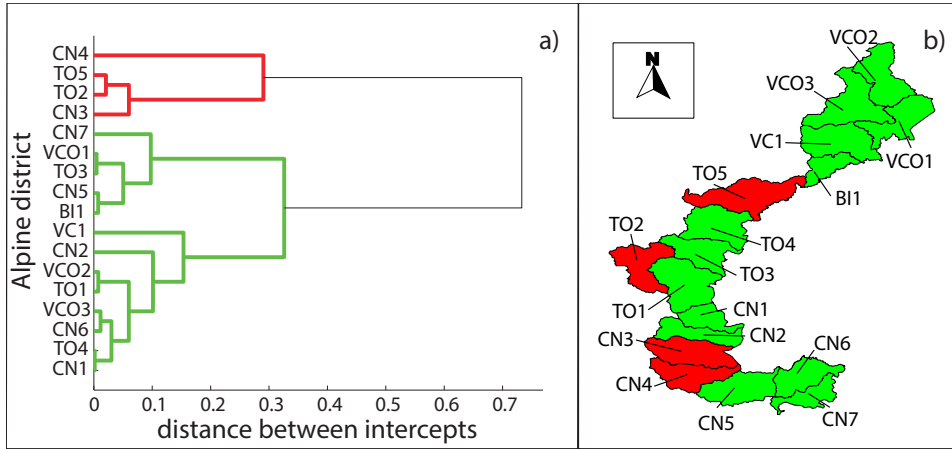
Figure 4.7: *Clusters identified in the univariate growth rate - male density model, obtained using the algorithm explained in the main text. Panel a) the cluster tree; Panel b) map of the Alpine districts. The districts belonging to the same cluster are coloured with the same colour (red or green).*

slope, a Ricker-like model can be written for each of them:

$$\log(\lambda_{t,c}) = \begin{cases} \beta_0^{\mathbf{1}} + \beta_M M_{t,c} + \varepsilon_{t,c}, & \text{if } c \in cluster \ \mathbf{1} \\ \beta_0^{\mathbf{2}} + \beta_M M_{t,c} + \varepsilon_{t,c}, & \text{if } c \in cluster \ \mathbf{2} \end{cases} \tag{4.9}$$

Fitting this model, the coefficient of determination R^2 is 0.28, and the correlation between growth rate and density is significant for both clusters ($p < 0.001$). The values of the model parameters are: $\hat{\beta}_0^2 = 0.52 \pm 0.065$, $\hat{\beta}_0^1 = 0.798 \pm 0.101$ and the common slope is $\hat{\beta}_M = 0.132 \pm 0.015$. The carrying capacities, measured as the non-trivial equilibrium of the equation 4.9 ($\overline{M} = -\frac{\beta_{0,c}}{\beta_M}$) solved for each cluster, are 3.97 for *cluster* **2** and 6.04 for *cluster* **1**. Notice that both the equilibria of the deterministic version of the Ricker model are stable since $0 < \beta_{0,c} < 2$. In figure 4.8 we show the growth rate as a function of the male densities, together with the best fit models.

BMA Model

In the multivariate model, the number of potential covariate is $k = 12$, thus leading to $2^k = 4096$ possible models, while the number of observations is 169. The model space was exhaustively explored and the expected posterior model dimension, measured as the number of included independent variables, was 3.25.
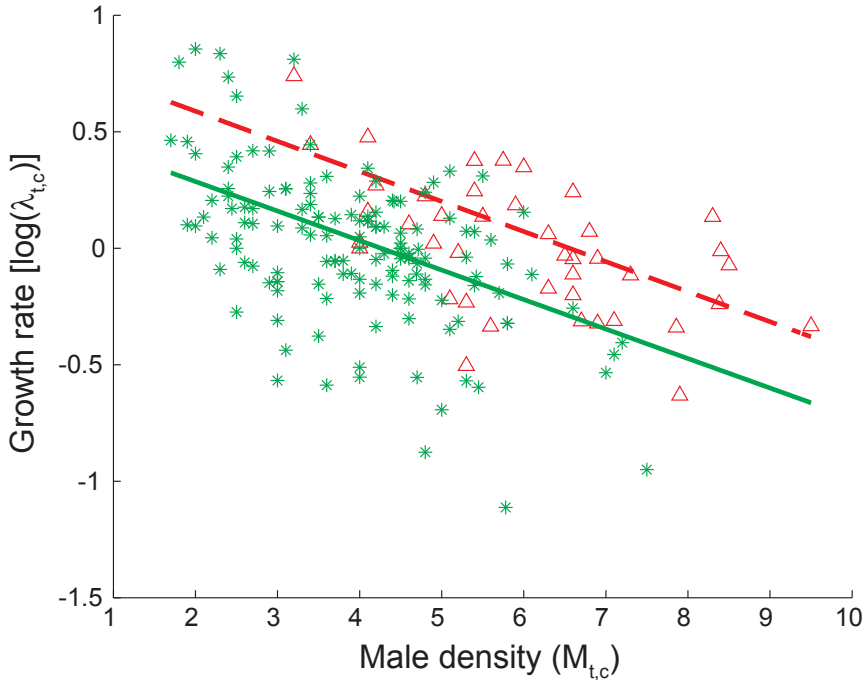
Figure 4.8: *Scatter plot of the growth rate [$\log(\lambda_{t,c})$] as function of the male density $M_{t,c}$, and regression lines based on the two groups formed using the clustering algorithms described in the text. Using the colour of figure 4.7, the red triangles and the red dashed line represent, respectively, data and regression line for the group composed by districts CN3, CN4, TO2 and TO5. Green stars and solid green line represent data and regression line for the other cluster of districts.*

BMA measures the importance of single covariates to the final prediction as the sum of the posterior probabilities of the models in which the given covariate is included (see chapter 2). The posterior probability of inclusion of the single covariates is summarized in table 4.1, together with the posterior probability of the 5 best models. The variables with the highest posterior probability of inclusion are: the male density ($M_{t,c}$), which negatively affects $\log(\lambda_{t,c})$; the categorical variable that permits to adjust the intercept using the clusters found in the univariate analysis ($\Delta Intercept$); the mean temperature in late April ($Tm_{Apr2,1}$), which negatively affects $\log(\lambda_{t,c})$ and the amount of precipitations in early January of year t+1 ($P_{Jan1,t+1}$) included with a negative effect. Notice that the ranking of variables changed between the univariate (correlation) and the multivariate (BMA) analysis. For example, the meteorological variables $P_{Oct2,t}$ and $P_{Jan1,t}$, which are the most correlated variables in the univariate analysis, have a posterior probability of inclusion lower than 0.10. On the other hand, the variable $Tm_{Apr2,1}$, which is measured just before the period of lek formation, is the most important meteorological variable in both univariate and multivariate analysis.

Both male density and $\Delta Intercept$ have a posterior inclusion probability close to 1, and are included in the best five models of table 4.1. This confirms the importance of accounting for density dependence and separating the districts in two clusters. Notice that, following equation 4.5, the density is included as in the Ricker model. The coefficient of determination obtained on the training set with the BMA model is $R^2 = 0.35$ while the R^2 of the density dependence only model is 0.28. Therefore, the inclusion of the climatic conditions significantly improved the predictive ability of the model. Moreover, the values of the model parameters are similar in the univariate analysis and in the BMA. More precisely, in BMA the intercepts are slightly higher ($\beta_{0,c} = 0.53$ for *cluster 2* and $\beta_{0,c} = 0.83$ for *cluster 1*), while the slope is a bit steeper ($\beta_M = -0.136$, see again table 4.1).

Future projections

Figure 4.9 shows the results of the 1000 stochastic future projections for the growth rates and the male densities in the two clusters. For each simulation, the values assigned to each cluster are the average of the values obtained in all the districts belonging to the cluster. The difference between the 1000 simulations is due to a different extraction of the environmental noise from the variance-covariance matrix of residuals, while the variability of the climatic model is not taken into account because only a realization of

Table 4.1: *Posterior probability of inclusion of the independent variables (covariates) and structure of the best models in BMA. x_i is the name of the independent variable, **PIP** its probability of inclusion, $\overline{\beta}_j$ the posterior mean of the parameter β_j and σ_{β_j} its standard deviation. $\text{sign}(\beta_j)$ is the probability that β_j is positive, conditioned on the fact of being included in the model. In the last five columns, the structure of the first five best models is shown, labelling with a "1" the rows which correspond to the variables included in the model, and with "0" the variables that are not included. In the last row, the posterior probability for each of the five best models is reported.*

x_i	PIP	$\overline{\beta}_j$	σ_{β_j}	$\text{sign}(\beta_j)$	Best models				
$Intercept$	1.000	0.534	-	-	1	1	1	1	1
$M_{t,c}$	1.000	-0.136	0.016	0.00	1	1	1	1	1
$\Delta Intercept$	0.999	0.296	0.61	1.00	1	1	1	1	1
$Tm_{Apr2,t}$	0.492	-0.099	0.114	0.00	1	0	0	0	1
$P_{Jan1,t+1}$	0.245	-0.067	0.133	0.00	0	0	1	1	0
$P_{Jun2,t}$	0.100	-0.012	0.044	0.00	0	0	0	1	1
$P_{Oct2,t}$	0.091	0.008	0.035	1.00	0	0	0	0	0
$P_{Nov2,t}$	0.062	-0.003	0.016	0.00	0	0	0	0	0
$P_{Jan1,t}$	0.057	0.005	0.040	0.91	0	0	0	0	0
$P_{Mar2,t}$	0.056	0.008	0.044	0.94	0	0	0	0	0
$\Delta T_{Nov2,t}$	0.053	0.002	0.018	0.93	0	0	0	0	0
$\Delta T_{Apr1,t}$	0.051	-0.002	0.017	0.07	0	0	0	0	0
$P_{Mar1,t}$	0.047	0.004	0.032	1.00	0	0	0	0	0
Posterior model probability: $P(m_i|D)$					0.31	0.16	0.11	0.02	0.02
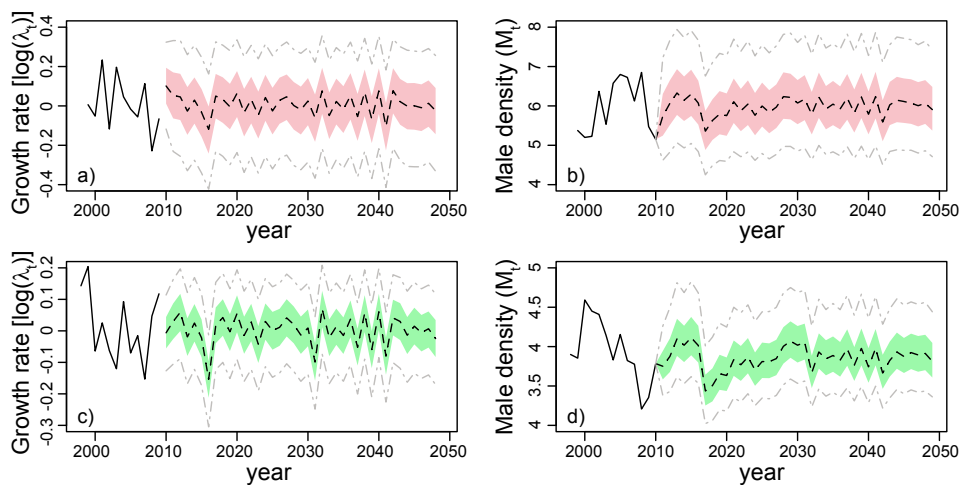
Figure 4.9: *Data (solid line) and future projections of the male densities (M_t) and the growth rate ($\log[\lambda_t]$) in the two clusters of figure 4.7, made using the BMA model and the meteorological projections given by the PROTHEUS model. Panel a and b refer to cluster 1, while panels c and d to cluster 2. The median value of the 1000 simulations are black dashed lines, interquartile ranges are coloured areas (following figure 4.7), while the fifth and the 95th percentile are grey dashed lines.*

the process is available. Even if the projections of the growth rate show a high uncertainty, the projections of the male density never goes below 4 males/100 ha (*cluster 1*) or 3 males/100 ha (*cluster 2*). Demographic simulations on both clusters, have in some years quite unusual behaviours, such as for the growth rate drop in 2006 and the consequent drop of the male density in 2017. Figure 4.10 reveals why: for example in 2016, the particular realization of the PROTHEUS model used for the simulations shows a very high value of $Tm_{Apr2,t}$, which is the most important meteorological variable in the model. Although such an effect had no serious consequences in the present case, it reveals that climate change might seriously affect the dynamics if the unfortunate conditions occur for some consecutive years.
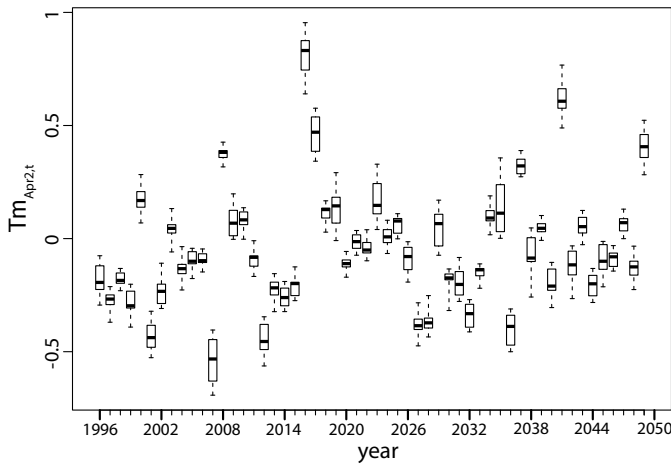
Figure 4.10: *Boxplot of the values of the standardized meteorological variable $Tm_{Apr2,t}$ given by a realization of the PROTHEUS model. The intra-annual variability is given by the variability among districts.*

4.5.2 Fertility components

Correlation with meteorological variables

Figure 4.11 summarizes the results obtained calculating the Pearson's correlation coefficients for the correlation between the fertility components and the meteorological variables. In the figure, only the significant ($\alpha = 0.5$) correlations are reported. Notice that, even if the value of α used in the plot for the fertility components is much higher than for the growth rate, many variables are found to influence the fertility rates of the population (see figure 4.6 for comparison).
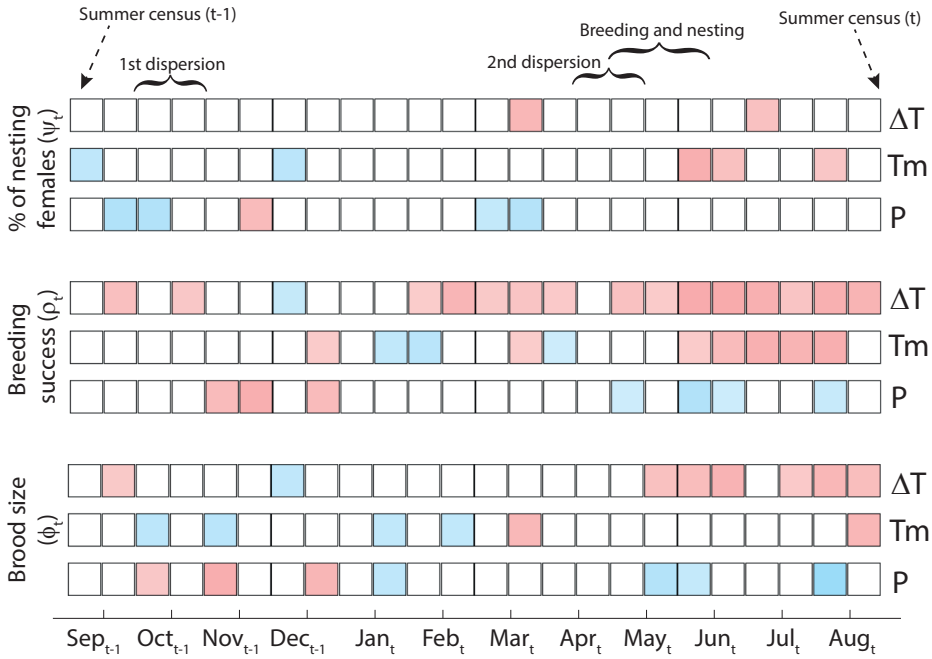
Figure 4.11: *Correlations between the fertility components and the semi-monthly meteorological variables: the average of the standardized precipitation P; the average of the standardized daily temperature range ΔT; the average of the standardized mean temperature Tm. Every cell in the plot refers to a single correlation between the growth rate and a meteorological variable. For each month label on the x-axis, the left column of cells refers to the first half of the month while the right column of cells to the second half of the month. Red [blue] cells indicate a positive [negative] and significant ($\alpha = 0.05$) correlation, and the intensity of the colours is proportional to the Pearson correlation coefficient. On the top of the figure, we reported the timing of the late summer censuses used to calculate the fertility components and of some important events in the black grouse life cycle.*

The percentage of nesting females is significantly correlated with only few meteorological variables and, as for the growth rate, it is not possible to clearly identify intervals of consequent semi-months that affect this rate. The variable that is more positively correlated with the percentage of nesting females is the mean temperature in early June ($Tm_{Jun1,t}$, $R = 0.27$, $p = 0.0017$), thus, even our Alpine populations confirm the importance of the post-hatching period in influencing the number of females that successfully nest, as it was found in lowland populations.

As for the brood size, the most important variables, are the amount of precipitations in early August of year t, $P_{Aug1,t}$, which negatively affects the rate ($R = -0.33$, $p = 1.1 \cdot 10^{-4}$), and precipitation in early November of year $t-1$ ($P_{Nov1,t-1}$), which has a positive effect ($R = 0.28$, $p = 0.0013$) on the rate. The former underlines both the risks of high precipitations, which can be the cause of nests destruction, and the importance of summer conditions in the survival of chicks, which are not yet able to thermoregulate. The latter suggest that snowy late autumns favours the conditions at which the hens access the breeding season, possibly increasing the availability of a good snowpack to dig the winter shelters. Even if with a weaker effect, the temperature ranges are important in all the late spring/early summer period with a positive effect. This result confirms the importance of clear skies and sunny days in the breeding period, including mating, nesting, hatching and weaning.

The same effect of the late spring temperature ranges is present in the results obtained for the breeding success. Moreover, $\Delta T_{Jun2,t}$ is the meteorological variable mostly (and positively) correlated with the breeding success ($R = 0.29$, $p = 5.64 \cdot 10^{-5}$). On the other hand, $P_{Jun1,t}$ is the meteorological variable mostly negatively correlated with this rate ($R = -0.24$, $p = 0.001$), thus confirming the negative effects of high precipitations in the nesting success and the chick survival.

Density dependence and Clustering

The clustering procedure performed as explained in the methodological section identified a unique cluster for the percentage of nesting females, three clusters for the breeding success and eight clusters for the brood size (with 4 different slopes and 8 different intercepts). Moreover, we found that the male density is significantly correlated with the brood size ($R = 0.27$, $p = 3.709 \cdot 10^{-4}$) and the breeding success ($R = 0.15$, $p = 0.038$), but it is not correlated with the percentage of nesting females ($R = -0.05$, $p = 0.506$). The results of the statistical tests carried out to create the

clusters are reported in appendix 4.A.

The compositions of the clusters is summarized in Figure 4.12, where, for a given fertility component, the same colours are used to identify the same clusters in the clustering trees (a,b), the geographical maps (b, e) and the regression lines between the male density and the fertility components (c, f). Clusters are labelled with letters (used to identify slope clusters) and numbers (used to identify intercept clusters).

For the breeding success, three clusters are defined, having the same slope but different intercepts:

- *cluster* **1**: VC1, TO4, CN5, CN3, CN2;

- *cluster* **2**: TO5, CN7, CN6, CN1, CN4, BI1;

- *cluster* **3**: VCO1, TO2, TO3, VCO3, VCO2, TO1.

For the brood size, the eight clusters are labelled with the same letter when they have the same slope:

- *cluster* **a1**: CN2, CN5, TO1. The slope $\beta_M^{\mathbf{a}} = 0$.

- *cluster* **b1**: CN1.

- *cluster* **b2**: TO4.

- *cluster* **c1**: CN3,CN6

- *cluster* **c2**: CN4

- *cluster* **c3**: VC1, TO3, TO2, VCO3,VCO1

- *cluster* **d1**: VCO2

- *cluster* **d2**: CN7, TO5, BI1

In many cases, adjacent districts belong to the same cluster; see clusters formed by districts {TO1, TO2, TO3} and {VCO1, VCO2, VCO3} according to their values for the breeding success, or {VC1, VCO1, VCO3} for the brood size. The articulated clustering structures that we obtained underline the importance of considering the spatial structure of the information to develop an accurate predictive model, in particular for the brood size.
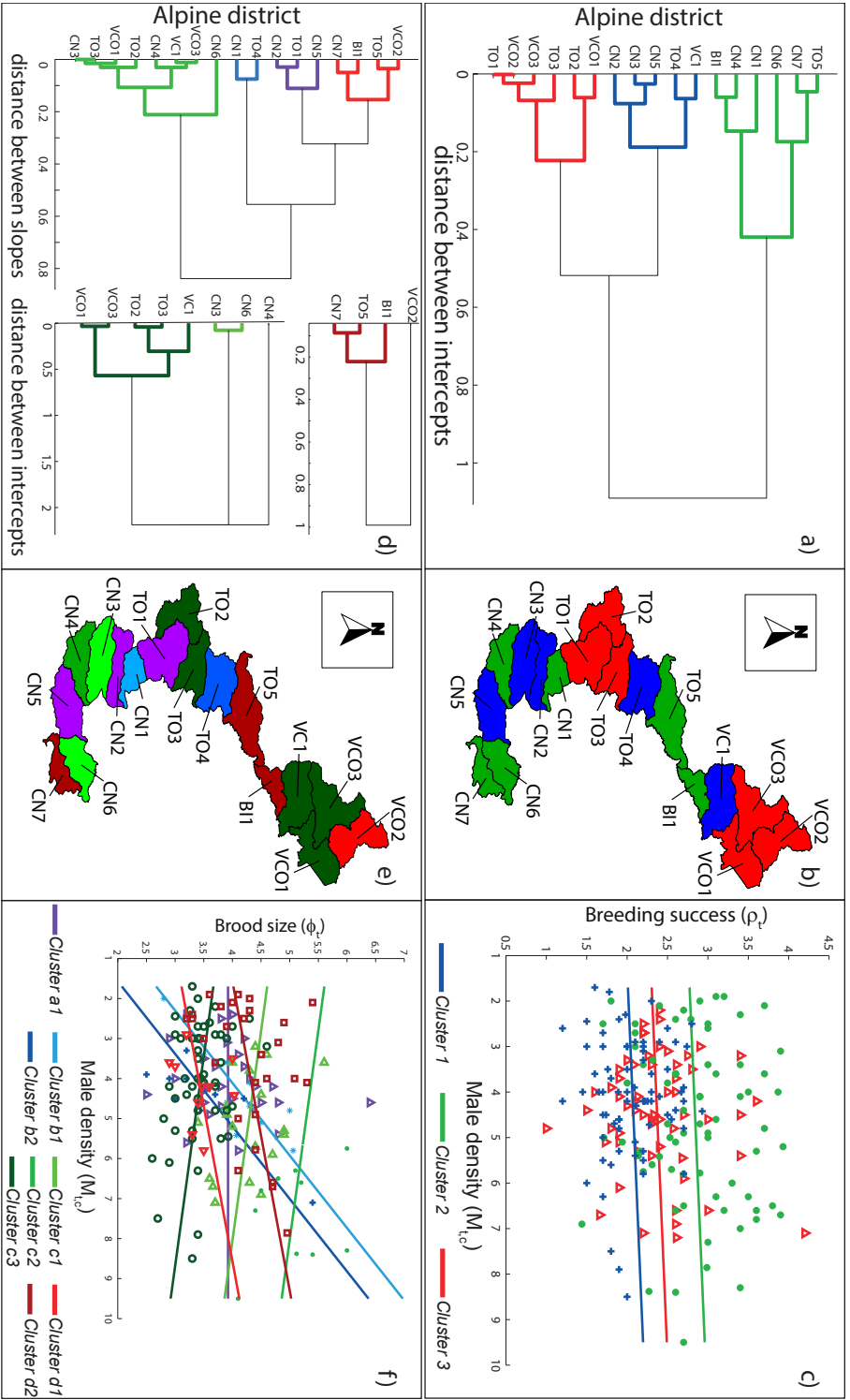
Figure 4.12: *Clusters identified for the breeding success (rho_t, first row of plots) and the brood size (phi_t, second row of plots), obtained using the algorithm explained in the main text. Panel a and d) report the cluster tree; Panel b) and e) the map of the Alpine districts; Panel c) and f) the scatter plot of the fertility component as function of the male density M_{t,c}, and regression lines based on the groups formed using the clustering algorithms. The districts belonging to the same cluster are coloured with the same colour.*

BMA model

The potential number of covariates to be included in the model is 31 for the %of nesting females, 50 for the breeding success and 46 for the brood size. According to BMA, the posterior model dimension (pmd), measured as the mean number of covariates included in the model, and the coefficient of determination R^2 are, respectively: $pmd = 1.10$ and $R^2 = 0.268$ for the percentage of nesting females, $pmd = 3.90$ and $R^2 = 0.552$ for the breeding success, $pmd = 8.23$ and $R^2 = 0.640$ for the brood size.

In the BMA, the importance of the independent variables is measured as their posterior probability of inclusion, calculated as the sum of the posterior probability of the models in which they are included. Table 4.2 reports such values for the variables with a posterior probability of inclusion greater or equal than 0.15, together with the compositions (variables included) and the posterior probability of the five best models for each fertility component. For all the fertility components, and in particular for the brood size, the posterior probability of the models is widely spread in the model space, thus supporting the choice of a multimodel approach.

For the percentage of nesting females, the model with the greater posterior probability is the constant model. Thus, the variability of this fertility component is weakly explained by the meteorological conditions and the male density. However, the most important meteorological variable is the mean temperature in early June ($Tm_{Jun1,t}$), included with a positive sign. This result confirms the results obtained in the univariate analysis on the importance of the post hatching period.

For the model of breeding success, the most important meteorological variables are the amount of precipitations in the second half of November of year t-1 ($P_{Nov2,t-1}$) with a positive effect and in the first half of June of year t ($P_{Jun1,t}$) with a negative effect. The latter effect further underlines the detrimental effect of high rainfalls in the post-hatching period, while the former effect is of difficult interpretation and is probably linked to the conditions at which the individuals access the winter. Moreover, the two $\Delta Intercept$ variables have an high probability of inclusion, confirming the importance of considering the three defined clusters. Conversely, the male density has a small probability of inclusion (0.056), thus the density dependence has a negligible effect on the breeding success.

For the brood size, the importance of the eight clusters defined above is confirmed by the presence, in the variables with the highest posterior inclusion probability, of all the 7 $\Delta Intercepts$, and the slope variables $slope_b$, $slope_c$ and $slope_d$, which represent the presence of the variable $M_{t,c}$ for the

Table 4.2: *Posterior probability of inclusion of the independent variables (covariates) and structure of the best models in BMA. Only the variables with a probability of inclusion greater or equal than 0.15 are shown. x_i is the name of the independent variable, **PIP** its probability of inclusion, $\bar\beta_j$ the posterior mean of the parameter β_j and σ_{β_j} its standard deviation. sign(β_j) is the probability that β_j is positive, conditioned on the fact of being included in the model. In the last five columns, the structure of the first five best models is shown, labelling with a "1" the rows which correspond to the variables included in the model, and with "0" the variables that are not included. For each fertility component, we report in the last row the posterior probability of the best five models.*

ψ_t

x_i	PIP	$\bar\beta_j$	σ_{β_j}	sign(β_j)		Best models			
$Intercept$	1.000	59.44	-	-	1	1	1	1	1
$Tm_{Jun1,t}$	0.177	1.758	4.067	1.000	0	1	0	0	0
Posterior model probability: $P(m_i|D)$					0.285	0.125	0.042	0.041	0.034

ρ_t

x_i	PIP	$\bar\beta_j$	σ_{β_j}	sign(β_j)		Best models			
$Intercept$	1.000	1.888	-	-	1	1	1	1	1
$\Delta Intercept_3$	1.000	0.660	0.109	1.000	1	1	1	1	1
$P_{Nov2,t-1}$	0.753	0.235	0.152	1.000	1	0	1	1	1
$\Delta Intercept_2$	0.657	0.211	0.170	1.000	1	1	0	1	1
$P_{Jun1,t}$	0.202	-0.045	0.096	0.000	0	0	0	0	0
Posterior model probability: $P(m_i|D)$					0.119	0.101	0.064	0.034	0.023

ϕ_t

x_i	PIP	$\bar\beta_j$	σ_{β_j}	sign(β_j)		Best models			
$Intercept$	1.000	3.853	-	-	1	1	1	1	1
$\Delta Intercept_{c2}$	0.973	1.361	0.582	1.000	1	1	1	1	1
$\Delta Intercept_{d1}$	0.901	-0.771	0.339	0.000	1	1	1	1	1
$\Delta Intercept_{b2}$	0.716	-1.627	1.354	0.000	1	1	1	1	1
$slope_b$	0.601	0.293	0.267	0.994	1	0	1	1	1
$\Delta Intercept_{c1}$	0.591	0.536	0.502	0.999	0	1	0	0	0
$\Delta Intercept_{b1}$	0.569	-1.159	1.140	0.025	1	1	1	1	1
$\Delta Intercept_{c3}$	0.547	-0.386	0.385	0.006	1	0	0	0	1
$slope_d$	0.508	0.061	0.070	0.999	1	1	1	1	1
$P_{Jan2,t}$	0.445	-0.618	0.781	0.000	1	1	1	1	1
$slope_c$	0.423	-0.038	0.057	0.076	0	0	1	1	0
$P_{May2,t}$	0.244	-0.045	0.090	0.002	1	1	0	1	1
$P_{Jun1,t}$	0.188	-0.063	0.148	0.000	0	0	0	0	0
$\Delta Intercept_a$	0.177	-0.059	0.148	0.003	0	0	1	0	0
Posterior model probability: $P(m_i|D)$					0.007	0.005	0.005	0.004	0.004

clusters b, c and d. The most important meteorological variables are the amount of precipitations in the second half of January ($P_{Jan2,t}$), the second half of May($P_{May2,t}$) and the first half of June ($P_{Jun1,t}$) of year t. The importance of rainfall in late May and early June can be interpreted along the same line of the early June rainfall for the breeding success. On the other hand, too abundant rainfalls in January are probably snowfalls, which, if too abundant, can completely cover the shrubs and reduce the food availability.

Future projections
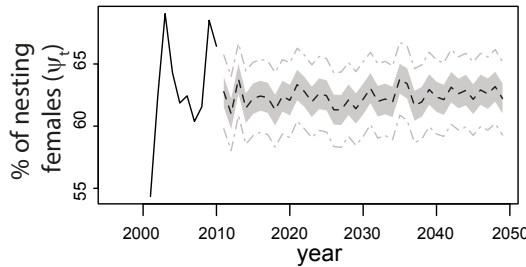
Figure 4.13: *Data and future projections of percentage of nesting females made using the BMA model and the meteorological projections given by the PROTHEUS model. Data are shown with a black solid line, median value of the 1000 simulations as black dashed lines, interquartile ranges as coloured areas, the fifth and the 95th percentile as grey dashed lines.*

The future projections, obtained using equations 4.8 are reported, for each defined cluster, in figures 4.13, 4.14 and 4.15 for, respectively, the the percentage of nesting females, the breeding success and the brood size.

For the percentage of nesting females the simulated values oscillate around 62%, showing a small variability both among the different years and the different simulations. The effect of climate seems therefore to be very limited for this rate. In fact, the percentage of nesting females is the fitness component for which the developed models have the lowest explanatory power. However, the highest peak in the simulations occurs in the years 2035 and 2036, in which the realization of the Protheus model predict an high value for the variable $Tm_{Jun1,t}$, which is the most important for this rate (see table 4.2). The future values of $Tm_{Jun1,t}$ are reported in figure 4.16.

Simulations for the breeding success are instead more variable, but even in this case no clear trends can be detected for the future, and the rate is predicted to oscillate around values already reached in the past. In this
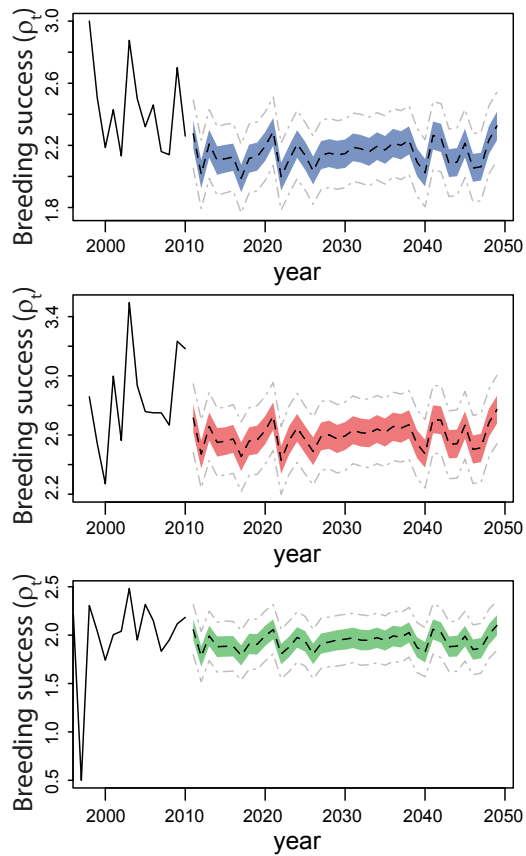
Figure 4.14: *Data and future projections of the breeding success made using the BMA model and the meteorological projections given by the PROTHEUS model. Data are shown with a black solid line, median value of the 1000 simulations as black dashed lines, interquartile ranges as coloured areas (as figure 4.12), the fifth and the 95th percentile as grey dashed lines.*

case, the effect of the meteorological variables on the system have a larger effect that in the case of the percentage of nesting females. However, the peaks of the single most important variable, $P_{Nov2,t-1}$, shown in figure 4.16, do not corresponds to the peaks obtained simulating the breeding success. Thus, in this case, the main oscillations cannot be guessed looking only at the most influential meteorological variable.
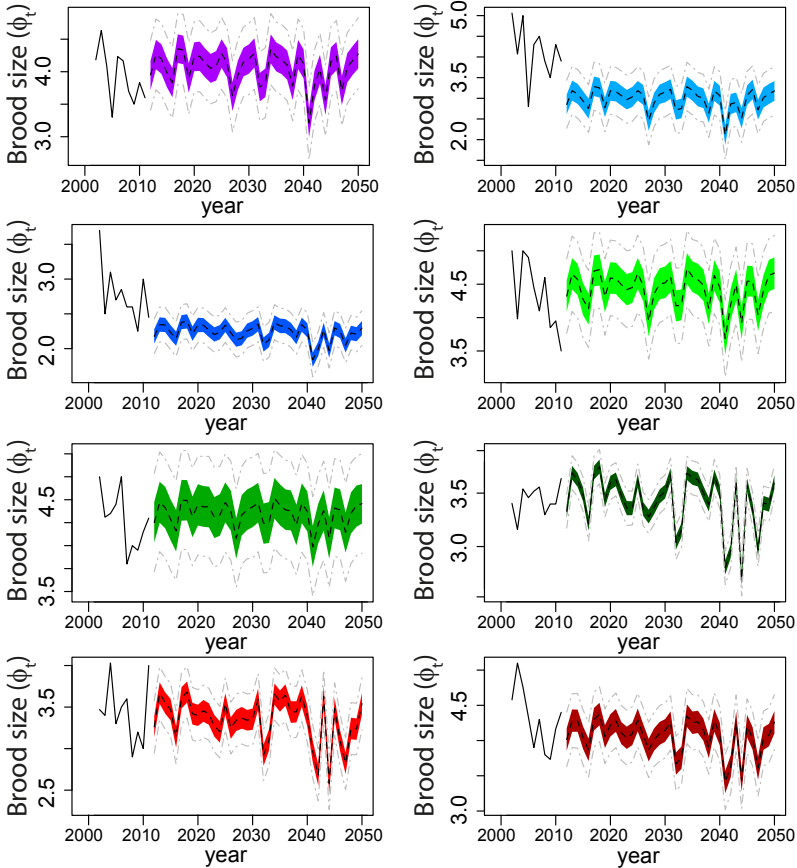
Figure 4.15: *Data and future projections of the brood size made using the BMA model and the meteorological projections given by the PROTHEUS model. Data are shown with a black solid line, median value of the 1000 simulations as black dashed lines, interquartile ranges as coloured areas (as figure 4.12), the fifth and the 95th percentile as grey dashed lines.*

For the brood size, the simulations are more highly variable than for the other two fertility rates. Moreover, they are, in many years and for all the clusters, out of the historical range of data. In particular, for clusters *b1*

and *b2* (in light blue and dark blue in figure 4.15), the expected brood size is clearly smaller than recorded in the past. The simulations have a high variability at the end of their temporal extent, between 2040 and 2050, as a consequence of the high variability that is predicted by the Protheus realization in the same years for the variable $P_{Jan2,t}$ (see figure 4.16). This meteorological variable is the most important, according to the BMA analysis, for the model of brood size, and can influence the conditions at which the females or the males access the leks.

(a) $\Delta T_{Jun1,t}$

(b) $Tm_{Nov2,t-1}$

(c) $Tm_{Jan2,t}$
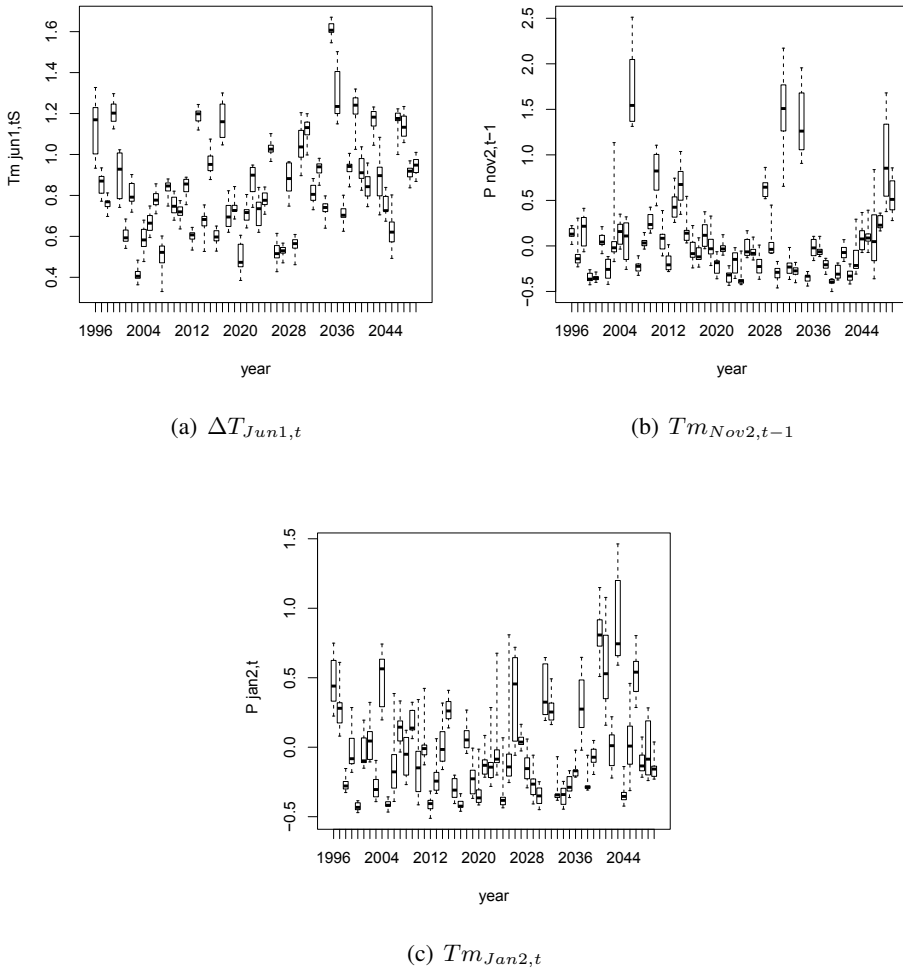
Figure 4.16: *Boxplots of the values of the most important standardized meteorological variable according to the BMA models for the fertility components.*

4.6   Discussion and conclusions

In this chapter, we studied the influence of density dependence, spatial position and meteorological variables on the growth rate and the fertility components of the black grouse populations in the Piedmont region.

Growth rate is clearly affected by density dependence in all districts and in almost each district. Moreover, the parameter that measures the intraspecific competition is not significantly different among districts, thus showing that density dependence is mostly an intrinsic trait of the population, weakly affected by the different environmental conditions that occur in different geographical positions. Two clusters of districts characterized by a different carrying capacity can be found. The cluster with the highest carrying capacity includes only 4 out 17 of districts, which positions do not suggest a clear spatial structure.

The meteorological variable with the greatest influence on the growth rate is, in both the univariate and the multivariate analysis, the mean temperature measured in late April of year t, just before the period of lek formation. The growth rate decreases in fact with the increase of temperatures in late April. A possible explanation is that an higher mean temperature in the first half of April leads to an anticipation of the lek formation, thus to an hatching period occurring when conditions are not optimal for the newborns. A similar effect is in fact described by Ludwig & Alatalo (2006) for a Finnish population of black grouse. In the present case, this hypothesis is supported by the fact that, during the study period, mean temperatures increased significantly (Mann-Kendall test) in the in late April ($p = 2.00 \cdot 10^{-11}$), while they decreased in early June ($p = 5.02 \cdot 10^{-6}$), as we show in figure 4.17. In the same period the population abundance decreased, at least in the cluster of districts with a low carrying capacity (see the bottom right panel of figure 4.9). The meteorological variable ranked 2$^{\text{nd}}$ for importance in BMA is the amount of precipitations in early January, which has a negative effect on the growth rate. Our hypothesis is that too high precipitations in the middle of winter (much probably snow) makes the search for food more difficult for the individuals.

The results on the fertility components confirm the importance of the environmental conditions in the critical post-hatching period, about early June. In fact, high precipitations in the post-hatching period are detrimental for the brood size and the breeding success, while high temperatures favour the nesting and lead to an increase in the percentage of nesting females. These results confirm what was found in lowland populations; heavy rain can in fact wash away the eggs from the nests, and cause thermoregulation
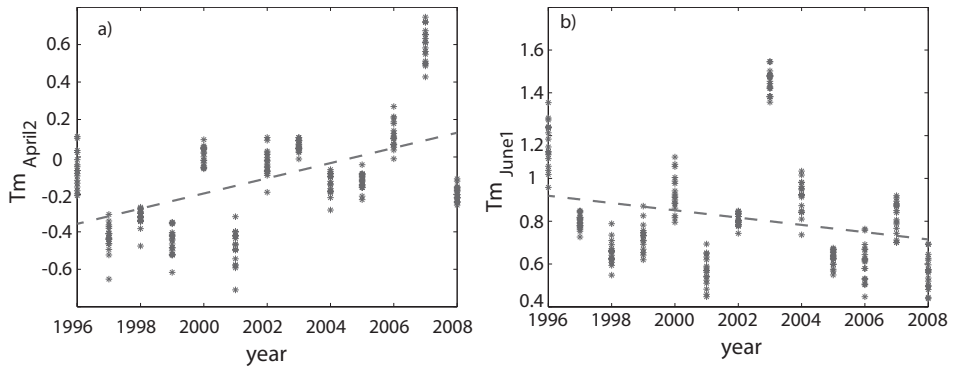
Figure 4.17: *Mean temperature data in the in late April (panel a) and early June (panel b) of year t. For each available year, the value measured in each Alpine district is shown as a grey star. The dashed grey line is the linear fitting.*

problems to chicks just after hatching (Hannon & Martin, 2006); moreover, the availability of insects in summer (Thacker *et al.*, 1997) decreases if summer precipitations are abundant. High precipitations in late January are also detrimental for the brood size, thus likely confirming the importance of the winter conditions in determining the status of the population, as we found for the growth rate. On the other hand, the breeding success is favoured by high precipitations in early winter, probably because of the presence of a snowpack suitable for sheltering.

Quite surprisingly, male density significantly and positively affects brood size and breeding success, even though its effect is weak and its contribution in the predictive models remains limited. Nevertheless, this result on fertility helps to understand the density dependence effects on the growth rate described above. In fact, the negative effect on growth rate contrast with the positive effect on fertility components. Therefore, it is likely that the male density might negatively affect the growth rate by reducing the winter survival, rather than by affecting fertility.

The future projections of the demographic parameters and of the population densities suggest that, although some strong inter-annual variability is clearly visible, the expected climatic conditions for the next 40 years will not directly represent a major danger for the conservation of black grouse. However, they also show that the oscillations caused by changes in the meteorological conditions are consistent. It would be therefore interesting to repeat the simulations including the variability of climate forecasting, using more than only one realization of the climatic model.

Another important improvement of this work would consist in repeat-

ing the analysis properly redefining the meteorological variables that might influence the rates. For example, we could use indicators that better represent the occurrence of extreme precipitation events, such as the maximum quantity of precipitation in a given period, or the mean precipitation obtained by using only the rainy days rather than all the semi-month (which include also non-rainy days). Another example could be the use of minimum temperatures in winter, which can probably better represent the risk of death for the species. The definition of such indicators needs to take into account the results of the present and the past studies, as to involve experts of the species, to better understand which mechanisms can "a-priori" affect the species.

Density, meteorological variables and other effects linked to geographical position affect the demographic rates of black grouse in different ways. To assess the potential future status of the population, it is therefore useful to consider all these aspects, if data are available, not focusing on population growth rate only. Indeed, the study on the fertility components permitted us to have a better understanding on the effects of both climate and density on the population dynamics.

In the next two chapters, we present the study of the dynamics of a long-living species: *Capra ibex ibex*. In that case, the need for separating the effects of climate and density on the different components of the fitness is enhanced by the fact that the individuals can change their sensitivity to environmental conditions according to the age or the sex. Moreover, the age-structure can mask the effects of density dependence and climate if only the total number of individuals is considered for studying the population dynamics. In the next chapters, we tackle the problem of considering a coarse (chapter 5) and a fine (chapter 6) age structure in modelling the population dynamics.

Bibliography

Arlettaz, R. & Patthey, P. 2007: Spreading free-riding snow sports represent a novel serious threat for wildlife. Proceedings of the Royal Society B 274: 1219–1224.

Artale, V., Calmanti, S. & Carillo, A. 2010: An atmosphere–ocean regional climate model for the Mediterranean area: assessment of a present climate simulation. Climate Dynamics 35: 721–740. doi: 10.1007/s00382-009-0691-8.

Barnagaud, J.Y., Crochet, P.A., Magnani, Y., Bernard Laurent, A., Menoni, E., Novoa, C. & Gimenez, O. 2011: Short-term response to the North Atlantic Oscillation but no long-term effects of climate change on the reproductive success of an alpine bird. Journal of Ornithology 152(3): 631–641. doi:10.1007/s10336-010-0623-8.

BirdLife International 2012: Tetrao tetrix. In IUCN 2013. IUCN Red List of Threatened Species, www.iucnredlist.org.

Boggs, C., Norris, E. & Steen, J. 1977: Behavioural and physiological temperature regulation in young chicks of the willow grouse (*Lagopus lagopus*). Comparative Biochemistry and Physiology Part A: Physiology 58: 371–372.

Bolker, B.M., Brooks, M.E., Clark, C.J., Geange, S.W., Poulsen, J.R., Stevens, M.H.H. & White, J.S.S. 2009: Generalized linear mixed models: a practical guide for ecology and evolution. Trends in Ecology & Evolution 24: 127–135.

Brichetti, P. & Fracasso, G. 2004: Ornitologia italiana, vol. 2 - Tetraonidae-Scolopacidae. Alberto Perdisa Editore, Bologna.

Caizergues, A. & Ellison, L. 2002: Natal dispersal and its consequences in black grouse Tetrao tetrix. Ibis 1: 478–487.

Caizergues, A. & Ellison, L.N. 2000: Age-specific reproductive performance of black grouse Tetrao tetrix females. Bird Study 47(February 2012): 37–41. doi:10.1080/00063650009461194.

Cattadori, I.M. & Hudson, P.J. 1999: Temporal dynamics of grouse populations at the southern edge of their distribution. Ecography 22: 374–383. doi:10.1111/j.1600-0587.1999.tb00574.x.

Clarke, J. & Johnson, R. 1992: The influence of spring snow depth on white-tailed ptarmigan breeding success in the Sierra Nevada. Condor 94: 622–627.

Dahlgren, D., Elmore, R.D., Smith, D.A., Hurt, A., Arnett, E.B. & Connelly, J.W. 2012: Use of Wild Dogs in Wildlife Research and Management. In N. Silvy, ed., Wildlife Techniques Manual, Vol. 1, The Wildlife Society Inc., Washington, D.C., USA, (pp. 140–153).

Dell'Aquila, A. & Calmanti, S. 2012: Impacts of seasonal cycle fluctuations in an A1B scenario over the Euro-Mediterranean. Climate Research 52: 135–157. doi:10.3354/cr01037.

Geary, M., Fielding, A.H. & Marsden, S.J. 2012: The anatomy of population change in a black grouse population 1992-2008. Oecologia 168(1): 73–81. doi:10.1007/s00442-011-2062-5.

Hannon, S.J. & Martin, K. 2006: Ecology of juvenile grouse during the transition to adulthood. Journal of Zoology 269: 422–433. doi:10.1111/j.1469-7998.2006.00159.x.

Jain, A.K. & Dubes, R.C. 1988: Algorithms for clustering data. Prentice Hall PTR.

Loneux, M., Lindsey, J. & Vandiepenbeeck, M. 2003: Climatic influence on Black Grouse population dynamic in Belgian Hautes-Fagnes Nature Reserve: an update. Sylvia 39 (suppl.): 53–57.

Ludwig, G. & Alatalo, R. 2006: Short-and long-term population dynamical consequences of asymmetric climate change in black grouse. Proceedings of the Royal Society B 273: 2009–2016. doi:10.1098/rspb.2006.3538.

Marjakangas, A. & Kiviniemi, S. 2005: Dispersal and migration of female Black Grouse *Tetrao tetrix* in eastern central Finland. Ornis Fennica 82: 107–116.

Novoa, C., Besnard, A., Brenot, J. & Ellison, L. 2008: Effect of weather on the reproductive rate of Rock Ptarmigan Lagopus muta in the eastern Pyrenees. Ibis 150: 270–278. doi:10.1111/j.1474-919X.2007.00771.x.

Ortigosa, G., Antonelli, R. & Gatto, M. 2003: Influenza dell'ambiente naturale e antropizzato sulla demografia del fagiano di monte (Tetrao

tetrix) in Trentino. In R. Casagrandi & P. Melià, eds., Atti del XIII Congresso Nazionale della Società Italiana di Ecologia (Como, 8-10 settembre 2003). Aracne, Roma.

Patthey, P., Wirthner, S., Signorell, N. & Arlettaz, R. 2008: Impact of outdoor winter sports on the abundance of a key indicator species of alpine ecosystems. Journal of Applied Ecology 45: 1704–1711.

Schweiger, A., Nopp-Mayr, U. & Zohmann, M. 2012: Small-scale habitat use of black grouse (*Tetrao tetrix L.*) and rock ptarmigan (*Lagopus muta helvetica* Thienemann) in the Austrian Alps. European Journal of Wildlife Research 58: 35–45.

Selås, V., Sonerud, G.a., Framstad, E., Kå lås, J.A., Kobro, S., Pedersen, H.B., Spidsø, T.K. & Wiig, O. 2010: Climate change in Norway: warm summers limit grouse reproduction. Population Ecology 53(2): 361–371. doi:10.1007/s10144-010-0255-0.

Storch, I. 2007: Grouse: Status Survey and Conservation Action Plan 2006–2010 IUCN. Gland, Switzerland : IUCN; Fordingbridge, UK : World Pheasant Assoc. ISBN 9782831710099 283171009X, 112 pp.

Summers, R. & Green, R. 2004: An experimental study of the effects of predation on the breeding productivity of capercaillie and black grouse. Journal of Applied Ecology 41: 513–525. doi:10.1111/j.0021-8901.2004.00891.x.

Thacker, J.I., Thieme, T. & Dixon, A.F.G. 1997: Forecasting of periodic fluctuations in annual abundance of the bean aphid: the role of density dependence and weather. Journal of Applied Entomology 121(1-5): 137–145. doi:10.1111/j.1439-0418.1997.tb01383.x.

Vaida, F. & Blanchard, S. 2005: Conditional Akaike information for mixed-effects models. Biometrika 92: 351–370.

Viterbi, R. 2012: Climate and animal biodiversity: analysis of risk factors in western Alpine protected areas. Ph.D. Thesis. Università degli Studi di Genova.

Wang, G. & Hobbs, N.T. 2002: Relationships between climate and population dynamics of white-tailed ptarmigan *Lagopus leucurus* in Rocky Mountain National Park, Colorado, USA. Climate Research 23: 81–87.

4.A Clustering details for fertility components

Here we report the details of the statistical tests performed in the clustering procedure summarized in the flowchart of figure 4.5. The results are reported for the breeding success (ρ_t), the brood size (ϕ_t) and the percentage of nesting females (ψ_t).

Percentage of nesting females

- Using all the data (from all the 17 Alpine districts) pooled together, the percentage of nesting females is not significantly correlated with the male density ($R = -0.052$, $p = 0.506$).

- In the ANOVA, the *F-test* is not passed ($F = 1.624$, $p = 0.071$), thus there is no evidence for estimating different intercepts.

- All the districts are clustered together in a unique group.

Breeding success

- Using all the data (from all the 17 Alpine districts) pooled together, the breeding success is significantly and positively correlated with the male density ($R = 0.145$, $p = 0.038$).

- The $F - test$ on the slope is not passed ($F = 0.880$, $p = 0.593$), thus we define a unique slope for all the districts.

- In the ANOVA, the *F-test* is passed ($F = 5.246$, $p = 4.855 \cdot 10^{-9}$), thus the intercept significantly differ among the districts.

- Intercept clustering is therefore performed. Three clusters are defined, having the same slope abut three different intercepts, as reported in the main text.

Brood size

- Using all the data (from all the 17 Alpine districts) pooled together, the brood size is significantly and positively correlated with the male density ($R = 0.272$, $3.709 \cdot 10^{-4}$).

- The $F - test$ on the slope is passed ($F = 2.049$, $p = 0.014$), thus there is evidence that the slope is not the same in all the clusters.

- The slope clustering procedure produces four clusters ($cluster$ **a**, ..., $cluster$ **d**):

  - $cluster$ **a**, including districts CN2, CN5 and TO1.

    The correlation with density is, for this cluster, not significant using $\alpha = 0.2$ ($R = 0.190$, $p = 0.32$). Therefore we set $\beta_M^a = 0$. In the ANOVA, the *F-test* is not passed ($F = 2.224$, $p = 0.127$), thus the intercept is the same for all the districts.

  - $cluster$ **b**, including districts CN1 and TO4.

    The correlation with density is, for this cluster, significant using $\alpha = 0.2$ ($R = 0.729$, $p = 0.0003$).

    In the ANCOVA, the *F-test* is passed ($F = 7.996$, $p = 0.0116$), thus the intercept is not the same for all the districts, and an intercept clustering is performed. Two intercept clusters are obtained: $cluster$ **b1** including only the district CN1 and $cluster$ **b2**, including only TO4.

  - $cluster$ **c**, including districts CN3, CN4, CN6, TO2, TO3, VC1, VCO1 and VCO3.

    The correlation with density is, for this cluster, significant using $\alpha = 0.2$ ($R = 0.329$, $p = 0.0031$).

    In the ANCOVA, the *F-test* is passed ($F = 19.62$, $p = 2.813 \cdot 10^{-14}$), thus the intercept is not the same for all the districts, and an intercept clustering is performed. Three intercept clusters are obtained: $cluster$ **c1** including districts CN3 and CN6, $cluster$ **c2** including only CN4 and $cluster$ **c3**, including districts VC1, TO3, TO2, VCO3 and VCO1.

  - $cluster^d$, including districts BI1, CN7, TO5 and VCO2.

    The correlation with density is, for this cluster, significant using $\alpha = 0.2$ ($R = 0.197$, $p = 0.193$).

    In the ANCOVA, the *F-test* is passed ($F = 7.095$, $p8.29 \cdot 10^{-4}$), thus the intercept is not the same for all the districts, and an intercept clustering is performed. Two intercept clusters are obtained: $cluster$ **d1** including only VCO2 and $cluster$ **d2** including districts CN7, TO5 and BI1.

4.B Additional tables

The following tables report the posterior probability of inclusion of the independent variables and posterior expected values of the parameters for the fertility components. In the header of the table, x_i is the name of the independent variable, **PIP** its probability of inclusion, $\overline{\beta}_j$ the posterior mean of the parameter β_j and σ_{β_j} its standard deviation. $\text{sign}(\beta_j)$ is the probability that β_j is positive, conditioned on the fact of being included in the model. Table 4.6 report the mean values of the demographic quantities.

Table 4.3: *BMA for the percentage of nesting females ψ_t.*

x_i	PIP	$\overline{\beta}_j$	σ_{β_j}	sign(β_j)
$Intercept$	1.000	59.44	-	-
$Tm_{Jun1,t}$	0.177	1.758	4.067	1.000
$P_{Oct1,t-1}$	0.101	-0.304	0.989	0.000
$P_{Nov2,t-1}$	0.084	0.369	1.336	0.999
$P_{Oct2,t-1}$	0.072	-0.341	1.347	0.002
$\Delta T_{Mar2,t}$	0.066	0.412	1.707	0.998
$Tm_{Sep1,t-1}$	0.054	-0.545	2.554	0.000
$P_{Mar2,t}$	0.053	-0.773	3.620	0.001
$\Delta T_{Jul1,t}$	0.046	0.289	1.496	1.000
$Tm_{Jun2,t}$	0.038	0.360	2.064	0.999
$P_{Aug2,t}$	0.038	0.388	2.229	1.000
$\Delta T_{Nov2,t-1}$	0.036	-0.187	1.098	0.001
$Tm_{Dec1,t-1}$	0.027	-0.199	1.414	0.023
$Tm_{Aug1,t}$	0.027	0.143	1.124	0.914
$P_{Mar1,t}$	0.023	-0.187	1.479	0.005
$Tm_{Jul2,t}$	0.022	0.210	1.717	0.987
$\Delta T_{Jan1,t}$	0.022	0.090	0.747	0.995
$\Delta T_{Sep1,t-1}$	0.021	-0.074	0.616	0.008
$Tm_{Nov1,t-1}$	0.018	0.124	1.191	0.979
$P_{May1,t}$	0.018	-0.057	0.520	0.005
$P_{Apr2,t}$	0.018	0.096	0.943	0.969
$Tm_{Apr2,t}$	0.017	0.115	1.109	0.987
$Tm_{Apr1,t}$	0.016	-0.144	1.494	0.028
$Tm_{Oct2,t-1}$	0.016	-0.111	1.144	0.011
$\Delta T_{May1,t}$	0.015	0.057	0.614	0.961
$\Delta T_{Mar1,t}$	0.015	0.052	0.543	0.990
$P_{Sep1,t-1}$	0.014	0.040	0.433	0.994
$Tm_{Feb1,t}$	0.013	-0.044	0.514	0.035
$\Delta T_{Jun1,t}$	0.011	0.034	0.444	0.967
$\Delta T_{Aug1,t}$	0.010	0.022	0.450	0.843
$Tm_{May2,t}$	0.009	-0.073	1.111	0.107
$\Delta T_{Oct2,t}$	0.007	0.010	0.374	0.749

Table 4.4: *BMA for the breeding success ρ_t.*

x_i	PIP	$\overline{\beta}_j$	σ_{β_j}	sign(β_j)
$Intercept$	1.000	1.888	-	-
$\Delta Intercept_3$	1.000	0.660	0.109	1.000
$P_{Nov2,t-1}$	0.753	0.235	0.152	1.000
$\Delta Intercept_2$	0.657	0.211	0.170	1.000
$P_{Jun1,t}$	0.202	-0.045	0.096	0.000
$Tm_{Feb1,t}$	0.136	-3.96E-02	0.109	0.001
$Tm_{Jul2,t}$	0.084	4.23E-02	0.161	0.992
$Tm_{Mar1,t}$	0.074	-1.60E-02	0.066	0.034
$\Delta T_{Feb2,t}$	0.056	1.47E-02	0.069	1.000
M_t	0.053	2.54E-03	0.012	1.000
$Tm_{Aug1,t}$	0.052	1.77E-02	0.096	0.874
$Tm_{Feb2,t}$	0.040	-7.92E-03	0.046	0.018
$Tm_{Jan2,t}$	0.037	-7.80E-03	0.047	0.016
$Tm_{Jul1,t}$	0.036	1.41E-02	0.094	0.939
$\Delta T_{Nov2,t-1}$	0.031	-6.40E-03	0.046	0.081
$\Delta T_{Jun2,t}$	0.030	7.47E-03	0.053	0.992
$\Delta T_{Dec1,t-1}$	0.030	-6.02E-03	0.042	0.004
$Tm_{Dec1,t-1}$	0.029	-7.65E-03	0.055	0.018
$Tm_{Nov1,t-1}$	0.028	-1.31E-02	0.100	0.039
$\Delta T_{Jan1,t}$	0.028	4.57E-03	0.033	0.996
$\Delta T_{May2,t}$	0.023	2.67E-03	0.024	0.941
$Tm_{Jun1,t}$	0.022	5.89E-03	0.054	0.867
$Tm_{Mar2,t}$	0.022	5.62E-03	0.048	0.973
$P_{Nov1,t-1}$	0.021	3.27E-03	0.034	0.903
$Tm_{Aug2,t}$	0.020	5.06E-04	0.062	0.456
$\Delta T_{Sep2,t-1}$	0.018	1.48E-03	0.017	0.957
$\Delta T_{Oct2,t-1}$	0.018	3.12E-03	0.030	0.999
$Tm_{Nov2,t-1}$	0.016	-2.64E-05	0.021	0.324
$Tm_{Jun2,t}$	0.016	2.78E-03	0.031	0.978
$P_{Mar1,t}$	0.015	-2.88E-03	0.035	0.023
$Tm_{Apr1,t}$	0.014	2.85E-04	0.028	0.642
$Tm_{Dec2,t}$	0.013	1.91E-03	0.033	0.800
$\Delta T_{Apr1,t}$	0.012	1.15E-03	0.020	0.790
$\Delta T_{Jul1,t}$	0.012	6.70E-04	0.016	0.789
$\Delta T_{Jan2,t}$	0.012	9.22E-05	0.018	0.606
$\Delta T_{Aug1,t}$	0.012	7.31E-04	0.016	0.812
$\Delta T_{Mar1,t}$	0.012	-2.86E-05	0.015	0.561
$\Delta T_{Jul2,t}$	0.012	3.54E-04	0.018	0.671
$\Delta T_{Aug2,t}$	0.011	3.12E-05	0.014	0.655
$P_{Aug1,t}$	0.011	-1.23E-03	0.031	0.206
$\Delta T_{Feb1,t}$	0.010	1.14E-03	0.019	0.948
$P_{May1,t}$	0.010	-2.99E-05	0.010	0.336
$P_{Aug2,t}$	0.010	1.56E-03	0.027	0.877
$\Delta T_{Mar2,t}$	0.010	4.50E-04	0.019	0.649
$\Delta T_{May1,t}$	0.010	4.82E-04	0.014	0.762
$P_{Dec2,t}$	0.009	2.29E-03	0.055	0.854
$P_{Jun2,t}$	0.009	1.93E-03	0.044	0.803
$P_{Mar2,t}$	0.009	5.60E-04	0.032	0.741
$P_{Oct2,t-1}$	0.009	-1.77E-04	0.009	0.383
$P_{Jul2,t}$	0.008	1.22E-03	0.036	0.736

Table 4.5: *BMA for the brood size ϕ_t.*

x_i	PIP	$\bar{\beta}_j$	σ_{β_j}	$\text{sign}(\beta_j)$
$Intercept$	1.000	3.853	-	-
$\Delta Intercept_{c2}$	0.973	1.361	0.582	1.000
$\Delta Intercept_{d1}$	0.901	-0.771	0.339	0.000
$\Delta Intercept_{b2}$	0.716	-1.627	1.354	0.000
$slope_b$	0.601	0.293	0.267	0.994
$\Delta Intercept_{c1}$	0.591	0.536	0.502	0.999
$\Delta Intercept_{b1}$	0.569	-1.159	1.140	0.025
$\Delta Intercept_{c3}$	0.547	-0.386	0.385	0.006
$slope_d$	0.508	0.061	0.070	0.999
$P_{Jan2,t}$	0.445	-0.618	0.781	0.000
$slope_c$	0.423	-0.038	0.057	0.076
$P_{May2,t}$	0.244	-0.045	0.090	0.002
$P_{Jun1,t}$	0.188	-0.063	0.148	0.000
$\Delta Intercept_a$	0.177	-0.059	0.148	0.003
$P_{Nov1,t-1}$	0.132	0.043	0.128	0.988
$Tm_{Mar2,t}$	0.129	0.059	0.187	0.948
$\Delta T_{Nov1,t-1}$	0.125	-0.031	0.097	0.005
$\Delta T_{Jan1,t}$	0.116	0.035	0.114	0.991
$P_{Aug1,t}$	0.110	-0.060	0.201	0.003
$Tm_{Jul1,t}$	0.104	0.068	0.240	0.965
$\Delta T_{May2,t}$	0.102	0.023	0.084	0.959
$Tm_{Aug2,t}$	0.097	0.050	0.189	0.987
$Tm_{Oct1,t-1}$	0.090	-0.048	0.196	0.062
$Tm_{Nov1,t-1}$	0.089	-0.050	0.197	0.034
$Tm_{May2,t}$	0.079	0.055	0.232	0.993
$\Delta T_{Jun1,t}$	0.076	0.021	0.091	0.971
$P_{Nov2,t-1}$	0.073	0.012	0.059	0.981
$P_{Oct1,t}$	0.055	0.006	0.032	0.961
$Tm_{Jan2,t}$	0.048	-0.005	0.063	0.288
$\Delta T_{Feb2,t}$	0.045	0.007	0.048	0.952
$Tm_{Feb1,t}$	0.044	-0.007	0.049	0.072
$Tm_{Feb2,t}$	0.040	-0.002	0.049	0.339
$\Delta T_{Dec1,t}$	0.039	-0.004	0.040	0.207
$Tm_{Aug1,t}$	0.039	-0.002	0.070	0.595
$Tm_{Apr2,t}$	0.038	0.005	0.078	0.602
$Tm_{Apr1,t}$	0.036	-0.006	0.086	0.288
$\Delta T_{Jul1,t}$	0.035	-0.005	0.048	0.181
$P_{Aug2,t}$	0.034	-0.003	0.075	0.412
$\Delta T_{Oct2,t}$	0.032	-0.001	0.031	0.423
$P_{Dec2,t}$	0.031	0.004	0.126	0.597
$\Delta T_{Aug2,t}$	0.030	-0.002	0.035	0.313
$Tm_{Jun2,t}$	0.029	0.005	0.060	0.821
$\Delta T_{Aug1,t}$	0.029	3.52E-05	0.035	0.525
$\Delta T_{Jul2,t}$	0.025	-0.002	0.040	0.293
$\Delta T_{Jun2,t}$	0.025	0.000	0.042	0.481
$\Delta T_{Mar1,t}$	0.025	0.000	0.026	0.536

Table 4.6: *Temporal mean (μ) and standard deviation σ of the demographic quantities used in the study, for all the 17 districts. The last row, named "mean", refers to a mean over the 17 districts.*

	M_t males/100ha		Brood size $\%B_{t,c}/F_{t_c}$		Breeding success $J_{t,c}/F_{t,c}$		Brood size $J_{t,c}/B_{t,c}$		Growth rate $log(\lambda_{t,c})$	
	μ	σ	μ	σ	μ	σ	μ	σ	μ	σ
BI1	3.57	1.76	$6.46 \cdot 10$	$1.09 \cdot 10$	2.74	$6.43 \cdot 10^{-1}$	4.08	$8.15 \cdot 10^{-1}$	$-4.11 \cdot 10^{-2}$	$4.81 \cdot 10^{-1}$
CN1	4.49	1.06	$6.07 \cdot 10$	$2.25 \cdot 10$	2.63	$5.77 \cdot 10^{-1}$	4.13	$6.74 \cdot 10^{-1}$	$-1.29 \cdot 10^{-2}$	$4.14 \cdot 10^{-1}$
CN2	5.81	1.59	$5.01 \cdot 10$	$2.18 \cdot 10$	2.29	$6.75 \cdot 10^{-1}$	4.12	1.04	$3.87 \cdot 10^{-2}$	$3.24 \cdot 10^{-1}$
CN3	5.53	1.32	$5.48 \cdot 10$	$1.94 \cdot 10$	2.49	$5.57 \cdot 10^{-1}$	4.30	$6.19 \cdot 10^{-1}$	$3.69 \cdot 10^{-2}$	$3.90 \cdot 10^{-1}$
CN4	7.14	1.28	$5.71 \cdot 10$	$2.39 \cdot 10$	2.82	$7.92 \cdot 10^{-1}$	5.06	$6.36 \cdot 10^{-1}$	$-8.27 \cdot 10^{-3}$	$2.30 \cdot 10^{-1}$
CN5	3.63	0.768	$5.53 \cdot 10$	5.93	2.30	$2.47 \cdot 10^{-1}$	4.11	$4.18 \cdot 10^{-1}$	$-1.66 \cdot 10^{-2}$	$2.60 \cdot 10^{-1}$
CN6	4.58	0.978	$6.54 \cdot 10$	6.35	2.87	$5.76 \cdot 10^{-1}$	4.37	$5.81 \cdot 10^{-1}$	$2.03 \cdot 10^{-2}$	$2.39 \cdot 10^{-1}$
CN7	2.80	0.859	$7.25 \cdot 10$	7.44	2.98	$4.28 \cdot 10^{-1}$	4.18	$4.96 \cdot 10^{-1}$	$3.69 \cdot 10^{-2}$	$3.73 \cdot 10^{-1}$
TO1	4.33	0.944	$4.43 \cdot 10$	$3.06 \cdot 10$	2.10	$3.25 \cdot 10^{-1}$	3.54	$4.76 \cdot 10^{-1}$	$-3.69 \cdot 10^{-2}$	$2.31 \cdot 10^{-1}$
TO2	5.54	1.43	$5.84 \cdot 10$	$1.31 \cdot 10$	1.99	$4.55 \cdot 10^{-1}$	3.35	$3.69 \cdot 10^{-1}$	$-8.27 \cdot 10^{-3}$	$2.89 \cdot 10^{-1}$
TO3	3.20	0.759	$5.69 \cdot 10$	$2.11 \cdot 10$	2.13	$4.63 \cdot 10^{-1}$	3.55	$3.57 \cdot 10^{-1}$	$-3.08 \cdot 10^{-3}$	$2.44 \cdot 10^{-1}$
TO4	4.63	1.15	$6.51 \cdot 10$	$1.18 \cdot 10$	2.43	$7.86 \cdot 10^{-1}$	3.55	$8.28 \cdot 10^{-1}$	$-4.55 \cdot 10^{-2}$	$2.16 \cdot 10^{-1}$
TO5	5.59	1.25	$5.64 \cdot 10$	$3.22 \cdot 10$	3.08	$5.49 \cdot 10^{-1}$	4.56	$3.44 \cdot 10^{-1}$	$-2.52 \cdot 10^{-2}$	$2.71 \cdot 10^{-1}$
VC1	3.90	1.22	$6.26 \cdot 10$	9.00	2.39	$4.60 \cdot 10^{-1}$	3.79	$4.42 \cdot 10^{-1}$	$-5.51 \cdot 10^{-3}$	$3.43 \cdot 10^{-1}$
VCO1	2.98	1.02	$5.42 \cdot 10$	$2.13 \cdot 10$	1.95	$3.82 \cdot 10^{-1}$	3.35	$2.15 \cdot 10^{-1}$	$4.64 \cdot 10^{-2}$	$5.49 \cdot 10^{-1}$
VCO2	4.12	0.862	$5.56 \cdot 10$	2.03	2.10	$3.26 \cdot 10^{-1}$	3.44	$3.74 \cdot 10^{-1}$	$1.10 \cdot 10^{-2}$	$1.89 \cdot 10^{-1}$
VCO3	4.48	1.16	$6.05 \cdot 10$	$2.31 \cdot 10$	2.13	$4.50 \cdot 10^{-1}$	3.15	$2.73 \cdot 10^{-1}$	$9.84 \cdot 10^{-3}$	$3.68 \cdot 10^{-1}$
mean	4.43	1.55	$5.84 \cdot 10$	$1.94 \cdot 10$	2.43	$6.17 \cdot 10^{-1}$	3.91	$7.33 \cdot 10^{-1}$	$-1.91 \cdot 10^{-4}$	$3.19 \cdot 10^{-1}$

Structured population models for Alpine ibex (*Capra ibex*) dynamics in the Gran Paradiso National Park

5.1 Abstract

Past analysis showed that the population dynamics of Alpine ibex are regulated by both population density and winter snow accumulation. However, recent time series of the ibex counts in the Gran Paradiso National Park shows interesting trends in comparison with historical snow data: while the winter snow depth has steadily decreased since the beginning of the 1980s, the ibex population experienced rapid growth during the 1980s and the early 1990s, followed by a strong decrease.

To explain these dynamics we build novel age structured population models in which demographic parameters depend on density and snow depth. They include a nonmonotonic effect of snow depth and density on the vital rates, the age and sex structure of the population, and spatial segregation between females and males. Using information criteria ($AICc$, BIC and SRM) and data from 1961, we select the best models and find that:

1. snow and population density interact in determining the demography of both males and females at all age classes, thus confirming that unfavourable climatic conditions intensify the density dependence of the population;

2. the effect of snow is nonmonotonic on weaning success and rate of demographic variation of kids, which are maximal at intermediate values of snow depth;

3. accounting for spatial segregation between sexes improves the fitting of the models, which suggests that the different use of space made by males and females influences intra-specific competition.

When the selected models are recalibrated on past data and used to simulate recent trends, they underestimate both the rapid growth of the 1980s-1990s and the recent decline of the population. However, using the novel sex and age-structured models, we find out that the underestimation of the peak is mainly due to deficiencies of adult demography models, while the overestimation of the recent population abundance is caused by shortcomings in the models of recruitment.

5.2   Introduction

The population dynamics of ungulates is strongly determined by both density dependence and environmental drivers (Forchhammer *et al.*, 2002; Lande, 1993; Post *et al.*, 1997; Sæ ther & Saether, 1997), which may operate in an interacting way (Gaillard & Yoccoz, 2003). Jacobson *et al.* (2004) were first in showing that the population dynamics of Alpine ibex (*Capra ibex ibex*) is significantly affected by a specific environmental variable, the average snow depth during winter. Since Alpine ecosystems are extremely sensitive to climate change (Fischlin *et al.*, 2007) and snow depth has been decreasing in the Alps in recent years (e.g. Terzago *et al.*, 2010), studying how population dynamics of high-altitude species is influenced by abiotic disturbances and trends is of paramount importance.

The exceptionally long time series of Alpine ibex counts in the Gran Paradiso National Park (GPNP) provides a unique opportunity to study the complex interplay between population density and climatic conditions operating in the species dynamics. To reproduce the dynamics of the population and to possibly make predictions into its near future, different models have been proposed. The simple but powerful approach put forth by Jacobson *et al.* (2004) explored various possible relationships of total ibex popu-

lation increase with both total animal density and snow depth. The analysis performed by the authors revealed that the population rate of increase is significantly different in years characterized by low vs high snow depth. This observation led the authors to include in their model suite what they called *threshold-models*, in which different functional relationships are used for years of high and low snow depth. The process of parameter calibration and model selection actually picked up two threshold models as the best candidates. Both models acceptably reproduce the increase of the 1980s and the population peak occurring at the beginning of the 1990s, while the subsequent decline is only partially captured (see Fig. 3 in Jacobson *et al.*, 2004). Unfortunately, if used to simulate more recent trends emerging from newly available data, such models largely overestimate the total abundance of ibex (see also the last three simulated years in Jacobson *et al.*, 2004).

The models proposed by Jacobson *et al.* (2004) have been expanded in various ways. For example, Corani & Gatto (2007) found that a slightly modified version of Jacobson *et al.*'s threshold models, obtained by introducing two different values of the intrinsic rate of increase at low and high snow depth, had better performances in terms of model selection criteria. Other authors tried to avoid the use of thresholds and proposed smoother functional forms for the rate of increase. Bianchi *et al.* (2006), for example, used local linear models instead of a piecewise linear system while Lima & Berryman (2006) proposed nonparametric, nonlinear versions of the dynamic model using the so-called Generalized Additive Modeling (GAM) approach of Hastie & Tibshirani (1990). Although these models provided technical insights into the potential limitations of the approach followed in Jacobson *et al.* (2004), none of them neither significantly altered the main biological assumptions of the original study nor was able to reproduce the population dynamics during the low-density phase in the last ten years.

In the present chapter we follow the lines suggested by Yoccoz & Gaillard (2006) and improve over existing models by incorporating peculiarities of the ibex life cycle that have never been included in previous modelling attempts, despite their ecological importance (Jacobson *et al.*, 2006). The most evident among these characteristics are sexual dimorphism and age structure. Also, we contrast the threshold models by Jacobson *et al.* (2004) and Corani & Gatto (2007) with differentiable models (hereafter called continuous models) where we use second-order polynomial approximations of nonlinear unknown functional forms.

The effects of sex and age are quite strong in Alpine ibex and must be taken into account to understand how density and environmental drivers might affect the various fitness components of ibex populations (Gaillard

et al., 1998, 2000). According to sex and age, in fact, animals live in spatially segregated groups, using different habitat types. Males and females usually join only during the very narrow breeding season, from mid-November to mid-January (Nievergelt, 1974). Kids live with their mothers throughout their first year of life while male yearlings gradually depart from female groups and form bachelor groups (2-3 years old) that join adult males (Villaret & Bon, 1995). Recruitment and juvenile survival are usually considered more sensitive to both density and environmental variability than adult survival. Among adults, female survival is larger and more buffered against limiting factors than male survival (Gaillard *et al.*, 1998; Toïgo *et al.*, 2003, 2007), although the difference is perhaps smaller for ibex than for other large mammals (Toïgo *et al.*, 1997). Since males and females (with kids) are almost always spatially segregated, it is reasonable to imagine that intraspecific competition can involve members of the same sex only. In the present work, this hypothesis will be contrasted against the alternative that intraspecific competition occurs among all individuals in the population.

Data for kids, yearlings, adult males and adult females are actually available, although they have never been used to formulate structured population models (Appendix E of Jacobson *et al.* (2004)). Here we fill the gap and use this detailed information to build models for the rate of demographic variation in kids and adults (both males and females), and for the weaning success. These sex- and age-structured models not only allow the demographic projection in time of specific population compartments, but can reveal which demographic processes are most influenced by biotic (e.g. population density) or abiotic (snow) factors.

5.3 Material and methods

5.3.1 Population and data

The GPNP is located in the Northwestern Italian Alps ($45°$ $25'$ N, $7°$ $34'$ E). The wardens of the GPNP perform two counts every year, one in late spring and one in the autumn, counting the population by walking over established routes. The numbers of ibex in the two counts are highly correlated (von Hardenberg *et al.*, 2000); also, the autumn counts include all summer newborns (discounted for neonatal mortality). Therefore we will use the autumn counts for our analysis. Details on the counts techniques used to obtain the data are provided in Appendix A of Jacobson *et al.* (2004). In the same Appendix, on the basis of the correlation between the two count

series, the authors suggest that counts are reliable.

The replication of counts within the same year, together with outliers identification, has been suggested by Largo *et al.* (2008) as a methodology to make the ibex counts more reliable and to avoid huge underestimates of the population size. The authors define as obvious outliers the data of years with a growth rate > 1.35. In the GPNP case, this value is never exceeded. Nevertheless, the minimum and the maximum of the growth rate occur in two consecutive years, in 1976 ($N_{t+1}/N_t = 0.64$) and in 1977 ($N_{t+1}/N_t = 1.28$). Counts of 1977 are then candidate to be a notable underestimate of the actual population size. We therefore compared these growth rate values with those obtained using spring counts, which are $N_{t+1}/N_t = 0.61$ in 1976 and $N_{t+1}/N_t = 1.25$ in 1977. Thus, the growth rate values are comparable using the two different counts and we therefore decided to include 1977's data in the analysis. Moreover, 1976 is the year characterized by the largest snow depth in the time series, so that a very low growth rate is not surprising.

Data of the ibex population in the Park are available from 1956 till today and constitute one of the longest continuous existing time series of mountain ungulate counts worldwide. In addition, the data are structured in age and sex classes, which, for clarity, we will call hereafter population compartments. Fig. 5.1a shows the total number of ibex (autumn counts) while Fig. 5.1b reports the counts of each of four population compartments: kids ($0 - 1$ years), yearlings ($1 - 2$ years), adult (> 2 years) females and males.

Fig. 5.1a reports the mean winter snow depth (S_t) measured at the IREN ENERGIA meteorological station at Lake Serrù (45° 16' N, 7° 8' E, 2 240 m), averaged from November of year t to May of year $t+1$. In the threshold models by Jacobson *et al.* (2004), the critical value of $\bar{S} = 154$ cm is chosen as the average plus half a standard deviation of the snow time series in the period 1961-2000.

From 1961 to 1982 the total number of ibex in GPNP fluctuated around a mean value of about 3 300 individuals. Then, an interesting temporal pattern clearly emerged: the total abundance in fact displayed a rapid increase (from ca. 3 250 individuals in 1982 to almost 5 000 in 1993) and then a sharp decrease, with only ca. 2 700 ibex surviving in 2008. This unimodal variation of the population size occurred under a monotonically decreasing trend of snow depth, somehow suggesting that the interaction between climatic conditions and population numbers is not at all as simple as one might hope for.

Figure 5.1: *Available data for Alpine ibex in the GPNP. (A) Fall counts of the total population abundance (solid) and mean winter snow depth S_t (dashed) estimated at Serrù station as the average from November of year t to May of year $t + 1$. (B) Number of ibex in the four population compartments: adult males (solid), adult females (dashed), yearlings (dotted) and kids (dash-dotted).*
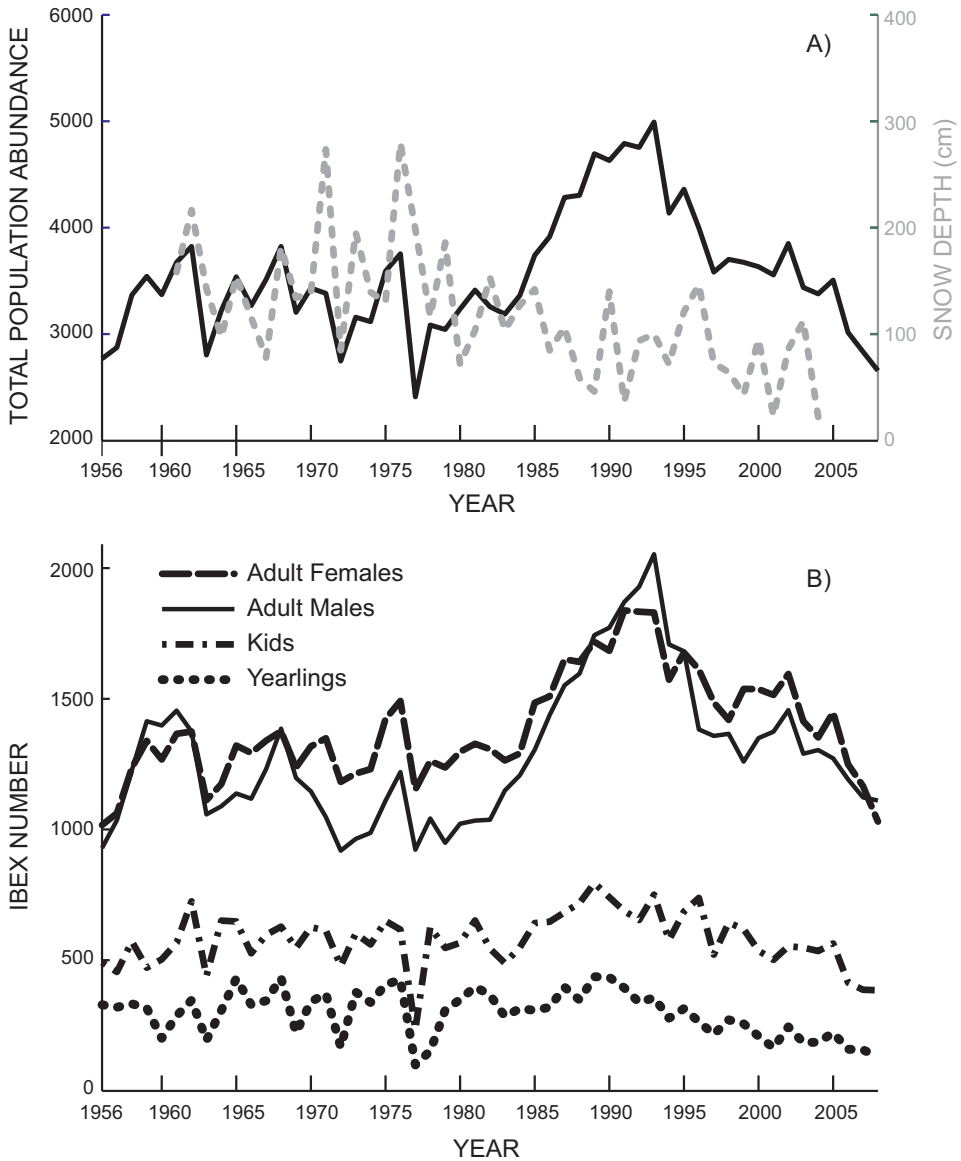
5.3.2 Unstructured and sex- and age-structured models

The use of thresholds (Jacobson *et al.*, 2004; Corani & Gatto, 2007, as done by) represents a form of non-linearity in the demographic growth rate model. We wish to extend this approach in order to better capture the non-linearities of the system. To this end we consider continuous models that incorporate all the quadratic terms in the explanatory variables. In its complete form, a model of this type has the polynomial expression

$$\log \left(\frac{N_{t+1}}{N_t} \right) = \beta_0 + \beta_1 N_t + \beta_2 S_t + \beta_3 S_t N_t + \beta_4 S_t^2 + \beta_5 N_t^2 + \rho_t \quad (5.1)$$

where N_t is the total population density, S_t is the mean winter snow depth and ρ_t is a stochastic factor representing environmental noise and un-modeled processes. In previous models, the parameters β_4 and β_5 were set to zero. Continuous models of this kind can be viewed as a 2-nd order Taylor expansion of a more general model $\log (N_{t+1}/N_t) = f (N_t, S_t)$ around the average ibex density and snow depth.

The second extension formulated here is the introduction of sex- and a simplified age-structure. Since adult counts are not partitioned into yearly age classes, the models we propose are not fully age-structured; however, they provide a first attempt toward the bottom-up approach to ibex demography invoked by Jacobson *et al.* (2006) and Yoccoz & Gaillard (2006). Moreover, in the next chapter, we describe the first attempts to consider the complete age structure of eh population starting from the available censuses

According to the counts data reported in Fig. 5.1, in each year t the population is partitioned into four compartments: kids K_t, yearlings Y_t, adult males M_t and adult females F_t. Juvenile classes K_t and Y_t include animals of both sexes that are not yet reproductive. At year t, the rate of demographic variation of kids ($\sigma_{K,t}$), males (yearlings and adults, $\sigma_{M,t}$) and females (yearlings and adults, $\sigma_{F,t}$), as well as the weaning success w_t can

be defined as

$$\sigma_{K,t} = \frac{Y_{t+1}}{K_t} \tag{5.2a}$$

$$\sigma_{M,t} = \frac{M_{t+1}}{M_t + \frac{1}{2}Y_t} \tag{5.2b}$$

$$\sigma_{F,t} = \frac{F_{t+1}}{F_t + \frac{1}{2}Y_t} \tag{5.2c}$$

$$w_t = \frac{K_{t+1}}{F_{t+1}} \tag{5.2d}$$

Definitions of the rates of demographic variation σ_M and σ_F implicitly entail the assumptions of balanced sex ratio at birth and no ratio distortion in the juveniles (kids and yearlings). For the realism of these assumptions, see Stüwe & Grodinsky (1987) and Toïgo *et al.* (1997).

By using the same approach introduced above for the unstructured counterparts, structured models are defined through nonlinear relationships between the logarithms of rates (5.2) and two covariates: the average snow depth S_t and the density $D_{\mathcal{C},t}$ of animals that is relevant for intraspecific competition within each compartment $\mathcal{C}$ (see below). As in the unstructured case, such nonlinear relationships can be continuous, i.e.

$$\log(\sigma_{\mathcal{C},t}) = \beta_{0,\mathcal{C}} + \beta_{1,\mathcal{C}} D_{\mathcal{C},t} + \beta_{2,\mathcal{C}} S_t + \beta_{3,\mathcal{C}} S_t D_{\mathcal{C},t} + \beta_{4,\mathcal{C}} S_t^2 + \beta_{5,\mathcal{C}} D_{\mathcal{C},t}^2 + \rho_{\mathcal{C},t} \tag{5.3}$$

with $\mathcal{C}$ $(= K, F,$ or $M)$ and

$$\log(w_t) = \beta_{0,w} + \beta_{1,w} D_{w,t} + \beta_{2,w} S_t + \beta_{3,w} S_t D_{w,t} + \beta_{4,w} S_t^2 + \beta_{5,w} D_{w,t}^2 + \rho_{w,t} \tag{5.4}$$

or, alternatively, they may be discontinuous. In this latter case, they contain fewer terms ($\beta_4 = \beta_5 = 0$), but the parameters β_0, β_1, β_2, β_3 can take different values in years characterized by snow depths above or below the critical threshold $\bar{S}$.

Apart from the short breeding season, Alpine ibex live in groups spatially segregated by age and/or sex (Villaret *et al.*, 1997). Therefore, in addition to accounting for dependence on total density ($D_{\mathcal{C},t} = D_{w,t} = N_t$), we also consider the case of sexually-segregated density dependence. Although not all male yearlings depart from their mothers, we consider the simple hypothesis of two separate groups, one with "males" (adult males plus male yearlings) and the other with "females" (mothers with all kids plus female yearlings). For eqs. (5.3) and (5.4) above, this translates into

considering $D_{w,t} = D_{F,t} = D_{K,t} = F_t + K_t + Y_t/2$ and $D_{M,t} = M_t + Y_t/2$. Note that Eq. (5.4) is dynamical, in the sense that weaning success in the spring of year $t + 1$ is dependent on the state of the population in the autumn of year t and average snow depth in the winter between year t and year $t + 1$. In fact, meteorological conditions and population density of the year preceding births can well describe the physiological state of mothers during the reproduction period (see the 'tap-hypothesis' in Grøtan *et al.*, 2008).

5.3.3   Model evaluation

The number of candidate models that emerge from the scheme outlined in the previous section is quite large. In fact, we define two families of models: unstructured and sex- and age-structured. Every unstructured model is fully characterized by the function relating the total population growth rate $(\log (N_{t+1}/N_t))$ to the different covariates. Every structured model instead requires the mathematical description of 4 demographic quantities $(\log (\sigma_K), \log (\sigma_M), \log (\sigma_F)$ and $\log (w))$ that can be either related to the density of the entire population (no spatial segregation) or to the compartment-specific density of "males" or "females", as defined in the previous section (spatial segregation). Each of the above rates can be related to the covariates by either a continuous formulation (like in eq.s 5.1, 5.3 and 5.4) or a threshold formulation. Independent of the chosen formulation, candidate models include all possible combinations obtained from the most complex formulation in which one or more terms are dropped, with the only exception of the constant term β_0. Simple combinatorics reveal that there are 32 continuous formulations and 8 threshold formulations for the suite of unstructured models. For the structured case, because of the two different hypotheses on density dependence (with or without spatial segregation) and considering that some of the models depend on snow only, we have a total of 74 potential model candidates for each of the 4 demographic parameters.

To orient ourselves inside the model space, we use standard model selection techniques: the second order Akaike's Information Criterion ($AICc$, equation 2.19), the Bayesian Information Criterion ($AICc$, equation 2.20) and a criterion based on Structural Risk Minimization ($AICc$, equation 2.22), which are described in section 2.2. we use here multiple criteria rather than a unique selection method, because their different way of accounting for model parsimony can produce a difference in the results that is worth investigation.

In general, model selection does not provide one winner model, but a hierarchical set of optimal models, i.e. a set of models that are "near" the model that shows the best value for the criterion. The number of these optimal models vary between criteria and is not known a priori. The strategies used to define the set of optimal models are reported, for each criterion, in section 2.2. In this case, we merge the results obtained using the three criterion, qualifying as best models those with the lowest number of estimated parameters among the models that meet all these conditions: $\Delta AICc < 4$, $\Delta BIC < 2$ and SRM < 1.06SRM$_{\text{best}}$. In principle, it might be possible that no model satisfies simultaneously the three conditions, but this is not our case.

For the best models we also calculate the adjusted R^2, which is a variation of the classical coefficient of determination that takes into account the model complexity:

$$\hat{R}^2 = 1 - \frac{n-1}{n-k-1} \frac{SSE}{\sum_{i=1}^{n}(y_i - \overline{y})^2} \tag{5.5}$$

where k is the number of parameters of the model, n the number of observations, $\overline{y}$ the mean value of the observations and SSE the sum of squares of residuals (see equation 2.1).

To evaluate errors of parameter estimates we use bootstrap (Efron, 1979). The bootstrap method provides an unbiased estimation of each parameter (but see caveats in Efron *et al.*, 1993) and an estimation of their variances. The statistics reported in Appendix I are obtained by calibrating the parameter values over $1\,000$ bootstrap samples, each consisting of n data values drawn with replacement from the original n-sized dataset.

In order to assess the predictive ability of the best models over longer time scales, we repeat the same parameter tuning and simulation experiments performed in Jacobson *et al.* (2004). To compare our results with theirs, we recalibrate all parameters of the selected models using only the first 20 years of data (1961-1980). Then, based on the recalibration, we simulate the ibex population trends until 2005 with both unstructured and structured models.

Simulating population trends after 1980 with the unstructured models is quite simple, because it is sufficient to initialize the systems with N_{1981} and use the snow depth series $S_{1981}, S_{1982}, \ldots, S_{2004}$ as inputs. To predict the total population abundance with structured models is more cumbersome, because the different rates of demographic variations and the weaning success of the structured models must be aggregated into one global model.

The main advantage of structured models is to provide information on the role played by covariates in each specific demographic process (i.e. adult rates of demographic variation, kid rate of demographic variation, weaning success). Also, structured models can be used to understand whether simulations of any particular population compartment deviate from data significantly more than others, thus pointing out the weakest links of the chain in the global model. To specifically investigate this point, we have performed additional simulations with global models in which part of the state variables are computed via the model equations, while others are directly equated to data. More precisely, we have predicted the number of adult males and females from yearling counts using the following equations

$$\hat{M}_{t+1} = \left(\hat{M}_t + \frac{Y_t}{2} \right) \hat{\sigma}_{M,t}$$
$$\hat{F}_{t+1} = \left(\hat{F}_t + \frac{Y_t}{2} \right) \hat{\sigma}_{F,t}$$

(5.6)

where Y_t is the measured number of yearlings in year t, while $\hat{M}_t$ and $\hat{F}_t$ are the model-predicted numbers of adult males and females, respectively, and $\hat{\sigma}_{M,t}$ and $\hat{\sigma}_{M,t}$ are the best-estimated rates of demographic variations. Similarly, we have predicted the number of kids from the mother counts and the number of yearlings from the kid counts using

$$\hat{K}_t = F_t \hat{w}_t$$
$$\hat{Y}_{t+1} = K_t \hat{\sigma}_{K,t}$$

(5.7)

where $\hat{w}_t$ and $\hat{\sigma}_{K,t}$ are the best estimates of weaning success and rate of demographic variation of kids.

The estimated total population abundance $\hat{N}_t$ can be derived by simply summing the abundances of all compartments. A direct comparison of the long-term prediction obtained from structured vs unstructured models is then possible. As an index of predictive ability we use the root mean square error between $\hat{N}$ and N:

$$RMSE_N = \sqrt{\frac{\sum_{t=1982}^{2005} \left(N_t - \hat{N}_t \right)^2}{2005 - 1981}}$$

To better evaluate the performance of the different models throughout the simulation period, it is also convenient to define the root square error averaged from the beginning of simulation (year 1981) to year k, i.e.

135

$$RMSE_N(k) = \sqrt{\frac{\sum_{t=1982}^{k}\left(N_t - \hat{N}_t\right)^2}{k - 1981}}$$

5.4 Results

In subsection 5.4.1 we present the models selected and their performance for one-step-ahead predictions, while in subsection 5.4.2 we illustrate the results when using the same models in long-term simulations.

5.4.1 Predictions

By using the selection criteria described in the previous section, we obtained the best models reported in Tab. 5.1. Within the family of unstructured models, the two selected systems are both discontinuous, in agreement with the original findings of Jacobson *et al.* (2004). NT1 includes pure density dependence and the interaction term $S_t N_t$, while NT2 includes pure snow-dependence and the interaction term. This latter model has the same structure as the model selected by Corani & Gatto (2007). Interestingly enough, the inclusion of higher order terms in the continuous systems (eq. 5.1) for the total growth rate does not result in better performance of the unstructured models.

The picture emerging from the analysis of structured models is more complex. First, we notice that the set of best models among the potential candidates is indeed very small (see again Table 5.1). Most interesting is the fact that the best density-dependent models selected by our procedure tend to be those with spatial segregation. That is, the dynamics of "males" is influenced more by "males" than by the entire population and the same is true for "females". The only exception is the rate of demographic variation of kids, for which both a model incorporating the segregation hypothesis (KC1, in which D_t = "females") and one excluding segregation (KC2, in which D_t = total population density) pass the model selection. As for the rate of demographic variation of males, three models that do not incorporate the spatial segregation hypothesis would also satisfy the Δ's criteria described above, but have been excluded because they are not as parsimonious as the others. While for females and kids two alternative models are selected, the rate of demographic variation of males and the weaning success have a unique best functional formulation.

Table 5.1: *List of best models according to selection criteria SRM, BIC and AICc as explained in the main text. The first letter of the Model ID indicates unstructured modelling (N) or structured modelling: females' (F), males' (M), and kids' rate of demographic variation (K) or weaning success (W). The second letter in Model ID is T for threshold formulations or C for continuous formulations. D_t is the compartment considered for density dependence: "all" indicates total population density (i.e., $D_t = N_t$), "females" stays for $D_t = F_t + K_t + Y_t/2$, while "males" indicates $D_t = M_t + Y_t/2$. p is the number of free model parameters (not including variance), while symbol "x" denotes inclusion of the corresponding polynomial term into the best models. The column $\hat{R}^2$ contains the adjusted R^2 considering the degrees of freedom of the model according to the formula $\hat{R}^2 = 1 - \frac{SSE(n-1)}{SST(n-p-1)}$, where n is the number of calibration data, SSE is the sum of squared prediction errors and SST is the total sum of squares. All indicators of model performances are calculated over the entire dataset. For all selection criteria reported in the relevant column, the corresponding indicator should be minimum.*

Model ID	Rate	D_t	p	$\beta_1[D_t]$	$\beta_2[S_t]$	$\beta_3[S_t,D_t]$	$\beta_4[S_t^2]$	SRM	BIC	AICc	$\hat{R}^2$
NT1	$\log\left(\frac{N_{t+1}}{N_t}\right)$	all	6	x	-	x	-	0.0108	-221.8	-231.2	0.73
NT2	$\log\left(\frac{N_{t+1}}{N_t}\right)$	all	6	-	x	x	-	0.0104	-223.5	-232.9	0.74
FT1	$\log(\sigma_F)$	females	6	x	x	-	-	0.0075	-237.6	-247.0	0.65
FT2	$\log(\sigma_F)$	females	6	x	-	x	-	0.0075	-237.5	-246.9	0.65
MT	$\log(\sigma_M)$	males	4	-	-	x	-	0.0113	-217.8	-225.2	0.54
KC1	$\log(\sigma_K)$	females	4	-	x	x	x	0.1167	-115.2	-122.5	0.52
KC2	$\log(\sigma_K)$	all	4	-	x	x	x	0.1159	-115.5	-122.8	0.53
WC	$\log(w)$	females	4	-	x	x	x	0.0285	-177.2	-184.6	0.48

For structured models, there is no systematic prevalence of threshold over continuous formulations. More precisely, while threshold models are best for adult compartments (male and female rates of demographic variation), continuous models are selected for kid demography and weaning success. These include the linear and quadratic terms in the snow depth S_t and the interaction term $D_t S_t$. A closer look at the signs of the best estimates of parameter values (see Appendix I, Tables 5.7, 5.8 and 5.9) reveals that the coefficients β_2 multiplying S_t are positive while the coefficients β_4 multiplying S_t^2 are negative, an indication that kid demography and weaning success have a nonmonotonic dependence on snow depth (see Fig. 5.2). This suggests that years characterized by particularly low snow depth can be detrimental to the juvenile compartments of the Alpine ibex, a result that is in keeping with the recently observed drop of the relevant rates (see von Hardenberg *et al.*, 2009).

In terms of adjusted R^2, the best performances are provided by models for the total population and for the rate of demographic variation of females, while the models for male and kid demography and weaning success display a poorer fit to the data lower explained variance.

Most coefficients of variation of the estimated parameters, as shown in the Appendix I (Tables I.1-7) are of the order of 10^{-1} (see also the Discussion), thus showing that best fits are rather robust. Using the bootstrapped parameter distributions, we assessed the predictive ability of the best models under parameter uncertainty. First, we performed one-step-ahead predictions, whose distribution (5th-95th percentile) was obtained from the 1 000 parameters of the bootstrap analysis. The result is shown in Fig. 5.3. Despite all models are calibrated on data over the entire period 1961-2004, the predictive ability deteriorates at the end of the 1970s. In fact, while data fall within the prediction range during the first part of the time series, deviations of predictions from data are more frequent after the beginning of the 1980s. Particularly evident is the mismatch in the case of the rate of demographic variation of kids.

5.4.2 Long-term simulations

Having selected two best models for the rates of demographic variation of females and kids and one best model for the other rates, we obtained four structured global models, namely $STR1$ (consisting of models MT, $FT1$, $KC1$ and WC), $STR2$ (MT, $FT2$, $KC1$ and WC), $STR3$ (MT, $FT1$, $KC2$ and WC) and $STR4$ (MT, $FT2$, $KC2$ and WC). Similarly to the case of unstructured models, the initial condition is considered as

Figure 5.2: *Models for kid rate of demographic variation (panel A) and weaning success (panel B) vs snow depth, where asterisks indicate the data and the the dotted vertical line corresponds to the snow threshold value of 154 cm. The continuous line shows the fit from models $KC1$ (A) and WC (B) while dashed lines correspond to optimal threshold models. As all the models include both the snow depth and the interaction between snow depth and density, curves are computed using the mean value of the population density over the entire study period.*
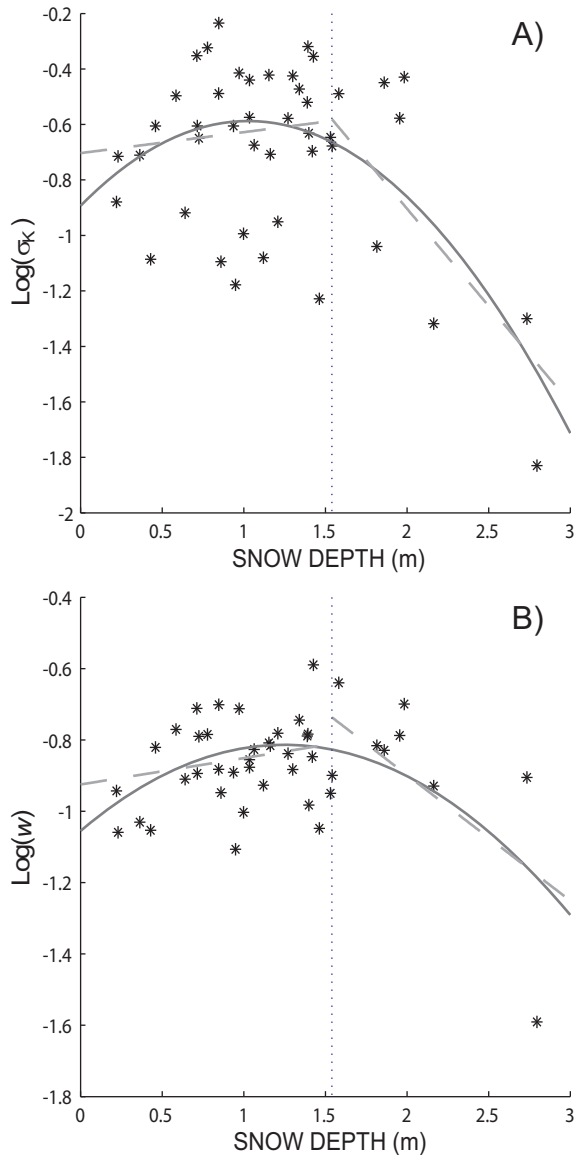
Figure 5.3: *One-step ahead prediction ranges of the best models (5th to 95th per-centile and mean, grey bars) vs the logarithm of observed vital rates (solid lines). Parameters, whose values and statistics are in tables of Appendix I, are calibrated by using 1 000 bootstrap samples from data along the entire times-pan. Panels (A) and (B) represent the total annual growth rates predicted by unstructured models NT1 and NT2, respectively. The other panels report results of structured modelling: (C) Female rate of demographic variation predicted by model FT1 (left axis) and FT2 (right axis); (D) Male rate of demographic vari-ation (model MT), (E) Kid rate of demographic variation predicted by model KC1 (left axis) and KC2 (right axis), and (F) weaning success (WC). The struc-ture of each model is summarized in Tab. 5.1.*
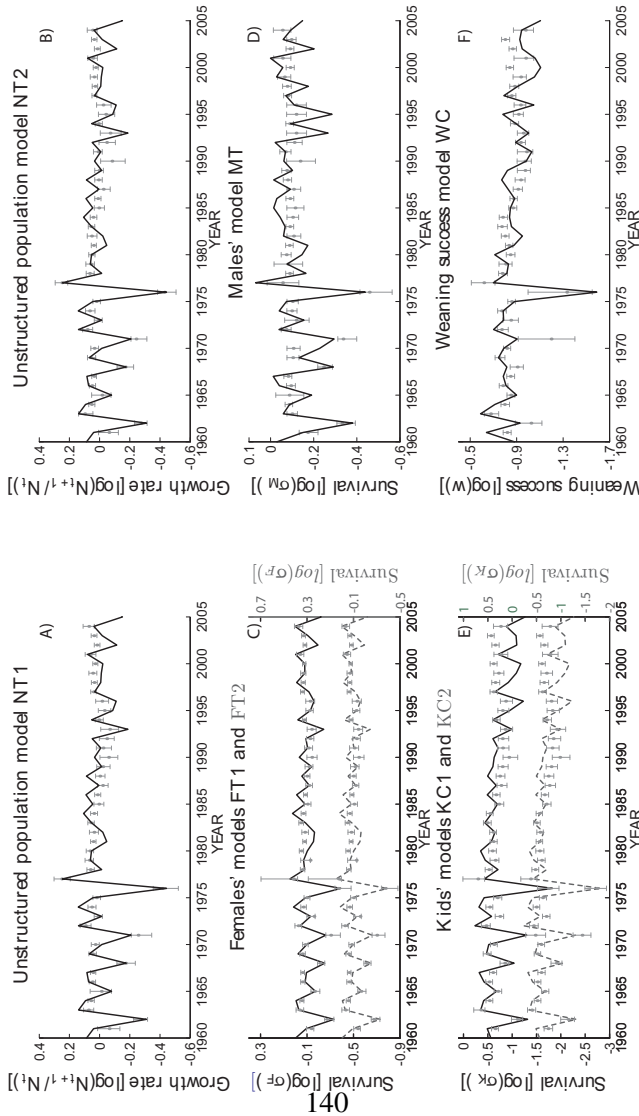
known ($\hat{X}_{1981} = X_{1981}$ for all X's) as well as the snow depth time-series S_t over the entire simulation horizon (from 1981 to 2004). Fig. 5.4 shows the distributions of values (in terms of 5th-95th interpercentile and 25th-75th interquartile) simulated with the best models under parameter uncertainty (evaluated via bootstrap). The plots reveal that the unstructured models NT1 and NT2 reproduce the recent trends in quite a similar way. The main difference is that model $NT2$ exhibits more oscillations than $NT1$. In terms of $RMSE_N$, the performances of the two unstructured models are comparable ($RMSE_N = 506$ for $NT1$ and 531 for $NT2$), and they are both significantly more effective than the model by Jacobson *et al.* (2004) ($RMSE_N = 852$) which did not include the double estimate of β_0.

The structured global models neither perform qualitatively better than the unstructured model, nor provide quantitatively significant improvements ($RMSE_N = 577$ for $STR1$, 570 for $STR2$, 524 for $STR3$ and 520 for $STR4$). As in the case of unstructured models, trends simulated with structured models underestimate the peak and overestimate the abundances of recent years (Fig. 5.4).

The temporal evolution of $RMSE_N(k)$ for the best structured and unstructured models is shown in Fig. 5.5. Structured models perform better than unstructured ones in terms of $RMSE_N(k)$ along almost the entire simulation period, with the exception of the first and last years. On the other hand, recent data are systematically included between the 5th and 95th percentile of all simulations obtained with unstructured models (see Fig. 5.4), while this is not true for simulations obtained with structured models. However, unstructured models display very high variability of long-term predictions, simulating unrealistic abundances as high as 10 000 individuals or more.

Even though structured models do not significantly improve the prediction of total population numbers, it is useful to explore what is the contribution of the different compartments to the simulated dynamics. The first three panels of Fig. 5.6 show the simulated numbers of adult males and females obtained from models (5.6) while considering the time series of yearlings Y_t as a known input. The two best models FT1 and FT2 perform rather similarly and both underestimate the population peak of the 1990s but reproduce fairly well the subsequent decreasing trend. The model for males is more precise than the two models for females. Observations are almost always included between the 5th and the 95th percentiles of bootstrapped simulations for both males and females. Simulations for the adult male compartment are more variable than those for females. This is expected because the coefficients of variation of the estimated parameters of

Figure 5.4: *Simulation ranges for the dynamics after 1980 of the total number of ibex obtained with unstructured models NT1 (A) and NT2 (B), and with global models STR1 (C), STR2 (D), STR3 (E) and STR4 (F). Parameter values are calibrated by using 1 000 bootstrap samples over the first 20 years of data. The dark gray areas include the 25th to 75th percentile, while light gray areas are for the range 5th to 95th percentile. The thick continuous line stands for data while the thin dashed line corresponds to the reference simulation obtained with the unbiased parameters reported in Tables of Appendix A.*
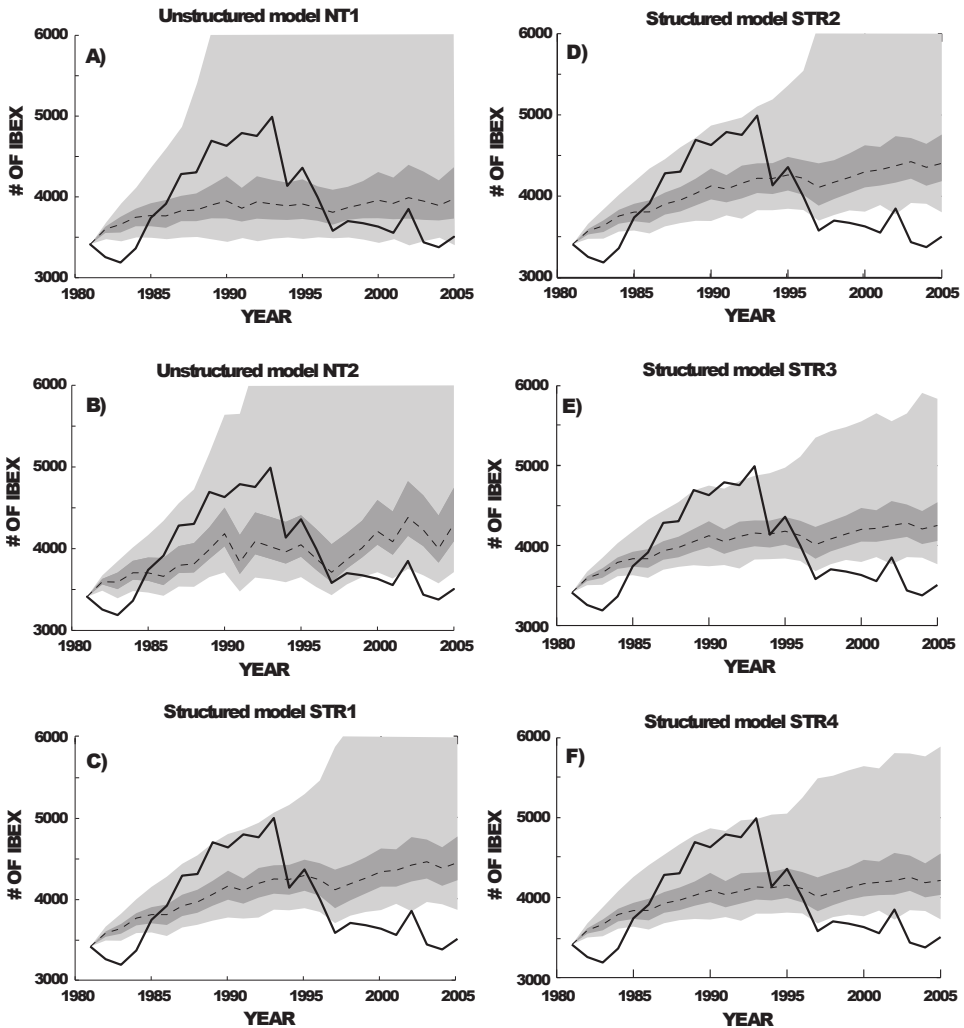
Figure 5.5: *Temporal evolution of $RMSE_N(k)$ as defined in the main text. All parameter values as in the reference simulations of Fig. 5.4.*
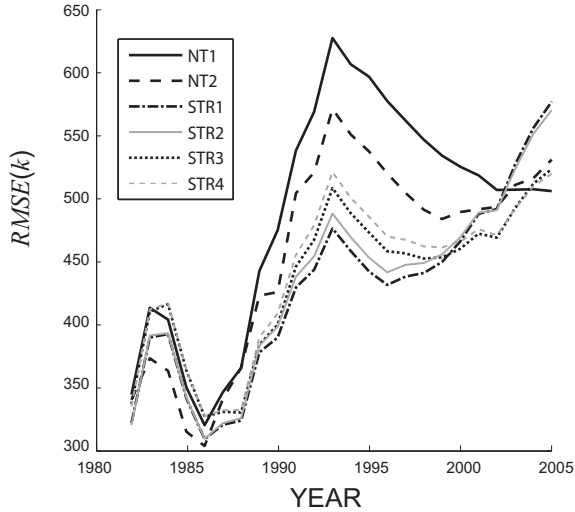
model MT are higher than unity when snow depth is below threshold (see Tab. 5.6). Panels (d), (e), and (f) of Fig. 5.6 focus on the juvenile compartments of kids and yearlings and are obtained with the first and second of equations (5.7). While the counts data are often included in the prediction range before and during the population peak, they are frequently below the 5th percentile starting from the mid-1990s, especially in the case of yearlings.

5.5   Discussion and conclusions

The models proposed and analysed in this study relate the total annual growth rate (unstructured models) or the rates of demographic variation and weaning success (structured models) to population density and snow depth. For the unstructured models the idea is not new, but here we account for richer functional forms than those available in the literature. As for the novel compartment-structured approach, we propose models aimed at including the likeliest factors impacting on the juvenile and adult ibex rates of demographic variation and on mother weaning success.

The sexually-segregated density dependence hypothesis almost systematically improves the model performance and is specifically selected for

Figure 5.6: *Simulations for adult males and adult females obtained with models (5.6) using parametrization as in FT1 (panel A), FT2 (panel B) and MT (panel C) respectively. Panels (D), (E) and (F) represent simulated kids and yearlings obtained with models (5.7). Parameter values and curve types are as in Fig. 5.4.*
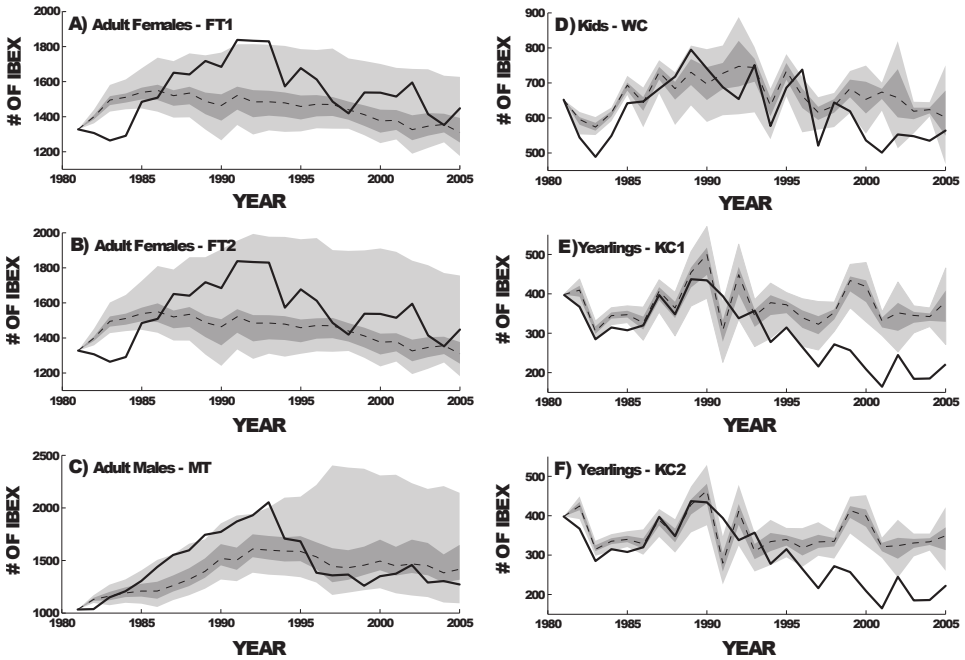
the female and male rates of demographic variation and for the weaning success. For kids, one of the two selected models is based on sexual segregation, while the other is not. With the only exception of one model for adult female demography, all the structured models selected among the many potential candidates include the interaction term between snow depth and density ($S_t D_t$). This result reinforces the evidence that climate strongly intensifies density dependence of ibex in GPNP, in accordance with the results of Jacobson *et al.* (2004). In fact, not only the total annual growth rate, but every single vital rate appears to be crucially dependent on the joint effect of snow depth and population density.

In contrast to what happens for the rate of demographic variation of adult males and females, the best models for kids and weaning success are continuous rather than threshold-like. Also, they reveal that an intermediate value of snow depth is optimal for both demographic parameters. This non-monotonic snow dependence is presumably related to different biological mechanisms. Winters with high snow cover are detrimental to all ibex, and especially adults, because food is scarcer than in low-snow winters and more energy is required to move in the high snowpack and dig out the dry grasses from below the snow. High ibex densities amplify the snow effect as in this case intraspecific competition becomes more severe. In addition, winters with large snow cover have a correspondingly higher probability of avalanches and the associated ibex casualties. This mechanism, where high winter snow is detrimental to ibex, have been thoroughly discussed in Jacobson *et al.* (2004).

Here, however, another effect has been discovered. Winters with very low snow cover (such as the winters in the last twenty years) are also detrimental to ibex, but this time through their effects on kid survival and weaning success. This seems to reflect a major sensitivity of juveniles to a lack of snow during winter. Pettorelli *et al.* (2007) have shown that, possibly because of climate change, the green-up of GPNP vegetation became faster. Indeed, the annual maximal increase in the normalized difference vegetation index (NDVI), a satellite-based measure that is strongly correlated with the net primary productivity, appeared to increase over time. This may lead to a shorter period of availability of high-quality forage over a large spatial scale, decreasing the opportunity for mountain ungulates to exploit high-quality forage. Kid rate of demographic variation might thus be influenced either directly or possibly via the state of mothers during lactation.

Although simulations obtained with the best structured and unstructured models show quite high variability within the range of bootstrapped parameter values, the actual time series of animal counts is not always included

in that range. Reference simulations made using unbiased parameters (see again Fig. 5.4) show that all models underestimate the population peak (occurred from the mid 1980s to the mid 1990s) and overestimate recent counts.

The long term simulations of each single compartment show an underestimation of the adult compartments during the growing phase of the peak and an overestimation of the juvenile compartments (kids and yearlings) during the population decline started from the mid-nineties. These results indicate that weaknesses in modelling adult rates of demographic variation are responsible for the underestimation of the population peak in the 1990s, while the overestimation of the recent declining trend can be mainly ascribed to inadequate modelling of recruitment and rate of demographic variation of kids.

Our findings suggest that mechanisms other than direct climate effects and population density could influence the dynamics of ibex in GPNP. As mentioned above, the recent drop of kid survival might also be related to the state of pastures. Another important, yet poorly explored factors are parasite infections and interspecific competition. In fact, emergence of parasitic infections that critically affect demography of ungulates have been recorded in different Arctic populations (Kutz *et al.*, 2004). Such epidemics appear to be favoured by climate warming. Modelling their effects on ibex population dynamics is thus a promising avenue for investigation (see for example Ferrari *et al.*, 2010). As for interspecific competition, it is known that ibex share their habitat with chamois (*Rupicapra rupicapra*) in the GPNP. Actually, the populations of chamois and ibex showed similar trends until 1993 (Picollo, 2002). After that year, however, chamois stayed approximately constant, while ibex started to decrease. Therefore, testing whether competition between the two species (documented in the literature since long time, see Pfeffer & Settimo, 1973) might be responsible for the decrease of ibex is worth exploring.

Finally, a big step ahead and a possible remedy to the shortcomings of currently available models would consist in formulating age-structured models that consider a more realistic subdivision into yearly classes of individuals of the same sex. Models at this finer scale would include the effects of senescence on male and female rates of demographic variation. These have been clearly documented, e.g. in a French population of ibex (Toïgo *et al.*, 2007). As reported for other species of large herbivores (Gaillard *et al.*, 2000), it is plausible that old ibex suffer much more than young individuals in years characterized by particularly unfavourable environmental conditions. Compartmented models, like those proposed in the present

chapter, cannot account for animal senescence, because all adults are included in the same class independent of their age. To develop complete age-structured models, one could integrate the count data with capture-mark-resight (CMR) data collected on cohorts of individually marked animals (currently under way at GPNP).

Even if CMR data are not available, other strategies can be used to reconstruct the age structure of the population and to use it in the dynamical models. The main focuses of the subsequent chapter are indeed the study of the effect of senescence in Alpine ibex dynamics and the reconstruction of the full age structure of the population.

Bibliography

Bianchi, M., Corani, G., Guariso, G. & Pinto, C. 2006: Prediction of ungulates abundance through local linear algorithms. Environmental Modelling and Software 21(10): 2004–2007. doi:10.1016/j.envsoft.2006.04.001.

Corani, G. & Gatto, M. 2007: Structural risk minimization: a robust method for density-dependence detection and model selection. Ecography 30(3): 400–416. doi:10.1111/j.2007.0906-7590.04863.x.

Efron, B. 1979: Bootstrap methods: another look at the jackknife. The annals of Statistics 7(1): 1–26.

Efron, B., Tibshirani, R. & Tibshirani, R. 1993: An introduction to the bootstrap. Chapman & Hall/CRC. ISBN 0412042312.

Ferrari, N., Rosà, R., Lanfranchi, P. & Ruckstuhl, K.E. 2010: Effect of sexual segregation on host-parasite interaction: model simulation for abomasal parasite dynamics in alpine ibex (Capraibex). International journal for parasitology 40(11): 1285–1293. doi:10.1016/j.ijpara.2010.03.015.

Fischlin, A., Midgley, G.F., Price, J., Leemans, R., Gopal, B., Turley, C., Rounsevell, M., Dube, P., Tarazona, J. & Velichko, A. 2007: Ecosystems, their properties, goods and services. In: Climate Change 2007: Impacts, Adaptation and Vulnerability. Contribution of Working Group II to the Fourth Assessment Report of the Intergovernmental Panel on Climate Change / Parry, M.L., Canziani, O. In Notes, Cambridge University Press, Cambridge, UK, chap. 4, (pp. 211–272).

Forchhammer, M., Post, E., Stenseth, N. & Boertmann, D. 2002: Global climate change and phenotypic variation among red deer cohorts. - Population Ecology 44: 113–120.

Gaillard, J.M., Festa-Bianchet, M. & Yoccoz, N.G. 1998: Population dynamics of large herbivores: variable recruitment with constant adult survival. - Trends in Ecology & Evolution 13(2): 58–63.

Gaillard, J.M., Festa-Bianchet, M., Yoccoz, N.G., Loison, A. & Toigo, C. 2000: Temporal variation in fitness components and population dynamics of large herbivores. Annual Review of Ecology and Systematics 31: 367–393.

Gaillard, J.M. & Yoccoz, N.G. 2003: Temporal variation in survival of mammals: a case of environmental canalization? Ecology 84(12): 3294–3306.

Grøtan, V., Sæther, B., Filli, F. & Engen, S. 2008: Effects of climate on population fluctuations of ibex. - Global Change Biology 14(2): 218–228. doi:10.1111/j.1365-2486.2007.01484.x.

von Hardenberg, A., Bassano, B., Percacino, V., Jacobson, A., von Hardenberg, J. & Provenzale, A. 2000: Preliminary analysis of the temporal variability of the Alpine ibex population in the Gran Paradiso National Park. - Ibex Journal of Mountain Ecology 5: 201–210.

von Hardenberg, A., Bassano, B. & Provenzale, A. 2009: Temporal variability in juvenile survival explains the strong population decline in the Alpine ibex Capra ibex population in Gran Paradiso National Park (North-Western Italian Alps). In V World Conference on Mountain ungulates. Granada (ESP).

Hastie, T. & Tibshirani, R. 1990: Generalized additive models. Chapman & Hall/CRC. ISBN 0412343908.

Jacobson, A., Provenzale, A., Von Hardenberg, A., Bassano, B. & Festa-Bianchet, M. 2004: Climate forcing and density dependence in a mountain ungulate population. Ecology 85(6): 1598–1610.

Jacobson, A.R., Festa-Bianchet, M., Provenzale, A., von Hardenberg, A. & Bassano, B. 2006: Comment on Lima & Berryman (2006): the Alpine ibex revisited. Climate Research 32(2): 137.

Kutz, S.J., Hoberg, E.P., Nagy, J., Polley, L. & Elkin, B. 2004: "Emerging" Parasitic Infections in Arctic Ungulates. Integrative and Comparative Biology 44(2): 109. doi:10.1093/icb/44.2.109.

Lande, R. 1993: Risks of Population Extinction from Demographic and Environmental Stochasticity and Random Catastrophes. - Global Change Biology 142(6): 911–927.

Largo, E., Gaillard, J., Festa-Bianchet, M. & C 2008: Can ground counts reliably monitor ibex Capra ibex populations. Wildlife Biology .

Lima, M. & Berryman, A. 2006: Predicting nonlinear and non-additive effects of climate: the Alpine ibex revisited. Climate Research 32(2): 129.

Nievergelt, B. 1974: The Behaviour of Ungulates and its relations to Management, Geist & Walther (Eds.), IUCN Publ., chap. A comparison of rutting behaviour in the Ethiopian and Alpine ibex., (pp. 324–340).

Pettorelli, N., Pelletier, F., von Hardenberg, A., Festa-Bianchet, M. & Côoté, S.D. 2007: Early onset of vegetation growth vs. rapid green-up: impacts on juvenile mountain ungulates. Ecology 88(2): 381–390.

Pfeffer, P. & Settimo, R. 1973: Deplecements saisonniers et competition vitale entre mouflons, chamois et bouquetins dans la reseve du Mercantour (Alpes Maritimes). Mammalia 37(2): 203–219.

Picollo, M. 2002: Effetti della variabilitá climatica su ecosistemi alpini. Master's thesis, Facoltá di Scienze Matematiche, Fisiche e Naturali, Universitá degli studi di Torino.

Post, E., Stenseth, N., Langvatn, R. & Fromentin, J. 1997: Global climate change and phenotypic variation among red deer cohorts. - Proceedings of the Royal Society of London. Series B: Biological Sciences 264: 1317–1324.

Sæ ther, B. & Saether, B.E. 1997: Environmental stochasticity and population dynamics of large herbivores: a search for mechanisms. Trends in Ecology & Evolution 12(4): 143–149.

Stüwe, M. & Grodinsky, C. 1987: Reproductive biology of captive Alpine ibex (Capra i. ibex). Zoo biology 6(4): 331–339.

Terzago, S., Cassardo, C., Cremonini, R. & Fratianni, S. 2010: Snow Precipitation and Snow Cover Climatic Variability for the Period 1971–2009 in the Southwestern Italian Alps: The 2008–2009 Snow Season Case Study. Water 2(4): 773–787.

Toïgo, C., Gaillard, J. & Michallet, J. 1997: Adult survival pattern of the sexually dimorphic Alpine ibex (Capra ibex ibex). Canadian Journal of Zoology 75(1): 75–79.

Toïgo, C., Gaillard, J.M. & Töigo, C. 2003: Causes of sex-biased adult survival in ungulates: sexual size dimorphism, mating tactic or environment harshness? Oikos 101(2): 376–384.

Toïgo, C., J.M., G., Festa-Bianchet, M., Largo, E., Michallet, J., Maillard, D., Töigo, C. & Gaillard, J.M. 2007: Sex-and age-specific survival of the highly dimorphic Alpine ibex: evidence for a conservative

life-history tactic. Journal of Animal Ecology 76(4): 679–686. doi: 10.1111/j.1365-2656.2007.01254.x.

Villaret, J. & Bon 1995: Social and spatial segregation in alpine ibex (Capra ibex) in Bargy, French Alps. - Ethology 101(4): 291–300.

Villaret, J., Bon, R. & Rivet, A. 1997: Sexual segregation of habitat by the alpine ibex in the French Alps. Journal of Mammalogy 78(4): 1273–1281.

Yoccoz, N.G. & Gaillard, J.M. 2006: Age structure matters for Alpine ibex population dynamics: comment on Lima & Berryman (2006). Climate Research 32(2): 139.

5.A   Appendix I

The following tables contain parameter values of the selected best models, together with their statistics. The labelling scheme of models and parameters is explained in the main text (see as references eqs. 5.3 and 5.4 in the main text). Since there is no risk of confusing $\beta_{i,\mathcal{C}}$ with $\beta_{i,w}$ or viceversa, we omit the second subscript in the tables. For threshold models, the superscripts refer to parameters calibrated using data of years with snow depth lower (L) or higher (H) than the threshold of $\bar{S} = 154$ cm used in (Jacobson *et al.*, 2004). The column "Best fit" indicates the best fitted value of the parameter obtained by minimizing the square errors (data until 1980), while "Unbiased value" stays for the bias-corrected parameter as suggested in Efron *et al.* (1993). The column $\mu \pm SE$ represents the mean $\pm$ the standard deviation of the parameter values obtained by using the bootstrapped 1 000 samples (see main text for details). CV is the coefficient of variation.

Table 5.2: *Parameters for the logarithm of the total annual growth rate qualifying the unstructured threshold model NT1*

Parameter	Best fit	Bootstrap analysis			
		$\mu \pm SE$		CV	Unbiased value
β_0^L	$4.46{\cdot}10^{-1}$	$4.26{\cdot}10^{-1}$	$\pm$ $2.20{\cdot}10^{-1}$	$5.16{\cdot}10^{-1}$	$4.66{\cdot}10^{-1}$
β_1^L	$-1.08{\cdot}10^{-4}$	$-1.04{\cdot}10^{-4}$	$\pm$ $7.21{\cdot}10^{-5}$	$6.94{\cdot}10^{-1}$	$-1.12{\cdot}10^{-4}$
β_2^L	-	-		-	-
β_3^L	$-7.13{\cdot}10^{-6}$	$-6.19{\cdot}10^{-6}$	$\pm$ $1.94{\cdot}10^{-5}$	3.14	$-8.07{\cdot}10^{-6}$
β_0^H	1.05	1.05	$\pm$ $1.76{\cdot}10^{-1}$	$1.68{\cdot}10^{-1}$	1.04
β_1^H	$-1.86{\cdot}10^{-4}$	$-1.87{\cdot}10^{-4}$	$\pm$ $6.92{\cdot}10^{-5}$	$3.70{\cdot}10^{-1}$	$-1.86{\cdot}10^{-4}$
β_2^H	-	-		-	-
β_3^H	$-7.32{\cdot}10^{-5}$	$-7.39{\cdot}10^{-5}$	$\pm$ $2.00{\cdot}10^{-5}$	$2.71{\cdot}10^{-1}$	$-7.25{\cdot}10^{-5}$

Table 5.3: *Parameters for the logarithm of the total annual growth rate qualifying the unstructured threshold model NT2*

Parameter	Best fit	Bootstrap analysis			
		$\mu \pm SE$		CV	Unbiased value
β_0^L	$9.59 \cdot 10^{-2}$	$9.43 \cdot 10^{-2}$	$\pm \quad 6.86 \cdot 10^{-2}$	$7.26 \cdot 10^{-1}$	$9.76 \cdot 10^{-2}$
β_1^L	-	-		-	-
β_2^L	$3.25 \cdot 10^{-1}$	$3.03 \cdot 10^{-1}$	$\pm \quad 2.04 \cdot 10^{-1}$	$6.72 \cdot 10^{-1}$	$3.46 \cdot 10^{-1}$
β_3^L	$-1.08 \cdot 10^{-4}$	$-1.01 \cdot 10^{-4}$	$\pm \quad 5.76 \cdot 10^{-5}$	$5.71 \cdot 10^{-1}$	$-1.14 \cdot 10^{-4}$
β_0^H	$3.71 \cdot 10^{-1}$	$3.80 \cdot 10^{-1}$	$\pm \quad 1.41 \cdot 10^{-1}$	$3.73 \cdot 10^{-1}$	$3.62 \cdot 10^{-1}$
β_1^H	-	-		-	-
β_2^H	$3.46 \cdot 10^{-1}$	$3.38 \cdot 10^{-1}$	$\pm \quad 1.71 \cdot 10^{-1}$	$5.05 \cdot 10^{-1}$	$3.55 \cdot 10^{-1}$
β_3^H	$-1.69 \cdot 10^{-4}$	$-1.68 \cdot 10^{-4}$	$\pm \quad 3.58 \cdot 10^{-5}$	$2.13 \cdot 10^{-1}$	$-1.70 \cdot 10^{-4}$

Table 5.4: *Parameters for the logarithm of the adult female rate of demographic variation of the age-structured model FT1*

Parameter	Best fit	Bootstrap analysis			
		$\mu \pm SE$		CV	Unbiased value
β_0^L	$1.34 \cdot 10^{-1}$	$1.64 \cdot 10^{-1}$	$\pm \quad 1.57 \cdot 10^{-1}$	$9.56 \cdot 10^{-1}$	$1.04 \cdot 10^{-1}$
β_1^L	$-1.23 \cdot 10^{-4}$	$-1.39 \cdot 10^{-4}$	$\pm \quad 7.29 \cdot 10^{-5}$	$5.26 \cdot 10^{-1}$	$-1.08 \cdot 10^{-4}$
β_2^L	$4.64 \cdot 10^{-2}$	$4.81 \cdot 10^{-2}$	$\pm \quad 4.68 \cdot 10^{-2}$	$9.73 \cdot 10^{-1}$	$4.46 \cdot 10^{-2}$
β_3^L	-	-		-	-
β_0^H	$9.13 \cdot 10^{-1}$	1.06	$\pm \quad 2.65 \cdot 10^{-1}$	$2.49 \cdot 10^{-1}$	$7.63 \cdot 10^{-1}$
β_1^H	$-4.08 \cdot 10^{-4}$	$-4.82 \cdot 10^{-4}$	$\pm \quad 1.33 \cdot 10^{-4}$	$2.75 \cdot 10^{-1}$	$-3.35 \cdot 10^{-1}$
β_2^H	$-1.23 \cdot 10^{-1}$	$-1.20 \cdot 10^{-1}$	$\pm \quad 3.86 \cdot 10^{-2}$	$3.21 \cdot 10^{-1}$	-1.26E-0.1
β_3^H	-	-		-	-

Table 5.5: *Parameters for the logarithm of the adult female rate of demographic variation of the age-structured model FT2*

Parameter	Best fit	Bootstrap analysis			
		$\mu \pm SE$		CV	Unbiased value
β_0^L	$1.91 \cdot 10^{-1}$	$2.16 \cdot 10^{-1}$	$\pm \quad 1.54 \cdot 10^{-1}$	$7.14 \cdot 10^{-1}$	$1.66 \cdot 10^{-1}$
β_1^L	$-1.53 \cdot 10^{-4}$	$-1.65 \cdot 10^{-4}$	$\pm \quad 8.35 \cdot 10^{-5}$	$5.05 \cdot 10^{-1}$	$-1.40 \cdot 10^{-4}$
β_2^L	-	-		-	-
β_3^L	$2.39 \cdot 10^{-5}$	$2.46 \cdot 10^{-5}$	$\pm \quad 2.75 \cdot 10^{-5}$	1.12	$2.32 \cdot 10^{-5}$
β_0^H	$6.66 \cdot 10^{-1}$	$8.29 \cdot 10^{-1}$	$\pm \quad 2.96 \cdot 10^{-1}$	$3.57 \cdot 10^{-1}$	$5.02 \cdot 10^{-1}$
β_1^H	$-2.96 \cdot 10^{-4}$	$-3.75 \cdot 10^{-4}$	$\pm \quad 1.68 \cdot 10^{-4}$	$4.48 \cdot 10^{-1}$	$-2.16 \cdot 10^{-4}$
β_2^H	-	-		-	-
β_3^H	$-5.59 \cdot 10^{-5}$	$-5.46 \cdot 10^{-5}$	$\pm \quad 2.60 \cdot 10^{-5}$	$4.77 \cdot 10^{-1}$	$-5.71 \cdot 10^{-5}$

Table 5.6: *Parameters for the logarithm of the adult male rate of demographic variation of the age-structured model MT*

Parameter	Best fit	Bootstrap analysis		
		$\mu \pm SE$	CV	Unbiased value
β_0^L	$-2.51 \cdot 10^{-2}$	$-2.28 \cdot 10^{-2}$ $\pm$ $1.04 \cdot 10^{-1}$	4.56	$-2.73 \cdot 10^{-2}$
β_1^L	-	-	-	-
β_2^L	-	-	-	-
β_3^L	$-4.89 \cdot 10^{-5}$	$-4.92 \cdot 10^{-5}$ $\pm$ $2.27 \cdot 10^{-3}$	1.46	$-4.85 \cdot 10^{-5}$
β_0^H	$3.22 \cdot 10^{-1}$	$3.27 \cdot 10^{-1}$ $\pm$ $1.54 \cdot 10^{-1}$	$4.70 \cdot 10^{-1}$	$3.16 \cdot 10^{-1}$
β_1^H	-	-	-	-
β_2^H	-	-	-	-
β_3^H	$-1.96 \cdot 10^{-4}$	$-2.00 \cdot 10^{-4}$ $\pm$ $6.38 \cdot 10^{-5}$	$3.19 \cdot 10^{-1}$	$-1.92 \cdot 10^{-4}$

Table 5.7: *Parameters for the logarithm of the kid rate of demographic variation of the age-structured model KC1*

Parameter	Best fit	Bootstrap analysis		
		$\mu \pm SE$	CV	Unbiased value
β_0	$-3.65 \cdot 10^{-1}$	$-4.20 \cdot 10^{-1}$ $\pm$ $2.46 \cdot 10^{-1}$	$5.85 \cdot 10^{-1}$	$-3.11 \cdot 10^{-1}$
β_1	-	-	-	-
β_2	$9.85 \cdot 10^{-1}$	1.12 $\pm$ $4.03 \cdot 10^{-1}$	$3.59 \cdot 10^{-1}$	$8.47 \cdot 10^{-1}$
β_3	$-1.88 \cdot 10^{-1}$	$-2.01 \cdot 10^{-1}$ $\pm$ $1.12 \cdot 10^{-1}$	$5.59 \cdot 10^{-1}$	$-1.75 \cdot 10^{-1}$
β_4	$-4.07 \cdot 10^{-4}$	$-4.45 \cdot 10^{-4}$ $\pm$ $1.58 \cdot 10^{-4}$	$3.55 \cdot 10^{-1}$	$-3.69 \cdot 10^{-4}$
β_5	-	-	-	-

Table 5.8: *Parameters for the logarithm of the kid rate of demographic variation of the age-structured model KC2*

Parameter	Best fit	Bootstrap analysis		
		$\mu \pm SE$	CV	Unbiased value
β_0	$-4.72 \cdot 10^{-1}$	$-5.19 \cdot 10^{-1}$ $\pm$ $2.35 \cdot 10^{-1}$	$4.53 \cdot 10^{-1}$	$-4.25 \cdot 10^{-1}$
β_1	-	-	-	-
β_2	1.15	1.21 $\pm$ $3.78 \cdot 10^{-1}$	$3.13 \cdot 10^{-1}$	1.08
β_3	$-2.33 \cdot 10^{-1}$	$-2.47 \cdot 10^{-1}$ $\pm$ $1.08 \cdot 10^{-1}$	$4.37 \cdot 10^{-1}$	$-2.19 \cdot 10^{-1}$
β_4	$-2.53 \cdot 10^{-4}$	$-2.55 \cdot 10^{-4}$ $\pm$ $6.47 \cdot 10^{-5}$	$2.54 \cdot 10^{-1}$	$-2.51 \cdot 10^{-4}$
β_5	-	-	-	-

Table 5.9: *Parameters for the logarithm of the kid rate of demographic variation of the age-structured model WC*

Parameter	Best fit	Bootstrap analysis			
		$\mu \pm SE$		CV	Unbiased value
β_0	$-9.42 \cdot 10^{-1}$	$-9.31 \cdot 10^{-1}$	$\pm$ $2.15 \cdot 10^{-1}$	$2.31 \cdot 10^{-1}$	$-9.54 \cdot 10^{-1}$
β_1	-	-		-	-
β_2	$7.60 \cdot 10^{-1}$	$7.75 \cdot 10^{-1}$	$\pm$ $4.04 \cdot 10^{-1}$	$5.21 \cdot 10^{-1}$	$7.44 \cdot 10^{-1}$
β_b	$-1.43 \cdot 10^{-1}$	$-1.24 \cdot 10^{-1}$	$\pm$ $1.11 \cdot 10^{-1}$	$8.99 \cdot 10^{-1}$	$-1.63 \cdot 10^{-1}$
β_3	$-2.11 \cdot 10^{-4}$	$-2.37 \cdot 10^{-4}$	$\pm$ $1.18 \cdot 10^{-4}$	$4.98 \cdot 10^{-1}$	$-1.85 \cdot 10^{-4}$
β_c	-	-		-	-

CHAPTER 6

The role of senescence in the population dynamics of Alpine ibex

6.1 Abstract

In the previous chapter we emphasized the joint role played by population density and climatic conditions in determining ibex population dynamics. Here we extend the study investigating whether they can be affected by temporal variations in the age-structure of the population. It is in fact known from past studies that survival rates decrease with age in both sexes and old individuals become more sensitive to harsh conditions (senescence). Moreover, the fertility increases with age for young females (maturation) and decreases for old females (senescence). Available census data for Gran Paradiso National Park (GPNP) population do not include age-specific counts, so we build the age-structure of the adults by accumulating data on different cohorts of yearlings. We contrast models characterized by different families of senescence and maturation functions and, within these families, by different parameters on abiotic (snow depth) and/or biotic (population density) factors. We selected the best models according to the second order Akaike's Information criterion (AIC_c). Since model selection is highly un-

157

certain, we produced the predictions using multimodel inference based on Akaike's weights. The structures of the best models suggest that considering maturation and senescence is particularly important to model the adult females survival and the survival of kids, but less important for the survival of adult males and the weaning success. The role of snow depth and density found in the previous chapter is almost completely confirmed, even if the nonlinear effects are less strongly detected. Nevertheless, considering the population structure decreases the importance of density dependence, because the fraction of old individuals and the population density increases at the same time. The work highlights how one of the important drivers of Alpine ibex dynamics in GPNP is the variation of the population structure. However, to confirm the hypothesis, the results should be matched with real data on the population structure (e.g. CMR data).

6.2 Introduction

The main shortcoming of the models discussed in literature and those proposed in the previous chapter for the dynamics of the Alpine ibex in the GPNP is the poor predictive power on the recent decreasing trend of the population (e.g. see figure 5.6 at page 143). The results obtained using the age and sex structured models presented above have shown that this drawback is mainly due to some lacks in the models for the compartment of juveniles. Recent studies have confirmed that the main cause of the ibex drop is the decrease in the survival of kids (A. Provenzale, personal communication). As mentioned in the previous chapter, one of the possible explanation for this phenomenon is the worsening of the state of the pastures (Pettorelli *et al.*, 2007). Another sound alternative hypothesis is that the dynamics were influenced by the variation of the population structure and the increase of the fraction of senescent individuals.

Senescence is defined as the decrease of vital functions of an individual (or its cells) near the end of its typical lifespan. In particular, we use here the term *senescence* to intend a decrease with age of (i) the survival, (ii) the weaning success and (iii) the ability of the mothers to breed their kids to adulthood. Moreover, individuals of many species usually have, at the beginning of their life, a period before the full development characterized by a high mortality and a low production of offspring. Along with these effects, senescent and young individuals are also less able to face harsh environmental conditions. Most of the studies on senescence are focused on the human species and the age-related changes in the risk of mortality (Monaghan *et al.*, 2008). However, senescence on other components of

the fitness have been found for different phyla of the animal kingdom (see Benton *et al.* (2008) for an example on mites and Martin & Service (1995) for an example on birds).

Gaillard *et al.* (2000) show that, regardless of the environmental conditions, female survival and fecundity are high in large herbivores and have a low variability in adults, while they are lower but more variable for kids and old adults, and moderately variable for prime-age adults. They show also that the overall population dynamics are more affected by a variation in the adult survival (less variable) than in recruitment (more variable) thus leading to a damped effects of detrimental conditions in the short period (see also Gaillard & Yoccoz, 2003). However, if detrimental conditions occurs for many consecutive years, the long term dynamics can be driven by the variations in recruitment, as happened in the Alpine ibex population of the GPNP. Other authors report evidences of senescence in ungulates, underlining how adverse climatic conditions and high densities affect more older individuals than younger (White *et al.*, 2011; Garrott & Eberhardt, 2003; Mysterud *et al.*, 2001).

Unfortunately, in long living mammals, it is often hard to distinguish between density dependence and senescence of the population, because populations at high densities have, usually, also a high proportion of old individuals (Festa-Bianchet *et al.*, 2003). The recruitment tends in fact to decrease as the density increases, thus leading to a population with many senescent individuals, and a smaller growth rate. Festa-Bianchet *et al.* (2003) found that, if the age structure is taken into account, often the strength of the detected density dependence effect decreases.

Toïgo *et al.* (1997) specifically studied the senescence in the survival of males and females for a French population of Alpine ibex. They confront different Gompertz or Weibull functions, as suggested by Gaillard *et al.* (2004), and found that in both cases the Gompertz model better fits their data. Moreover, they show that the decrease of survival with age is steeper for males than for females, and females survival is more bufferd against environmental variations. Functions to model the age-specific fecundity of mammalian population are typically unimodal with a maximum for the mature adults. For example, Gage (2001) proposes the use of three competing models: the Gamma distribution, the Hadwiger function, and the Brass polynomial. However, it is very rare to find studies that model (and not only describe) the age-specific fecundity of ungulates. Loison *et al.* (2002) reports, for a reintroduced population of ibex, a fertility of 43% at the age of two and a fertility of 87% from year three onwards. On the other hand, Giacometti & Ratti (1994) report, for a Swiss population, a fecundity rate

that is lower for old females (14-16 years), intermediate for young females (3 years) and higher for mature adult females (4-13 years).

In this chapter, we develop a state space model for the dynamics of the Alpine ibex population of the GPNP. The model permits to reconstruct the structure of the population of the last years through the accumulation of several cohorts of yearlings. Moreover, proposed models potentially include functions that describe the interplay between population density, snow depth, development time and senescence in determining the age specific survivals and fertilities.

6.3 Methods

6.3.1 The state-space model

A generic state-space model is a model representation that includes both a measurement and a state transition process. The measurement equations describe the relationship between the state of the system and the measurements, while the transition equations describe how the state of the system evolves through time. We modelled our system including the age structure of the population in the state vector, and using the censuses as our measurements. According to the results of the last chapter, we hypothesize that the male density does not affect neither reproduction nor male survival. Thus, to simplify the description of the model, we first define the equations for the female population only.

Following the available censuses, we define the measurement vector as $\boldsymbol{y}_t = [\log(K_t), \log(Y_t), \log(F_t)]'$, where K_t, Y_t and F_t are, respectively, the number of kids, yearlings and females measured at year t and the symbol ' stays for transposed.

The state vector is $\boldsymbol{x}_t = [F_{II,t} \ldots F_{XX,t}, F_{1,t}, \ldots, F_{20,t}]'$, where $F_{j,t}$ is the number of female kids made by a female of age j if j is a Roman numeral; conversely, if j is an Arabic numeral, $F_{j,t}$ is the number of females of age j at year t. Notice that the state vector includes the age structure of the population. Moreover, kids (females of age 0) are partitioned according to age of the mother. The age of an adult female can in fact influence not only its own survival rate and its weaning success, but also the chances of its offspring to survive the first year of life, for example because of an age-dependent ability of parental care. Notice also that $F_{1,t}$ are female yearlings.

The state transition and the observation equations are defined as

$$x_{t+1} = \Phi_t(\bullet)x_t + w_t \tag{6.1}$$

$$y_t = \log(H_t x_t) + v_t \tag{6.2}$$

where w_t and v_t are the process and measurement noise vectors and $\Phi_t(\bullet)$ is defined as the square matrix:

$$
\begin{array}{cccccccccc}
II & III & \ldots & XX & 1 & 2 & \ldots & 19 & 20 \\
\end{array}
$$

$$
\begin{pmatrix}
0 & 0 & \ldots & 0 & \frac{1}{2}\sigma_1(\cdot)f_2(\cdot) & 0 & \ldots & 0 & 0 \\
0 & 0 & \ldots & 0 & 0 & \frac{1}{2}\sigma_2(\cdot)f_3(\cdot) & \ldots & 0 & 0 \\
\vdots & \ddots & \ddots & \ddots & \ddots & \ddots & \ddots & \ddots & \vdots \\
0 & 0 & \ldots & 0 & 0 & 0 & \ddots & \frac{1}{2}\sigma_{19}(\cdot)f_{20}(\cdot) & 0 \\
\sigma_{II}^K(\cdot) & \sigma_{III}^K(\cdot) & \ldots & \sigma_{XX}^K(\cdot) & 0 & \ldots & \ldots & 0 & 0 \\
0 & 0 & \ldots & 0 & \sigma_1(\cdot) & 0 & \ddots & 0 & 0 \\
0 & 0 & \ldots & 0 & 0 & \sigma_2(\cdot) & \ddots & 0 & 0 \\
\vdots & \ddots & \ddots & \ddots & \ddots & \ddots & \ddots & \vdots \\
0 & 0 & \ldots & 0 & 0 & 0 & \ldots & \sigma_{19}(\cdot) & 0 \\
\end{pmatrix} \tag{6.3}
$$

where the age specific fertilities, $f_j(\cdot)$, and survivals, $\sigma_j(\cdot)$ and $\sigma_j^K(\cdot)$, are functions of the the population density ($D_t = F_t + Y_t/2 + K_t$) and of the mean winter snow depth (S_t). $\Phi_t(\bullet)$ is a Leslie-like transition matrix properly designed to take memory of the mother's age for each kid. The survival functions identified by a Roman number represent the probability of survival for a kid as dependent on the age of its mother; for example, $\sigma_{XIX}^K(\cdot)$ is the survival of a kid whose mother has 19 years. The weaning success rates $f_j(\cdot)$ are defined as the number of kids per females, and are multiplied by 0.5 because we hypothesize a balanced sex ratio for both kids and yearlings. Notice also that the last age class (20 years) is not fertile and its survival is equal to zero. In the measurement equation, H_t is defined as:

$$
H_t =
\begin{array}{c}
\begin{array}{ccccccc}
II & \ldots & XX & 1 & 2 & \ldots & 20 \\
\end{array} \\
\begin{pmatrix}
2 & \ldots & 2 & 0 & \ldots & \ldots & 0 \\
0 & \ldots & 0 & 2 & 0 & \ldots & 0 \\
0 & \ldots & 0 & 0 & 1 & \ldots & 1 \\
\end{pmatrix}
\end{array} \tag{6.4}
$$

6.3.2 Weaning success and survival functions

The fertilities and the survival functions reported in equation 6.3 are functions that depend on the age (j) of the individuals or, for kids only, of their

mothers. To limit the degrees of freedom, we constrained the weaning success and the survival of kids to vary with age according to specified functional forms, suitably chosen to take into account the contributes of senescence and maturity. Moreover, fertilities and survivals potentially varies with the population density (D_t) and the mean winter snow depth (S_t). The equations for weaning success and survival can be therefore written has:

$$\sigma_j^K(\cdot) = \sigma(j, D_t, S_t) \qquad (6.5)$$
$$\sigma_j(\cdot) = \sigma(j, D_t, S_t) \qquad (6.6)$$
$$f_j(\cdot) = f(j, D_t, S_t) \qquad (6.7)$$

where functions are time-dependent if D_t and/or S_t are included in the model.

To model the variation of adult survival with age, we used monotonic descending functions, under the hypothesis that from age 2 the survival can only decrease, as described in Toïgo *et al.* (2007). For weaning success and survival of kids, j is the age of their mothers. Under the hypothesis that, as shown in literature (e.g. see Loison *et al.*, 2002), from the first year of maturity a female needs some years to reach its maximal fertility rate, and that after the peak there is a decrease due to senescence, we tested unimodal functions for weaning success. For the variation of kids survival with the age of the mother there are few informations in literature, thus we tested both monotonically decreasing and unimodal functions. Using the unimodal functions, we are assuming that the ability of a female to take care of its offspring increases with the age, reaches a maximum, then decreases as senescence occurs. Using a monotonic function we are instead considering that this ability can only decrease in time. For kids' survival, the candidate functional forms are the same used for weaning success and adult survival.

Adult survival functions

Using age-structured data from a French population of Alpine ibex, Toïgo *et al.* (1997) calibrated age-dependent adult survival functions based on the Gompertz and the Weibull distributions. To compute the discrete-time survival, the authors use an approximate solution of the Weibull and the Gompertz functions (Gaillard *et al.*, 2004). However, the integrals of the Weibull and the Gompertz functions can be solved analytically without approximations, as we show below. We consider five different competing age-dependent model structures for the survival:

- constant survival between age 1 and 8, then a Gompertz function until age 20;

- constant survival between age 1 and 8, then a Weibull function until age 20;

- a Weibull function from age 1 to age 20;

- a Gompertz function from age 1 to age 20;

- constant survival from age 1 to age 20.
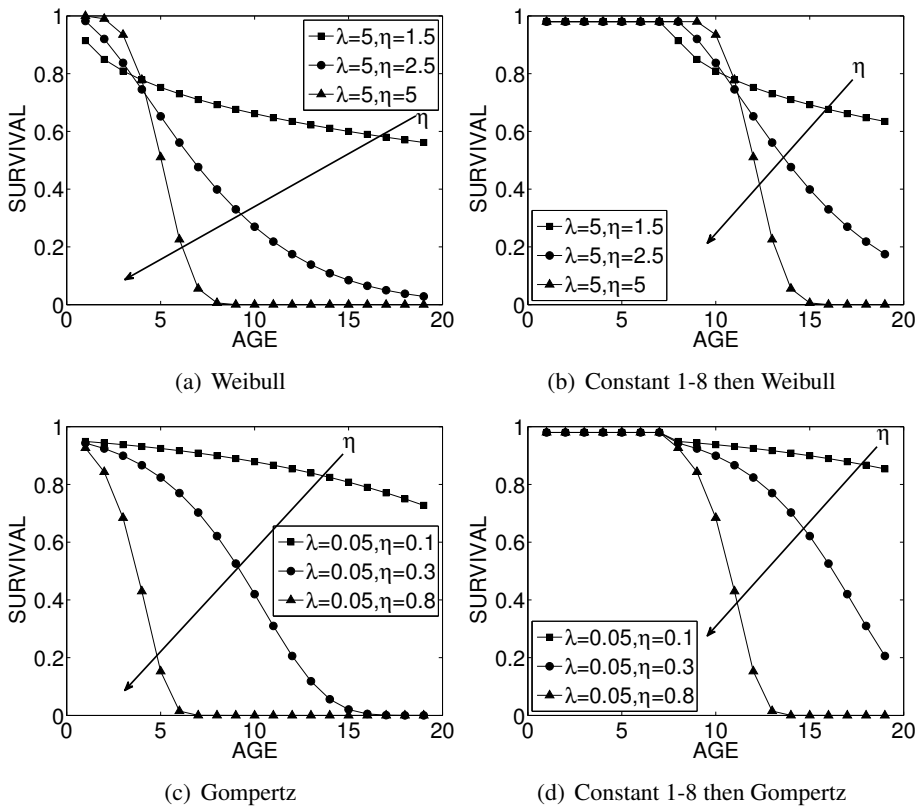
Figure 6.1: *Examples of the age-dependent survival functions, obtained using four of the five tested senescence functions listed in the main text: panel a) Weibull; panel b) constant survival from age 1 to age 8, then Weibull; panel c) Gompertz; panel b) constant survival from age 1 to age 8, then Gompertz. We show the value of the functions obtained using different values of the senescence parameter, while the other parameters are kept constant.*

Weibull: The hazard rate of the Weibull distribution is

$$h(t) = \frac{\eta}{\lambda^\eta} t^{(\eta-1)} \tag{6.8}$$

where $\eta > 0$ is the shape parameter and $\lambda > 0$ is the scale parameter. The shape parameter determines if the failure (death) rate increases ($\eta > 1$), decreases ($\eta < 1$) or is constant ($\eta = 1$) over ages, thus η defines the senescence rate. Starting from the hazard rate, the probability that an individual has at birth to survive until age j is:

$$p(j) = e^{-\int_0^j h(t)\,dt} = e^{-\left(\frac{j}{\lambda}\right)^\eta} \tag{6.9}$$

and the discrete time survival between age j and $j+1$ is

$$\sigma(j) = \frac{p(j+1)}{p(j)} = \frac{e^{1-\left(\frac{j+1}{\lambda}\right)^\eta}}{e^{1-\left(\frac{j}{\lambda}\right)^\eta}} = e^{\frac{j^\eta - (j+1)^\eta}{\lambda^\eta}} \tag{6.10}$$

Gompertz: The hazard rate of the Gompertz distribution is of the form:

$$h(t) = \lambda e^{(\eta t)} \tag{6.11}$$

where η is the shape parameter (senescence factor) and λ is the scale parameter. Over the age, the mortality rate increases if $\eta > 0$, decreases if $\eta < 0$ and it is constant if $\eta = 0$. The probability at birth to survive until age j ($p(j)$) and the survival between age j and $j+1$ ($\sigma(j)$) are defined as

$$p(j) = e^{-\int_0^j h(t)\,dt} = e^{-\left[\frac{\lambda}{\eta}\left(e^{\eta j}-1\right)\right]} \tag{6.12}$$

$$\sigma(j) = \frac{p(j+1)}{p(j)} = e^{\frac{\lambda}{\eta}\left(e^{\eta j}-e^{\eta(j+1)}\right)} \tag{6.13}$$

Weaning success functions

For the weaning success (number of kids per females), we used distributions that are potentially unimodal, because we expect, starting from the age of maturity, an increase in the weaning success due to maturation and then a decrease due to senescence. The two candidate functional forms are the *Gamma* and the *Beta* distributions, along with a model in which the weaning success is constant over the ages.
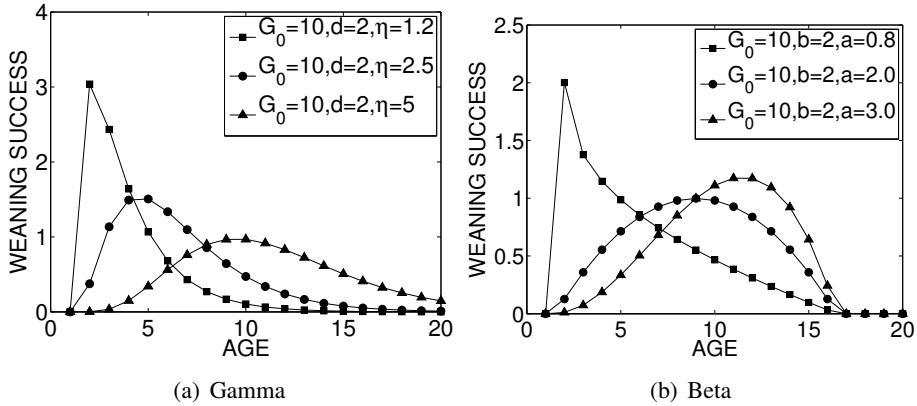
(a) Gamma

(b) Beta

Figure 6.2: *Examples of the age-dependent weaning success functions, obtained using two of the three tested senescence functions listed in the main text: panel a) Gamma; panel b) Beta. We show the value of the functions obtained using different values of the parameter η for the Gamma (see equation 6.16) and a for the Beta (see equation 6.19), while the other parameters are kept constant.*

Gamma: The Gamma model assumes that the continuous weaning success rate is:

$$\psi(j) = \begin{cases} \frac{G_0(j-j_0)^{(\eta-1)}e^{-\left(\frac{j-j_0}{d}\right)}}{d^\eta \Gamma(\eta)}, & \text{if } j > j_0 \\ 0, & \text{if } j \leq j_0 \end{cases} \qquad (6.14)$$

where j_0 is the age at first reproduction, G_0 is the gross reproduction rate, d is a scale parameter, η is a shape parameter and $\Gamma(\eta) = \int_0^\infty t^{\eta-1}e^{-t}dt$ is the Gamma function. For Alpine ibex, the system is discrete because the reproduction occurs only once a year in a specific period. The corresponding cumulative function is

$$\Psi(j) = G_0 \int_{j_0}^{j} \psi(t) = G_0 \frac{\gamma(\eta, (j-j_0)/d)}{\Gamma(\eta)} \qquad (6.15)$$

where $\gamma(\eta, (j-j_0)/d) = \int_0^{(j-j_0)/d} t^{\eta-1}e^{-t}dt$ is the *lower incomplete gamma function*. Thus, in the discrete time case the Gamma weaning success model becomes:

165

$$f(j) = \begin{cases} \frac{G_0}{\Gamma(\eta)} \left(\gamma(\eta, (j - j_0)/d) - \gamma(\eta, (j - 1 - j_0)/d) \right), & \text{if } j > j_0 \\ 0, & \text{if } j \leq j_0 \end{cases}$$

$$(6.16)$$

According to literature (see the introduction of this chapter), the females start to be fertile at the age of two, therefore we fixed $j_0 = 1$. Since j_0 is fixed, the free parameters are the senescence parameter (η), the scale parameter d and the gross reproduction rate (G_0).

Beta   The *Beta* function is here properly modified to be defined between the age of first reproduction j_0 and the last fertile age j_l. The weaning success in a continuous system is described by the *Beta* as:

$$\psi(j) = \begin{cases} \frac{G_0 z(j)^{(a-1)} [1 - z(j)]^{(b-1)}}{B(a,b)}, & \text{if } j_0 \leq j \leq j_l \\ 0, & \text{else} \end{cases}$$

$$(6.17)$$

where $z(j) = (j - j_0)/(j_l - j_0)$, G_0 is again the gross reproduction rate, while b and a are two shape parameters. The corresponding cumulative function, for $j_0 \leq j \leq j_l$ is

$$\Psi(j) = G_0 I_{z(j)}(a, b)$$

$$(6.18)$$

where $I_{z(j)}$ is the *regularized incomplete beta function*. Thus, the discrete time form of the weaning success is

$$f(j) = \begin{cases} G_0 \left(I_{z(j)}(a, b) - I_{z(j-1)}(a, b) \right), & \text{if } j_0 \leq j \leq j_l \\ 0, & \text{else} \end{cases}$$

$$(6.19)$$

We here fix the reproductive limits to $j_0 = 2$ and $j_l = 16$, according to the biology of the species. Fixing these two parameters, the parameters to be calibrated are the gross production rate and the two shape parameters.

Dependence on climate and density

The dependencies on the snow depth and on the population density are taken into account in two different ways: i) as a multiplicative factor or ii) to determine the value of the shape parameter η (a for the *Beta* distribution) of the function. Let $g(j)$ be a generic weaning success or survival function, the multiplicative models are defined as

$$g(j, S_t, D_t) = f(j) * e^{\left(\beta_1 D_t + \beta_2 S_t + \beta_3 S_t D_t + \beta_4 S_t^2 + \beta_5 D_t^2 \right)}$$

$$(6.20)$$

In the other case (ii), the density and the snow depth affect the senescence parameters; in other words we are assuming that old individuals suffer the harsh conditions more than young individuals, as reported for many ungulates (see the introduction of this chapter). Thus, parameter η becomes function of the density and the snow depth:

$$\eta(S_t, D_t) = \eta_0 + \beta_1 D_t + \beta_2 S_t + \beta_3 S_t D_t + \beta_4 S_t^2 + \beta_5 D_t^2 \qquad (6.21)$$

To define the model set, for each age dependent survival or weaning success function, we consider the complete model as expressed in equations 6.20 or 6.21 and all the possible models defined setting to zero one or more β_i terms.

6.3.3 Model identification

The aims of our model are to reconstruct the complete age structure of the population and to simulate the population dynamics. The use of a classical Kalman filtering techniques is not possible here because several requirements to apply the filter are not satisfied by the system. In particular the initial state, the parameter values and the variance-covariance matrices of measurement and process errors are unknown, and the model is not linear. Several methods have been developed to overcome these problems. For example the extended and the unscented Kalman filters are suitable for nonlinear systems with Gaussian noises (Julier & Uhlmann, 1997), while particle filtering techniques, based on Montecarlo method, deal both with model nonlinearities and non-Gaussian noises. De Valpine & Hastings (2002) specifically developed a method for fitting nonlinear and non-Gaussian models of population abundance, where the probability calculations are carried out numerically. Even using these advanced methods, the problem of estimating the initial conditions is till open and can be solved only under particular circumstances. If the parameters of the model are known and under the hypothesis that the system is at the equilibrium, the initial population can be approximated using the stationary distribution. If these conditions are not satisfied (as for the system under study in this chapter), another interesting possibility is to treat the initial state of the system as an additional unknown parameter and to recursively estimate it, like suggested in Dennis *et al.* (2006).

However, even estimating the initial state of the system is not an efficient solution for the system under study. In fact, the state vector x_t has 39 elements and, consequently, so that the vector w_t. If these vectors are

treated as parameters to be estimated, the dimensionality of the model increases excessively, especially taking into account that only 44 years of data are available for calibration. Therefore we decided to simplify the problem setting $w_t = 0$ and incorporating all the noise in the measurement error v_t, thus saving the calibration of 39 parameters. The measurement error is distributed as $v_t = N_3(0, \Sigma)$, where:

$$\Sigma = \begin{pmatrix} \sigma_K^2 & 0 & 0 \\ 0 & \sigma_Y^2 & 0 \\ 0 & 0 & \sigma_F^2 \end{pmatrix} \quad (6.22)$$

Moreover, to avoid the definition of 38 more parameters for the initial state (Y_0 is measured, thus its estimate can be avoided), we used the first 18 years of yearlings counts to accumulate cohorts and completely reconstruct the adult population structure and the structure of kids at year 19. Thus, we used only the last 26 years of data to calibrate and test the model. Note that, using this strategy, we saved the calibration of more than two parameters for each year used to accumulate the cohorts and therefore we strongly improved the ratio between data and parameters to be estimated.

In order to calibrate the models, we need to define the figure of merit that has to be optimized. The problem is indeed much more complicated than in the previous chapter, in which we easily calibrate the sub-models of weaning success, kids' survival and adult females survival. The same separation of sub-models is not straightforward in this chapter, because the age structure of the adult population is not measured, nor the age of the mothers is available to define the structure of kids.

If the sub-models are not separated, one of the alternatives is to use a figure of merit which represent the overall dynamic of the population, such as the population growth rate. One of the main issue in adopting such strategy is that it would lead to estimate of many parameters with relatively few data. Moreover, calculating a unique figure of merit at each time step (t), thus merging the separate counts of kids, yearlings and adults, most of the information contained in the counts is discarded. On the other hand, it is also possible to define more than one figure of merit, separately looking at the different measures (K_t, Y_t and F_t). However, this implies to solve a multi-objective problem, which is computationally too expensive. Moreover, having more than one objective, some of them can be conflictual, i.e. impossible to be contemporary optimized. In this case, a good solution for the optimization is to find many Pareto optimal solutions instead of a unique optimum.

To overcome all these problems, we developed a method to perform a sequential optimisation of three sub-models: (i) adult females survival, (ii) weaning success and (iii) survival of kids. The main idea is to first calibrate the adult survival model and to reconstruct the age-structure of the adult females ($F_{2,t}, ..., F_{20,t}$), using the counts of yearlings as inputs. Starting from the reconstructed structure of adult females, it is then possible to calibrate the model of weaning success and to reconstruct the structure of kids (i.e. fraction of kids having a mother of a given age, $F_{II,t}...F_{XIX,t}$). Using the kids' structure it is finally possible to calibrate the parameters of the models for the survival of kids. This permits to avoid the definition of a single score and allows to separately use the counts of kids, yearlings and females. Thus, we aimed at separately minimizing three sum of squared simulation errors calculated as:

- $SSE^F = \sum_t \left(\log(\hat{F}_t) - \log(F_t) \right)^2$ for the adult female survivals

- $SSE^K = \sum_t \left(\log(\hat{K}_t) - \log(K_t) \right)^2$ for weaning success

- $SSE^Y = \sum_t \left(\log(\hat{Y}_t) - \log(Y_t) \right)^2$ for the kids' survival

where the hatted variables are the simulated values of the corresponding measured variables (not hatted). The three submodels used for sequential optimisation are summarized in figure 6.3 and explained in detail in the following three subsections.

To select the best models for each sub-model, we used the second order Akaike's Information Criterion (AICc, equation 2.19 at page 36). We selected as best all the models that have $AICc \leq AICc_{best} + 4$. If more than one model was selected, predictions were made using the AIC_c multimodel inference as described in section 6.3.3 at page 171. We decided to use this approach, which is more empirical than a rigorous BMA, because the system is strongly nonlinear and the model posteriors are thus extremely hard to be computed.

First sub-model: adult females survival

The first identification step is the calibration of the model for the adult females survival. The state space model is defined as a sub-model of equations 6.1, 6.3 and 6.4, properly modified to include the counts of yearlings as a forcing factor. The state transition equation for this sub-model thus becomes:

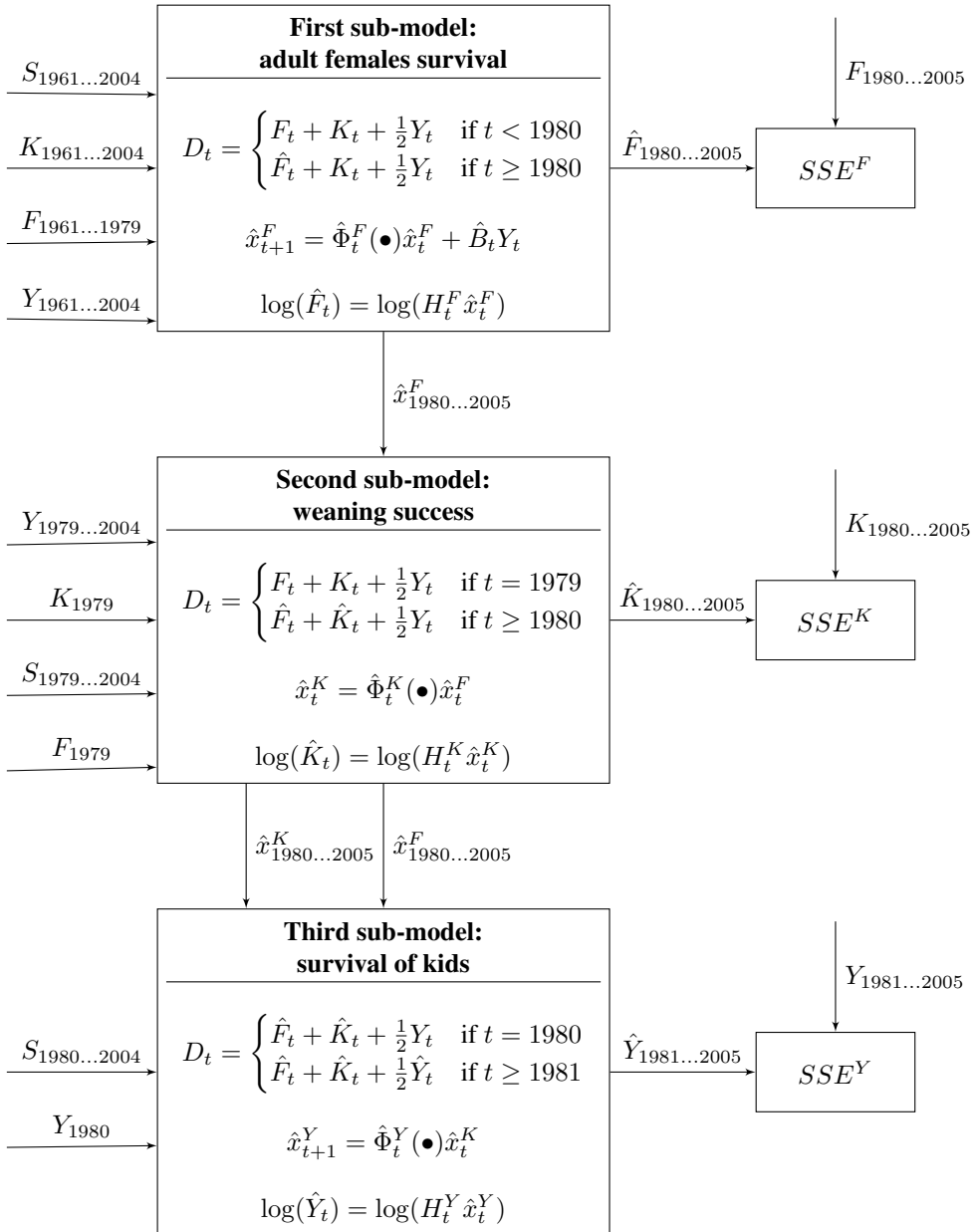$$x_{t+1}^F = \Phi_t^F(\bullet)x_t^F + B_t(\bullet)Y_t \qquad (6.23)$$

Figure 6.3: *Block diagram of the three submodels used for the sequential optimization described in the main text.*

where $x_t^F = [F_{2,t}, \ldots, F_{20,t}]'$ is a subset of the state vector x_t, $B_t(\bullet) = [\sigma_{1,t}(\bullet), 0, \ldots, 0]$ is a 19x1 matrix, and Φ_t^F is the squared matrix:

$$
\Phi_t^F = \begin{pmatrix}
0 & 0 & \ldots & 0 & 0 \\
\sigma_{2,t}(\cdot) & 0 & \ldots & 0 & 0 \\
0 & \sigma_{3,t}(\cdot) & \ddots & 0 & 0 \\
\vdots & \ddots & \ddots & \ddots & \vdots \\
0 & 0 & \ldots & \sigma_{19,t}(\cdot) & 0
\end{pmatrix}
\tag{6.24}
$$

The output equation of this sub-model is:

$$
\log(F_t) = \log(H_t^F x_t^F) + v_t^F
\tag{6.25}
$$

where $v_t^F \sim N(0, \sigma_F^2)$, and $H_t^F = [1, \ldots, 1]$ is a 1x19 vector.

The starting year for simulation is 1961 because is the first year in which snow depth data is available. Following the logic of iteratively replenishing the state vector with a plausible age structure of adults, the initial state vector is set to $x_{1961}^F = [0, \ldots, 0]'$. Equation 6.23 permits to estimate x_{1962}^F as

$$
\hat{x}_{1962}^F = [Y_{1961}\sigma_{1,1961}, 0, \ldots, 0]
$$

Iteratively applying equation 6.23, the state vector x_t^F is completely reconstructed in 1980, and an estimate of F_t can be therefore calculated, in the same year, as $\hat{F}_t = H_t^F \hat{x}_t^F$. The sum of squared simulation errors, to be minimized, is then calculated using all the time steps in which the population is completely reconstructed, thus from 1980 to the first year after the last data on snow depth:

$$
SSE^F = \sum_{t=1980}^{2005} \left(\log(\hat{F}_t) - \log(F_t) \right)^2
\tag{6.26}
$$

Second sub-model: weaning success

According to the equations of the state-space model, the complete structure of kids x_t^K can be calculated only when the structure of adult females x_t^F is completely defined, thus from 1980 to 2005. The state transition equation for the survival sub-model is:

$$
x_t^K = \Phi_t^K(\bullet)\hat{x}_t^F
\tag{6.27}
$$

where $x_t^K = [K_{II,t}, \ldots, K_{XIX,t}]'$, and Φ_t^K is the $[19 \times 19]$ squared matrix:

$$\Phi_t^K = \begin{pmatrix} \frac{1}{2}f_{2,t}(\cdot) & 0 & \dots & 0 \\ 0 & \frac{1}{2}f_{3,t}(\cdot) & \ddots & 0 \\ \vdots & \ddots & \ddots & \vdots \\ 0 & 0 & 0 & \frac{1}{2}f_{20,t}(\cdot) \end{pmatrix} \quad (6.28)$$

Notice that, with respect to the matrix in equation 6.3, the survivals of adult females do not appear in this matrix, but they have already been used to calculate the estimate $\hat{x}_t^F$.

The output equation of this sub-model is:

$$\log(K_t) = \log(H_t^K x_t^K) + v_t^K \quad (6.29)$$

where $v_t^K \sim N(0, \sigma_K^2)$, and $H_t^F = [2, \dots, 2]'$ is a $1x19$ vector that permits to sum the kids, either males and females, produced by each mother.

Naming $\hat{K}_t$ the estimate of K_t, produced by using equations 6.28 and 6.29, the sum of squared simulation error, to be minimized, is calculated as:

$$SSE^K = \sum_{t=1980}^{2005} \left(\log(\hat{K}_t) - \log(K_t) \right)^2 \quad (6.30)$$

Third sub-model: survival of kids

Starting from the reconstructed structure of kids $\hat{x}_t^K$, we calibrated the models of kids survival. The state transition equation for this sub-model is defined as:

$$x_{t+1}^Y = \Phi_t^Y(\bullet)\hat{x}_t^K \quad (6.31)$$

where $x_t^Y = [F_{1,t}]$ and $\Phi_t^Y = [\sigma_{II}^K(\cdot), \sigma_{III}^K(\cdot), \dots, \sigma_{XX}^K(\cdot)]$. The output equation of this sub-model is:

$$\log(Y_t) = \log(x_t^Y) + v_t^Y \quad (6.32)$$

where $v_t^Y \sim N(0, \sigma_Y^2)$. The sum of squared simulation errors, to be minimized, is calculated as:

$$SSE^Y = \sum_{t=1981}^{2005} \left(\log(\hat{K}_t) - \log(K_t) \right)^2 \quad (6.33)$$

where $\hat{Y}_t$ is the estimate of the number of yearlings at time t, and it is available only starting from 1981, one year after the structure of kids is completely reconstructed. Therefore, the calibration of the model is, for this sub-model, based on 25 years of data instead of 26.

Adult male sub-model

In analogy with the first sub-model of female survival, starting from measured yearlings, we also developed a model for the adult male survival. The strategies for model development were the same used for adult females, with only few differences. The first difference is that, for male survival, the density considered for density dependence is $D_t = M_t + 1/2Y_t$, to take into account the spatial segregation of adult males (see chapter 5). The second difference is that the maximum life length for males is set to 16 years, so that the age structure of adults is completely defined 4 years before female, thus in 1976. Therefore, the sum of squared errors is calculated as:

$$SSE^M = \sum_{1976}^{2005} \left(\log(\hat{M}_t) - \log(M_t) \right)^2 \tag{6.34}$$

where M_t and $\hat{M}_t$ are, using the usual convention, the measured and the estimated numbers of adult males at year t. Notice that, for adult males, 30 years of data are available for calibration.

Optimization strategy and simulations

The widespread nonlinearities of the system made the parameter calibration of the models particularly complicated. First of all we calibrated all the models using the genetic algorithm implemented in the GA toolbox in MATLAB®. We started from different initial points, and constrained the survivals and the fertilities, where needed, to have ecologically feasible values (i.e. to be less than one). Then, for a given rate and a given functional form, we used all the parameter sets of the last generation of the genetic calibration as starting points of a nonlinear least-squares curve fitting (Coleman & Li, 1994). Finally, we chose for each sub-model the parameter setting that minimizes the sums of squared errors as defined above, in equations 6.26, 6.30, 6.33 and 6.34. Once the sets of best models were selected, we estimated the standard deviations of all the models' parameters repeating the calibration using 2000 bootstrapped samples of the dataset. For each bootstrap sample, the final predictions are obtained as the weighted sum of the predictions produced by each best model, where the weights of the model predictions are the AIC_c weights (see the multimodel inference section 6.3.3 at page).

Finally, to check the performances of the complete model, we simulated the entire system as described by the equations 6.1, 6.3 and 6.4. In these simulations, the measured number of yearlings Y_t is used to "feed"

the model only until the adult females structure is completely reconstructed (i.e. 1980), and the weaning success and kids' survival functions can therefore be used to predict the number of kids and yearlings. The parameters used for the simulations of the entire systems are those calibrated with the bootstrap samples.

6.4 Results

Following the procedures described in the methods, we found that the model selection is highly uncertain for all the sub-models. In fact, in all the cases there are many competing models that have a ΔAIC_c smaller than four. More specifically, 23 best models were selected for the survival of females, 20 for the survival of males, 25 for the weaning success and 27 for the kids' survival. Moreover, even for the same sub-model, a similar fitting can be reached using models that include competing senescence functions.

In analogy with the concept of *posterior inclusion probability* described for the BMA (see the theory at section 2.3.2 at page 41 and the applications in chapters 3 and 4), we measured the importance of the covariates (density and snow depth) summing the AICc weights (w_m, where m is the index of the model) of the models that include the given covariate, as reported in table 6.1. In the first part of the table we report the sum of the AIC_c weights of the best models that include the covariate listed in the first column, namely D_t, S_t, $S_t * D_t$, S_t^2 and D_t^2. The rows corresponding to S_{tot} and D_{tot} report the sum of the AIC_c weights of the best models in which at list one covariate calculated using, respectively, the snow depth or the population density, is included. The full structures of the best models are reported in the appendices, tables 6.2, 6.3, 6.4 and 6.5. We calculated the importance of each possible senescence function using the same strategy, thus summing the AIC_c weights of the best models that include the given senescence function. We remark that the number of possible model structures is the same for all the senescence functions. Given the senescence function and the choice between model of the type described in equation 6.20 or in equation 6.21, the different model structures are in fact obtained combining the density and the snow depth covariates in all the possible ways, obtaining 2^5 model structures. Thus, we gave the same a-priori weight to all the possible senescence functions and it is therefore possible to compare the sum of the AIC_c weights as described above.

For the survival of adult females, five different types of senescence functions are selected in the pool of best models: Gompertz, multiplica-

Table 6.1: *Characteristics of the best models selected for the four submodels. In the first part of the table we report, for each of the submodels, the number of best models that include the covariate listed in the first column. Alongside the number of models, in parenthesis, the sum of their AIC_c weights is reported. The meaning of the covariates is presented in the main text. The last line of the first part reports the weighted mean of the model dimensionality, made using the AIC_c weights. In the second part of the table we show, in analogy with the first part, the number of models that have the maturation and senescence functions listed in the first column. If the name of the function is followed by "M", the model is "multiplicative", thus snow depth and density enter as in equation 6.20, otherwise they enter as in equation 6.21. In the header, F surv. is the survival of females, M surv. the survival of males, and K surv. the survival of kids. $npar$ in the weighted mean number of free parameters, obtained using the Akaike's weights.*

		F surv.	M surv.	Weaning success	K surv.
Covariates	D	8 (0.27)	8 (0.31)	7 (0.26)	0 (-)
	S	7 (0.23)	9 (0.41)	5 (0.13)	5 (0.10)
	$S \cdot D$	14 (0.67)	8 (0.29)	5 (0.12)	5 (0.11)
	S^2	7 (0.26)	14 (0.79)	5 (0.14)	5 (0.10)
	D^2	10 (0.34)	7 (0.39)	12 (0.45)	3 (0.07)
	S_{tot}	23 (1.00)	20 (1.00)	14 (0.38)	15 (0.31)
	D_{tot}	23 (1.00)	17 (0.76)	7 (0.72)	8 (0.18)
Senescence functions	No senescence	8 (0.26)	9 (0.51)	14 (0.58)	1 (0.02)
	Gompertz	9 (0.49)	11 (0.49)		1 (0.06)
	Gompertz M	1 (0.03)			5 (0.12)
	Weibull				5 (0.21)
	Weibull M	2 (0.06)			5 (0.23)
	Weibull 8+ M	3 (0.17)			
	Beta				1 (0.07)
	Beta M			4 (0.19)	4 (0.12)
	Gamma			3 (0.10)	1 (0.06)
	Gamma M			4 (0.13)	4 (0.11)
	npar	4.68	4.68	3.95	3.73

tive Gompertz, multiplicative Weibull from age 8 onwards and constant (or no senescence). Despite the large number of senescence functions, the Gompertz is far more likely than the others, with a score of 0.49 (out of 1), followed by the constant function ($\sum w_m = 0.29$), i.e. no senescence. The contest between the Gompertz and the no senescence is by far in favour of Gompertz, because the mean value of the AIC_c weight of the models with a Gompertz senescence function is much larger than the mean AIC_c weight of the constant model. The number of Gompertz models in the pool of best models is in fact only one more than the number of "constant" models, while the AIC_c weights sum is almost the double. The importance of the Gompertz model, with a non multiplicative effect of snow depth and density (see equation 6.21), confirms our hypothesis that the harsh conditions affects more the older individuals.

As in the best models of the previous chapter, population density and snow depth are included in all the best models for females survival ($\sum w_m$ for S_{tot} and N_{tot}), and they are more likely to be included through the interaction term $S_t \cdot D_t$ ($\sum w_m = 0.67$). The simulations separately obtained with each of the 23 best models for females are reported in figure 6.4.a, and show that, despite the differences in the structure of the models, the simulations follow almost the same patterns and predict quite well the population dynamics. In the appendix (figure 6.8.a), we report the simulations of the female populations obtained using the Akaike's multimodel inference and 2000 bootstrap extractions of the calibration set. Even if data are not always included in the 5$^{\text{th}}$-95$^{\text{th}}$ percentiles, the general patterns are well reproduced.

For the male survival, only two senescence functions are included in the pool of best models: Gompertz and constant. The sum of the AIC_c weights is similar for the two senescence functions. The snow depth is the most important variable ($\sum w_m = 1$ for S_{tot}), especially in its quadratic term ($\sum w_m = 0.79$ for S^2). Of course, even the population density is important, as known from previous modelling attempts in literature, with a score of 0.72. More specifically, the density dependence is always included if the senescence function is the constant, thus suggesting that the effects of density and senescence are difficult to disentangle looking at the counts data (Festa-Bianchet *et al.*, 2003). As a consequence, the term of interaction between the snow depth and the population density has a smaller importance than in the models developed in the previous chapter. In figure 6.4.d, we report the simulations separately obtained with each of the 20 best models for male survival. In this case, the simulations obtained with the best models are even less different from each other than in the case of adult females

(a) Adult females

(b) Kids

(c) Yearlings

(d) Adult males
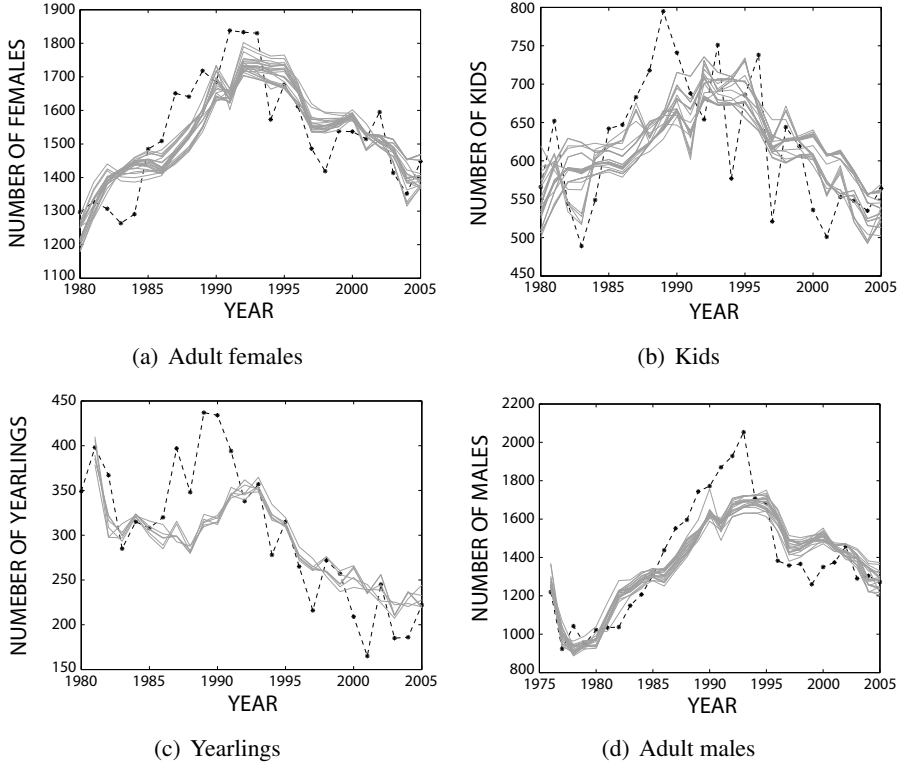
Figure 6.4: *Simulations of the population abundance made, separately for each population compartment, using the best models selected for the different rates. Black dashed lines represent measured data while grey thin lines the simulations obtained using the best models. panel a) simulations of the number of adult females made using the 23 best models for female survival; panel b) simulations of the number of kids made using the 20 best models for weaning success and the adult females structure obtained using the best models of females survival; panel c) simulations of the number of yearlings made using the 27 best models for the survival of kids and the kids' mothers structure obtained using the best models of weaning success; panel d) simulations of the number of males made using the 25 best models for male survival.*

survival. The populations dynamics are well reproduced, especially in the first ten years of the simulations, while the very peak observed in the data is not reached by the simulations. These behaviours are confirmed by the multimodel bootstrap simulations reported in figure 6.8.d.

In the weaning success models the senescence is less important than in the models for the survival of adults. The most likely senescence function is in fact the constant ($\sum w_m = 0.58$), while the remaining score is spread through the *Beta* (multiplicative), and the *Gamma* (multiplicative or not). The population density is very important for this rate ($\sum w_m = 0.72$), especially on its quadratic term, while the snow depth has a more marginal effect ($\sum w_m = 0.38$). This result is surprising because in the previous chapter, in which the fine age structure is not taken into account, the best model for weaning success includes three terms calculated using the snow depth. The simulations separately made using the best models are shown in figure 6.4.b, and have an higher variability than the simulations for the adult population. The bootstrap simulations (figure 6.8.b) reproduce the data fairly well, with the exception of the late 80's, characterized by a particularly high weaning success. The last simulation year shows a drop in the bottom of the simulation range, as a consequence of the same drop in the simulation of adult females.

For the survival of kids, 27 models have a $\Delta AIC_c < 4$ and they have a wide variety of senescence functions: Gompertz, Weibull, *Beta* and *Gamma* in both their multiplicative and non-multiplicative version, and the *costant*. The most likely types of models are those including a Weibull senescence function, thus highlighting the importance of considering a decrease with age in the ability of the mothers to successfully breed their offspring until the first year of life. Density and snow depth are included in the best models with a small weight and, confirming what we found in the previous chapter, snow depth is more important than density in driving the survival of kids. The simulations separately made using the best models (figure 6.4.c), show that there is only a small variability among the predictions of the different models, and the first part of the dataseries is not well reproduced. However, this shortcoming is also due to the errors made in the models of adult females survival and fertility, since the starting population of kids is the population reconstructed using these model compartments.

Since we used the multimodel approach to investigate the role of the covariates and of the senescence functions, it is interesting to look at the shapes of the senescence functions with the same approach. Using the AIC_c weights, the survival [or the weaning success] corresponding to an individual of age j [or with a mother of age j], is therefore calculated as the

weighted mean of the survival [or the weaning success] obtained with each of the best models. To investigate the role of snow and density in shaping the age-survival [or age-weaning success] curves, we tested five different combination of values, based on the historical values of the variables:

1. **maxDmaxS** $= \{\max_t D_t, \max_t S_t\}$

2. **maxDminS** $= \{\max_t D_t, \min_t S_t\}$

3. **meanDmeanS** $= \{1/n \sum_t S_t, 1/n \sum_t D_t\}$

4. **minDmaxS** $= \{\min_t D_t, \max_t S_t\}$

5. **minDminS** $= \{\min_t D_t, \min_t S_t\}$

where n is the amount of available time steps. The obtained curves are reported in figure 6.5.

   The functions for adult females survival, in figure 6.5.a, show that the survival is really high for the first year of life and it can drastically drop, according to the values of density and snow depth, in the older ages. The numerical results are similar to those reported in literature (see Toïgo *et al.*, 1997), in particular in the conditions **meanDmeanS**. The drop in survival at age eight can be explained with the inclusion of three models for which the survival starts to decrease at that age (Weibull 8+ M). A high snow depth can strongly decrease the survival of old individuals (see the lines for which the minimum value of snow was considered) while the effect of density is less strong. For example if the value of snow is at its minimum, the survival tends to be high whether density is low or high. Notice that, if both density and snow depth are minimal, the survival function is quite flat.

   The weaning success functions, showed in figure 6.5.b, are really interesting because they are the result of an ensemble in which either constant, *Beta* and *Gamma* functions are considered, even if with different weights. The weaning success has in fact an impressive drop after age 16, at which the constant and the *Beta* functions go to zero, but there is still a low weaning success at the older ages because of the inclusion of the *Gamma* functions. Overall and consistently with previous studies (see Giacometti & Ratti, 1994; Largo *et al.*, 2008), the weaning success value is ~ 0.4 and the highest weaning success occurs at the mature stages, between 4 and 8 years. In this case, the density is the major driver of the variability of the function, since the curves calculated using the maximum [minimum] value of density are consistently below [above] the curve calculated using **meanDmeanS**.

   The results obtained for the survival of kids are reported in figure 6.5.c and show that survival of kids can decrease with the age of the mother. The

(a) Female survival

(b) Weaning success

(c) Kids' survival
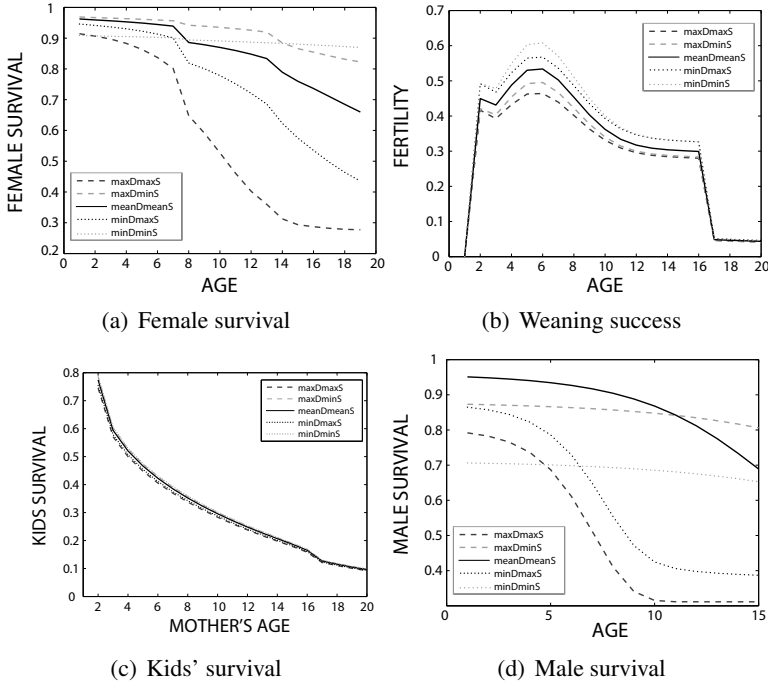
(d) Male survival

Figure 6.5: *Multimodel maturation and senescence functions for the four different rates: panel a) survival of adult females; panel b) weaning success; panel c) survival of kids; panel d) survival of adult males. The curves are obtained using the AIC_c weighted sum of the curves defined by each of the best models. For each panel, we report the response to the different values of snow depth and male density, as described in the main text.*

survival of kids is smaller if the values of snow depth and density are high, the former with a stronger effect than the first. This results highlights the importance of the population structure over the environmental conditions in driving the variations in the survival of kids. However, the results are also driven also by the errors in the models of fertility. Thus, it would be interesting to further investigate this compartment, possibly matching the obtained results with some field data, which are not available at present.

For male survival we report the survival functions in figure 6.5.d. As for females, the survival is high (but more variable) in the early ages and it decreases rapidly for older ages if snow is high. Otherwise, if the snow depth is low, the survival is smaller at younger ages and varies only a little during the lifetime. Moreover it is worth noticing that, due to the nonlinearities in the inclusion of snow depth and density, the effects of the maximum and

minimum densities are opposite if snow is maximal or minimal. In fact, if snow is minimal, a high density favours the survival, while it is the opposite for maximal values of the snow depth. Overall, the values obtained for the male survival are similar to those reported in Toïgo *et al.* (2007).

(a) Adult females structure

(b) Adult males structure

(c) Kids' mothers structure
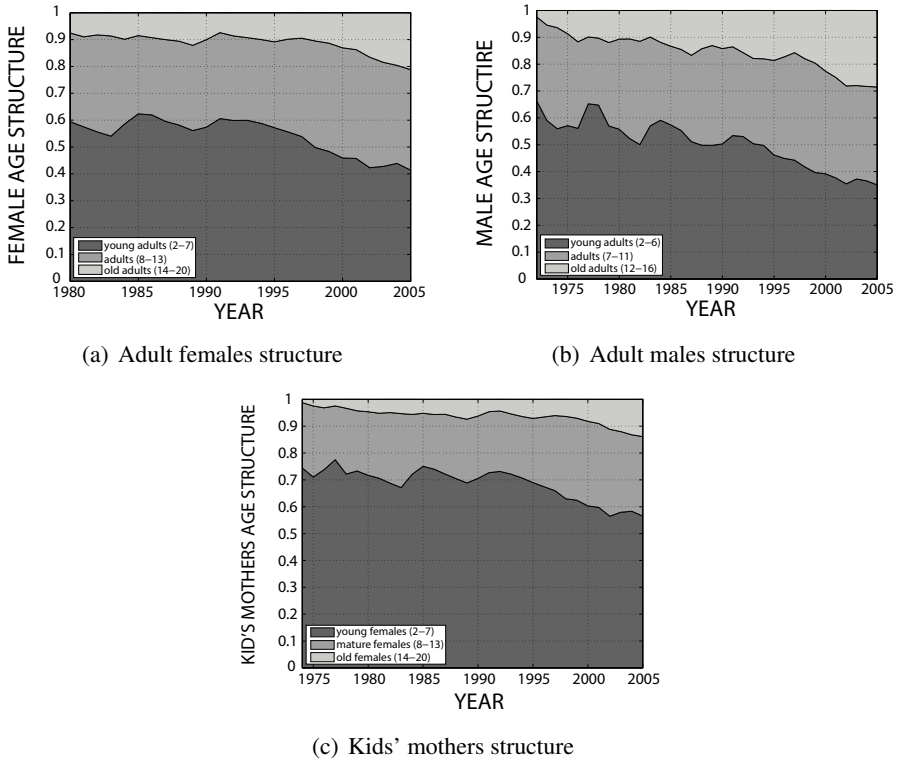
Figure 6.6: *Dynamics of the reconstructed adult population structure, dividing the population into three age classes (young adults, middle-age adults and old adults) as reported in the legend. The panels report the proportion of individuals belonging to each age class: panel a) structure of adult females; panel b) structure of adult males; panel c) structure of kids' mothers.*

Using the models selected for survivals of males, we were able to fully reconstruct the population structure. In Fig.6.6, we report the reconstructed structure of adult females, adult males and kids' mothers. The adults are divided in three categories which differ between females and males: young adults, middle-age adults and old (or senescent) adults. For females, the model predicts that young adults passed from $\sim 60\%$ to $\sim 40\%$ in the period 1980-2005, while the senescent part of the population passed from $\sim 5\%$ to $\sim 25\%$ in the same period. The middle-age adult population seems

instead to remain at $\sim 35\%$ in all the period. Dynamics of the male structure show an even steeper decrease, with a really small portion of senescent adults at the beginning of the simulation ($\sim 2\%$), which increases up to $\sim 30\%$ at the end of the simulation. The young adults show a similar but opposite variation, passing from $\sim 68\%$ to $\sim 36\%$. As for females, the proportion of middle-age males is quite consistent during the study period. The structure of the kids' mothers has a similar but less pronounced change, with an increase of older mothers from $\sim 1\%$ to $\sim 14\%$, a decrease of younger mothers from $\sim 74\%$ to $\sim 58\%$ and a proportion of middle-age adults that always remains around 25%. The recent variation in the population structure suggest that the Alpine ibex population of the GPNP is getting older and that, as a consequence, the contribute of old females to recruitment is increasing. As we discuss in the next section, these dynamics suggest that taking into account population structure is important to understand recent population trends.

Using the selected best models, we can simulate the dynamics of the entire population starting from the first year in which the adult population is completely reconstructed. In these "complete" simulations the number of yearlings used to reconstruct the adult population is the estimate given by the models of weaning success and the survival of kids. In figure 6.7 we report the simulated population abundances for the four population groups and for the total population, calculated as the sum of the simulations for the other compartments. The simulations are produced using the 2000 bootstrapped calibrations of the parameters described at the end of the methodological section of this chapter. The simulations show that the generic pattern is reproduced and there are only few observations out of the 5th to 95th percentile range. However this is not true if the interquartile range is considered, thus highlighting that the models have a low probability to generate the measured data. Moreover, the most important shortcoming is the lack in reproducing the growth phase in the population peak, similarly to the models proposed in the previous chapter. Nonetheless, the simulations between 1995 and 2005 well reproduce the data, at least for adults and kids.

6.5   Discussion and conclusions

In this chapter, we improve our previous study of the Alpine ibex population dynamics in GPNP, using a modelling approach that permits to consider the fine age structure of the population, even if data report a coarser age structure. Using the fine age structure, we investigated the interplay of maturation time, senescence, density dependence and environmental drivers (snow

(a) Adult females

(b) Kids

(c) Yearlings

(d) Adult males

(e) Total population
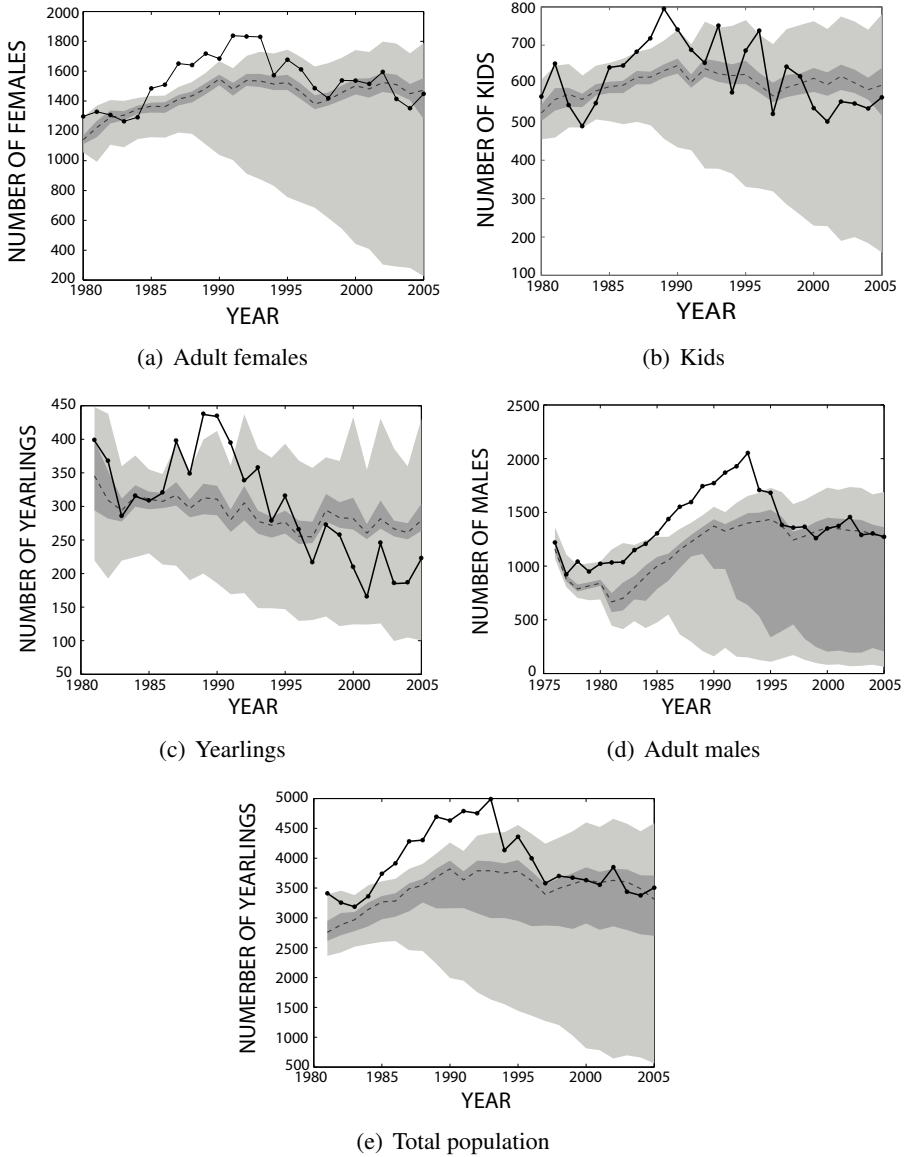
Figure 6.7: *Simulations of the complete model, made using the parameters cali-brated separating the submodels. The variability of the simulations is obtained using the 2000 bootstrapped calibration of the parameters. The dark grey ar-eas include the 25th to 75th percentile, while light grey areas are for the range 5th to 95th percentile. The thick continuous line stands for data while the thin dashed line corresponds to the 50th percentile.*

depth) in driving the population dynamics.

Our results show that there is a high uncertainty in the selection of the best model among the set of candidates. In part, this is perhaps due to the fact that only a relatively small fraction of the dataset has been used for calibration, thus novel data would be needed to better discriminate among models. Also, the high model uncertainty suggests the use of a multimodel approach. The pool of best models selected for each rate (adult female survival, adult male survival, survival of kids and weaning success) gives information on the main mechanisms that is worth to take into account to model the system under study.

Taking into account the effects of senescence clearly improves the modelling of the adult females survival and the survival of kids, which varies with the age of the mothers. Conversely, for adult male survival and weaning success, even models that do not consider senescence or maturation are likely to be selected as best models. For adults, continuous senescence functions are more likely than discontinuous, thus supporting the idea that senescence does not occur suddenly in the life history of the individuals, but it is a continuous process that, however, accelerate with the age.

In the adult survival components, if models with senescence functions are selected, the multiplicative models have a marginal role, thus highlighting that harsh conditions do not equally effect the individuals of all ages, but are particularly detrimental for older individuals.

The information about the fine age structure can potentially change the role of density and snow depth in driving the dynamics with respect to the results of the previous chapter. For the survival of females, the results of the previous chapter are confirmed, since both snow depth and density are fundamental, and are more likely to be included through the interaction term. For male survival, the role of snow depth is confirmed but the effects of density dependence is less clear. In fact, while density is always included in models without senescence, the evidences for its inclusion are smaller if senescence is taken into account. The decrease in survival that occur at high densities can in fact be the consequence of both an actual density dependence and/or a high average age of the population. This effect, for which the density dependence effect is overestimated if senescence is not considered, is known as apparent density dependence (Festa-Bianchet *et al.*, 2003).

The models selected for the survival of kids confirm that snow depth is more important than density in this compartment, even if none of them appears to have a crucial role once the structure of kids is taken into account. For the weaning success, taking into account the senescence of the mothers

reduces the importance of snow depth and population density, while previous results are confirmed if models without senescence are used. However, simple models tend to be selected because the time series used for calibration is short. As a consequence, the unimodal effect of snow described in the previous chapter is not reported.

The analysis of the variation of the population structure in time shows that, during the population increase and decrease that characterize the 1990's peak discussed in the previous chapter, the proportion of old individuals increased while a corresponding decrease in young adults occurred. In the meanwhile, the proportion of middle age adults remained almost stable. This innovative result suggests an evolutionary strategy for which the fraction of middle-age adults, which are the part of the population that mostly contributes to reproduction, tends to be preserved even if the environmental conditions and the population density change. This strategy could help the population to overcome unsuitable periods. The analysis of the variation of population structure shows also an asymmetry between the change in adult females structure and the structure of kids' mothers. The proportion of old individuals increased in fact much more rapidly in the adult females than in the mothers, thus suggesting that a change in the adult female structure can strongly alter the productivity of the population. In this sense, the change in the population structure can explain the recent decrease in the number of kids and yearlings.

To confirm the obtained results they should be matched with the population structure retrieved from the CMR data, which are existing but not publicly available (Apollonio *et al.*, 2013). Moreover, it will be interesting to include more recent data in the analysis. Another interesting improvement would be to properly redefine the optimization to directly fit the entire model, and not the submodels separately. This could also permit to use also the first years of data in calibration, for example fixing the initial conditions through simulation, using past data (before 1960) randomly generated under appropriate assumptions. Using all the available data for calibration would also permit to better identify the nonlinear effects of snow on the juvenile compartments, as done in the previous chapter.

Bibliography

Apollonio, M., Brivio, F., Rossi, I., Bassano, B. & Grignolio, S. 2013: Consequences of snowy winters on male mating strategies and reproduction in a mountain ungulate. Behavioural processes 98: 44–50. doi: 10.1016/j.beproc.2013.05.001.

Benton, T.G., St Clair, J.J.H. & Plaistow, S.J. 2008: Maternal effects mediated by maternal age: from life histories to population dynamics. Journal of Animal Ecology 77(5): 1038–1046. doi:10.1111/j.1365-2656.2008.01434.x.

Coleman, T.F. & Li, Y. 1994: On the convergence of interior-reflective Newton methods for nonlinear minimization subject to bounds. Mathematical Programming 67(1): 189–224.

De Valpine, P. & Hastings, A. 2002: Fitting Population Models Incorporating Process Noise and Observation Error. Ecological Monographs 72(1): 57. doi:10.2307/3100085.

Dennis, B., Ponciano, J.M.J., Lele, S.R.S., Taper, M.L. & Staples, D.F. 2006: Estimating Density Dependence, Process Noise, and Observation Error. Ecological Monographs 76(3): 323–341. doi:10.1890/0012-9615(2006)76[323:EDDPNA]2.0.CO;2.

Festa-Bianchet, M., Gaillard, J.M., Côté, S.D. & Festa-Bianchet, M. 2003: Variable age structure and apparent density dependence in survival of adult ungulates. Journal of Animal Ecology 72(4): 640–649.

Gage, T.B.T. 2001: Age-specific fecundity of mammalian populations: A test of three mathematical models. Zoo Biology 20(6): 487–499. doi: 10.1002/zoo.10029.

Gaillard, J.M., Festa-Bianchet, M., Yoccoz, N.G., Loison, A. & Toigo, C. 2000: Temporal variation in fitness components and population dynamics of large herbivores. Annual Review of Ecology and Systematics 31: 367–393.

Gaillard, J.M., Viallefont, A., Loison, A. & Festa-Bianchet, M. 2004: Assessing senescence patterns in populations of large mammals. Animal Biodiversity and Conservation 27(1): 47–58.

Gaillard, J.M. & Yoccoz, N.G. 2003: Temporal variation in survival of mammals: a case of environmental canalization? Ecology 84(12): 3294–3306.

Garrott, R. & Eberhardt, L. 2003: Climate-induced variation in vital rates of an unharvested large-herbivore population. Canadian Journal of Zoology 81(1): 33–45.

Giacometti, M. & Ratti, P. 1994: Zur Reproduktionsleistung des Alpensteinbockes (Capra i. ibex L.) in der Freilandkolonie Albris (Graubünden, Schweiz). Z. Saeugetierk. 59: 174–180.

Julier, S.J. & Uhlmann, J.K. 1997: A New Extension of the Kalman Filter to Nonlinear Systems. (pp. 182–193).

Largo, E., Gaillard, J., Festa-Bianchet, M. & C 2008: Can ground counts reliably monitor ibex Capra ibex populations. Wildlife Biology .

Loison, A., Toigo, C., Appolinaire, J. & Michallet, J. 2002: Demographic processes in colonizing populations of isard (Rupicapra pyrenaica) and ibex (Capra ibex). Journal of Zoology 256: 199–205. doi: 10.1017/S0952836902000237.

Martin, K. & Service, C.W. 1995: Patterns and Mechanisms for Age-dependent Reproduction and Survival in Birds. Integrative and Comparative Biology 35(4): 340–348. doi:10.1093/icb/35.4.340.

Monaghan, P., Charmantier, a., Nussey, D.H. & Ricklefs, R.E. 2008: The evolutionary ecology of senescence. Functional Ecology 22(3): 371–378. doi:10.1111/j.1365-2435.2008.01418.x.

Mysterud, A., Yoccoz, N.G.N., Stenseth, N.C. & Langvatn, R. 2001: Effects of age, sex and density on body weight of Norwegian red deer: evidence of density–dependent senescence. Proceedings of the Royal Society of London. Series B: Biological Sciences 268(1470): 911. doi: 10.1098/rspb.2001.1585.

Pettorelli, N., Pelletier, F., von Hardenberg, A., Festa-Bianchet, M. & Côoté, S.D. 2007: Early onset of vegetation growth vs. rapid green-up: impacts on juvenile mountain ungulates. Ecology 88(2): 381–390.

Toïgo, C., Gaillard, J. & Michallet, J. 1997: Adult survival pattern of the sexually dimorphic Alpine ibex (Capra ibex ibex). Canadian Journal of Zoology 75(1): 75–79.

Toïgo, C., J.M., G., Festa-Bianchet, M., Largo, E., Michallet, J., Maillard, D., Töigo, C. & Gaillard, J.M. 2007: Sex-and age-specific survival of the highly dimorphic Alpine ibex: evidence for a conservative

life-history tactic. Journal of Animal Ecology 76(4): 679–686. doi: 10.1111/j.1365-2656.2007.01254.x.

White, K., Pendleton, G., Crowley, D., Griese, H.J., Hundertmark, K.J., Mcdonough, T., Nichols, L., Robus, M., Smith, C.A. & Schoen, J.W. 2011: Mountain goat survival in coastal Alaska: effects of age, sex, and climate. The Journal of Wildlife Management 75(8): 1731–1744.

6.A Appendix I

We report in this appendix the main characteristics of the best models (ΔAIC_c<4) selected for the weaning success (table 6.4) and the survival of females (table 6.2), males (table 6.3) and kids (table 6.5).

The first column report the type of maturation/senescence function included in the model: "G" for Gompertz, "W" for Weibull, "β" for the *Beta*, "γ" for the *Gamma* and "No sen" for the constant. If the dependency on the snow depth is multiplicative (see equation 6.20), an "m" is added to the label reported in the first column. Moreover, for adult survival, the text "8+" is added after the "W" or the "G" if the survival is considered to be constant until age 8.

Columns from 2 to 5 summarize the dependencies on population density and snow depth, showing the sign of the coefficient β that multiplies the covariate. If the covariate is not included in the model, a blank space is left. We remark here that, while in multiplicative and constant models a negative sign corresponds to a negative effect on survival or weaning success, the same sign has the effect of reducing the strength of senescence in non-multiplicative models (see equation 6.21). In analogy, a positive sign has the opposite effects.

The other columns report: SSE the sum of squared errors, K the number of parameters including error variance, AIC_c the value of the AIC_c criterion, ΔAIC_c the difference between the AIC_c of the given model and $AIC_{c,best}$, w the *Akaike's weight*.

Table 6.2: *Characteristics of the best models for female survival.*

Sen.fun.	$\beta_1 D_t$	$\beta_2 S_t$	$\beta_3 S_t D_t$	$\beta_4 S_t^2$	$\beta_5 D_t^2$	SSE ($\cdot 10^3$)	K	AIC_c	ΔAIC_c	w
G	+		+			4.25	4	-132.07	0	0.17
G	+	+				4.24	5	-129.05	3.02	0.04
G	+	+	+			4.19	5	-129.37	2.70	0.04
G			+	+		4.35	5	-128.40	3.67	0.03
G	+	-	+		+	4.20	5	-129.31	2.76	0.04
G		+				4.15	5	-129.61	2.46	0.05
G		+	+	-	+	4.23	5	-129.12	2.95	0.04
G			+		+	4.18	5	-129.41	2.66	0.04
G			+	+	+	4.27	5	-128.85	3.22	0.03
G m	+		-		-	3.80	6	-128.44	3.63	0.03
W m						4.96	4	-128.08	3.99	0.02
W m	+			-	-	3.70	6	-129.13	2.94	0.04
W8+ m			-			3.89	5	-131.31	0.76	0.12
W8+ m		+	-			3.81	6	-128.43	3.64	0.03
W8+ m			-		+	3.86	6	-128.07	4	0.02
No sen						5.32	3	-129.06	3.01	0.04
No sen	-		-			4.94	4	-128.14	3.93	0.02
No sen	-	+	-	-		4.70	4	-129.47	2.60	0.05
No sen		+	-		-	4.92	4	-128.28	3.79	0.03
No sen		-			-	4.94	4	-128.17	3.90	0.02
No sen			-	-	-	4.92	4	-128.27	3.80	0.03
No sen						4.67	4	-129.61	2.46	0.05
No sen	+	+	-		-	3.85	6	-128.16	3.91	0.02

Table 6.3: *Characteristics of the best models for male survival.*

| Sen.fun.	$\beta_1 D_t$	$\beta_2 S_t$	$\beta_3 S_t D_t$	$\beta_4 S_t^2$	$\beta_5 D_t^2$	$SSE\ (\cdot 10^3)$	K	AIC_c	ΔAIC_c	w
G		+				12.33	4	-104.38	0.96	0.09
G			+			13.85	4	-101.37	3.98	0.02
G				+		11.95	4	-105.21	0.14	0.13
G	+	+				11.93	5	-102.16	3.19	0.03
G	-		+			12.23	5	-101.51	3.84	0.02
G	+			+		11.63	5	-102.82	2.53	0.04
G		+	+			11.98	5	-102.05	3.30	0.03
G		+		+		11.87	5	-102.27	3.07	0.03
G		+			+	11.81	5	-102.41	2.93	0.03
G			+	+		11.57	5	-102.93	2.41	0.04
G				+	+	11.56	5	-102.96	2.39	0.04
No sen	-			-		12.66	4	-103.70	1.65	0.06
No sen				-	-	11.88	4	-105.34	0	0.14
No sen	-	+		-		11.60	5	-102.87	2.48	0.04
No sen	-		+	-		11.90	5	-102.22	3.13	0.03
No sen	+			-	-	11.69	5	-102.67	2.68	0.04
No sen		+	-	-		11.21	5	-103.77	1.57	0.06
No sen		+		-	-	11.44	5	-103.23	2.12	0.05
No sen			+	-	-	11.69	5	-102.68	2.67	0.04
No sen	+	+	-	-	-	8.55	7	-103.60	1.75	0.06

Table 6.4: *Characteristics of the best models for weaning success.*

| Sen.fun.	$\beta_1 D_t$	$\beta_2 S_t$	$\beta_3 S_t D_t$	$\beta_4 S_t^2$	$\beta_5 D_t^2$	SSE ($\cdot 10^3$)	K	AIC_c	ΔAIC_c	w
γ m	−					12.35	4	-104.33	2.10	0.04
γ m						11.11	5	-104	2.43	0.04
γ m						11.14	5	-103.92	2.51	0.04
γ m			−		−	10.32	6	-102.50	3.93	0.02
γ						12.35	4	-104.33	2.10	0.04
γ						11.24	5	-103.70	2.73	0.03
γ	+			+	+	11.31	5	-103.54	2.90	0.03
β m						10.56	5	-105.31	1.13	0.07
β m		−		−	−	9.76	6	-103.95	2.48	0.04
β m			−		−	9.88	6	-103.62	2.81	0.03
β m				−	−	9.53	6	-104.57	1.87	0.05
No sen						14.02	2	-106.43	0	0.12
No sen	−					13.06	3	-105.71	0.73	0.09
No sen		−				14.01	3	-103.87	2.56	0.03
No sen				−		13.98	3	-103.92	2.51	0.04
No sen					−	14.02	3	-103.87	2.57	0.03
No sen			−			13.14	3	-105.55	0.88	0.08
No sen	−	−				13.06	4	-102.90	3.54	0.02
No sen	−		−			13.06	4	-102.90	3.54	0.02
No sen				−		13.04	4	-102.93	3.50	0.02
No sen		+			+	12.47	4	-104.10	2.34	0.04
No sen		−	−			13.23	4	-102.55	3.88	0.02
No sen	−	−	−			13.14	4	-102.74	3.69	0.02
No sen			−		−	13.13	4	-102.74	3.69	0.02
No sen				−	−	13.12	4	-102.76	3.67	0.02

Table 6.5: *Characteristics of the best models for the survival of kids.*

Sen.fun.	$\beta_1 D_t$	$\beta_2 S_t$	$\beta_3 S_t D_t$	$\beta_4 S_t^2$	$\beta_5 D_t^2$	$SSE\ (\cdot 10^3)$	K	AIC_c	ΔAIC_c	w
γ m						49.06	4	-65.37	1.14	0.06
γ m		-				48.34	5	-62.58	3.93	0.02
γ m			-			47.92	5	-62.80	3.71	0.02
γ m				-		48.16	5	-62.67	3.83	0.02
γ						49.20	4	-65.30	1.21	0.06
β m						48.63	4	-65.59	0.92	0.07
β m		-				48.19	5	-62.66	3.85	0.02
β m			-			47.68	5	-62.92	3.58	0.02
β m				-		48.46	5	-62.52	3.99	0.01
β						48.63	4	-65.59	0.92	0.07
G						55.44	3	-65.17	1.34	0.06
W						52.55	3	-66.51	0	0.11
W		+				52.62	4	-63.62	2.89	0.03
W			+			52.61	4	-63.62	2.88	0.03
W				+		52.55	4	-63.65	2.86	0.03
W					+	52.55	4	-63.65	2.85	0.03
G m						55.44	3	-65.17	1.34	0.06
G m		-				54.95	4	-62.53	3.97	0.02
G m			-			54.41	4	-62.78	3.72	0.02
G m				-		54.85	4	-62.58	3.93	0.02
G m					-	54.23	4	-62.86	3.64	0.02
W m						52.58	3	-66.49	0.01	0.11
W m		-				52.07	4	-63.88	2.62	0.03
W m			-			51.49	4	-64.16	2.35	0.03
W m				-		51.92	4	-63.95	2.55	0.03
W m					-	52.54	4	-63.65	2.85	0.03
No sen						67.66	2	-62.79	3.72	0.02

6.B   Appendix II

(a) Adult females

(b) Kids

(c) Yearlings

(d) Adult males
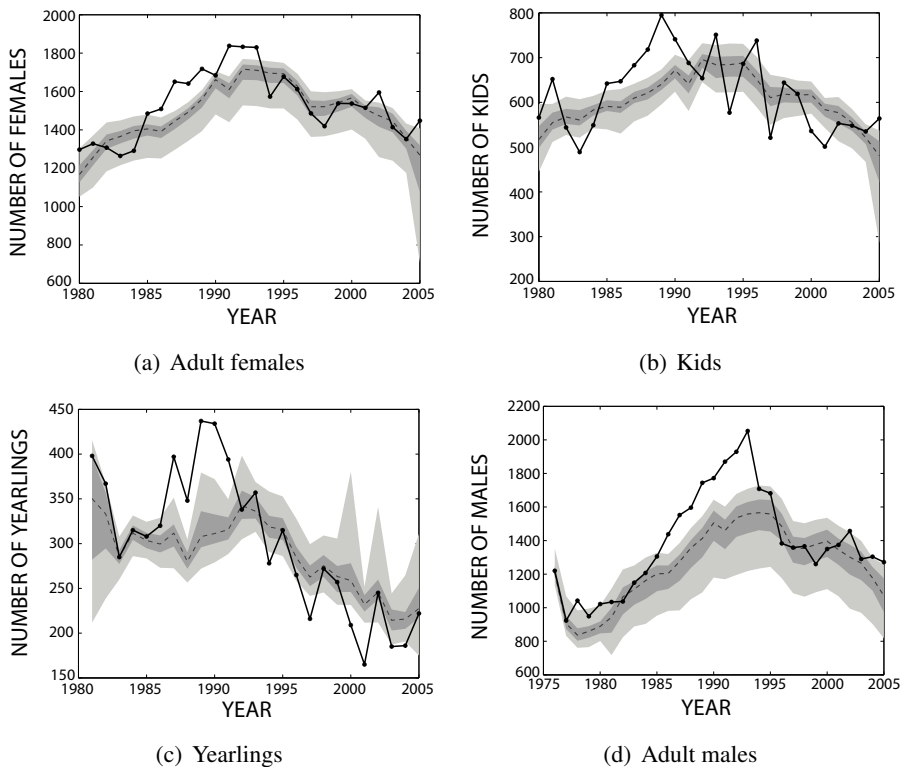
Figure 6.8: *Simulations of the separate submodels, made using the parameters calibrated using the 2000 bootstrapped samples of calibration data. The dark grey areas include the 25th to 75th percentile, while light grey areas are for the range 5th to 95th percentile. The thick continuous line stands for data while the thin dashed line corresponds to the 50th percentile.*
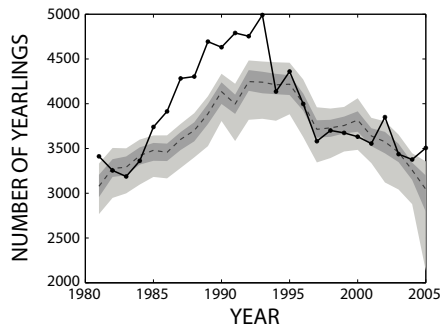
Figure 6.9: *Simulations of the total population, made summing the simulations of the separate submodels reported in figure 6.8. The dark grey areas include the 25th to 75th percentile, while light grey areas are for the range 5th to 95th percentile.The thick continuous line stands for data while the thin dashed line corresponds to the 50th percentile.*

Conclusions

Using data about three remarkably important high altitude species of fauna in the Alps, we developed models to study either their species distribution or their population dynamics. High altitude Alpine regions are characterized by a great ecological importance and a strong sensitivity to climatic conditions. Moreover, high altitude environments are regarded as early indicators of climate change. Climate change is affecting the mountain biota in several interacting ways, rather direct, e.g. through the increase in temperatures and the variation of the precipitation regime, and indirect through the variation of the abiotic components of the environment (e.g. the reduction of the glaciers). The ecological responses to these pressures depend on the specific characteristics of each species. Moreover, the responses of the single species can lead to a variation in the interaction among different species at the same or at different trophic level, and to a more general variation of the ecological communities. In this context characterized by many interacting effects and a high uncertainty, it is difficult to define a priori, for each problem, a single deterministic model to describe the system under study. In each of the tackled case studies, the starting point is in fact a substantial uncertainty on which specific characteristics of the species and/or which environmental variables are the most important to be included in the

models.

The study of species distribution and demographic rates has been carried out considering, in the pool of potential drivers, climatic variables or environmental variables that have already been shown to be clearly affected by the climate change. In particular, for the models of species distribution, we used precise information on the vegetation type; uphill shift of vegetation and changes in flora communities are in fact two of the most evident impacts of climate change on the Alpine biome. On the other hand, in the dynamical models we included meteorological variables as potential drivers of the demographic rates. The three high altitude species under study, chosen according to their already known sensitivities to the environmental conditions, are: the Alpine marmot, a small mammal that hibernates during winter; the black grouse, a tetraonid bird that lives just above the tree line; the Alpine ibex, a long-living large mammal that uses several different types of habitat during the year.

In the following paragraphs we summarize the main results obtained in modelling each of the three species, and in the last two paragraphs we present the more general conclusion of the thesis.

In chapter 3 we studied the fine scale species distribution of the Alpine marmot in a high altitude valley which is not affected by human disturbance. The positional data of the burrows were personally collected in a valley near the borders of the Stelvio National Park (Italy). The availability of a high resolution vegetation map permitted to study the fine scale influence of vegetation type on the suitability of the habitat for the marmots. We found, in fact, that the vegetation cover is one of the most important factors that determines the suitability of the habitat for the Alpine marmot. Moreover, including the fine scale vegetation in the study reduces the importance of the Altitude, which can be considered a proxy of the temperatures. The upper bound of the altitude range of Alpine marmot appears to be regulated by the transition between the Alpine meadows and the pioneer vegetation. The potential speed of uphill shifting of Alpine marmot distribution can be therefore limited by the rapidity of vegetation changes, which follow precise successional stages. The most important topographical variables are related to (i) sun exposure, which can regulate both winter conditions and snowmelt in spring, and (ii) a burrow position favourable to defend against predators and to avoid extreme weather conditions. For each burrow, we also collected many local characteristics that it would be useful to include in the species distribution model to (partially or completing) substitute the variables retrieved from the digital terrain map. However, to use that information in modelling, a similar collection of data have to be carried out

also in locations of the valley in which marmot is not present. To study the dynamics of colonizations, it would also be interesting to track the changes in the position of the upper bound of marmot distribution in the valley, alongside with the existing monitoring of the vegetation status.

The dynamical models developed for both the Alpine ibex and the black grouse underline the sensitivity of the most fragile population compartments on the meteorological conditions and the expected climate changes. In both cases, the density dependence is a key mechanism for driving the dynamics, thus highlighting the limited carrying capacity of the extreme Alpine environment.

In chapter 4, we studied the influence of climate, density dependence and spatial position on the demographic rates of the black grouse, using wildlife monitoring data about the 17 Alpine districts of the Piedmont region (Italy). Currently, few studies have investigated the role of the climatic influence on the Alpine populations of Tetrao tetrix, while most of the studies refer to lowland populations. The considered demographic rates are the population growth rate, calculated using the male portion of the population, and three fertility rates, calculated using the information on the number of females, hens and chicks. Our results show that, despite the different environment, the effect of meteorological conditions on the demographic rates are mostly consistent with the results published for lowland populations. In fact, high temperatures in the breeding season reduce the growth rate while the fertility decreases with the amount of rainfalls in hatching period, when the newborns are more sensitive to harsh conditions. The winter precipitations, which have not a clear role in the past studies, are likely to negatively affect the population growth rate and the condition of the birds, probably through a reduction of the food availability in the critical winter period. Notice that the most important climatic variables that affect the demographic rates are linked with key periods of the life cycle (breeding, hatching, winter survival), thus they are likely to interfere with the phenology of the species. The study of the influence of population density on the demographic rates show that the direct (negative) density dependence is the main driver for growth rate, while a weak but significant inverse (positive) density dependence influences the fertility rates. Matching the two results, since the productivity is not negatively affected by population density, the negative effect of population density on growth rate is likely to be caused by an adult survival that, for the effects of the intraspecific competition, decreases as densities increase. Our approach permitted also to separate two group of districts that are characterized by a different carrying capacity. Future projections show that the variations in climate have the potentiality

to strongly affect dynamics, even if no clear future trends are detected in the values of the demographic rates. However, only one realization of the regional climatic model was available. Therefore, to confirm the obtained results and to calculate the extinction risks linked with the climate change, it would be useful to repeat the projections under different realizations of the climatic models, maybe using the updated scenarios provided in the fifth assessment report of the IPCC.

In chapters 5 and 6 we studied the dynamics of the Alpine ibex population in the Gran Paradiso National Park, extending the models proposed in literature along many directions. Past studies on the same population concentrate only on the growth rate of the total population and found a negative effect of high winter snow depth. Despite the fact that the winter snow depth is constantly and clearly decreasing in the study area, the initial increase in the number of individuals was followed by a strong unexpected decrease. Alpine ibex is a long living mammal characterized by a strong age and sex structure; we therefore developed dynamical models that take into account of the population structure with different levels of precision.

In chapter 5 we consider four population groups according to the age and the sex of the individuals, as reported in the population counts. We relate the growth rate and the demographic rates (adult male survival, adult females survival, weaning success and survival of kids) to the linear and non linear effects of winter snow depth and population density. Ibex population is divided into spatially segregated groups composed by individuals of the same sex; we found that the demographic rates related to a specific population group are more likely to be affected by the density of that group only and not of the total population. The values of all the demographic rates are clearly determined by the interaction between population density and snow depth. Moreover, we found that the nonlinear effects of snow depth are important for the juvenile compartments. Weaning success and survival of kids are in fact favoured by intermediate levels of snow depth. However, considering the population groups instead of the total population does not satisfactorily explain the occurred dynamics, especially the recent population decline.

We therefore developed, as presented in chapter 6, more sophisticated models that permit to reconstruct the complete age structure of the population. Using that models, we studied the effects of maturation time and senescence (decrease of the individual fertility and/or survival with the age) to determine the population dynamics. Maturation and senescence are mechanisms which have been reported for many long living mammals, and specifically for ibex. However, they were never explicitly included

in models for the Alpine ibex population dynamics. Our results underline that taking into account senescence is particularly important to explain the survival of adult females and their ability of breeding kids, while is less important for adult males and weaning success. Moreover, harsh environmental conditions are likely to enhance the senescence rate, and, thus, their effects are stronger in old individuals. The simulation of the population structure dynamics shows that the number of old individuals increased in the last 25 years of the study, at the expense the fraction of young adults. The stability in the fraction of middle age adults, which are characterized by both an high survival and an high weaning success, can be interpreted as a strategy to damp the short term effects of harsh conditions. However, this strategy might start to be ineffective if harsh conditions occur for several consecutive years. Even if they can not be directly compared with models of chapter 5, the models that consider the complete age structure reproduce quite well the recent population decrease. However, as explained in the discussion of the specific chapter, they still have much room for improvement, especially in the estimation of the initial age structure of the population.

Overall, the results of the population dynamics models developed for black grouse and Alpine ibex highlight the particular sensitivity of the more fragile population compartments to the climate change. Meteorological conditions are in fact critical for black grouse in the breeding and the hatching period, while for Alpine ibex the juvenile compartments show a very specific preference for intermediate levels of snow depth and the old individuals respond in a more pronounced way to the environmental variations.

The methodologies adopted in this thesis are a sound solution to tackle the problem of studying the spatial distribution and the demography of the species in the climate change context, even using very different datasets. Our models permit in fact to investigate the role of climate-sensitive variables, such as the status of the vegetation and the meteorological variables, in affecting the spatial and temporal dynamics of the case-study populations, taking also into account the peculiar characteristics of each species. Using model selection criteria we were able to find the most likely mathematical laws and the most important variables that drive the systems under study. This kind of analysis is crucial for conservation purposes for several reasons. Without precise modelling studies that include the peculiarities of the species it is in fact difficult to predict and understand the expected impacts of climate change on the populations. Indeed, using the species specific results to make generalizing conclusions can be misleading because each species has different characteristics and different vulnerabilities. Our results highlight which are the most critical areas (for marmot and

grouse), periods of the year (for grouse and ibex) or periods of life cycle (for grouse and ibex) on which is worth to put more effort in future studies. These results can in fact serve, for example, as a basis to design future data collections focusing the available and unfortunately limited resources on precise population characteristics or population compartments. Moreover, our models can be used to predict the expected species distributions and population dynamics using future projections of the explanatory variables, such as meteorological variables or vegetation status.

On the other hand, the addressed topic is complex and the proposed approaches have some structural limitations related to the data quality and the simplifications applied to design models. In fact, available long term data of ecological populations were not usually collected with the specific aim of studying the responses of the given species to the climate change. A clear example provided in this thesis are the counts of black grouse, which were performed as a support for the management of the species and to decide hunting regulation. The use of poor quality data can be only partially compensated by the use of modern statistical techniques, thus, availability of good quality data is a crucial factor in determining the quality of research in this field. Moreover, to improve our knowledge on the expected impacts of climate change we should consider both the interaction and the synergies among the climatic pressures and the ecological responses. To do that, the ecologists need to work alongside with the experts of other earth science disciplines, such as climatology and glaciology. For example, if the aim is to predict the future status of a species at a population level, the reliability of ecological models strongly depends on the availability of good climatic models properly downscaled. Considering all these issues, a lot of work is still needed to study the spatial and the temporal dynamics of the Alpine ecological populations at high altitude, both at the level of single populations, as done in this thesis, and at the level of interspecific interactions.